

Coulomb interaction in the Eliashberg theory of Superconductivity

Dissertation

zur Erlangung des akademischen Grades
Doctor rerum naturalium (Dr. rer. nat.)

der

Naturwissenschaftlichen Fakultät II – Chemie, Physik und Mathematik
der Martin-Luther-Universität Halle-Wittenberg

vorgelegt

von Arkadiy Davydov

geboren am 15.09.1986 in Severouralsk, UdSSR

Gutachter:

Prof. Dr. Eberhard K. U. Gross, MPI Halle
Prof. Dr. Ingrid Mertig, MLU Halle-Wittenberg
Prof. Dr. Lilia Boeri, TU Graz

Halle (Saale), den 25.04.2018

Contents

| | |
|--|-----------|
| Acronyms | 4 |
| Introduction | 5 |
| 1 Normal state properties | 7 |
| 1.1 Introduction | 7 |
| 1.2 Kohn-Sham system | 7 |
| 1.2.1 LDA | 9 |
| 1.3 Phonon contribution | 9 |
| 1.3.1 Born-Oppenheimer approximation | 9 |
| 1.3.2 Phonons | 10 |
| 1.3.3 Electron-phonon interaction | 13 |
| 1.4 Direct Coulomb contribution | 14 |
| 1.4.1 Screening | 14 |
| 1.4.1.1 Dielectric function, reducible and irreducible polarizability | 14 |
| 1.4.1.2 Thomas-Fermi screening | 15 |
| 1.4.1.3 Random Phase Approximation (RPA) | 16 |
| 1.4.1.4 TDDFT framework | 18 |
| 1.4.1.5 Frequency and q -dependent f_{xc} in homogeneous case. Dielectric function | 19 |
| 1.4.2 Coulomb matrix | 20 |
| 1.4.3 Isotropic limit | 21 |
| 1.4.4 Plasmon pole approximation. | 22 |
| 1.4.5 Lindhard theory | 22 |
| 1.4.6 Coulomb kernel: examples | 23 |
| 2 A novel approach to the Eliashberg theory of Superconductivity | 28 |
| 2.1 Perturbation theory in the Nambu formalism | 29 |
| 2.1.1 Hamiltonian | 29 |
| 2.1.2 Green's Function | 30 |
| 2.1.2.1 Approximations for \bar{G} | 32 |
| 2.1.3 Self-energy | 32 |
| 2.1.3.1 Phonon part | 33 |
| 2.1.3.2 Exact Coulomb part | 34 |
| 2.1.3.3 Coulomb part in the Nambu-GW approximation | 35 |
| 2.1.3.4 Coulomb part - $\bar{\Sigma}^A$ and the spin fluctuation contribution | 35 |
| 2.1.4 Summary of the self energy | 37 |
| 2.2 Eliashberg equations | 37 |
| 2.2.1 χ and v^{xc} | 38 |

| | | |
|----------|--|-----------|
| 2.2.2 | Connection to experimental observables | 38 |
| 2.2.3 | Isotropic limit | 39 |
| 2.2.3.1 | Phonon interaction kernel. | 40 |
| 2.2.3.2 | Paramagnon interaction kernel | 41 |
| 2.3 | Using the SCDFT-Kohn-Sham GF in the Eliashberg method | 41 |
| 2.4 | Numerical aspects and approximations | 42 |
| 2.4.1 | Meshes and numerical integrations | 43 |
| 2.4.2 | Special integrations and approximations in the Coulomb part | 44 |
| 2.4.2.1 | Plasmon pole approximation | 44 |
| 2.4.2.2 | Static contribution | 45 |
| 2.4.2.3 | μ^* approach | 46 |
| 2.4.3 | Summary of approximation schemes and nomenclature | 47 |
| 2.5 | Convergence and tests | 47 |
| 2.5.1 | Models | 48 |
| 2.5.2 | Model A | 49 |
| 2.5.3 | Model B: Convergence of the mass renormalization (Z) | 50 |
| 2.5.4 | Model B: Convergence of the gap (ϕ) | 51 |
| 2.5.5 | Static Coulomb kernel | 52 |
| 2.5.6 | Comparison with the μ^* approach | 53 |
| 3 | Applications | 54 |
| 3.1 | Superconductivity of Nb and MgB ₂ within the static Coulomb interaction | 54 |
| 3.1.1 | Normal state properties and pairing interactions | 54 |
| 3.1.1.1 | DOS | 55 |
| 3.1.1.2 | Electron-phonon interaction | 55 |
| 3.1.1.3 | Static Coulomb kernel | 56 |
| 3.1.2 | Solution of the Eliashberg equations for Nb and MgB ₂ | 58 |
| 3.1.3 | Excitation spectrum and tunneling | 61 |
| 3.2 | Ab-initio static calculations on a larger set of materials | 62 |
| 3.2.1 | Test set of materials | 63 |
| 3.2.2 | Critical temperatures and comparison with experiments | 63 |
| 3.3 | Dynamical screening | 65 |
| 3.3.1 | Electron gas | 67 |
| 3.3.1.1 | Result with the Eliashberg scheme | 67 |
| 3.3.1.2 | Approach with SCDFT self energy | 70 |
| 3.3.2 | Applications to real materials | 71 |
| 3.3.2.1 | Eliashberg scheme | 74 |
| 4 | Summary, Conclusions and Outlook | 76 |
| A | Translational symmetry | 78 |
| A.1 | Lattice | 78 |
| A.1.1 | Direct lattice | 78 |
| A.1.2 | Reciprocal lattice | 78 |
| A.1.3 | Periodic boundary conditions | 79 |
| A.2 | Fourier transforms | 79 |
| A.2.1 | Nuclear coordinates | 79 |
| A.2.2 | Electronic coordinates | 79 |
| A.2.3 | Applications: Coulomb matrix elements | 81 |

| | | |
|----------|---|------------|
| A.2.4 | Applications: KS response | 82 |
| A.2.5 | Analytical properties of χ_0 | 82 |
| B | MBPT | 84 |
| B.1 | Green's function in KS basis | 84 |
| B.2 | Polarization propagator | 86 |
| B.3 | EOM for \tilde{G}_0 and D | 87 |
| B.4 | MBPT for magnetic perturbations | 89 |
| B.5 | Spectral function of spin fluctuations | 91 |
| C | Convergence properties of the Coulomb kernel | 93 |
| C.1 | Static case. Superconducting calculations | 93 |
| C.2 | Dynamical case. Lindhard kernel integrations | 93 |
| C.3 | Dynamical case. Superconducting calculations | 95 |
| C.4 | Gross-Kohn approximation for the ω and q -dependent f_{xc} | 99 |
| D | Eliashberg equations | 103 |
| D.1 | Review of the different sets of Eliashberg equations | 103 |
| D.2 | Block-band resolved approach | 104 |
| D.3 | Model A (details) | 105 |
| | Bibliography | 107 |
| | Acknowledgements | 115 |
| | Curriculum Vitae | 116 |
| | Eidesstattliche Erklärung | 116 |

Acronyms

| | |
|-------|--|
| ALDA | Adiabatic LDA |
| BCS | Bardeen, Cooper, Schrieffer |
| BO | Born-Oppenheimer |
| BZ | Brillouin zone |
| DFPT | Density Functional Perturbation Theory |
| DFT | Density Functional Theory |
| DOS | Density of State |
| ET | Eliashberg Theory |
| FC | Fourier Component |
| FS | Fermi Surface |
| FT | Fourier Transform |
| GF | Green's Function |
| KS | Kohn-Sham |
| LDA | Local Density Approximation |
| MBPT | Many-Body Perturbation Theory |
| PBE | Perdew, Burke, Ernzerhof |
| RPA | Random Phase Approximation |
| SC | Superconductivity |
| SCDFT | Superconducting DFT |
| SE | Self-Energy |
| TDDFT | Time-Dependent Density Functional Theory |
| TF | Thomas-Fermi |
| UC | Unit cell |
| WZ | Wigner-Seitz |

Introduction

In the past century superconductivity (SC) has been one of the most challenging fields in solid state physics. The first microscopic description (by Bardeen, Cooper and Schrieffer BCS in 1957 [1]) appeared only 46 years after the discovery of the phenomenon (by Onnes 1911 [2]). Still, more than 50 years after BCS we have no commonly accepted theoretical description for several classes of superconductors (among which are the so called high T_c superconductors, like pnictides and cuprates) [3, 4, 5]. Within BCS theory, the driving force for SC was identified as an *attraction* between Fermi surface electrons due to electron-phonon interaction [6], although the BCS model does not necessarily require the phononic nature of this attraction. Moreover in the BCS theory, this attractive pairing is quite oversimplified, leading to a qualitatively correct picture, without, however, any quantitative predictive power.

A formally exact approach to SC was then formulated in the sixties, by means of many body perturbation theory (MBPT) [7, 8], leading to the Eliashberg theory (ET) [9], which is at the heart of this work. This method is, in principle, capable to include the electron-phonon interaction in an accurate way. In particular, it naturally takes into account the different timescales of phonons and electrons. At the time the ET was first formulated, its predictive power was relatively low, mainly because it was not yet possible to compute accurately phonons and the related electronic coupling. Nowadays we are able to calculate fully *ab-initio* phonons and the electron-phonon interaction with reasonable accuracy [10, 11]. This allows us to use the Eliashberg framework to perform calculations on real materials.

One major problem survives in the way Coulomb interactions are handled, namely as a BCS-like static potential, which is reduced to an effective parameter μ^* [12, 13]. This parameter is usually *fitted* to get the experimental T_c , thus reducing an accurate *ab-initio* theory to a semi-empirical one. Typical values for μ^* in simple superconductors range from 0.09 to 0.16, although for more complex systems μ^* can lay outside of this specific interval [14]. Moreover, in the case of multiband superconductivity, where different bands of the material show different superconducting behavior, no thumb rule applies to estimate μ^* [15].

The aim of this work is to revisit the original Eliashberg approach and to improve it in such a way that Coulomb interactions are included in order to promote it to a genuine *ab-initio* level. We will proceed by reviewing the many body perturbation expansion leading to the conventional Eliashberg equations, and account for the Coulomb interaction in a similar way as it is done in GW theory [16, 17] and in DFT for superconductors (SCDFT [18]).

The central point of any superconducting theory based on MBPT is the non SC ground state, that is assumed to be well understood and characterized. This may not be always the case, like in high- T_c superconductors [3, 4, 5]. However, in this work we will assume that conventional density functional theory (DFT) schemes [19] do provide a description of this “normal state” that is accurate enough. The superconducting state is then formed by two-body correlations omitted in conventional DFT approximations: those due to the scattering of electron pairs with opposite spin and momenta i.e., Cooper pairs.

If one is mostly interested in the prediction of the critical temperature, the pairings can be

computed ignoring feedback effects due to SC, i.e., in the normal state¹. Phonons will be and are usually computed within the so-called Born-Oppenheimer approximation (BO) [20]. The calculation of a Coulomb part is less straightforward and involves the estimation of the screening properties. The simplest and completely parameter free approach to the screening is the random phase approximation (RPA) [21]. To introduce correlation corrections [22, 23] is also possible and can be done conveniently by means of time dependent DFT (TDDFT).

The RPA is a popular approximation in theoretical optical spectroscopy and is commonly used in SCDF. However so far in the SCDF literature, the RPA has been used mostly in the static limit, and very little is known on the role of dynamical effects [24]. In fact, those are associated with plasmons, which are the source of the superconducting pairing according to some unconventional theories of superconductivity [25, 26]. The first step towards an *ab-initio* analysis of the plasmon-induced superconducting pairing is done in ref. [27]. It is constructed using a plasmon pole approximation for the effective interaction and resulted in a weak superconducting pairing leading to a sensible critical temperature at extremely low densities. The second work we refer to is by Rietschel and Sham [28], which relies on the Eliashberg approach with Lindhard's theory for the corresponding interaction. Both of these works study Coulomb-only driven superconductivity. In this thesis we revise the whole effect of the Coulomb interaction in its static and full dynamic limits from a fully *ab-initio* perspective using correspondingly adopted Eliashberg approach. Moreover our implementation allows to study the interplay between phonon, plasmon and magnon² mediated pairings at the same time.

The thesis starts (chap. 1) by giving a review on the techniques used to describe the normal state properties. In particular, we will discuss the screened Coulomb interaction, the calculation of which was implemented during this work in the open source code ELK [29].

In chap. 2 we discuss the MBPT leading to the Eliashberg equations. We achieve a form of the equations that allow us to include the full Coulomb interaction. Details on the implementation are given in the appendices.

Results are presented in chap. 3. In sec. 3.2.2 a systematic study of the method is presented in the limit of a static Coulomb interaction: we calculate the critical temperatures of several phononic superconductors and compare them with experiment. The effect of dynamical screening and plasmonic couplings is discussed in sec. 3.3.

¹As long as the SC transition is of II order

²Although electron-magnon pairings will be treated in a simplified way.

Chapter 1

Normal state properties

1.1 Introduction

The normal state DFT approach is conveniently obtained by solving a system of single-particle equations. These are known as Kohn-Sham (KS) equations [19] and are presented in sec. 1.2.

Then we will introduce methods to compute phonons and electron-phonon coupling, standard approximations and methods will be discussed in sec. 1.3. Approximations and methods to compute the Coulomb part of the electronic interactions are discussed in sec. 1.4 including specific approximations developed in this work.

1.2 Kohn-Sham system

A description of the system of interacting electrons is formally given by the Schrödinger equation¹. Ignoring for a moment the nuclear motion², we write this equation for electronic degrees of freedom:

$$\begin{aligned}\hat{H}\Psi(\mathbf{r}_1\mathbf{r}_2..\mathbf{r}_{N_e}) &= (\hat{T} + \hat{W} + \hat{V}_0)\Psi(\mathbf{r}_1\mathbf{r}_2..\mathbf{r}_{N_e}) \\ &= \left(-\frac{1}{2} \sum_i \nabla_{\mathbf{r}_i}^2 + \frac{1}{2} \sum_{i \neq j} \frac{1}{|\mathbf{r}_i - \mathbf{r}_j|} + \sum_i v_{ext}^0(\mathbf{r}_i) \right) \Psi(\mathbf{r}_1\mathbf{r}_2..\mathbf{r}_{N_e}) \\ &= E\Psi(\mathbf{r}_1\mathbf{r}_2..\mathbf{r}_{N_e})\end{aligned}\tag{1.2.1}$$

in atomic units ($m = \hbar = e = 1$). The $\mathbf{r}_1\mathbf{r}_2..\mathbf{r}_{N_e}$ is the set of electronic coordinates. The first term in the Hamiltonian \hat{H} is the total kinetic energy contribution, the second one is the electron-electron Coulomb interaction, while the $v_{ext}^0(\mathbf{r})$ is an external potential assumed to be produced by a fixed nuclear system. Due to electron-electron interactions this Schrödinger equation is not separable in single particle equations and is too complex to solve for large systems and crystals even with the most powerful modern computers.

An alternative treatment is found within the Density Functional Theory (DFT) [30]. The key object in DFT is the ground state density (i.e., Ψ_0 is the ground state wave function):

$$n_0(\mathbf{r}) = N_e \int d\mathbf{r}_2..d\mathbf{r}_{N_e} |\Psi_0(\mathbf{r}\mathbf{r}_2..\mathbf{r}_{N_e})|^2.\tag{1.2.2}$$

¹To describe something in quantum theory is equivalent to knowing the many-body wavefunction Ψ , which is a solution of the mentioned Schrödinger equation.

²This approximation is reviewed in sec. 1.3.1.

The Hohenberg-Kohn (HK) theorem [31] proves (1) that there is a one-to-one correspondence between the ground state density and the external potential:

$$V_0 \leftrightarrow \Psi_0 \leftrightarrow n_0, \quad (1.2.3)$$

(2) that the energy functional:

$$E[n] = \langle \Psi[n] | \hat{T} + \hat{W} + \hat{V}_0 | \Psi[n] \rangle, \quad (1.2.4)$$

is minimized by the ground state density n_0 (for V_0) for which it gives the ground state energy of the system. Computational applications of this DFT approach are mostly implemented in the Kohn-Sham (KS) [19] scheme. Kohn and Sham considered a system of fictitious non-interacting electrons (KS electrons), which possess the same density as an original interacting many-electron system. The total energy functional can be rewritten as:

$$E[n] = T_{KS}[n] + W_H[n] + V_0[n] + E_{xc}[n], \quad (1.2.5)$$

where $T_{KS}[n]$ is the kinetic energy of KS system, W_H is a classical (Hartree) contribution to the energy³ and a so-called exchange-correlation energy is simply given by:

$$E_{xc}[n] = T[n] - T_{KS}[n] + W[n] - W_H[n]. \quad (1.2.6)$$

This approach leads to the set of one-particle equations (KS equations):

$$\left(-\frac{1}{2}\nabla^2 + v_{KS}(\mathbf{r}) \right) \phi_i(\mathbf{r}) = \epsilon_i \phi_i(\mathbf{r}), \quad (1.2.7)$$

$$n_0(\mathbf{r}) = 2 \sum_{i=1}^{N_e/2} |\phi_i(\mathbf{r})|^2. \quad (1.2.8)$$

The factor of two in the last line is responsible for spin. The one body potential v_{KS} is a functional of the density and is given by:

$$v_{KS}[n](\mathbf{r}) = v_{ext}^0(\mathbf{r}) + v_H[n](\mathbf{r}) + v_{xc}[n](\mathbf{r}), \quad (1.2.9)$$

$$v_H[n](\mathbf{r}) = \int d\mathbf{r}' n(\mathbf{r}') v(\mathbf{r} - \mathbf{r}'), \quad (1.2.10)$$

where $v(\mathbf{r})$, as in the following, is used for the bare Coulomb interaction and the so-called exchange-correlation potential v_{xc} is directly related to the E_{xc} by:

$$v_{xc}[n](\mathbf{r}) = \frac{\delta E_{xc}[n]}{\delta n(\mathbf{r})} \quad (1.2.11)$$

The solutions of eqs. 1.2.7, 1.2.8 and 1.2.9 are found iteratively. First, the density n at eq. 1.2.8 is evaluated (usually out of the atomic orbitals), then it is used to get $v_{KS}[n](\mathbf{r})$ from eq. 1.2.9, and finally, eigenfunctions of eq. 1.2.7, ϕ_i (KS orbitals) are used to compute the density for the subsequent iteration step (again, eq. 1.2.8). When self-consistency is reached the resulting density is the ground state density of interacting system, $n_0(\mathbf{r})$.

The KS scheme is constructed to produce $n_0(\mathbf{r})$, but a major advantage of the scheme lies in the fact, that the KS eigenvalues (ϵ_i) and eigenfunctions ($\phi_i(\mathbf{r})$) are usually a good approximation to quasiparticle⁴ energies and orbitals respectively.

³ $W_H[n] = \int d\mathbf{r} \int d\mathbf{r}' n(\mathbf{r})n(\mathbf{r}')/|\mathbf{r} - \mathbf{r}'|$

⁴The quasiparticle in a given context is an bare (i.e. as it would be free) electron plus the ‘‘cloud’’ of other electrons interacting with it [32].

1.2.1 LDA

The KS scheme would not be of practical use without a valid approximation for $E_{xc}[n]$. The earliest and still one of the most successful approximation to $E_{xc}[n]$ is given by the local density approximation (LDA):

$$E_{xc}[n] = \int d\mathbf{r} n(\mathbf{r}) \epsilon_{xc}(n(\mathbf{r})), \quad (1.2.12)$$

$$\epsilon_{xc}(n) = \epsilon_x(n) + \epsilon_c(n), \quad (1.2.13)$$

where exchange (ϵ_x) and correlation (ϵ_c) energy per electron are defined for the homogeneous electron system of density n . In this way the ϵ_{xc} becomes just a *function* of the density. The exchange-correlation potential in eq. 1.2.9 is now also a *function* of the density at point \mathbf{r} :

$$\begin{aligned} v_{xc}(n(\mathbf{r})) &= \frac{\delta E_{xc}[n]}{\delta n} = \frac{\partial \{n \epsilon_{xc}(n)\}}{\partial n} \\ &= \epsilon_{xc}(n) + n(\mathbf{r}) \frac{\partial \epsilon_{xc}(n)}{\partial n}. \end{aligned} \quad (1.2.14)$$

For the homogeneous electron gas the exchange contribution is

$$\begin{aligned} \epsilon_x(n) &= -3/(4\pi\alpha r_s), \\ \alpha &= (4/9\pi)^{1/3}, \quad r_s(n) = \left[\frac{3}{4\pi} \frac{1}{n} \right]^{1/3}, \end{aligned}$$

while the correlation part (ϵ_c) comes from quantum Monte-Carlo calculations (see ref. [30] p. 176-183 for the complete review).

1.3 Phonon contribution

1.3.1 Born-Oppenheimer approximation

To be able to describe phononic superconductivity we need to evaluate the interaction between electrons and lattice vibrations (electron-phonon coupling). The problem of the electron-ion interaction is far from trivial and a large branch of solid state research is devoted to this topic. However close to equilibrium it is possible to adopt the Born Oppenheimer (BO) approximation [20], which allows to deal with this problem with sufficient accuracy for our scope. In this section we will review its basics.

Starting from the most general formulation, a full Schrödinger equation for electron-nuclear system is written as:

$$\hat{H}\Psi(\underline{\mathbf{R}}, \underline{\mathbf{r}}) = E\Psi(\underline{\mathbf{R}}, \underline{\mathbf{r}}), \quad (1.3.1)$$

$$\hat{H} = \hat{T}^e(\underline{\mathbf{r}}) + \hat{T}^n(\underline{\mathbf{R}}) + \hat{U}^{ee}(\underline{\mathbf{r}}) + \hat{U}^{en}(\underline{\mathbf{R}}, \underline{\mathbf{r}}) + \hat{U}^{nn}(\underline{\mathbf{R}}), \quad (1.3.2)$$

where $\underline{\mathbf{r}}$ and $\underline{\mathbf{R}}$ are sets of all electron (e) and all nuclear (n) coordinates respectively, where:

$$\begin{aligned} \hat{T}^e(\underline{\mathbf{r}}) &= -\frac{1}{2} \sum_i \nabla_{\mathbf{r}_i}^2, \quad \hat{T}^n(\underline{\mathbf{R}}) = -\sum_i \frac{1}{2M_i} \nabla_{\mathbf{R}_i}^2, \\ \hat{U}^{ee}(\underline{\mathbf{r}}) &= \frac{1}{2} \sum_{i \neq j} \frac{1}{|\mathbf{r}_i - \mathbf{r}_j|}, \quad \hat{U}^{en}(\underline{\mathbf{R}}, \underline{\mathbf{r}}) = -\sum_{ij} \frac{Z_i}{|\mathbf{R}_i - \mathbf{r}_j|}, \\ \hat{U}^{nn}(\underline{\mathbf{R}}) &= \frac{1}{2} \sum_{i \neq j} \frac{Z_i Z_j}{|\mathbf{R}_i - \mathbf{R}_j|}, \end{aligned} \quad (1.3.3)$$

with Z_i and M_i being the charge and the mass of i 'th nucleus, respectively. In the BO approximation it is assumed, that electrons follow moving nuclei instantaneously which is reasonable due to the huge difference between electronic and nuclear velocities. This allows to split the eq. 1.3.1 into nuclear and electronic parts:

$$\Psi(\underline{\mathbf{R}}, \mathbf{r}) = \chi_{\underline{\mathbf{R}}}(\mathbf{r})\Phi(\underline{\mathbf{R}}), \quad (1.3.4)$$

$$[\hat{T}^n + E^{BO}(\underline{\mathbf{R}})]\Phi(\underline{\mathbf{R}}) = E\Phi(\underline{\mathbf{R}}), \quad (1.3.5)$$

$$\hat{H}_{\underline{\mathbf{R}}}^{BO}(\mathbf{r})\chi_{\underline{\mathbf{R}}}(\mathbf{r}) = E^{BO}(\underline{\mathbf{R}})\chi_{\underline{\mathbf{R}}}(\mathbf{r}), \quad (1.3.6)$$

where the BO Hamiltonian is defined:

$$\hat{H}_{\underline{\mathbf{R}}}^{BO}(\mathbf{r}) = \hat{T}^e(\mathbf{r}) + \hat{U}^{ee}(\mathbf{r}) + \hat{U}^{en}(\underline{\mathbf{R}}, \mathbf{r}) + \hat{U}^{nn}(\underline{\mathbf{R}}). \quad (1.3.7)$$

The dependence of eq. 1.3.6 on $\underline{\mathbf{R}}$ is parametric, i.e., one should solve this equation for different nuclear configurations $\underline{\mathbf{R}}^\nu$, in this way constructing the BO energy surface $E^{BO}(\underline{\mathbf{R}})$, and then solve the eq. 1.3.5 with this surface as a potential. In principle, the last property can be obtained solving a corresponding KS problem of sec. 1.2 for each nuclear configuration $\underline{\mathbf{R}}^\nu$ and adding a last term of eq. 1.3.7 to the total energy functional:

$$E^{BO}(\underline{\mathbf{R}}^\nu) = E[n_{0\underline{\mathbf{R}}^\nu}(\mathbf{r})] + \frac{1}{2} \sum_{i \neq j} \frac{Z_i Z_j}{|\underline{\mathbf{R}}_i^\nu - \underline{\mathbf{R}}_j^\nu|}, \quad (1.3.8)$$

where $n_{0\underline{\mathbf{R}}^\nu}(\mathbf{r})$ is the ground state density obtained with the KS scheme with an external potential constructed from the given nuclear configuration:

$$v_{ext}^0(\mathbf{r}) = - \sum_i \frac{Z_i}{|\underline{\mathbf{R}}_i^\nu - \mathbf{r}|}. \quad (1.3.9)$$

Solutions of eq. 1.3.5 are found expanding the BO energy surface around its minimum (equilibrium position of the nuclei⁵, see the next section):

$$E^{BO}(\underline{\mathbf{R}}) = E_0 + \frac{1}{2} \sum_{ij} \frac{\partial^2 E^{BO}(\underline{\mathbf{R}})}{\partial R_i^a \partial R_j^b} \delta R_i^a \delta R_j^b. \quad (1.3.10)$$

First derivative terms vanish at the surface minimum and higher order terms are truncated. The E_0 obtained in this way is a full energy of interacting electron-nuclear system with nuclei being in equilibrium position and the derivative term (the $\partial^2 E^{BO}(\underline{\mathbf{R}})/\partial R_i^a \partial R_j^b$ is the so-called Hessian matrix) is used to construct the contribution from the lattice vibrations (phonons) in harmonic approximation.

The method described above normally gives good estimations to vibrational properties of physical systems. Picking up a ground state energies in eq. 1.3.6 makes the DFT framework applicable to produce $E^{BO}(\underline{\mathbf{R}})$, and hence, providing a well-defined method to get phonons [10, 11].

1.3.2 Phonons

The position of an ion in a crystal is specified with a position vector:

$$\mathbf{R}_i \equiv \mathbf{R}_{n\alpha} = \mathbf{R}_n + \mathbf{R}_\alpha + \mathbf{u}_{n\alpha}, \quad (1.3.11)$$

where displacement around equilibrium is described by vectors $\mathbf{u}_{n\alpha}$ ($\mathbf{R}_n + \mathbf{R}_\alpha$ gives the equilibrium position of the α 'th atom in the n 'th unit cell, see A.1). The following Fourier transformation (FT) for $\mathbf{u}_{n\alpha}$ is defined:

$$\mathbf{u}_{q\alpha} = \frac{1}{\sqrt{N_n}} \sum_{\mathbf{R}_n \in \Omega} \mathbf{u}_{n\alpha} e^{-iq\mathbf{R}_n}, \quad (1.3.12)$$

⁵a sum over tensor components a, b is implied

where the sum goes over all N_n cells in a macroscopic piece of solid with volume Ω . The inverse transformation is also given:

$$\mathbf{u}_{\mathbf{n}\alpha} = \frac{1}{\sqrt{N_n}} \sum_{\mathbf{q} \in BZ} \mathbf{u}_{\mathbf{q}\alpha} e^{i\mathbf{q}\mathbf{R}_n}. \quad (1.3.13)$$

The sum is over \mathbf{q} in the first Brillouin zone, see A.2.1. Each component, $u_{\mathbf{n}\alpha}^a$ is real and hence the condition $u_{\mathbf{q}\alpha}^{a*} = u_{-\mathbf{q}\alpha}^a$ is fulfilled in transformations above.

Eq. 1.3.10 can be rewritten in Fourier components (ignoring the constant E_0 term) as:

$$\begin{aligned} \frac{1}{2} \sum_{\mathbf{nm}\alpha\beta} \frac{\partial^2 E^{BO}(\mathbf{R})}{\partial u_{\mathbf{n}\alpha}^a \partial u_{\mathbf{m}\beta}^b} \hat{u}_{\mathbf{n}\alpha}^a \hat{u}_{\mathbf{m}\beta}^b &= \frac{1}{2} \sum_{\mathbf{nm}\alpha\beta} A_{\mathbf{nm}\alpha\beta}^{ab} \hat{u}_{\mathbf{n}\alpha}^a \hat{u}_{\mathbf{m}\beta}^b \\ &= \frac{1}{2N_n} \sum_{\mathbf{nm}\alpha\beta} \sum_{\mathbf{q}\mathbf{q}' \in BZ} \hat{u}_{\mathbf{q}\alpha}^a \hat{u}_{\mathbf{q}'\beta}^b e^{i\mathbf{q}\mathbf{R}_n} e^{i\mathbf{q}'\mathbf{R}_m} A_{\mathbf{nm}\alpha\beta}^{ab} \\ &= \frac{1}{2N_n} \sum_{\alpha\beta} \sum_{\mathbf{q}\mathbf{q}' \in BZ} \hat{u}_{\mathbf{q}\alpha}^a \hat{u}_{\mathbf{q}'\beta}^b \sum_{\mathbf{n}} e^{i(\mathbf{q}+\mathbf{q}')\mathbf{R}_n} \sum_{\mathbf{m}} e^{i\mathbf{q}'(\mathbf{R}_m - \mathbf{R}_n)} A_{\mathbf{nm}\alpha\beta}^{ab}. \end{aligned} \quad (1.3.14)$$

That translational symmetry provides $A_{\mathbf{nm}\alpha\beta}^{ab} = A_{\mathbf{0}(\mathbf{m}-\mathbf{n})\alpha\beta}^{ab}$ resulting in the fact that the potential energy operator becomes:

$$\frac{1}{2N_n} \sum_{\alpha\beta} \sum_{\mathbf{q}\mathbf{q}' \in BZ} \hat{u}_{\mathbf{q}\alpha}^a \hat{u}_{\mathbf{q}'\beta}^b \sum_{\mathbf{n}} e^{i(\mathbf{q}+\mathbf{q}')\mathbf{R}_n} A_{\mathbf{q}'\alpha\beta}^{ab} \quad (1.3.15)$$

with FT:

$$A_{\mathbf{q}\alpha\beta}^{ab} = \sum_{\mathbf{m}} e^{i\mathbf{q}(\mathbf{R}_m - \mathbf{R}_n)} A_{\mathbf{0}(\mathbf{m}-\mathbf{n})\alpha\beta}^{ab}. \quad (1.3.16)$$

The sum $\sum_{\mathbf{n}} e^{i\mathbf{k}\mathbf{R}_n}$ is non-zero only if \mathbf{k} is equal to a reciprocal lattice vector \mathbf{G} :

$$\sum_{\mathbf{n}} e^{i\mathbf{k}\mathbf{R}_n} = N_n \sum_{\mathbf{G}} \delta_{\mathbf{k},\mathbf{G}}, \quad (1.3.17)$$

this relation allows to rewrite eq. 1.3.15 as:

$$\begin{aligned} \frac{1}{2} \sum_{\alpha\beta} \sum_{\mathbf{q}\mathbf{q}' \in BZ} \hat{u}_{\mathbf{q}\alpha}^a \hat{u}_{\mathbf{q}'\beta}^b A_{\mathbf{q}'\alpha\beta}^{ab} \sum_{\mathbf{G}} \delta_{\mathbf{q}+\mathbf{q}',\mathbf{G}} &= \frac{1}{2} \sum_{\alpha\beta} \sum_{\mathbf{q}' \in BZ} \hat{u}_{-\mathbf{q}'\alpha}^a \hat{u}_{\mathbf{q}'\beta}^b A_{\mathbf{q}'\alpha\beta}^{ab} \\ &= \frac{1}{2} \sum_{\alpha\beta} \sum_{\mathbf{q} \in BZ} \hat{u}_{\mathbf{q}\alpha}^{a\dagger} \hat{u}_{\mathbf{q}\beta}^b A_{\mathbf{q}\alpha\beta}^{ab}. \end{aligned} \quad (1.3.18)$$

By definition of the first Brillouin zone, $|\mathbf{q} + \mathbf{q}'| < |\mathbf{G}|$ for any $\mathbf{G} \neq \mathbf{0}$, so we are left only with the $\mathbf{G} = \mathbf{0}$ contribution. The expression above is a quadratic form of $3N_a$ variables with respect to the combined $l = \{\alpha a\}$ index ($l = 1..3N_a$, N_a is the number of atoms in the unit cell). Then we perform the following change of variables:

$$\begin{aligned} \frac{1}{2} \sum_{\alpha\beta} \sum_{\mathbf{q} \in BZ} \hat{u}_{\mathbf{q}\alpha}^{a\dagger} \hat{u}_{\mathbf{q}\beta}^b A_{\mathbf{q}\alpha\beta}^{ab} &= \frac{1}{2} \sum_{\alpha\beta} \sum_{\mathbf{q} \in BZ} \sqrt{M_\alpha} \hat{u}_{\mathbf{q}\alpha}^{a\dagger} \sqrt{M_\beta} \hat{u}_{\mathbf{q}\beta}^b \left(\frac{1}{\sqrt{M_\alpha M_\beta}} A_{\mathbf{q}\alpha\beta}^{ab} \right) \\ &= \frac{1}{2} \sum_{\alpha\beta} \sum_{\mathbf{q} \in BZ} \hat{u}_{\mathbf{q}\alpha}^{a\dagger} \hat{u}_{\mathbf{q}\beta}^b D_{\mathbf{q}\alpha\beta}^{ab} \end{aligned} \quad (1.3.19)$$

The Dynamical matrix $D_{\mathbf{q}}^{ll'} = \frac{1}{\sqrt{M_\alpha M_\beta}} A_{\mathbf{q}\alpha\beta}^{ab}$ is symmetric, which means that the given quadratic form can be diagonalized:

$$\frac{1}{2} \sum_{\mathbf{q} \in BZ} \sum_{j=1}^{3N_a} \hat{Q}_{j\mathbf{q}}^\dagger \hat{Q}_{j\mathbf{q}} \omega_{j\mathbf{q}}^2, \quad (1.3.20)$$

where $\hat{Q}_{j\mathbf{q}}$ is the normal coordinate, $\omega_{j\mathbf{q}}^2$ is an eigenvalue of $D_{\mathbf{q}}^{ll'}$, while its eigenvector $\mathbf{e}_{j\mathbf{q}}$ (in $3N_a$ dimensions) is a polarization vector for the phonon of branch j . If $\mathbf{e}_{j\mathbf{q}}$ is normalized to unity, the unitary matrix:

$$Y_{\mathbf{q}} = \begin{pmatrix} e_{1\mathbf{q}}^1 & \cdots & e_{3N_a\mathbf{q}}^1 \\ \vdots & \ddots & \vdots \\ e_{1\mathbf{q}}^{3N_a} & \cdots & e_{3N_a\mathbf{q}}^{3N_a} \end{pmatrix} \quad (1.3.21)$$

gives the desired transformations:

$$\tilde{u}_{\mathbf{q}} = Y_{\mathbf{q}} Q_{\mathbf{q}}, \quad D_{\mathbf{q}} = Y_{\mathbf{q}} \begin{pmatrix} \omega_{1\mathbf{q}}^2 & 0 & 0 \\ 0 & \ddots & 0 \\ 0 & 0 & \omega_{3N_a\mathbf{q}}^2 \end{pmatrix} Y_{\mathbf{q}}^\dagger \quad (1.3.22)$$

A similar discussion holds for the nuclear kinetic energy operator \hat{T}^n of eq. 1.3.3. First, we define the FT for nuclear momentum operator:

$$\begin{aligned} \hat{P}_i^a &= -i \frac{\partial}{\partial R_i^a} = -i \frac{\partial}{\partial u_{\mathbf{n}\alpha}^a} = -i \sum_{\mathbf{q} \in BZ} \frac{\partial u_{\mathbf{q}\alpha}^b}{\partial u_{\mathbf{n}\alpha}^a} \frac{\partial}{\partial u_{\mathbf{q}\alpha}^b} \\ &= -i \sum_{\mathbf{q} \in BZ} \frac{1}{\sqrt{N_n}} \sum_{\mathbf{R}_m \in \Omega} \delta_{a,b} \delta_{\mathbf{m},\mathbf{n}} e^{-i\mathbf{q}\mathbf{R}_m} \frac{\partial}{\partial u_{\mathbf{q}\alpha}^b} \\ &= \frac{1}{\sqrt{N_n}} \sum_{\mathbf{q} \in BZ} e^{-i\mathbf{q}\mathbf{R}_n} \left(-i \frac{\partial}{\partial u_{\mathbf{q}\alpha}^a} \right) = \frac{1}{\sqrt{N_n}} \sum_{\mathbf{q} \in BZ} e^{-i\mathbf{q}\mathbf{R}_n} \hat{P}_{\mathbf{q}\alpha}^a \end{aligned} \quad (1.3.23)$$

The inverse transformation is:

$$\hat{P}_{\mathbf{q}\alpha}^a = \frac{1}{\sqrt{N_n}} \sum_{\mathbf{R}_n \in \Omega} e^{i\mathbf{q}\mathbf{R}_n} \hat{P}_{\mathbf{n}\alpha}^a. \quad (1.3.24)$$

Now we are able to rewrite the kinetic energy operator in terms of the transformed operators:

$$\begin{aligned} \hat{T}^n &= \sum_i \frac{1}{2M_i} \hat{P}_i^a \hat{P}_i^a = \sum_{\alpha} \frac{1}{2M_{\alpha}} \frac{1}{N_n} \sum_{\mathbf{q}\mathbf{q}' \in BZ} \sum_{\mathbf{n}} e^{-i(\mathbf{q}+\mathbf{q}')\mathbf{R}_n} \hat{P}_{\mathbf{q}\alpha}^a \hat{P}_{\mathbf{q}'\alpha}^a \\ &= \frac{1}{2} \sum_{\alpha} \sum_{\mathbf{q} \in BZ} \frac{1}{\sqrt{M_{\alpha}}} \hat{P}_{-\mathbf{q}\alpha}^a \frac{1}{\sqrt{M_{\alpha}}} \hat{P}_{\mathbf{q}\alpha}^a = \frac{1}{2} \sum_{\alpha} \sum_{\mathbf{q} \in BZ} \hat{P}_{\mathbf{q}\alpha}^{a\dagger} \hat{P}_{\mathbf{q}\alpha}^a \end{aligned} \quad (1.3.25)$$

Passing to normal coordinates, the momentum operator changes, $\hat{P}_{normal} = -i \frac{\partial}{\partial Q}$. In ref. [33] it was shown that momentum operator transforms with the same matrices $Y_{\mathbf{q}}$ as the coordinates themselves, and as soon as the transformation is unitary, the dot product ($\hat{P}_{\mathbf{q}\alpha}^{a\dagger} \hat{P}_{\mathbf{q}\alpha}^a$) is invariant. Thus, we are free to write (for momentum operator in new coordinates we used the same symbol P with branch index j):

$$\hat{T}^n = \frac{1}{2} \sum_j \sum_{\mathbf{q} \in BZ} \hat{P}_{j\mathbf{q}}^\dagger \hat{P}_{j\mathbf{q}} \quad (1.3.26)$$

We then arrive to the following nuclear Hamiltonian form:

$$\hat{H}^{ph} = \frac{1}{2} \sum_j \sum_{\mathbf{q} \in BZ} \left[\hat{P}_{j\mathbf{q}}^\dagger \hat{P}_{j\mathbf{q}} + \omega_{j\mathbf{q}}^2 \hat{Q}_{j\mathbf{q}}^\dagger \hat{Q}_{j\mathbf{q}} \right] \quad (1.3.27)$$

This can be rewritten in terms of Bose field operators:

$$\hat{b}_{j\mathbf{q}} = \frac{1}{\sqrt{2\omega_{j\mathbf{q}}}} \left(\omega_{j\mathbf{q}} \hat{Q}_{j\mathbf{q}} + i\hat{P}_{j\mathbf{q}}^\dagger \right) \quad (1.3.28)$$

$$\hat{b}_{j\mathbf{q}}^\dagger = \frac{1}{\sqrt{2\omega_{j\mathbf{q}}}} \left(\omega_{j\mathbf{q}} \hat{Q}_{j\mathbf{q}}^\dagger - i\hat{P}_{j\mathbf{q}} \right) \quad (1.3.29)$$

as:

$$\hat{H}^{ph} = \sum_j \sum_{\mathbf{q} \in BZ} \omega_{j\mathbf{q}} \left(\hat{b}_{j\mathbf{q}}^\dagger \hat{b}_{j\mathbf{q}} + \frac{1}{2} \right) \quad (1.3.30)$$

The expectation value of the $\hat{b}_{j\mathbf{q}}^\dagger \hat{b}_{j\mathbf{q}}$ operator gives the number of phonons in $j\mathbf{q}$ state.

1.3.3 Electron-phonon interaction

At this point two essential results are obtained. The first one is that the ground state KS problem is solved at fixed nuclear positions. (sec. 1.2). At the same time the resulting KS energies and orbitals are assumed to those of the physical quasiparticle states⁶, and a relevant Hamiltonian for us is the KS Hamiltonian \hat{H}^{KS} built out of mentioned KS solutions and discussed later in sec. 2.1.1. Second, the BO phonons are obtained within the adiabatic approximation (sec. 1.3.1), i.e., assuming electrons adopting to nuclear motion instantaneously. It means that electrons do not excite when nuclei move.

Such effects are added as a perturbation on top of the KS Hamiltonian. The nuclear distortion causes the change of the KS potential⁷ (eq. 1.2.9) and hence, corresponding perturbation on top of the KS system should have a following form:

$$\hat{H}^{el-ph} = \sum_{kk'\sigma} (\delta\hat{v})_{kk'\sigma} \hat{c}_{k'\sigma}^\dagger \hat{c}_{k\sigma} \quad (1.3.31)$$

If we work with crystals, k stands for a combined band (b) and wave vector (\mathbf{k}) index, i.e., $k = \{b, \mathbf{k}\}$ and σ stands for the z projection of the spin ($\sigma = \pm\frac{1}{2}$ or equivalently, $\sigma = \uparrow\downarrow$).

The $\delta\hat{v}$ is decomposed around equilibrium (with notations of sec. 1.3.2):

$$\begin{aligned} \delta\hat{v} &= \sum_{\mathbf{n}\alpha} \frac{\partial v_{KS}[n](\mathbf{r})}{\partial u_{\mathbf{n}\alpha}^a} \hat{u}_{\mathbf{n}\alpha}^a = \sum_{\alpha} \sum_{\mathbf{q} \in BZ} \frac{\partial v_{KS}[n](\mathbf{r})}{\partial u_{\mathbf{q}\alpha}^a} \hat{u}_{\mathbf{q}\alpha}^a \\ &= \sum_{\alpha j} \frac{1}{\sqrt{M_\alpha}} \sum_{\mathbf{q} \in BZ} \frac{\partial v_{KS}[n](\mathbf{r})}{\partial u_{\mathbf{q}\alpha}^a} e_{j\mathbf{q}}^{a\alpha} \frac{1}{\sqrt{2\omega_{j\mathbf{q}}}} \left(\hat{b}_{j\mathbf{q}} + \hat{b}_{j,-\mathbf{q}}^\dagger \right) \end{aligned} \quad (1.3.32)$$

The matrix element of this potential should be calculated as:

$$\begin{aligned} (\delta\hat{v})_{kk'\sigma} &= \sum_{j\mathbf{q}} \frac{1}{\sqrt{2\omega_{j\mathbf{q}}}} \left\langle k\sigma \left| \sum_{\alpha a} \frac{\partial v_{KS}[n](\mathbf{r})}{\partial \hat{u}_{\mathbf{q}\alpha}^a} e_{j\mathbf{q}}^{a\alpha} \right| k'\sigma \right\rangle \left(\hat{b}_{j\mathbf{q}} + \hat{b}_{j,-\mathbf{q}}^\dagger \right) \\ &= \sum_{j\mathbf{q}} g_{kk'}^{j\mathbf{q}} \left(\hat{b}_{j\mathbf{q}} + \hat{b}_{j,-\mathbf{q}}^\dagger \right) \end{aligned} \quad (1.3.33)$$

The $g_{kk'}^{j\mathbf{q}}$ is non-zero, when the condition $\mathbf{k}' - \mathbf{k} = \mathbf{q} + \mathbf{G}$ is fulfilled by some reciprocal vector \mathbf{G} ($\mathbf{k}' - \mathbf{k}$ may fall outside the first BZ, while a \mathbf{q} is defined inside), i.e., when the momentum is conserved. The reason for that is in the lattice periodicity of $v_{KS}[n](\mathbf{r})$.

⁶which already account for exchange and correlations due to Coulomb interaction between electrons.

⁷Although in a rather complex and non-linear way. The nuclear distortion provides the change of the external potential v_{ext} in eq. 1.2.9. The density then changes as a functional of the v_{ext} . But the Kohn-Sham potential v_{KS} is a functional of the density, thus has a non-linear $v_{KS}[n[v_{ext}(\mathbf{R})]]$ dependence on nuclear positions \mathbf{R} .

In superconductivity one deals usually with paramagnetic systems, meaning that KS spin 'up' and spin 'down' orbitals are degenerate and identical in their spatial part, which makes the matrix element $g_{kk'}^{j\mathbf{q}}$ to be spin independent. The perturbation therefore can be cast in the final form:

$$\hat{H}^{el-ph} = \sum_{jkk'\sigma} g_{kk'}^j \hat{\varphi}_{j(\mathbf{k}'-\mathbf{k})} \hat{c}_{k'\sigma}^\dagger \hat{c}_{k\sigma} \quad (1.3.34)$$

$$\hat{\varphi}_{j\mathbf{q}} = \hat{b}_{j\mathbf{q}} + \hat{b}_{j,-\mathbf{q}}^\dagger \quad (1.3.35)$$

The last equation shows that electron scattering is accompanied by creating or absorbing a phonon and $g_{kk'}^j$ gives a probability of such process.

1.4 Direct Coulomb contribution

Coulomb interactions among electrons are actually the most important force in material science. However, their main contribution is already included in the properties of the normal state and accounted usually in DFT by the Hartree and exchange correlation functionals, for example in LDA. Despite of this, there are cases where DFT-LDA scheme fails to give KS eigenvalues and orbitals that reproduce the physical quasiparticles⁸, and one has to reconsider the effect of the Coulomb interaction within a proper framework to describe electronic excitations like GW or Bethe-Salpeter Equations (BSE) [35].

In the superconducting state, moreover, Coulomb interactions contribute additionally by scattering the Cooper pairs. What this electronic interaction is will be discussed extensively and in a more rigorous way in chapter 2. The essential point will be the concept of charge screening meaning the interaction between two classical particles that are embedded in the system. This can be exactly expressed in terms of the inverse dielectric function (ϵ^{-1}) and the bare Coulomb interaction (v):

$$V^c \sim \epsilon^{-1}v, \quad (1.4.1)$$

This is already an approximated form of the electronic interaction since, as we will discuss in chapter 2, it does not account for exchange/correlation effects between the interacting particles and those involved in the screening. However since the dielectric function of the normal state will be a key object in our superconducting interaction we will now introduce it together with the main approximation schemes used in this work.

1.4.1 Screening

1.4.1.1 Dielectric function, reducible and irreducible polarizability

Following the ref. [23], we start the discussion with the first-order (linear) density response $\delta n^1(x)$ ($x = \{\mathbf{r}t\}$ and $\int dx = \int d\mathbf{r} \int dt$ in the following) to the time-dependent external perturbation $\delta v_{ext}(x')$ (a total external potential now is time-dependent⁹ $v_{ext}(x') = v_{ext}^0(\mathbf{r}') + \delta v_{ext}(x')$). The total density then is:

$$\begin{aligned} n(x) &= n_0(\mathbf{r}) + \delta n^1(x) + \dots \\ &= n_0(\mathbf{r}) + \int dx' \chi(xx') \delta v_{ext}(x') + \dots, \end{aligned} \quad (1.4.2)$$

⁸For example, band gaps of insulators are usually underestimated within the LDA [34].

⁹The $\delta v_{ext}(x')$ is switched on at initial time $t = 0$, i.e., $\delta v_{ext}(x') \sim \Theta(t)$

where a linear density-density response function χ also called the *reducible polarizability* is introduced. Higher order terms in the eq. 1.4.2 are neglected for small δv_{ext} , as we assume in the following.

The second important quantity is the *irreducible polarizability* P , which allows to express the same $\delta n^1(x)$ in an alternative way:

$$\delta n^1(x) = \int dx' P(xx') \delta v_{tot}(x'), \quad (1.4.3)$$

where the change of the total potential enters. The $\delta v_{tot}(x')$ includes the $\delta v_{ext}(x')$ itself, but also depends on the induced Hartree potential $\delta v_{ind}(x) = \int d\mathbf{r}' \delta n(\mathbf{r}', t) / |\mathbf{r} - \mathbf{r}'|$:

$$\delta v_{tot}(x') = \delta v_{ext}(x') + \delta v_{ind}(x')$$

And finally, the *inverse dielectric function* ϵ^{-1} allows to express $\delta v_{tot}(x')$ via the $\delta v_{ext}(x')$:

$$\delta v_{tot}(x) = \int dx' \epsilon^{-1}(xx') \delta v_{ext}(x')$$

Our goal is to find this dielectric function, but normally one operates first with P or χ . Hence, the relations between ϵ (or, its inverse ϵ^{-1}), P and χ are important [23]:

$$\epsilon^{-1}(x_1 x_2) = \delta_{x_1 x_2} + \int dx_3 v(x_1 x_3) \chi(x_3 x_2), \quad (1.4.4)$$

$$\epsilon(x_1 x_2) = \delta_{x_1 x_2} - \int dx_3 v(x_1 x_3) P(x_3 x_2), \quad (1.4.5)$$

$$\chi(x_1 x_2) = P(x_1 x_2) + \int \int dx_3 dx_4 P(x_1 x_3) v(x_3 x_4) \chi(x_4 x_2), \quad (1.4.6)$$

where¹⁰ the term due to the bare Coulomb interaction is given by:

$$v(x_1 x_2) = \frac{\delta_{t_1 t_2}}{|\mathbf{r}_1 - \mathbf{r}_2|} \quad (1.4.7)$$

and the eq. 1.4.6 is solved for $\chi(P)$ if $P(\chi)$ is known.

Using the notations of this section, we rewrite the screened Coulomb interaction V^c of the eq. 1.4.1 in the following way:

$$V^c(x_1 x_2) = \int dx_3 \epsilon^{-1}(x_1 x_3) v(x_3 x_2), \quad (1.4.8)$$

In sec. 1.4.1.2 the ϵ^{-1} is directly estimated using the Thomas-Fermi (TF) model. In sec. 1.4.1.3 we introduce the so-called Random Phase Approximation (RPA). It is important to note that the resulting screening will be the one in the KS system, not in the real one. To obtain a real screening, we may use the methods of the Time-Dependent Density Functional Theory (TDDFT), which will be given in sec. 1.4.1.4 and 1.4.1.5.

1.4.1.2 Thomas-Fermi screening

One of the simplest and older methods to describe the screening in metals is the Thomas Fermi (TF) model [36]. It cuts the range of the bare Coulomb interaction in accordance to the parameter q_{TF} :

¹⁰ $\delta_{x_1 x_2}$ is a delta function in space and time, i.e., $\delta_{x_1 x_2} = \delta(\mathbf{r}_1 - \mathbf{r}_2) \delta(t_1 - t_2)$

$$V^c(\mathbf{r}) = \frac{1}{|\mathbf{r}|} e^{-q_{TF}|\mathbf{r}|}, \quad (1.4.9)$$

In the case of the free electron gas, the matrix elements of such interaction are simply:

$$V_{kk'}^c = \frac{4\pi}{|\mathbf{k} - \mathbf{k}'|^2 + (q_{TF})^2}, \quad (1.4.10)$$

with

$$(q_{TF})^2 = 4\pi N_F, \quad (1.4.11)$$

where N_F is the DOS at the Fermi level.

The screened potential (eq. 1.4.10) differs from the bare one by a dielectric function:

$$\epsilon_{TF}(\mathbf{q}) = 1 + \left(\frac{q_{TF}}{|\mathbf{q}|} \right)^2. \quad (1.4.12)$$

The model is valid only as long as the system behaves similarly to an electron gas, like in the case of simple metals. In a more complicated situation we have to appeal to a more advanced solution to be discussed in the following section.

1.4.1.3 Random Phase Approximation (RPA)

One of the drawbacks of the TF model lies in the presence of the parameter q_{TF} , which maps the real system onto the electron gas model. Secondly, for some applications, like optical spectroscopy, dynamical (or, time-dependent) effects are essential, and a frequency-dependent dielectric function¹¹ is needed [23]. Dynamical effects may be important in superconductivity as well, they go beyond conventional treatment, and corresponding effects will be investigated at the end of this work (chap. 3) within the Eliashberg theory of superconductivity (chap. 2).

In order to compute properly the screening properties (i.e., the dielectric function) of real systems one has to abandon model approaches like the TF and go beyond. The theory of screening in metals is one of the most advanced in solid state physics, but a pillar to many *ab-initio* approaches is the RPA [21, 23, 37].

In the eq. 1.4.5 we gave already the expression for the dielectric function via the irreducible polarizability P (not known yet). Let us take a closer look to that formula in the Fourier components (FC). A time Fourier Transform (FT) is trivial, since the bare Coulomb interaction is time-independent $v(x_1 x_2) \sim \delta(t_1 - t_2)$. The FT with respect to spatial coordinates takes the following form (see ref. [23] and sec. A.2.2) for periodic crystals:

$$\epsilon(\mathbf{q}\mathbf{G}_1\mathbf{G}_2\omega) = \frac{1}{\Omega} \int \int d\mathbf{r}_1 d\mathbf{r}_2 e^{-i(\mathbf{q}+\mathbf{G}_1)\mathbf{r}_1} \epsilon(\mathbf{r}_1\mathbf{r}_2\omega) e^{-i(\mathbf{q}+\mathbf{G}_2)\mathbf{r}_2} \quad (1.4.13)$$

$$\begin{aligned} &= \delta_{\mathbf{G}_1\mathbf{G}_2} - v(\mathbf{q}_1\mathbf{G}_1)P(\mathbf{q}_1\mathbf{G}_1\mathbf{G}_2\omega), \\ v(\mathbf{q}\mathbf{G}) &= \frac{4\pi}{|\mathbf{q} + \mathbf{G}|^2}, \end{aligned} \quad (1.4.14)$$

where the $\mathbf{G}_1\mathbf{G}_2$ are reciprocal lattice vectors and \mathbf{q} is defined within the first BZ. If we neglect off-diagonal part ($\mathbf{G}_1 = \mathbf{G}_2 = \mathbf{G}$), the ϵ can be trivially inverted:

$$\epsilon^{-1}(\mathbf{q} + \mathbf{G}, \omega) = \frac{1}{1 - v(\mathbf{q} + \mathbf{G})P(\mathbf{q} + \mathbf{G}, \omega)}, \quad (1.4.15)$$

otherwise one should perform a matrix inversion. The ϵ is a non-local object. It depends on both \mathbf{r}_1 and \mathbf{r}_2 and this is reflected in the dependence of the FC on both \mathbf{G}_1 and \mathbf{G}_2 , which corresponds to the inclusion of so-called *local field effects* (LFE) related to the microscopic structure of solid.

¹¹I.e., what is given by the eq. 1.4.12 is a static limit, $\omega \rightarrow 0$.

Knowing explicitly the P allows immediately to calculate the ϵ^{-1} . In the general definition the eq. 1.4.3 connects the density response with variation of the total potential via irreducible polarizability P we are searching for. The RPA in the DFT context corresponds to approximating the P by the Kohn-Sham response χ_0 [23]:

$$\delta n^1(x) = \int dx' \chi_0(xx') \delta v_{KS}(x'), \quad (1.4.16)$$

i.e., which relates a linear density response with the potential variation of the KS scheme (eq. 1.2.9). We skip the derivation for this well-known function in the section, as soon as it explores the elements of the MBPT (which will be introduced in chap. 2), but place one possible derivation in the appendix B.2. The χ_0 in position/frequency space is constructed out of the solutions (ξ_k and ϕ_k) of the KS scheme:

$$\chi_0(\mathbf{r}_1 \mathbf{r}_2 \omega) = 2 \sum_{kk'} \frac{(f_{k'} - f_k) \phi_k(\mathbf{r}_1) \phi_k^*(\mathbf{r}_2) \phi_{k'}(\mathbf{r}_2) \phi_{k'}^*(\mathbf{r}_1)}{\omega - (\xi_k - \xi_{k'}) + i0^+},$$

where f_k is a Fermi distribution. Taking the FT of this quantity (in the same style as for eq. 1.4.13) we arrive to:

$$\chi_0(\mathbf{q} \mathbf{G}_1 \mathbf{G}_2 \omega) = \frac{2}{N\Omega} \sum_{kk'} (f_{k'} - f_k) \frac{\langle k' | e^{-i(\mathbf{q} + \mathbf{G}_1) \mathbf{r}_1} | k \rangle \langle k | e^{i(\mathbf{q} + \mathbf{G}_2) \mathbf{r}_2} | k' \rangle}{\omega - (\xi_k - \xi_{k'}) + i0^+}, \quad (1.4.17)$$

where a prefactor $1/\Omega$ comes from the FT and a $1/N$ from the normalization condition (see sec. A.2.4 for more details). Normalizing our KS wave functions to the unit cell (or Wigner-Seitz (WS) cell) i.e., $\langle k | k' \rangle_{WS} = \delta_{kk'}$, we rewrite the expression as:

$$\chi_0(\mathbf{q} \mathbf{G}_1 \mathbf{G}_2 \omega) = \frac{2}{\Omega_{WS}} \sum_{kk'} (f_{k'} - f_k) \frac{\rho_{kk'}^*(\mathbf{q} \mathbf{G}_1) \rho_{kk'}(\mathbf{q} \mathbf{G}_2)}{\omega - (\xi_k - \xi_{k'}) + i0^+}, \quad (1.4.18)$$

where a *polarization matrix* $\rho_{kk'}(\mathbf{q} \mathbf{G})$ is given by:

$$\rho_{kk'}(\mathbf{q} \mathbf{G}) = \frac{1}{N} \langle k | e^{i(\mathbf{q} + \mathbf{G}) \mathbf{r}} | k' \rangle = \langle k | e^{i(\mathbf{q} + \mathbf{G}) \mathbf{r}} | k' \rangle_{WS}. \quad (1.4.19)$$

A dielectric function obtained with χ_0 as an approximation for the irreducible polarizability P will be named as ϵ_{RPA} (and the inverse one as ϵ_{RPA}^{-1}).

We also would like to give an alternative formulation of the ϵ_{RPA}^{-1} via the reducible polarizability χ_{RPA} , as in the eq. 1.4.4. The reducible polarizability is expressed via χ_0 using eq. 1.4.6:

$$\chi_{RPA}(\mathbf{q} \omega) = [1 - \chi_0(\mathbf{q} \omega) v(\mathbf{q})]^{-1} \chi_0(\mathbf{q} \omega), \quad (1.4.20)$$

which is a matrix equation in $\mathbf{G}_1 \mathbf{G}_2$ indices. Consequently, for the inverse dielectric function we have:

$$\begin{aligned} \epsilon_{RPA}^{-1}(\mathbf{q} \omega) &= 1 + v(\mathbf{q}) \chi_{RPA}(\mathbf{q} \omega) \\ &= 1 + \frac{v(\mathbf{q}) \chi_0(\mathbf{q} \omega)}{1 - \chi_0(\mathbf{q}) v(\mathbf{q})}, \end{aligned} \quad (1.4.21)$$

The response function χ_{RPA} does not give the true density response of the interacting system in eq. 1.4.2, as soon as the KS response was used instead of the exact P in that equation. The Time-Dependent Density Functional Theory (TDDFT) allows to go beyond this approximation and to compute a more realistic response function χ .

1.4.1.4 TDDFT framework

To go beyond the RPA one could directly use the Many Body Perturbation Theory (MBPT) in several forms and approximations: one could iterate the Hedin's cycle starting from the RPA [38], could perform a diagrammatic expansion [7], where the RPA is a low order approximation. However an alternative approach that is computationally very convenient is to make use of Time-Dependent Density Functional Theory (TDDFT) in the linear response regime. The step from the previous discussion to a formal linear-response TDDFT is in expressing the linear density response $\delta n^1(x)$ via the eq. 1.4.2 from one side and via the eq. 1.4.16 from the other side:

$$\delta n^1(x) = \int dx' \chi(xx') \delta v_{ext}(x') = \int dx' \chi_0(xx') \delta v_{KS}(x') \quad (1.4.22)$$

The $\delta v_{KS}(x)$ is deduced from the form of eq. 1.2.9, keeping only the first order density variations:

$$\begin{aligned} \delta v_{KS}(x) &= \delta v_{ext}(x) + \int dx' v(xx') \delta n^1(x') \\ &+ \int dx' f_{xc}[n_0](xx') \delta n^1(x'). \end{aligned} \quad (1.4.23)$$

Formally, the f_{xc} is a functional derivative of the time-dependent exchange-correlation potential $v_{xc}[n](x)$, where the derivative is evaluated at the unperturbed ground-state density n_0 . Plugging it back into the eq. 1.4.22 and writing all first order density variations in the form $\delta n^1(x) = \int dx' \chi(xx') \delta v_{ext}(x')$, we get an integral equation for χ :

$$\chi(xx') = \chi_0(xx') + \int dx_1 dx_2 \chi_0(xx_1) [v(x_1 x_2) + f_{xc}(x_1 x_2)] \chi(x_2 x'). \quad (1.4.24)$$

It can be transformed in FC, but we will use a symbolic notation which is independent on the representation:

$$\chi = \chi_0 + \chi_0 [v + f_{xc}] \chi \quad (1.4.25)$$

A further simplification, which implies an inversion, can be done, and the total density-density response is expressed as:

$$\chi = [1 - \chi_0 (v + f_{xc})]^{-1} \chi_0 \quad (1.4.26)$$

For the FC it reads:

$$\begin{aligned} \epsilon^{-1}(\mathbf{q}\omega) &= 1 + v(\mathbf{q}) \chi(\mathbf{q}\omega) \\ &= 1 + \frac{v(\mathbf{q}) \chi_0(\mathbf{q}\omega)}{1 - \chi_0(\mathbf{q}) [v(\mathbf{q}) + f_{xc}(\mathbf{q}\omega)]} \end{aligned} \quad (1.4.27)$$

which is a matrix equation in terms of $\mathbf{G}_1 \mathbf{G}_2$ (see the previous section).

Now, if we take the $f_{xc} = 0$, the equation above gives exactly the dielectric function of the RPA (eq. 1.4.21). Going beyond needs to consider the f_{xc} . Unlike conventional DFT, not many approximations are known for f_{xc} . The simplest and so far the most popular one is a generalization of LDA called adiabatic LDA (ALDA):

$$f_{xc}^{ALDA}(xx') = \delta_{xx'} \left. \frac{\delta v_{xc}^{ALDA}[n](x)}{\delta n(x')} \right|_{n_0(\mathbf{r})} = \delta_{xx'} \left. \frac{dv_{xc}^{LDA}(n)}{dn} \right|_{n_0(\mathbf{r})}. \quad (1.4.28)$$

What happened is that the $v_{xc}^{ALDA}[n](x)$ itself in ALDA is given by $v_{xc}^{LDA}(n(x))$, i.e., when the time dependent density is just inserted into the arguments of the ordinary LDA exchange-correlation potential (see seq. 1.2.1 for v_{xc}^{LDA} definition). The corresponding inverse dielectric function (i.e., eq. 1.4.27 with f_{xc}^{ALDA}) is noted as ϵ_{ALDA}^{-1} .

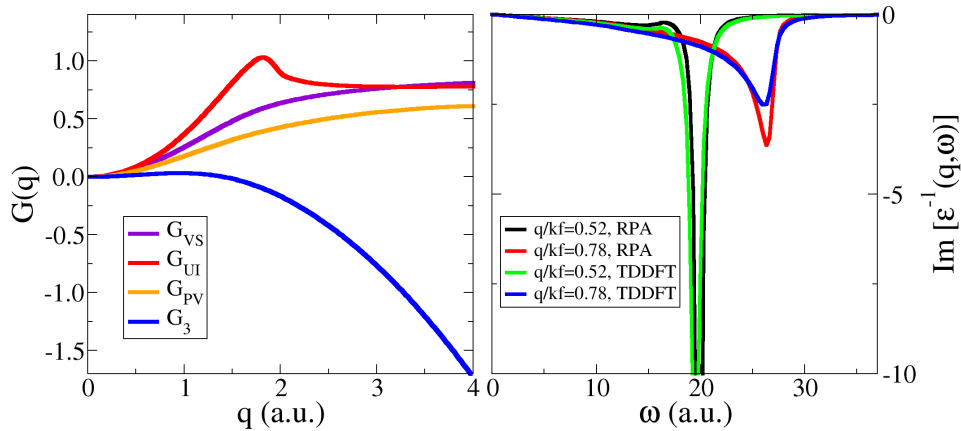


Figure 1.1: (left) Static (VS and UI) and high-frequency (PV, G3) limits of the local-field correction $G(q\omega)$. (right) Imaginary part of the inverse dielectric function obtained with RPA and with TDDFT using a frequency and q -dependent f_{xc} .

The last important observation here is that in ALDA the f_{xc} is static. The \mathbf{q} -dependence of f_{xc}^{ALDA} comes only from the \mathbf{q} -dependent density component. If the density is homogeneous then the f_{xc}^{ALDA} is \mathbf{q} -independent, which is apparently not the case for the exact functional. Approximate frequency and q -dependent f_{xc} is analyzed in the next section.

1.4.1.5 Frequency and q -dependent f_{xc} in homogeneous case. Dielectric function

There are some dynamical approximations to introduced f_{xc} like the method of Gross and Kohn [39], which could lead to important effects in solids, however little is known in literature. Therefore we will introduce it and compare its properties with RPA. Moreover, q -dependent corrections have also been introduced, and we refer for this to the work of Dabrowski [40], which explores the so-called local field correction G .

Following ref. [40], we are interested in the frequency and q -dependent local-field correction G , which is related to $f_{xc}(q, \omega)$ as:

$$f_{xc}(q, \omega) = -v(q)G(q, \omega). \quad (1.4.29)$$

For the G we write similar to Gross and Kohn [39]:

$$\text{Im}[G(q, \omega)] = \frac{a(q, n)\omega}{[1 + b(q, n)\omega^2]^{5/4}},$$

where the q -dependent a and b have the following form:

$$\begin{aligned} a(q, n) &= Cq^2 \left[\frac{G_0(q) - G_\infty(q)}{CDq^2} \right]^{5/3}, \\ b(q, n) &= \left[\frac{G_0(q) - G_\infty(q)}{CDq^2} \right]^{4/3}, \\ D &= 0.763 \quad C = 23\alpha r_s/60, \end{aligned} \quad (1.4.30)$$

and the $G_0(q)$ represents the static and $G_\infty(q)$ is a high-frequency limit of $G(q, \omega)$. Several approximations are known for these limits. In the static case the Utsumi-Ichimarui (UI, ref. [41]) or Vashishta-Singwi (VS, ref. [42]) forms are used. While the high-frequency expression is given by the Pathak-Vashishta (PV, ref. [43]) form or the result of Iwamoto [44] ($G_\infty(q)$ from this approach will be referred as a G_3). We try all listed forms for G_0 and G_∞ in the evaluation of the

$q\omega$ -dependent $G(q, \omega)$ and hence, the $f_{xc}(q, \omega)$. All the limiting $G_i(q)$ are shown in fig. 1.1. We found out that the resulting $q\omega$ -dependent $f_{xc}(q, \omega)$ at small q fits the best to the $f_{xc}(q \rightarrow 0, \omega)$ from ref. [45] with $G_{VS}(q)$ parameterizing the $G_0(q)$ and $G_3(q)$ parameterizing the $G_\infty(q)$ (see sec. C.4 for all details), and because of that we took this combination of G 's as a default one. The frequency-dependent dielectric function obtained with the corresponding (eq. 1.4.29) frequency-dependent f_{xc} (via eq. 1.4.27) is given together with the ϵ_{RPA}^{-1} ($f_{xc} = 0$) in the fig. 1.1. The main conclusion, which is important for us, is that $f_{xc}(q, \omega)$ slightly modified the shape of the plasmon dispersion and its damping, but did not significantly modified the low- q behavior of the dielectric function. Moreover, our tests show that it does not lead to important quantitative differences in the strength of the dynamical part (to be defined in the following) of the Coulomb interaction. Hence, we will not adopt this method in the chapter but we will consider the more conventional RPA to reproduce the dynamical screening.

1.4.2 Coulomb matrix

Coulomb matrix elements which are important for us [46, 47] are exchange integrals evaluated on the KS basis:

$$V_{kk'}^c(\omega) = \int d\mathbf{r}_1 d\mathbf{r}_2 \phi_k^*(\mathbf{r}_1) \phi_{k'}^*(\mathbf{r}_2) V^c(\mathbf{r}_1 \mathbf{r}_2 \omega) \phi_{k'}(\mathbf{r}_1) \phi_k(\mathbf{r}_2), \quad (1.4.31)$$

which according to the form of eq. 1.4.8 becomes:

$$V_{kk'}^c(\omega) = \int d\mathbf{r}_1 d\mathbf{r}_2 \phi_k^*(\mathbf{r}_1) \phi_{k'}^*(\mathbf{r}_2) \left[\int d\mathbf{r}_3 \epsilon^{-1}(\mathbf{r}_1 \mathbf{r}_3 \omega) v(\mathbf{r}_3 \mathbf{r}_2) \right] \phi_{k'}(\mathbf{r}_1) \phi_k(\mathbf{r}_2). \quad (1.4.32)$$

The FT follows the same steps as for the irreducible polarizability χ_0 (sec. A.2.3) and results in:

$$V_{kk'}^c(\omega) = \frac{1}{\Omega_{WS}} \sum_{\mathbf{q} \mathbf{G}_1 \mathbf{G}_2} \epsilon^{-1}(\mathbf{q} \mathbf{G}_1 \mathbf{G}_2 \omega) v(\mathbf{q} + \mathbf{G}_2) \rho_{kk'}(\mathbf{q} \mathbf{G}_1) \rho_{kk'}^*(\mathbf{q} \mathbf{G}_2), \quad (1.4.33)$$

where the polarization matrices $\rho_{kk'}(\mathbf{q} \mathbf{G})$ have the same meaning as in eq. 1.4.18.

Further we analytically continue it to the imaginary axis, which is needed in finite-temperature Green's functions formalism. The frequency dependence comes only from the dielectric function, for which the analytic continuation is done with the help of Kramers-Kronig relation:

$$\text{Re} [\epsilon^{-1}(\mathbf{q} \mathbf{G}_1 \mathbf{G}_2 z)] = \delta_{\mathbf{G}_1 \mathbf{G}_2} + \int_0^\infty \frac{2\omega \text{Im} [\epsilon^{-1}(\mathbf{q} \mathbf{G}_1 \mathbf{G}_2 \omega)]}{\pi (\omega^2 - z^2)} d\omega, \quad (1.4.34)$$

here, the ω is real but z can be any complex number. If we take z to be purely complex, $z = i\nu$, we get $\epsilon^{-1}(i\nu)$ being a hermitian matrix and is defined only by the anti-hermitian part of $\epsilon^{-1}(\omega)$ ¹²:

$$\epsilon^{-1}(\mathbf{q} \mathbf{G}_1 \mathbf{G}_2 i\nu) = \delta_{\mathbf{G}_1 \mathbf{G}_2} + \int_0^\infty \frac{2\omega \text{Im} [\epsilon^{-1}(\mathbf{q} \mathbf{G}_1 \mathbf{G}_2 \omega)]}{\pi (\omega^2 + \nu^2)} d\omega. \quad (1.4.35)$$

We proceed by inserting the eq. 1.4.35 into the eq. 1.4.33¹³:

$$\begin{aligned} V_{kk'}^c(i\nu) &= \sum_{\mathbf{q} \in \text{full space}} v(\mathbf{q}) \rho_{kk'}(\mathbf{q}) \rho_{kk'}^*(\mathbf{q}) + \int_0^\infty \frac{2\omega \tilde{V}_{kk'}^c(\omega)}{\pi (\omega^2 + \nu^2)} d\omega, \\ &= v_{kk'} + \tilde{V}_{kk'}^c(i\nu) \end{aligned} \quad (1.4.36)$$

¹²Hermitian and anti-hermitian parts respectively are: $\text{Re}[A] = \frac{1}{2}(A + A^\dagger)$, $\text{Im}[A] = \frac{1}{2i}(A - A^\dagger)$. See sec. A.2.5 for more details.

¹³We add an extra ' i ' factor in front of the frequency argument to distinguish the property defined in imaginary frequency domain.

where $\tilde{V}_{kk'}^c(\omega)$ is:

$$\tilde{V}_{kk'}^c(\omega) = \frac{1}{\Omega_{WS}} \sum_{\mathbf{q}\mathbf{G}_1\mathbf{G}_2} \mathbf{Im}[\epsilon^{-1}(\mathbf{q}\mathbf{G}_1\mathbf{G}_2\omega)] v(\mathbf{q} + \mathbf{G}_2) \rho_{kk'}(\mathbf{q}\mathbf{G}_1) \rho_{kk'}^*(\mathbf{q}\mathbf{G}_2). \quad (1.4.37)$$

The explicit appearance of the divergent $v_{kk'}$ can be avoided by rewriting eq. 1.4.36 as:

$$\begin{aligned} V_{kk'}^c(i\nu) &= V_{kk'}^c(0) + V_{kk'}^c(i\nu) - V_{kk'}^c(0) \\ &= V_{kk'}^{0c} + [v_{kk'} + \tilde{V}_{kk'}^c(i\nu)] - [v_{kk'} + \tilde{V}_{kk'}^c(i0)] \\ &= V_{kk'}^{0c} + \int_0^\infty \frac{2\omega}{\pi} \frac{\tilde{V}_{kk'}^c(\omega)}{\omega^2 + \nu^2} d\omega - \int_0^\infty \frac{2\omega}{\pi} \frac{\tilde{V}_{kk'}^c(\omega)}{\omega^2} d\omega \\ &= V_{kk'}^{0c} + \alpha_{kk'}^c(i\nu). \end{aligned} \quad (1.4.38)$$

Rewriting the interaction in this form makes a clear separation between static screening given only by $V_{kk'}^c(0) = V_{kk'}^{0c}$ and the dynamical correction $\alpha_{kk'}^c(i\nu)$, for which the final expression reads:

$$\alpha_{kk'}^c(i\nu) = \int_0^\infty \frac{2\omega}{\pi} \tilde{V}_{kk'}^c(\omega) \left[\frac{1}{\omega^2 + \nu^2} - \frac{1}{\omega^2} \right] d\omega \quad (1.4.39)$$

$$= \frac{2}{\pi} \int_0^\infty d\omega \frac{\tilde{V}_{kk'}^c(\omega)}{\omega} \frac{-\nu^2}{\omega^2 + \nu^2} \quad (1.4.40)$$

1.4.3 Isotropic limit

In certain cases¹⁴ the exact anisotropic structure of the interaction can be neglected by performing an isotropization. Such an isotropic approximation can be done by projecting the multidimensional index k (in solids, one dimension for band index, and three dimensions for \mathbf{k} -vector) to a one dimensional energy index ξ as follows:

$$K_{stat}^c(\xi\xi') = \frac{1}{N(\xi)N(\xi')} \sum_{kk'} V_{kk'}^c(0) \delta(\xi_k - \xi) \delta(\xi_{k'} - \xi'), \quad (1.4.41)$$

$$K_{dyn}^c(\xi\xi'\omega) = \frac{1}{N(\xi)N(\xi')} \sum_{kk'} \tilde{V}_{kk'}^c(\omega) \delta(\xi_k - \xi) \delta(\xi_{k'} - \xi'). \quad (1.4.42)$$

In other words, we perform the averages on isoenergy surfaces for each dimension, e.g., $A(\xi) = \overline{\{A_k\}}_{\text{over all } k: \xi_k=\xi}$. The object K_{stat}^c (\tilde{K}_{dyn}^c) later will be referenced as a static (or dynamic) *Coulomb kernel*.

In the electron gas limit, and within a Thomas Fermi model [51], the averaged static part (K_{stat}^c) can be expressed accurately in a completely analytic form:

$$\begin{aligned} K_{TF}^c(\xi\xi') &= \frac{\pi}{2\sqrt{\eta\eta'}} \ln \left[\frac{\eta + \eta' + 2\sqrt{\eta\eta'} + q_{TF}^2/2}{\eta + \eta' - 2\sqrt{\eta\eta'} + q_{TF}^2/2} \right], \\ &\eta = \xi + E_F, \end{aligned} \quad (1.4.43)$$

¹⁴It is well established that for many simple phononic superconductors anisotropy is rather weak and gives a negligible contribution to the critical temperature [48, 49]. The isotropic limit can also be achieved experimentally in presence of paramagnetic impurities [50].

with $q_{TF} = \sqrt{4\pi N(0)}$.

A similar electron gas-like approximation can also be done in the dynamical part (K_{dyn}^c), but the frequency dependence leads to considering the Lindhard theory for the electron gas [52] (or, equivalently the RPA for the electron gas), which will be discussed in sec. 1.4.5. Going to the imaginary frequency domain, we evaluate the total interaction kernel $K^c(\xi\xi'i\nu)$ out of $K_{stat}^c(\xi\xi')$ and $K_{dyn}^c(\xi\xi'\omega)$:

$$K^c(\xi\xi'i\nu) = K_{stat}^c(\xi\xi') + \alpha^c(\xi\xi'i\nu), \quad (1.4.44)$$

$$\alpha^c(\xi\xi'i\nu) = \int_0^\infty \frac{2\omega}{\pi} K_{dyn}^c(\xi\xi'\omega) \left\{ \frac{1}{\omega^2 + \nu^2} - \frac{1}{\omega^2} \right\} d\omega. \quad (1.4.45)$$

1.4.4 Plasmon pole approximation.

For test purposes it is also very useful to have an analytic form of the dynamical part of the Coulomb interaction (α^c). A popular one is the *plasmon pole approximation*. In this case, the imaginary part of the dielectric function and hence, the $K_{dyn}^c(\omega)$ itself is given by a delta peak at the plasma frequency (we use consequently the notation¹⁵ $K_{dyn}^c(\xi\xi'\omega) = K_{pl}^c(\xi\xi'\omega_p)\delta(\omega - \omega_p)$). Thus, from the eq. 1.4.45 it follows that¹⁶:

$$\alpha^{c,pl}(\xi\xi', i\nu) = \frac{2\omega_p}{\pi} K_{pl}^c(\xi\xi'\omega_p) \left\{ \frac{1}{\omega_p^2 + \nu^2} - \frac{1}{\omega_p^2} \right\} = C_{pl}(\xi\xi') \frac{-\nu^2}{(\omega_p^2 + \nu^2)}, \quad (1.4.47)$$

where the $C_{pl}(\xi\xi') = 2K_{pl}^c(\xi\xi'\omega_p)/[\pi\omega_p]$ now serves as independent normalization constant to set the scale of $\alpha^{c,pl}$. Later in sec. 2.5.4 we have to estimate the behavior of realistic *ab-initio* $\alpha^c(i\nu)$ for ν above the certain cutoff ν_{cut} . In this case (i.e., for $\nu > \nu_{cut}$) it is natural to approximate the *ab-initio* α^c with $\alpha^{c,pl}$, for which the norm $C_{pl}(\xi\xi')$ is chosen in a way to make those two functions equal at ν_{cut} , i.e., $\alpha^c(\xi\xi'i\nu_{cut}) = \alpha^{c,pl}(\xi\xi'i\nu_{cut})$ for each $\xi\xi'$ pair.

1.4.5 Lindhard theory

Since the consequences of dynamical screening in superconductivity have never been extensively investigated before and little is known from the existing literature [27, 28, 24] we will perform in this theoretical section a preliminary analysis by means of an electron gas model within the Lindhard theory. In particular following on general trends at high energy (ξ, ω) and the related convergence issues. The Lindhard approach, as discussed in ref. [52], gives an analytic form of the inverse dielectric function for the electron gas within the RPA approximation. We have seen that, $\epsilon^{-1}(\mathbf{q}\omega) = [1 - v(\mathbf{q})\chi_0(\mathbf{q}\omega)]^{-1}$, where χ_0 is the numerical KS response function (given by eq. 1.4.18). Lindhard theory gives an analytic result for χ_0 and thus, for ϵ^{-1} (ref. [52], p. 162, both spins):

$$\chi_0^{lind}(\mathbf{q}\omega) = N_F \frac{k_F}{q} \left[\Psi\left(\frac{\omega + i\eta_{lind}}{2qv_F} - \frac{q}{2k_F}\right) - \Psi\left(\frac{\omega + i\eta_{lind}}{2qv_F} + \frac{q}{2k_F}\right) \right], \quad (1.4.48)$$

$$\Psi(z) = \frac{z}{2} + \frac{1 - z^2}{4} \ln\left[\frac{z + 1}{z - 1}\right], \quad (1.4.49)$$

¹⁵Although the A_q in $Im[\epsilon^{-1}] = A_q\delta(\omega - \omega_p)$ can be estimated via a so-called f-sum rule:

$$2 \int_0^\infty d\omega \{\omega Im[\epsilon_q^{-1}(\omega)]\} = -\omega_p^2, \quad (1.4.46)$$

the corresponding coefficient (K_{pl}^c) in $K_{dyn}^c(\xi\xi'\omega)$ is left as a parameter.

¹⁶We also neglect here by a plasmon dispersion ($\omega_p = \omega_p(q) = const$).

where η_{lind} is a small parameter, which can be used as a smearing width for simpler numerics. The formula is written in Ry units, and the total DOS at Fermi level (N_F), k_F and v_F are all related to the Fermi energy parameter that sets the density of the electron gas (ref. [52], p. 161):

$$k_F = v_F = \sqrt{E_F}, \quad N_F = \frac{k_F}{2\pi^2} \quad (1.4.50)$$

The matrix element of the Coulomb interaction is given via ϵ_{lind}^{-1} ($v(\mathbf{q})$ is the bare interaction, $\mathbf{q} = \mathbf{k}' - \mathbf{k}$):

$$V_{\mathbf{k}\mathbf{k}'}^{c,lind}(\omega) = \epsilon_{lind}^{-1}(\mathbf{q}\omega)v(\mathbf{q}). \quad (1.4.51)$$

The isoenergy surface average to the dynamical part $\tilde{V}_{\mathbf{k}\mathbf{k}'}^{c,lind}$ ($\tilde{V}_{\mathbf{k}\mathbf{k}'}^{c,lind}(\omega) = \text{Im}[\epsilon_{lind}^{-1}]v$) that we call K_{lind}^c , has now to be constructed explicitly as:

$$K_{lind}^c(\xi\xi'\omega) = \frac{1}{S_{k'}} \int_0^\pi d\Theta \int_0^{2\pi} d\phi k'^2 \sin\Theta \tilde{V}_{\mathbf{k}\mathbf{k}'}^{c,lind}(\omega), \quad (1.4.52)$$

The azimuthal angle Θ and the polar angle ϕ defines the direction of \mathbf{k}' with respect to \mathbf{k} , $k'^2 \sin\Theta$ is Jacobian and $S_{k'}$ is a surface area of $\xi' = k'^2$ energy sphere. The $\text{Im}[\epsilon_{lind}^{-1}(\mathbf{q}\omega)]$ is finite at finite ω even in $q \rightarrow 0$ limit, which means that when $\xi = \xi'$ (equal energy spheres), it does not cancel the divergence of the bare Coulomb interaction $v(\mathbf{q})$ for $q \rightarrow 0$. The volume integral would still converge, however this surface average does not: the surface integral $K_{lind}^c(\xi\xi'\omega)$ diverges¹⁷ at $\xi = \xi'$. The same is true for *ab-initio* K_{dyn}^c in eq. 1.4.42. The key point here is that the divergence of K_{dyn}^c is integrable, later it will be plugged into the evaluation of the Self energy, i.e. $\Sigma(\xi) \sim \int d\xi' K_{dyn}^c(\xi\xi')G(\xi')$ (chap. 2).

The numerical investigation of this issue is done in sec. C.2. This investigation will show that the divergence numerically is relatively easy to handle by including a Gaussian smearing δ -function in the definition of the isotropic limit 1.4.41 and 1.4.42:

$$\delta_G(x, \eta_G) = \frac{1}{\sqrt{\pi}\eta_G} e^{-\frac{x^2}{\eta_G^2}}, \quad (1.4.53)$$

where the η_G is the smearing width. Such approach will be used for any *ab-initio* calculation, while for the electron gas the eq. 1.4.52 will be used for simplicity.

1.4.6 Coulomb kernel: examples

We conclude this chapter by presenting a visualization of the static and dynamic Coulomb kernel. We consider as example material Aluminum. Aluminum is electronically a simple system, and behaves similarly to an electron gas with $r_s \sim 2.08$.

Static kernel

Two cuts of the static Coulomb kernel for Aluminum are shown in fig. 1.2. For comparison we also show the corresponding kernel of the electron gas (as approximated by a TF model ($K_{TF}^c(\xi\xi')$, eq. 1.4.43)). The two results are clearly very similar. Both have maximum at the lowest energy corner and decay with increase of $\xi(\xi')$ arguments. Moreover, they both are smooth, i.e., do not possess a significant structures (peaks, dips) in the medium energy range. This supports the fact that Aluminum is a quite simple system and can be mapped into the electron gas model. But even in more complex situations (see fig. 3.10), the *ab-initio* $K_{stat}^c(\xi\xi')$ also tends to become smooth

¹⁷Basically, having the divergent integral from $1/q^2$ in 2D.

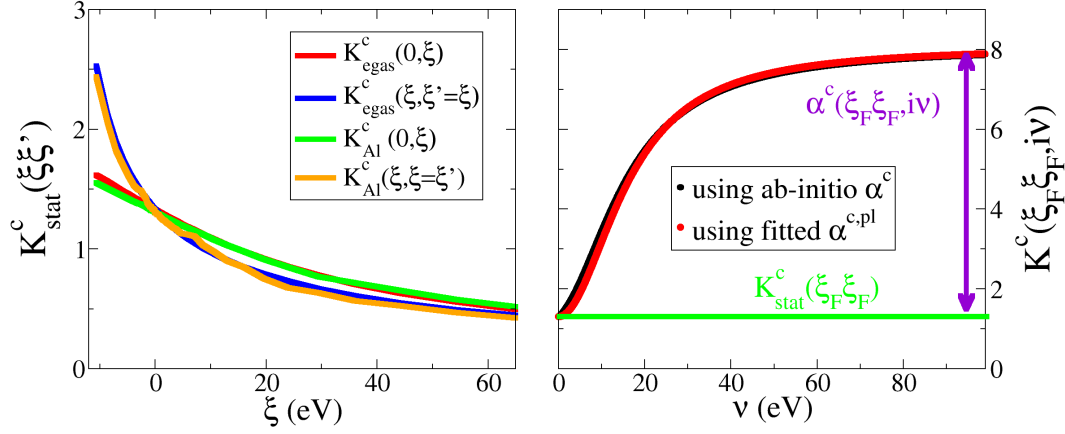


Figure 1.2: (left) Cuts of the static Coulomb kernel for Aluminum and the electron gas: $K_{stat}^c(\xi\xi' = \xi)$ and the one with the first argument fixed at Fermi energy (i.e., $K_{stat}^c(0, \xi)$). (right) Total kernel in imaginary frequency domain (eq. 1.4.44). Black is the fully *ab-initio* RPA result for aluminum, while red is given by the fully *ab-initio* static part K_{stat}^c (which is $\nu = 0$ limit marked with a green horizontal line), while the dynamical part α is fitted with the plasmon pole $\alpha^{c,pl}$ (eq. 1.4.47).

when its energy arguments exceed certain threshold. Hence, in the high energy range the Coulomb kernel of any material will be constructed using the eq. 1.4.43.

Dynamical kernel.

The dynamical part of the Coulomb interaction is far more complicated than its static part, as we have seen in sec. 1.4.2. Although we work on the imaginary axis, the spectral representation requires to use the dynamical Coulomb kernel on the real axis in its imaginary part (K_{dyn}^c). However, for completeness we will present here the real frequency kernel both in its real and imaginary part. Once again we use aluminum as example. The real¹⁸ (K_{dyn}^{Re}) and imaginary (K_{dyn}^c) parts of the interaction on the real frequency axis are shown respectively in fig 1.3 and 1.4.

Many effects are hidden and mixed together in this objects, but for simplicity we discuss only the main features. The low frequency limit of $K_{dyn}^{Re}(\xi\xi'\omega)$ is the static kernel $K_{stat}^c(\xi\xi')$ discussed above. It has a radial behavior around lower energy corner ($(\xi, \xi') = (-12, -12)$ eV) dictated by the weakly screened $1/q^2$ behavior at the bottom of the valence band. Approaching the plasma frequency $\omega_p \sim 16$ eV the low q divergence of the Coulomb interaction dominates the interaction on a larger energy scale leading to a marked diagonal structure in $K_{dyn}^{Re}(\xi\xi'\omega)$ (see sec. 1.4.5). Because of the pole structure, the kernel changes its sign twice from positive ($\omega \leq 7$) to negative ($7 < \omega \leq 16$) and then to positive again ($\omega > 16$). Strong diagonal enhancement happens not only in vicinity of the plasmon pole but also at high frequency limit due to the fact that at high frequencies the Coulomb interaction is completely unscreened and the low- q peak is very prominent.

The kernel K_{dyn}^c (fig. 1.4) on other hand is always negative and vanishes at high and low frequency limits. As for the real part (K_{dyn}^{Re}) at the plasma frequency the Coulomb kernel K_{dyn}^c is dominated by the low- q plasma peak, that induces a diagonal behavior in the average. At higher frequencies one can observe more complicated structures, however the absolute value of the kernel is extremely low and makes the K_{dyn}^c almost negligible in this range.

As we have seen, the $K_{dyn}^c(\xi\xi'\omega)$ is a complicated three dimensional object. Unlike phononic contribution, it is not straightforward to reduce it to an effective parameter as the BCS coupling strength λ . However a reasonable average can be made by considering that these kernels

¹⁸Defined as K_{dyn}^c (eqs. 1.4.42, 1.4.37) but with $\mathbf{Im}\epsilon^{-1} \rightarrow \mathbf{Re}\epsilon^{-1}$.

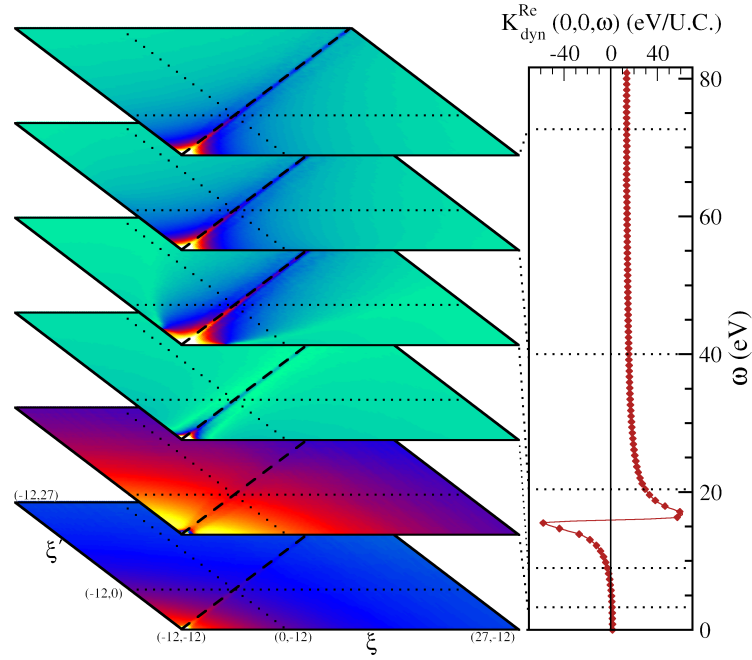


Figure 1.3: Real part of the screened Coulomb interaction in the real-frequency domain $K_{dyn}^{Re}(\xi\xi'\omega)$. Color maps on the left show the the $\xi\xi'$ dependence of the absolute value of $K_{dyn}^{Re}(\xi\xi'\omega)$ at specific frequency ω_i . The value of the frequency is indicated by a dashed line on the plot on the right. Hot/cold colors corresponds to larger/lower values which are always positive numbers. At each ω_i the color scale is normalized to its maximum. The actual value of the Kernel is shown in the plot on the right for $\xi = \xi' = \xi_F$. The pole at $\omega \sim 16$ eV is due to the plasmon, which changes the sign of K_{dyn}^{Re} with ω from positive to negative and then back to positive.

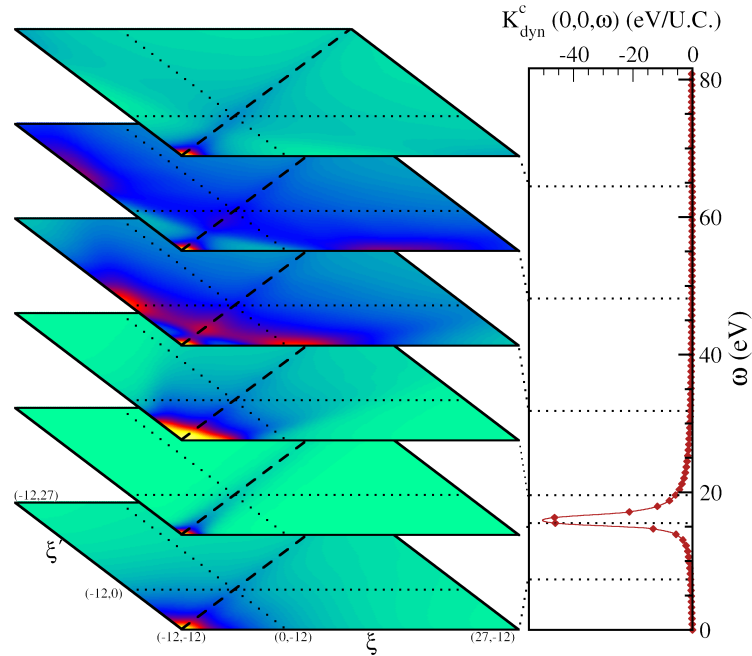


Figure 1.4: The same as in fig. 1.3, but for the $K_{dyn}^c(\xi\xi'\omega)$, which is the imaginary part of the screened Coulomb interaction in the real-frequency domain. It is always negative with plasmon enhancement at $\omega \sim 16$ eV.

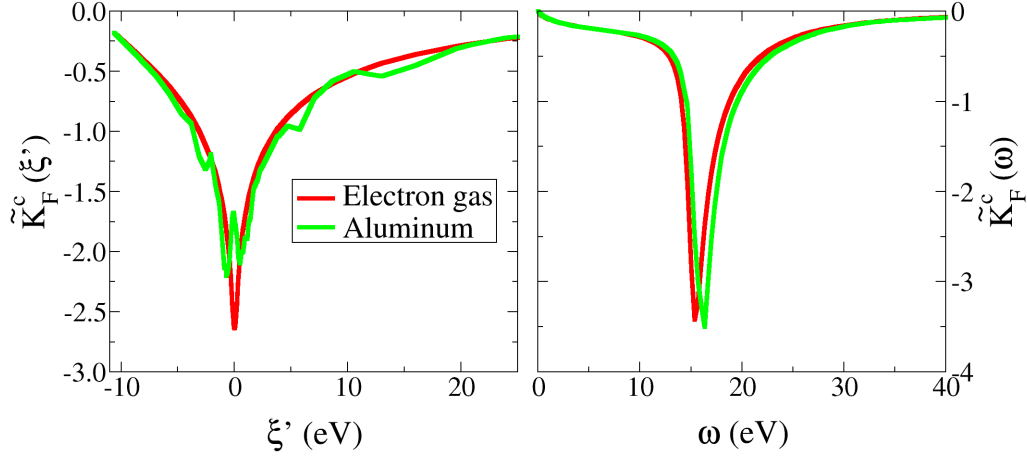


Figure 1.5: Comparing the (left) $\tilde{K}_F^c(\xi')$ and (right) $\tilde{K}_F^c(\omega)$ (eqs. 1.4.54 and 1.4.55 respectively) for aluminum with ones for an electron gas of $r_s = 2.08$ we can appreciate how similar aluminum is to the electron gas model.

in this work will be always integrated together with the electronic Green's function that has a characteristic $1/(\omega - \xi)$ behavior. Therefore we suggest the following average forms:

$$\tilde{K}_F^c(\xi') = N(\xi') \int_0^\infty d\omega K_{dyn}^c(\xi_F \xi' \omega) / \omega, \quad (1.4.54)$$

$$\tilde{K}_F^c(\omega) = \int_{-\infty}^\infty d\xi' N(\xi') K_{dyn}^c(\xi_F \xi' \omega) / (|\xi'| + \omega), \quad (1.4.55)$$

which are presented in fig. 1.5. For comparison in the same plot we also present electron gas calculations, for which we use $K_{dyn}^c = K_{lind}^c$ as discussed in sec. 1.4.5 (see eq. 1.4.52). The $\tilde{K}_F^c(\omega)$ for aluminum and electron gas are almost the same, while the $\tilde{K}_F^c(\xi')$ has an additional structure mediated by the DOS function.

In addition we consider the double integral:

$$I_F^c = \int d\omega \int d\xi' N(\xi') |K_{dyn}^c(\xi_F \xi' \omega)| / ([\xi']^2 + \omega^2), \quad (1.4.56)$$

that (as will be seen in chapter 2) has the relevant structure of the self energy¹⁹ and is treated as the measure of the dynamical coupling. As expected, electron gas and Aluminum present a very similar value of I_F^c : 1.50 for aluminum and 1.47 for a given electron gas model. For comparison with other materials see section 3.3.2 table 3.4.

Total kernel

Finally we present the total kernel $K^c(\xi\xi', i\nu) = K_{stat}^c(\xi\xi') + \alpha^c(\xi\xi' i\nu)$ for aluminum in the imaginary frequency domain (eq. 1.4.44): the full one in fig. 1.6 and the one with $\xi\xi'$ fixed at the Fermi level (i.e., showing only its imaginary-frequency dependence) in fig. 1.2. At low frequency it is given by purely static interaction (K_{stat}^c), while at finite frequency the positively-defined dynamical part α^c becomes relevant and dominates the structure. The divergence of the $K^c(\xi\xi', i\nu)$ at $\xi = \xi'$ is less pronounced as in the imaginary axis we are far away from the poles of the inverse dielectric

¹⁹Forgetting about imaginary frequency formulations. See further sec. 2.2 and 2.2.3.

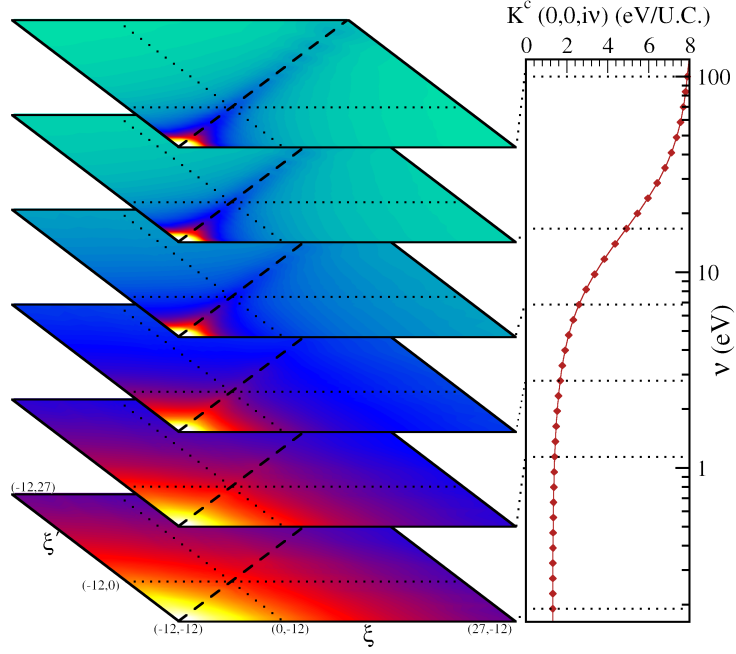


Figure 1.6: Color maps of the total kernel in imaginary frequency domain $K^c(\xi\xi'i\nu) = K_{stat}^c(\xi\xi') + \alpha^c(\xi\xi'i\nu)$ (eq. 1.4.44) plotted in the same way as the kernels in fig. 1.3 and 1.4. It is a real, positively defined quantity.

function, and all sharp features are smoothed out. However in the high $i\nu$ limit the kernel becomes constant and in this by analytic continuation identical to its real axis counterpart, i.e. identical to that in the high frequency limit (K_{dyn}^{Re}). And with this once again dominated by the low- q limit of the unscreened Coulomb interaction, with its characteristic diagonal structure. The decomposition of the $K^c(\xi\xi', i\nu)$ into static (K_{stat}^c) and dynamic (α^c) contributions is visualized in fig. 1.2 (right). In that figure one can see that the dynamical part α^c can be accurately fitted with the plasmon pole approximation in the way discussed in sec. 1.4.4.

Chapter 2

A novel approach to the Eliashberg theory of Superconductivity

The first experimental observable of a superconductor is the critical temperature (T_c). On the theory side, the easiest estimate of T_c is given by the McMillan formula [53] or its later improvement due to Allen and Dynes [54], which relates T_c to material-dependent quantities. The formula is obtained by solving the Eliashberg Equations [9] at variable input parameters. The mentioned Eliashberg approach has actually more power than just the prediction of T_c : it gives access to other experimental observables, like single particle excitation spectra [55]. It is also used for the inversion of tunneling spectra, which allows to extract the electron-phonon interaction [56, 57].

As will be detailed in sec. 2.1, it is based on an extension of conventional many body perturbation theory (MBPT) [7, 47] to allow for a symmetry broken ground state, where objects as the anomalous average $\langle \hat{c}_{k\uparrow} \hat{c}_{-k\downarrow} \rangle$ appear. This quantity is mathematically the most convenient order parameter for the SC condensation. The difference with respect to the normal MBPT is that both Green's function (GF) and self energy (SE) have a matrix form, in what is called the Nambu-Gor'kov formalism [58] introduced in sec. 2.1.1. As in conventional Green's function methods correlations are included within a Dyson like equation in the SE function (sec. 2.1.3). It will be natural to separate the SE into a phononic part and a Coulomb part. To the first belong all diagrams that contain phononic propagators and it describes the electron-phonon interaction. This issue will be discussed in sec. 2.2.1.

The first assumption of the Eliashberg theory is that the SE for the electron-phonon interaction is given by a first order term, which is conventionally the most relevant one due to Migdal's theorem [59]. The Coulomb part of the SE may have higher order contributions, which are cast into the many-body vertex part. Neglecting the vertex leads to a Coulomb SE that is the Nambu-Gor'kov analogue of the GW approximation¹, popular in photoemission spectroscopy studies [17, 16, 61, 34]. The Eliashberg approach is based on this form of the Coulomb SE part.

The screened Coulomb interaction discussed in chap. 1 is exactly the W in the above-mentioned Coulomb SE of the GW approximation. But in the traditional Eliashberg approach it is simplified by two further steps [58, 13, 12]. The first step consists in taking the static limit of the screened Coulomb interaction, i.e., ignoring completely its frequency (ω) dependence. And the second step consists in approximating this static interaction by a flat function of the electron energy (ξ) with sharp cut offs. These two approximations are conventionally reduced to a semi-empirical method with a single parameter (μ^*) describing the whole effect of the Coulomb interaction [13, 12]. Under these assumptions the Eliashberg method is cast into an effective approach that considers

¹As discussed in detail in ref. [60], for the sake of constructing a superconducting interaction, vertex corrections can also be cast into a GW form, by defining an *effective* W . This issue will be discussed in sec. 2.1.3, but here we keep the W in its original vertex-free sense.

only electronic degrees of freedom close to the Fermi surface. Our main goal is to keep the full dynamical Coulomb interaction in its full energy range.

In this thesis we have developed a novel approach that is based on a multiband-isotropic limit, which allows to consider the full scale of the electronic problem. To do so we will first review the original derivation of the Eliashberg equations in sec. 2.2. Then we will introduce our energy resolved isotropization scheme in sec. 2.2.3. Within this approach any pairing interaction can be fully included (*ab-initio*) in the calculation of the superconducting properties without any restriction on the energy scale or empirical cut-offs. This allows to address completely from first principles an old-issue in the theory of superconductivity, that is the possibility of a plasmon mediated pairing [28, 27].

2.1 Perturbation theory in the Nambu formalism

2.1.1 Hamiltonian

As seen in chapter 1, the introduction of the BO approximation allows one to split the total energy of the electron-nuclear system into an electronic part (E_0) with fixed nuclear positions (at the equilibrium) and a phononic part H^{ph} , describing the nuclear motion in the effective BO potential (eq. 1.3.10). Assuming as a starting point the KS Hamiltonian \hat{H}^{KS} , correlation effects due to exchange of phonons are described by the electron-phonon Hamiltonian \hat{H}^{el-ph} (sec. 1.3.3).

However, there are exchange and correlation effects due to the Coulomb interaction which practically are not included in the normal-state \hat{H}^{KS} . First of all, because we do not know the exact exchange-correlation potential, and second, because we have to account for this interaction in the superconducting state. Therefore, in the spirit of the GW theory [16, 34, 17], we add perturbatively a two-particle Coulomb interaction \hat{H}^c . In order to avoid a double counting (DC) problem the exchange-correlation and Hartree potential of the KS scheme is formally subtracted from \hat{H}^c . This issue will be discussed in sec. 2.2.1.

In addition to these conventional Hamiltonian terms, the many body Hamiltonian requires a further term related to the choice of the superconducting order parameter $\langle \hat{c}_{k\uparrow} \hat{c}_{-k\downarrow} \rangle$ that assumes a particle non-conserving ground state. This assumption is not problematic *per se* (as discussed in many references [62, 47, 58]), however it requires the inclusion of a symmetry breaking coupling term $\hat{H}^{\Delta^{ext}}$, which at the end of derivations should be set to zero. Hence, the total Hamiltonian which we study (collecting all statements) is the following:

$$\begin{aligned}
\hat{H} &= \hat{H}^{KS} + \hat{H}^{ph} + \hat{H}^{el-ph} + \hat{H}^c - \hat{H}^{Hxc} + \hat{H}^{\Delta^{ext}} \\
&= \sum_{k\sigma} \xi_{k\sigma} \hat{c}_{k\sigma}^\dagger \hat{c}_{k\sigma} + \sum_j \sum_{\mathbf{q} \in BZ} \omega_{j\mathbf{q}} (\hat{b}_{j\mathbf{q}}^\dagger \hat{b}_{j\mathbf{q}} + \frac{1}{2}) + \sum_{j,k,k',\sigma,\mathbf{q}} g_{kk'}^j \hat{\varphi}_{j\mathbf{q}} \hat{c}_{k'\sigma}^\dagger \hat{c}_{k\sigma} \\
&+ \frac{1}{2} \sum_{\substack{\mathbf{k}_1+\mathbf{k}_2=\mathbf{k}_3+\mathbf{k}_4 \\ k_1 k_2 k_3 k_4}} \langle k_1 k_2 | v | k_3 k_4 \rangle \hat{c}_{k_1\sigma}^\dagger \hat{c}_{k_2\sigma'}^\dagger \hat{c}_{k_4\sigma} \hat{c}_{k_3\sigma'} \\
&- \sum_{kk'\sigma} v_{kk'}^{Hxc} \hat{c}_{k\sigma}^\dagger \hat{c}_{k'\sigma} \\
&+ \sum_k (\Delta_k^{ext} \hat{c}_{k\uparrow}^\dagger \hat{c}_{-k\downarrow}^\dagger + \Delta_k^{ext*} \hat{c}_{-k\downarrow} \hat{c}_{k\uparrow}), \quad \Delta_k^{ext}, \Delta_k^{ext*} \rightarrow 0.
\end{aligned} \tag{2.1.1}$$

Here $\xi_{k\sigma}$ are KS band energies (with respect to chemical potential μ), the matrix of the bare Coulomb interaction v is evaluated on the given KS basis, as in the previous chapter $k = \{b, \mathbf{k}\}$ is

the band/k-vector pair, and the matrix $v_{kk'}^{Hxc} = \langle k|v^H + v^{xc}|k'\rangle$ is the sum of the Hartree and the exchange-correlation potential² of the KS scheme (sec. 1.2).

The additional symmetry-breaking term makes the form of this Hamiltonian quite unusual since it contains $\hat{c}\hat{c}$ and $\hat{c}^\dagger\hat{c}^\dagger$ field operators. However, it can be cast into a more common form by introducing Nambu field operators:

$$\hat{\psi}_k = \begin{pmatrix} \hat{c}_{k\uparrow} \\ \hat{c}_{-k\downarrow}^\dagger \end{pmatrix}, \quad \hat{\psi}_k^\dagger = (\hat{c}_{k\uparrow}^\dagger, \hat{c}_{-k\downarrow}), \quad (2.1.2)$$

which obey the anti-commutation relations, although using a different algebra:

$$\begin{aligned} \hat{\psi}_k \otimes \hat{\psi}_{k'}^\dagger + \hat{\psi}_{k'}^\dagger \otimes \hat{\psi}_k &= \delta_{kk'} \tau_0, \\ \hat{\psi}_k \otimes \hat{\psi}_{k'} + \hat{\psi}_{k'} \otimes \hat{\psi}_k &= 0, \end{aligned} \quad (2.1.3)$$

where the symbol \otimes denotes the tensor product (see eq. 2.1.7 how it acts), and τ_0 is one of the Pauli matrices:

$$\tau_0 = \begin{pmatrix} 1 & 0 \\ 0 & 1 \end{pmatrix} \quad \tau_1 = \begin{pmatrix} 0 & 1 \\ 1 & 0 \end{pmatrix} \quad \tau_2 = \begin{pmatrix} 0 & -i \\ i & 0 \end{pmatrix} \quad \tau_3 = \begin{pmatrix} 1 & 0 \\ 0 & -1 \end{pmatrix}. \quad (2.1.4)$$

The Hamiltonian above is rewritten as:

$$\begin{aligned} \hat{H} &= \hat{H}^{KS+\Delta^{ext}} + \hat{H}^{ph} + \hat{H}^{el-ph} + \hat{H}^c - \hat{H}^{Hxc} \\ &= \sum_k \hat{\psi}_k^\dagger \bar{\xi}_k \hat{\psi}_k + \hat{H}^{ph} + \sum_{j,k,k',\sigma,\mathbf{q}} g_{kk'}^j \hat{\phi}_{j\mathbf{q}} (\hat{\psi}_{k'}^\dagger \tau_3 \hat{\psi}_k) \\ &\quad + \frac{1}{2} \sum_{\substack{\mathbf{k}_1+\mathbf{k}_2=\mathbf{k}_3+\mathbf{k}_4 \\ k_1 k_2 k_3 k_4}} \langle k_1 k_2 | v | k_3 k_4 \rangle (\hat{\psi}_{k_1}^\dagger \tau_3 \hat{\psi}_{k_3}) (\hat{\psi}_{k_2}^\dagger \tau_3 \hat{\psi}_{k_4}) \\ &\quad - \sum_{kk'} v_{kk'}^{Hxc} \hat{\psi}_k^\dagger \tau_3 \hat{\psi}_{k'} \end{aligned} \quad (2.1.5)$$

where the symmetry-breaking term is combined with the normal state KS Hamiltonian in $\hat{H}^{KS+\Delta^{ext}}$ via:

$$\bar{\xi}_k = \begin{pmatrix} \xi_{k\uparrow} & \Delta_k^{ext} \\ \Delta_k^{ext*} & -\xi_{-k\downarrow} \end{pmatrix} \quad (2.1.6)$$

In the next section we discuss the formulation of many-body perturbation theory (MBPT), which allows to find the unknown interacting Green's function (GF) from the known non-interacting one and the interactions. The non-interacting GF is defined by a fixed normal state, which is in our case is given by $\hat{H}_0 = \hat{H}^{KS+\Delta^{ext}} + \hat{H}^{ph}$ part of Hamiltonian. While interactions are represented by $\hat{H}_{int} = \hat{H}^{el-ph} + \hat{H}^c - \hat{H}^{Hxc}$.

2.1.2 Green's Function

The corresponding finite-temperature Nambu Green's function (GF) is defined as 2×2 matrix given by the tensor product:

$$\begin{aligned} \bar{G}(kk'\tau) &= - \left\langle T_\tau \psi_k(\tau) \otimes \psi_{k'}^\dagger(0) \right\rangle = \begin{pmatrix} - \left\langle T_\tau \hat{c}_{k\uparrow}(\tau) \hat{c}_{k'\uparrow}^\dagger(0) \right\rangle & - \left\langle T_\tau \hat{c}_{k\uparrow}(\tau) \hat{c}_{-k'\downarrow}(0) \right\rangle \\ - \left\langle T_\tau \hat{c}_{-k\downarrow}^\dagger(\tau) \hat{c}_{k'\uparrow}^\dagger(0) \right\rangle & - \left\langle T_\tau \hat{c}_{-k\downarrow}^\dagger(\tau) \hat{c}_{-k'\downarrow}(0) \right\rangle \end{pmatrix} \\ &= \begin{pmatrix} G(kk'\tau) & F(kk'\tau) \\ F^\dagger(kk'\tau) & G^\dagger(kk'\tau) \end{pmatrix}, \end{aligned} \quad (2.1.7)$$

²Labels 'H' and 'xc' in v^H and v^{xc} are raised (in comparison with the previous chapter) for the matter of convenience

where the τ -dependence of the operators and the definition of T_τ (in the Fermionic case) are:

$$\hat{A}(\tau) = e^{\hat{H}\tau} \hat{A} e^{-\hat{H}\tau}, \quad (2.1.8)$$

$$T_\tau \hat{A}(\tau) \hat{B}(\tau') = \Theta(\tau - \tau') \hat{A}(\tau) \hat{B}(\tau') - \Theta(\tau' - \tau) \hat{B}(\tau') \hat{A}(\tau) \quad (2.1.9)$$

with \hat{H} given by eq. 2.1.5. The diagonal part of eq. 2.1.7 is the normal GF for an electron (G) and a hole (G^\dagger). The off-diagonal part is the so-called anomalous GF, the equal time limit ($\tau \rightarrow 0$) of which is the superconducting order parameter.

As soon as we deal with the finite-temperature formalism, the averages $\langle \dots \rangle$ in eq. 2.1.7 are taken as ensemble averages over many-particle states described by the full Hamiltonian presented by a fixed 'non-interacting' part and interactions (see the previous section):

$$\hat{H} = \hat{H}_0 + \hat{H}_{int} \quad (2.1.10)$$

If the interaction term \hat{H}_{int} vanishes, we are left with the non-interacting KS Hamiltonian plus the bare phononic Hamiltonian, and hence, we get a KS GF (in Nambu formalism) by using eq. 2.1.7 as well as the non-interacting phonon propagator $D_q(\tau)$. To obtain this result one uses the equation of motion for both (sec. B.3). For example, For the electron GF we get:

$$\left(-\frac{\partial}{\partial \tau} - \xi_k \tau_3\right) \bar{G}_0(kk'\tau) = \delta_\tau \delta_{kk'} \tau_0, \quad (2.1.11)$$

For phonons the propagator is somehow more complicated by the fact that it consist of two parts. The first one corresponds to the propagation of phonons, while the second one to the propagation of phonon 'holes' on the same footing. A more detailed discussion is presented in sec. B.3.

The equations are solved in Fourier components, which in the finite temperature formalism are defined on a discrete set of (Matsubara) frequencies for Fermions (ω_n) and Bosons (ν_n):

$$\bar{G}(k\tau) = T \sum_{\omega_n} e^{-i\omega_n \tau} \bar{G}(k, i\omega_n) \quad \text{Fermionic case} \quad (2.1.12)$$

$$D_{\mathbf{q}}(\tau) = T \sum_{\nu_n} e^{-i\nu_n \tau} D_{\mathbf{q}}(i\nu_n) \quad \text{Bosonic case} \quad (2.1.13)$$

$$\omega_n = (2n + 1)\pi T, \quad \nu_n = 2n\pi T, \quad n = 0, \pm 1, \pm 2, \dots \quad (2.1.14)$$

Using such transformations, we arrive from the eq. 2.1.11 to the explicit form of \bar{G}_0 in momentum/frequency representation:

$$[\bar{G}_0(k, i\omega_n)]^{-1} = i\omega_n \tau_0 - \xi_k \tau_3. \quad (2.1.15)$$

Now we add the interaction part \hat{H}_{int} . The corresponding interacting GF can be obtained in a perturbative way, i.e., calculating corrections to \bar{G}_0 . One can use different schemes for that, like the equation of motion, diagrammatic MBPT [7, 8] or Hedin's equations [38]. In this work we use a modification of MBPT for the Nambu GF, which is similar to ordinary MBPT with minor differences due to the matrix structure of \bar{G} [58]. This is because the Green's function/Hamiltonian have a similar form as in ordinary MBPT for conventional field operators.

A phononic GF also appears in a perturbation series for the electronic \bar{G} due to the presence of phononic field operator $\hat{\varphi}_{\mathbf{q}}$ in the \hat{H}^{el-ph} . We skip derivations on this part, as it is essentially

³It is clear, if we use hole creation (annihilation) operator $\hat{a}_{k\uparrow}^\dagger = \hat{c}_{-k\downarrow}$ ($\hat{a}_{k\uparrow} = \hat{c}_{-k\downarrow}^\dagger$), then $G^\dagger(kk'\tau) = -\langle T_\tau \hat{a}_{k\uparrow}(\tau) \hat{a}_{k'\uparrow}^\dagger(0) \rangle$.

unchanged with respect to standard textbook MBPT, and just write down the result for the non-interacting phononic GF in BO and harmonic approximation (see sec. 1.3.2 for details):

$$D_{\mathbf{q}}^j(i\nu_n) = \frac{-2\omega_{j\mathbf{q}}}{\nu_n^2 + \omega_{j\mathbf{q}}^2}, \quad (2.1.16)$$

where j is a phononic branch index. Since we work in a rather low-temperature regime and assume the dynamical stability of a crystal, the non-harmonic contributions can be neglected. Moreover, phonons in metals obtained within the presented scheme are usually in excellent agreement with experiments (see sec. 1.3.1, ref. [10, 11]), which supports the BO approximation as well. On the MBPT language a break down of above mentioned approximations corresponds to considering a perturbation series for D in a similar way as we do for the electronic Green's function \bar{G} .

2.1.2.1 Approximations for \bar{G}

The non-interacting GF \bar{G}_0 (eq. 2.1.15) is, by construction (see sec. B.1.12), diagonal both in the band index and the wave vector ($k = b\mathbf{k}$), i.e., it is completely defined by a single KS state index k .

We can however introduce two very useful approximations in order to conserve these quantum numbers also at the level of the interacting Green's function \bar{G} . First, we assume that transition to the superconducting state does not brake the translational symmetry of the crystal. This approximation makes the resulting interacting Nambu GF to be a diagonal in the \mathbf{k} -point index, i.e., $\sim \delta_{\mathbf{k}\mathbf{k}'}$.

Second, we assume a band-diagonal approximation for \bar{G} , leading to the following form:

$$\bar{G}(kk', i\omega_n) = \bar{G}(k, i\omega_n)\delta_{\mathbf{k}\mathbf{k}'}\delta_{bb'}. \quad (2.1.17)$$

This assumes that the inclusion of those Coulomb correlations that were not included on the level of the KS does not change the quasiparticle states and merely affects the quasiparticle energies and band widths. This constitutes the so-called *band decoupling approximation* and is often used in the normal-state GW calculations and in SCDFT [63, 51].

2.1.3 Self-energy

The connection between interacting and non-interacting GF in MBPT is given by the Dyson equation:

$$[\bar{G}(k, i\omega_n)]^{-1} = [\bar{G}_0(k, i\omega_n)]^{-1} - \bar{\Sigma}(k, i\omega_n), \quad (2.1.18)$$

where the self energy (SE) part $\bar{\Sigma}(k, i\omega_n)$ describes the effect of \hat{H}_{int} . In practice, $\bar{\Sigma}(k, i\omega_n)$ needs to be approximated. We discuss it in terms of Feynman diagrams. The rules to construct those objects are found in any textbook on MBPT [58, 7].

By default, we consider the so-called *proper* self energy function, the one which can not be separated into two pieces by cutting a single particle line [7]. First non-vanishing contributions from interactions of $\hat{H}_{int} = \hat{H}^{el-ph} + \hat{H}^c - \hat{H}^{Hxc}$ are given by:

where simple (or, bare) vertices (\bullet) are associated with τ_3 matrices, each dashed line corresponds to the bare Coulomb interaction, while a wavy line represents the phonon induced interaction. Hartree and exchange-correlation terms, which are two additive contributions to \hat{H}^{Hxc} , generate external potential -type diagrams (terms (5) and (6)) [64]. Closed particle loop in (1) and (3) corresponds to the trace $tr\{G(k, i\omega_n)\tau_3\}$ factor i.e., operates with the normal state (diagonal) part of \bar{G} . Moreover, together with (5) and (6) they give only $\sim \tau_3$ contribution to $\bar{\Sigma}$, while (2) and (4) contribute to all matrix components of $\bar{\Sigma}$. Let us discuss each contribution one by one.

(1) This first term is known as the Hartree self energy and is indeed the same as (5), these two compensate each other. However, if we (following the rules of MBPT) substitute all bare (thin) interaction/particle lines by dressed (bold) lines (in order to increase the number of diagrams) in the first term, correspondent additional contributions will not be compensated by V^H (or V^{xc}). If we assume that the KS charge is sufficiently accurate and that correlation effects in (1) are irrelevant then (1) and (5) compensate each other even in a "bold" form, and for this reason we will neglect them.

(2) This term contributes to all components of the Nambu self energy and at this moment is fully included in its renormalized version (i.e. with bold (dressed) interaction/particle lines). More details will be given in the following discussion.

(3) As (1), gives the phonon-mediated chemical potential $\sim \tau_3$ contribution and is naturally neglected due to the low energy scale of phonons.

(4) Included fully as (2). Here we remind only that interaction line should not be renormalized since we always work within the first order (non-interacting) phonons.

(5) Compensated by (1).

(6) For the time being this term will be included in our approach and discussed further in sec. 2.2.1.

All missing diagrams could formally be included by adding to (2) and (4) the effect of the many body vertex function. However, this vertex is difficult to obtain in a fully *ab-initio* way. We will discuss this object and related problems in secs. 2.1.3.1 and 2.1.3.2. Wrapping up the outcome of this section we can write the self energy in the following form:

$$\bar{\Sigma}(k, i\omega_n) = \bar{\Sigma}_{total}^c(k, i\omega_n) + \bar{\Sigma}^{ph}(k, i\omega_n) - v_k^{xc}\tau_3. \quad (2.1.19)$$

where $\bar{\Sigma}_{total}^c$ is the Coulomb part of the self energy that includes not only the dressed version the exchange diagram (2) but also vertex effects. We will now discuss in greater detail all the components of this self energy.

2.1.3.1 Phonon part

The $\bar{\Sigma}^{ph}(k, i\omega_n)$ is well studied in the literature [58, 14] in its *first order* exchange-like contribution:

$$\bar{\Sigma}^{ph} = \text{Diagram: } \overline{G} \text{ with } V_{ph} \text{ loop}$$

$$\bar{\Sigma}^{ph}(k, i\omega_n) = -T \sum_{k'\omega_{n'}} \tau_3 \bar{G}(k', i\omega_{n'}) \tau_3 V_{kk'nn'}^{ph}, \quad (2.1.20)$$

where the effective phonon-mediated interaction is $V_{kk'nn'}^{ph} = \sum_j |g_{kk'}^j|^2 D_{(\mathbf{k}'-\mathbf{k})nn'}^j$. The *next order* terms can be cast into the so-called many-body vertex correction, which should be inserted into the diagram above. If it contains only phononic interaction lines it can be neglected under the condition $\omega_D/E_F \sim v_s/v_F \ll 1$ fulfilled, where the ω_D, E_F, v_s and v_F are Debye frequency, Fermi energy, speed of sound and Fermi velocity respectively. This constitutes the so-called Migdal's theorem [59]. A more extensive discussion on the limits of the Migdal's theorem can be found in ref. [50]. If the vertex contains Coulomb interaction lines as well, not much can be said on its importance, and moreover, one probably would need to change the definition of the 'bare' $g_{kk'}^j$ coefficients in this case⁴. According to ref. [13] the Coulomb mediated vertex may lead to a prefactor in $g_{kk'}^j$. We nevertheless take the given above form as it is, referring to a high quantitative agreement of the SCDFT results [55, 49, 65, 66, 67, 68, 69] with the experimental data, where the 'bare' $g_{kk'}^j$ matrix is used as well.

2.1.3.2 Exact Coulomb part

Now we define the $\bar{\Sigma}_{total}^c(k, i\omega_n)$ from eq. 2.1.19. We assume without any further investigation that all phonon contributions to the vertex part (even in the Coulomb part of the self energy) are negligible. On the other hand, the Coulomb part of the vertex function is known to account for many important physical effects, among which the interaction between electrons and spin fluctuations [60, 70, 71, 72, 73, 74], which we would like to include in our work. Let us consider the Coulomb-only mediated $\bar{\Sigma}_{total}^c(k, i\omega_n)$ in its diagrammatic form given by:

$$\bar{\Sigma}_{total}^c = \text{Diagram: } \overline{G} \text{ with } V_c \text{ loop and } \bar{\Gamma} \text{ vertex}$$

where $\bar{\Gamma}$ is the many-body Coulomb mediated vertex part and its zero order term is just the simple vertex (\bullet). For $\bar{\Gamma}$ we use the conventions of ref. [60], where the problem is discussed in greater detail. $\bar{\Gamma}$ can be decomposed into a bare and a dressed vertex. The latter is expressed in terms of the particle-hole propagator Λ^P :

$$\begin{aligned} \bar{\Gamma} &= \bullet + \boxed{\Lambda^P} \\ \longrightarrow \quad \bar{\Sigma}_{total}^c &= \bar{\Sigma}^c + \bar{\Sigma}^A = \text{Diagram: } \overline{G} \text{ with } V_c \text{ loop} + \text{Diagram: } \overline{G} \text{ with } V_c \text{ loop and } \Lambda^P \text{ vertex} \end{aligned} \quad (2.1.21)$$

⁴Strictly speaking, the $g_{kk'}^j$ is calculated for the KS system and includes an essential part of the electron screening, hence is the bare one only with respect to the KS system.

One can see the GW-like [61, 16, 17] first order contribution $\bar{\Sigma}^c$, while the remaining $\bar{\Sigma}^\Lambda$ is proportional to Λ^P .

2.1.3.3 Coulomb part in the Nambu-GW approximation

The GW-like $\bar{\Sigma}^c$ (eq. 2.1.21) is given by:

$$\bar{\Sigma}^c(k, \omega_n) = -T \sum_{k' \omega_{n'}} \tau_3 \bar{G}(k', i\omega_{n'}) \tau_3 V_{kk'nn'}^c. \quad (2.1.22)$$

In this work we assume that the screened Coulomb interaction V_c is fixed to the one in the non-superconducting state, and calculated according to the discussion in sec. 1.4.2 and sec. 1.4.1. In other words, the feedback of superconducting correlations on the screening properties is neglected.

2.1.3.4 Coulomb part - $\bar{\Sigma}^\Lambda$ and the spin fluctuation contribution

As discussed in ref. [60] the part of the self energy containing vertex corrections contributes among many other effects to the interaction with magnetic fluctuations. These are very relevant effects and are believed to be responsible for the high- T_c superconductivity in pnictides [72, 73, 74]. In this work spin fluctuation effects will be considered as they give important repulsive effects on some classic superconductors.

As in ref. [60] we consider an effective interaction V_{eff} , which allows to rewrite $\bar{\Sigma}^\Lambda$ (in eq. 2.1.21) in an exchange-like form:

$$\bar{\Sigma}^\Lambda = \begin{array}{c} V_{eff} \\ \text{---} \text{---} \text{---} \\ \circ \text{---} \text{---} \text{---} \circ \end{array}$$

i.e., still keeping all vertex effects in the definition of V_{eff} . The definition of the bare vertex (\circ) is now different and will be revised below.

Instead of doing a complex diagrammatic derivation for the effective potential, we find an alternative approach [58] which is simpler and intuitive, although not completely *ab-initio*. First, we restrict ourselves to a class of systems in which the magnetic moments are localized at atomic sites and are due to the valence electrons (as they do in transitional metals like Nb and V). This allows us to treat the corresponding magnetic subsystem separately, by means of the spin operator of an atomic site a :

$$\hat{\mathbf{S}}_a = \langle \hat{\mathbf{S}}_a \rangle + \hat{\mathbf{S}}'_a. \quad (2.1.23)$$

Since the long range magnetism and superconductivity are strongly competing phases [47], we study the non-magnetic (or, paramagnetic) case only. It makes the average over the sites $\langle \hat{\mathbf{S}}_a \rangle$ vanish, and we are left only with the fluctuation part, i.e., $\hat{\mathbf{S}}_a = \hat{\mathbf{S}}'_a$. Instantaneous spin fluctuation at an ion site can induce magnetization of neighboring ion sites via exchange interactions, in this way magnetic waves can propagate in the crystal in what is called a *paramagnon*.

This leads to an additional perturbation term describing such scattering processes⁵:

$$\hat{H}_m = \int d\mathbf{r} \hat{\psi}_\alpha^\dagger(\mathbf{r}) V_{\alpha\beta}^m(\mathbf{r}) \hat{\psi}_\beta(\mathbf{r}), \quad (2.1.24)$$

⁵We use a real-space Hamiltonian for illustrative reasons.

where we assume the interaction V^m to be local. One of the form used in literature is due to Kasuya [75]:

$$V_{\alpha\beta}^m(\mathbf{r}) = \sum_a I(\mathbf{r} - \mathbf{R}_a) \hat{\sigma}_{\alpha\beta} \hat{\mathbf{S}}_a \quad (2.1.25)$$

where $I(\mathbf{r})$ is a so-called $s - d$ exchange integral. This perturbation can be decomposed on a KS basis:

$$\hat{H}^m = \sum_{kk'\alpha\beta} V_{kk'\alpha\beta}^m \hat{c}_{k\alpha}^\dagger \hat{c}_{k'\beta}, \quad (2.1.26)$$

and the matrix element is:

$$V_{kk'\alpha\beta}^m = \hat{\sigma}_{\alpha\beta} \hat{\mathbf{S}}_{\mathbf{q}} I_{kk'}, \quad (2.1.27)$$

$$I_{kk'} = \frac{1}{\sqrt{N}} \sum_{\mathbf{T}} \langle k | I(\bar{\mathbf{r}} - \mathbf{T}) | k' \rangle_{WS} e^{i\mathbf{q}\mathbf{T}}, \quad (2.1.28)$$

with $\mathbf{q} = \mathbf{k} - \mathbf{k}'$, and $\hat{\mathbf{S}}_{\mathbf{q}}$ is a FC of the $\hat{\mathbf{S}}_a$ operator, i.e., $\hat{\mathbf{S}}_a = \frac{1}{\sqrt{N}} \sum_{\mathbf{q}} \hat{\mathbf{S}}_{\mathbf{q}} e^{i\mathbf{q}\mathbf{R}_a}$. The important part of such interaction is that it flips the spins of the electrons in the Cooper state. This part is induced by so-called *transverse* spin-fluctuations and is associated with the following potential $V_{kk'\alpha\beta}^m$:

$$V_{kk'\alpha\beta}^{m\pm} = I_{kk'} \left\{ \hat{\sigma}_{\alpha\beta}^x \hat{S}_{\mathbf{q}}^x + \hat{\sigma}_{\alpha\beta}^y \hat{S}_{\mathbf{q}}^y \right\}. \quad (2.1.29)$$

Plugging it into the eq. 2.1.26 and summing up spin indices we get:

$$\begin{aligned} \hat{H}_{\pm}^m &= \sum_{kk'} I_{kk'} \left\{ [\hat{S}_{\mathbf{q}}^x - i\hat{S}_{\mathbf{q}}^y] \hat{c}_{k\uparrow}^\dagger \hat{c}_{k'\downarrow} + [\hat{S}_{\mathbf{q}}^x + i\hat{S}_{\mathbf{q}}^y] \hat{c}_{k\downarrow}^\dagger \hat{c}_{k'\uparrow} \right\} \\ &= \sum_{kk'} I_{kk'} \left\{ \hat{S}_{\mathbf{q}}^- \hat{c}_{k\uparrow}^\dagger \hat{c}_{k'\downarrow} + \hat{S}_{\mathbf{q}}^+ \hat{c}_{k\downarrow}^\dagger \hat{c}_{k'\uparrow} \right\}. \end{aligned} \quad (2.1.30)$$

It accounts for scattering processes in which the z projection of the total spin (the one of the scattered electron plus the spin of the ion) is conserved (rising and lowering operators ($\hat{S}_{\mathbf{q}}^+$ and $\hat{S}_{\mathbf{q}}^-$ respectively) change the z -projection of the ion's spin by 1).

One problem now arises from the fact that it is not possible to write this Hamiltonian within the 2×2 matrix Nambu formalism, because the combinations $c_{k\uparrow}^\dagger c_{k'\downarrow}$ (or $c_{k\downarrow}^\dagger c_{k'\uparrow}$) correspond to a magnetization of the electronic degrees of freedom and cannot be described by the $\psi_k^\dagger \tau_i \psi_{k'}$ products. One needs to adopt a 4×4 Nambu matrix formalism [58, 60, 76], which is then traced back to the normal 2×2 form, if the resulting interacting GF corresponds to a paramagnetic state (what is assumed at the beginning of the section). We do not follow this route because it complicates the discussion significantly. From the other hand, it is possible to construct the perturbation expansion for all components of the 2×2 Nambu GF, i.e., for G, G^\dagger, F and F^\dagger (see eq. 2.1.7) using the standard technique of MBPT⁶, and then contracting the resulting expressions back to the 2×2 matrix form. Such derivation can be found in appendix B.4). In this chapter we give just the final result.

The first non-vanishing perturbative contribution to the Nambu \bar{G} results to be:

$$\delta \bar{G}^2(k\tau) = - \int_0^{1/T} d\tau_1 d\tau_2 \sum_{k'} |I_{kk'}|^2 D_{(\mathbf{k}'-\mathbf{k})}^\pm \bar{G}_0 \tau_0 \bar{G}_0 \tau_0 \bar{G}_0, \quad (2.1.31)$$

⁶Wick's theorem [7]

where the transverse paramagnon propagator $D_{\mathbf{q}}^{\pm}(\tau) = -\langle T_{\tau} \hat{S}_{\mathbf{q}}^{-}(\tau) \hat{S}_{\mathbf{q}}^{+}(0) \rangle$ appears. The essential point is that our electron-paramagnon interaction of eq. 2.1.30 leads to an effective electron-electron scattering involving the propagation of magnetic excitation via $D_{\mathbf{q}}^{\pm}$. The same occurred for the electron-phonon interaction, where the phonon propagator $D_{\mathbf{q}}$ was involved. However this term acts differently in the Nambu space, via the τ_0 matrix instead of τ_3 appearing in the phonon and Coulomb SE.

The final SE due to the electron paramagnon interaction is:

$$\bar{\Sigma}^m(k, i\omega_n) = -T \sum_{k'\omega_{n'}} V_{kk'nn'}^m \tau_0 \bar{G}(k', i\omega_{n'}) \tau_0, \quad (2.1.32)$$

where the interacting GF is used instead of the non-interacting one, and $V_{kk'nn'}^m$ is what stands for the effective interaction due to spin fluctuations.

2.1.4 Summary of the self energy

To finalize the discussion on the SE, we collect all mentioned contributions and statements together and write explicitly the SE to proceed:

$$\begin{aligned} \bar{\Sigma}(k, i\omega_n) &= \bar{\Sigma}^{ph}(k, i\omega_n) + \bar{\Sigma}^c(k, i\omega_n) + \bar{\Sigma}^m(k, i\omega_n) - v_k^{xc} \tau_3 \\ &= -T \sum_{k'\omega_{n'}} \tau_3 \bar{G}(k', i\omega_{n'}) \tau_3 \left[V_{kk'nn'}^{ph} + V_{kk'nn'}^c \right] \\ &\quad - T \sum_{k'\omega_{n'}} \tau_0 \bar{G}(k', i\omega_{n'}) \tau_0 V_{kk'nn'}^m - v_k^{xc} \tau_3 \end{aligned} \quad (2.1.33)$$

2.2 Eliashberg equations

The main step to pass from the Dyson equation 2.1.18 to the Eliashberg equations is to expand the self-energy in the basis of Pauli matrices according to the following form:

$$\bar{\Sigma}(k, i\omega_n) = i\omega_n [1 - Z(k, i\omega_n)] \tau_0 + (\chi(k, i\omega_n) - v_k^{xc}) \tau_3 \quad (2.2.1)$$

$$+ \phi_1(k, i\omega_n) \tau_1 + \phi_2(k, i\omega_n) \tau_2, \quad (2.2.2)$$

where Z, χ and ϕ 's are state (k) and frequency ($i\omega_n$) -dependent coefficients. Inserting into the Dyson equation 2.1.18 determines the corresponding decomposition of the Nambu GF:

$$[\bar{G}(k, i\omega_n)]^{-1} = i\omega_n Z \tau_0 - (\xi_k + \chi - v_k^{xc}) \tau_3 - \phi_1 \tau_1 - \phi_2 \tau_2. \quad (2.2.3)$$

The Nambu GF then follows after inversion:

$$\begin{aligned} \bar{G}(k, i\omega_n) &= -\frac{i\omega_n Z \tau_0 + (\xi_k + \chi - v_k^{xc}) \tau_3 + \phi_1 \tau_1 + \phi_2 \tau_2}{\Theta(k, i\omega_n)} \\ &= -\frac{1}{\Theta(k, i\omega_n)} \begin{pmatrix} i\omega_n Z + (\xi_k + \chi - v_k^{xc}) & \phi_1 - i\phi_2 \\ \phi_1 + i\phi_2 & i\omega_n Z - (\xi_k + \chi - v_k^{xc}) \end{pmatrix}, \\ \Theta(k, i\omega_n) &= -\det(\bar{G}^{-1}) = [Z\omega_n]^2 + [\xi_k + \chi - v_k^{xc}]^2 + \phi_1^2 + \phi_2^2. \end{aligned} \quad (2.2.4)$$

In absence of magnetic fields (or, in a paramagnetic case), one can avoid the ϕ_2 term by choosing

a phase factor of total $\phi = \phi_1 + i\phi_2$. Inserting 2.2.1 and 2.2.4 into 2.1.33 one arrives to:

$$[1 - Z(k, i\omega_n)] i\omega_n = T \sum_{k'\omega_{n'}} \left[V_{kk'nn'}^{ph} + V_{kk'nn'}^m + V_{kk'nn'}^c \right] \frac{Z(k', i\omega_{n'}) i\omega_{n'}}{\Theta(k', i\omega_{n'})}, \quad (2.2.5)$$

$$\phi(k, i\omega_n) = -T \sum_{k'\omega_{n'}} \left[V_{kk'nn'}^{ph} - V_{kk'nn'}^m + V_{kk'nn'}^c \right] \frac{\phi(k', i\omega_{n'})}{\Theta(k', i\omega_{n'})}, \quad (2.2.6)$$

$$\chi(k, i\omega_n) = T \sum_{k'\omega_{n'}} \left[V_{kk'nn'}^{ph} + V_{kk'nn'}^m + V_{kk'nn'}^c \right] \frac{\chi(k', i\omega_{n'}) - v_k^{xc} + \xi_{k'}}{\Theta(k', i\omega_{n'})}. \quad (2.2.7)$$

The above is the anisotropic form of the Eliashberg equations.

One usually neglects the χ function, which is basically a chemical potential correction. This issue is to be discussed in the next section. Therefore, we will only consider the parts of the Eliashberg equations involving Z , which is called *mass renormalization* function, and obviously the non-diagonal part ϕ , which is the Eliashberg *gap function*.

2.2.1 χ and v^{xc}

The χ should include normal state corrections on top of the KS which are beyond ones accounted in the v^{xc} . From the sake of the low phonon/paramagnon energy scale in comparison with high chemical energy scale, we can safely ignore corresponding contributions into this function. The different situation is with the Coulomb mediated portion of χ . Keeping this part would correspond to the commonly adopted GW correction to the normal state, which is less important for metals in comparison with semiconductors, where the LDA band gap has to be corrected. Consequently, we assume that the χ is mostly compensated by the v_{xc} (both enter the equations as a difference) and ignore it completely.

One might think that under the assumption that the KS band structure is in a good agreement with the experimental spectrum one could also ignore the whole $\bar{\Sigma}_{11}^c$ part of the self energy (i.e. the Coulomb contribution to the Z as well). This is not at all the case. The mass renormalization function Z , which is not so important in the overall structure of the excitation spectrum [55], gives an essential contribution to the critical temperature, reducing it significantly, as we will see in the last chapter of this work. Thus, eqs. 2.2.5 and 2.2.6 will be considered as they are in the following discussion with $\chi - v^{xc}$ term omitted everywhere.

2.2.2 Connection to experimental observables

In principle, the Green's function formalism allows to compute much more than the critical temperature. In particular, from the Green's function it is possible to extract the excitation spectrum of the superconductor. However, this requires to obtain the retarded Green's function by analytically continuing the Matsubara Green's function to the real frequency axis. We adopt the Padé method [77, 78] that is simple and sufficiently accurate for our scope.

The physical Green's function is actually the 11 component of the Nambu \bar{G} on the real axis (see ref. [55]):

$$G_{11}(k\omega) = \frac{\omega Z_k(\omega) + \xi_k}{[\omega Z_k(\omega)]^2 - \xi_k^2 - [\phi_k(\omega)]^2}. \quad (2.2.8)$$

Poles of this function in the complex plane are defined by the equation:

$$z_p = \sqrt{[\xi_k/Z_k(z_p)]^2 + [\phi_k(z_p)/Z_k(z_p)]^2}. \quad (2.2.9)$$

The real part of z_p corresponds to the quasiparticle energy, while the imaginary part is an inverse lifetime. From the last formula it is clear that Z acts by scaling down the KS energies (ξ_k), i.e., causing a mass renormalization, (which is reflected in the name of this function). Z also scales the Eliashberg ϕ function giving the superconducting gap Δ :

$$\Delta_k = \phi_k/Z_k.$$

It is interesting to note that the superconducting gap at the excitation spectrum, which we name as a *fundamental gap*, is accessible without continuation to the real frequency domain, since it is measured in the low frequency limit:

$$\Delta_0(T) = \Delta(T, \omega = 0) = \frac{\phi(\xi_F, \omega = 0)}{Z(\xi_F, \omega = 0)} \equiv \frac{\phi(\xi_F, i\omega = i0)}{Z(\xi_F, i\omega = i0)}. \quad (2.2.10)$$

Integrating the spectral function $A_k(\omega) = \frac{1}{\pi} \text{Im}[G_{11}(k\omega)]$ over k , one gets the DOS of the superconductor [13]:

$$N_S(T, \omega) = \text{Re} \left[\frac{|\omega|}{\sqrt{\omega^2 - \Delta^2(T, \omega)}} \right]. \quad (2.2.11)$$

However the DOS is usually measured experimentally in a tunneling process as in Scanning Tunneling Microscopy (STM) or in tunneling through a barrier (for, example, insulating (I) oxide layer) between contacts of a superconducting (S) and a normal (N) phase, i.e., speaking about so-called $S - I - N$ junction. The tunneling current density $J(V)$ is given by [13]:

$$J(V) = J_0 \int d\omega N_S(\omega) N_N(\omega + V) [f(\omega) - f(\omega + V)] \quad (2.2.12)$$

as a function of the applied voltage V . The coefficient J_0 contains information about the tunneling matrix elements between the superconductor and the normal metal. The derivative of J with respect to the voltage gives the tunneling DOS:

$$\tilde{N}_{tun}(V) = \frac{\partial J(V)}{\partial V} = J_0 N_N \int d\omega N_S(\omega) \frac{\partial [f(\omega) - f(\omega + V)]}{\partial V}, \quad (2.2.13)$$

which at $T = 0$ is equal to $N_S(\omega)$ up to the constant $J_0 N_N$. Often, the reported $\tilde{N}_{tun}(V)$ curves are renormalized to $N_{tun}(V)$ such that $N_{tun}(V) \rightarrow \sim 1$ at $V \gg \Delta$, in order to get rid of the $J_0 N_N$ factor. The $N_{tun}(V)$ is also called as a *normalized conductance*. The essential difference between $N_S(V)$ and $N_{tun}(V)$ is in extra Fermi factors $f(\omega)$, which take into account the temperature effect on the single-particle occupation numbers in N and S contacts.

2.2.3 Isotropic limit

The anisotropic Eliashberg equations 2.2.5-2.2.6 are computationally quite expensive. However, the experience gained both by Eliashberg approaches and SCDFE ones [55, 49, 65, 66, 67, 68, 69] shows that the effect of this full \mathbf{k} and band resolution is weak in many materials, and an isotropic approximation like in conventional formulations of the Eliashberg approach [13, 12] is already sufficient, especially if one is mostly interested in the critical temperature rather than the details of the excitation spectrum. Even when anisotropy is essential, in the case of multiband superconductors (for example, MgB_2 [79, 80, 81] or the iron arsenides [3, 4]), it can be simplified to the level of a multiband but isotropic (within each band) approximation [81, 48, 49, 15].

The isotropic approximation⁷ is obtained by substituting the couplings by their isoenergy surface average:

$$V_{kk'nn'} \rightarrow K_{nn'}(\xi\xi') \equiv V_{nn'}(\xi_k\xi_{k'}) = \frac{1}{N(\xi')N(\xi)} \sum_{kk'} V_{kk'nn'} \delta(\xi_k - \xi) \delta(\xi_{k'} - \xi'). \quad (2.2.14)$$

Inserting this into the Eliashberg equations one immediately gets Z and ϕ dependent on the energy variable only⁸:

$$[1 - Z_n(\xi)] i\omega_n = T \sum_{\omega_{n'}} \int d\xi' N(\xi') \left\{ K_{nn'}^{ph}(\xi\xi') + K_{nn'}^m(\xi\xi') + K_{nn'}^c(\xi\xi') \right\} \frac{Z_{n'}(\xi') i\omega_{n'}}{\Theta_{n'}(\xi')}, \quad (2.2.15)$$

$$\phi_n(\xi) = -T \sum_{\omega_{n'}} \int d\xi' N(\xi') \left\{ K_{nn'}^{ph}(\xi\xi') - K_{nn'}^m(\xi\xi') + K_{nn'}^c(\xi\xi') \right\} \frac{\phi_{n'}(\xi')}{\Theta_{n'}(\xi')}, \quad (2.2.16)$$

$$\Theta_n(\xi) = [Z_n(\xi)\omega_n]^2 + \xi^2 + \phi_n^2(\xi). \quad (2.2.17)$$

The kernel $K_{nn'}^c(\xi\xi')$ is the isoenergy surface average of the full dynamically screened Coulomb interaction ($V_{kk'nn'}^c$) and is computed in the way discussed in sec. 1.4.3, using eq. 1.4.44. The phonon $K_{nn'}^{ph}(\xi\xi')$ and magnon $K_{nn'}^m(\xi\xi')$ kernels are discussed in the following subsections.

2.2.3.1 Phonon interaction kernel.

Following the general definition (eq. 2.2.14) the $K_{nn'}^{ph}(\xi\xi')$ is rewritten⁹:

$$\begin{aligned} K_{nn'}^{ph}(\xi\xi') &= \frac{1}{N(\xi')N(\xi)} \sum_{kk'} \sum_j V_{kk'nn'}^{ph} \delta(\xi_k - \xi) \delta(\xi_{k'} - \xi') \\ &= \frac{1}{N(\xi')N(\xi)} \int d\omega \sum_{kk'} \sum_j |g_{kk'}^j|^2 \delta(\xi_k - \xi) \delta(\xi_{k'} - \xi') \delta(\omega_{(\mathbf{k}'-\mathbf{k})}^j - \omega) D_{(\mathbf{k}'-\mathbf{k})nn'}^j \\ &= \frac{1}{N(\xi')} \int d\omega \alpha^2 F(\xi\xi'\omega) D_{nn'}(\omega), \end{aligned} \quad (2.2.18)$$

where $\alpha^2 F(\xi\xi'\omega)$ is the energy-resolved spectral function of the electron-phonon interaction and $D_{nn'}(\omega)$ now reads:

$$D_{nn'}(\omega) = \frac{-2\omega}{(\omega_n - \omega_{n'})^2 + \omega^2}. \quad (2.2.19)$$

It will be shown (sec. 2.5.3), that the energy (ξ') integral in the eqs. 2.2.15, 2.2.16 out of the $\sim K^{ph}$ terms converge quite fast, hence, the $K_{nn'}^{ph}(\xi\xi')$ can be taken as a constant with respect to $\xi\xi'$ and computed at the Fermi level ($\xi\xi' = \xi_F\xi_F$). Hence the $\xi\xi'$ arguments of the $K_{nn'}^{ph}(\xi\xi')$ will be omitted in the following, i.e., $K_{nn'}^{ph}(\xi\xi') \rightarrow K_{nn'}^{ph}$, which also implies a simplified definition of the *Eliashberg* spectral function:

$$\alpha^2 F(\omega) = \frac{1}{N_F} \sum_{kk'} \sum_j |g_{kk'}^j|^2 \delta(\xi_k) \delta(\xi_{k'}) \delta(\omega_{(\mathbf{k}'-\mathbf{k})}^j - \omega). \quad (2.2.20)$$

A simple measure of the electron-phonon coupling strength is given by the next integral:

$$\lambda^{ph} = 2 \int d\omega \alpha^2 F(\omega) / \omega. \quad (2.2.21)$$

⁷To keep the discussion simple here we discuss only the fully isotropic case, multiband isotropic being a rather simple generalization

⁸As discussed in sec. 2.2, we consider only equations for Z and ϕ . χ is neglected.

⁹the $1 = \int d\omega \delta(\omega_{\mathbf{q}}^j - \omega)$ was added in the second line

2.2.3.2 Paramagnon interaction kernel

The paramagnon interaction kernel is defined by the average:

$$K_{nn'}^m(\xi\xi') = \frac{1}{N(\xi)N(\xi')} \sum_{kk'} I_{kk'}^2 D_{(\mathbf{k}'-\mathbf{k})nn'}^\pm \delta(\xi_k - \xi) \delta(\xi_{k'} - \xi'). \quad (2.2.22)$$

The magnon energy is close to the phonon one [82] (~ 100 meV). Hence, as in the case of the phonon kernel $K_{nn'}^{ph}$, it will be mapped on the Fermi surface, i.e., $\xi\xi' \rightarrow \xi_F\xi_F$ and $K_{nn'}^m(\xi\xi') \rightarrow K_{nn'}^m$. Exchange integrals $I_{kk'}$ are generally hard for estimation and simplest solution is to assume it as a constant or to have a simple analytic dependence on $\mathbf{q} = (\mathbf{k}' - \mathbf{k})$ [71, 70]. We take it as a constant $I_{kk'} = I_{ex}$. Material-dependent estimations of this property were taken from ref. [83]. The same values were used in ref. [84].

The propagator D^\pm is written in the imaginary axis, but it can be expressed via the retarded propagator as:

$$D_{\mathbf{q}nn'}^\pm = \int_0^\infty \frac{2\omega}{\pi} \frac{\text{Im}[D_{\mathbf{q}}^\pm(\omega)]}{(\omega_n - \omega_{n'})^2 + \omega^2} d\omega \quad (2.2.23)$$

As with electron-phonon interaction, one introduces a spectral function $P(\omega)$ at the Fermi surface and writes consequently the kernel:

$$P(\omega) = \frac{I_{ex}^2}{N_F} \sum_{kk'} \left\{ -\frac{1}{\pi} \text{Im}[D_{(\mathbf{k}'-\mathbf{k})}^\pm(\omega)] \right\} \delta(\xi_k) \delta(\xi_{k'}) \quad (2.2.24)$$

$$K_{nn'}^m = \frac{1}{N_F} \int_0^\infty d\omega \frac{-2\omega}{(\omega_n - \omega_{n'})^2 + \omega^2} P(\omega) \quad (2.2.25)$$

Analogous to eq. 2.2.26, the corresponding coupling strength is given by:

$$\lambda_{sf} = 2 \int \frac{P(\omega)}{\omega} d\omega. \quad (2.2.26)$$

The details on computing the $P(\omega)$ are discussed in the appendix B.5.

2.3 Using the SCDF-T-Kohn-Sham GF in the Eliashberg method

The Superconducting Density Functional Theory (SCDF-T) is an effective *ab-initio* approach to superconductivity reviewed and developed in ref. [63, 51]. So far it was the only method to account the effect of the Coulomb interaction fully *ab-initio*, and which gave a reliable estimations of critical temperatures in a variety of compounds [55, 49, 65, 66, 67, 68, 69]. We incorporate its elements into our Eliashberg equations, calling the resulting scheme as 'Eliashberg+SCDF-T'.

The SCDF-T operates with quantities of a fictitious (Kohn-Sham) system of non-interacting 'bogoliubons', i.e. superconducting electrons described by a Bogoliubov single-particle equation, for which the corresponding superconducting Green's functions can be easily calculated. We concentrate on the anomalous Green's function due to KS, $F^s(\xi, i\omega_n)$. This is related to the many-body $F(\xi, i\omega_n)$ (off-diagonal component of the Nambu GF, see eq. 2.1.7 and 2.2.4) via equality of the order parameter χ^{OP} :

$$\chi^{OP}(\xi) = -T \sum_{\omega_n} F(\xi, i\omega_n) = -T \sum_{\omega_n} \frac{\phi_n(\xi)}{\Theta_n(\xi)}, \quad (2.3.1)$$

$$= -T \sum_{\omega_n} F^s(\xi, i\omega_n) = -T \Delta^s(\xi) \sum_{\omega_n} \frac{1}{\omega_n^2 + \xi^2 + [\Delta^s(\xi)]^2}, \quad (2.3.2)$$

where the Kohn-Sham gap Δ^s enters the definition of F^s [85]. The Matsubara sum in the last line can be taken analytically (see eqs. E.2-E.5 in ref. [64]):

$$\sum_{\omega_n} \frac{1}{\omega_n^2 + \xi^2 + [\Delta^s(\xi)]^2} = \frac{1 - 2f(E)}{2TE}, \quad (2.3.3)$$

where $E(\Delta^s, \xi) = \sqrt{\xi^2 + [\Delta^s(\xi)]^2}$. Hence, we can obtain the equation for Δ^s :

$$\Delta^s(\xi) = -\frac{2\chi^{OP}(\xi)E(\Delta^s, \xi)}{1 - 2f[E(\Delta^s, \xi)]},$$

which can be solved iteratively. The $\chi^{OP}(\xi)$ is defined from the total many-body ϕ and Θ (eq. 2.3.1) and defines the Δ^s , and this map always can be done.

We use this Δ^s in a very specific place. The gap function (eq. 2.2.16) further (sec. 2.4) will be split into additive contributions:

$$\phi = \phi^{ph,m} + \phi_{stat}^c + \phi^{c,dyn},$$

coming from the phonon/magnon interactions ($\phi^{ph,m}$), the static (ϕ_{stat}^c) and the dynamic ($\phi^{c,dyn}$) parts of the Coulomb interaction. Our Eliashberg+SCDFT scheme enters into the equations for ϕ_{stat}^c and $\phi^{c,dyn}$. Namely, we plug the Kohn-Sham gap into the right-hand side of the Coulomb gap equations (see further 2.4.13 and 2.4.14) as following:

$$\phi_{stat}^c(\xi) = -2T \sum_{\omega_{n'}} \int d\xi' N(\xi') K_{stat}^c(\xi\xi') \frac{\Delta^s(\xi')}{\omega_n^2 + \xi^2 + [\Delta^s(\xi')]^2}, \quad (2.3.4)$$

$$= -T \int d\xi' N(\xi') K_{stat}^c(\xi\xi') \chi^{OP}(\xi') \quad (2.3.5)$$

$$\phi_n^{c,dyn}(\xi) = -T \int d\xi' N(\xi') \sum_{\omega_{n'}} \alpha_{nn'}^c(\xi\xi') \frac{\Delta^s(\xi')}{\omega_n^2 + \xi'^2 + [\Delta^s(\xi')]^2}. \quad (2.3.6)$$

It corresponds to using the KS GF F^s instead of the many-body F for only this Coulomb-sourced parts of the self-energy. Note, that in the second line we use the independence of the static kernel K_{stat}^c on a Matsubara index. From this it follows that if one neglects the $\phi_n^{c,dyn}$ (taking a static limit) the remaining ϕ_{stat}^c will be independent on which equation we choose, eq. 2.3.4 or 2.4.13, since the order parameter is the same in both cases. But the modification above does make a difference in the dynamical case, which will be investigated in sec. 3.3.

2.4 Numerical aspects and approximations

Equations 2.2.15 and 2.2.16 are solved iteratively, as any Dyson-like equation, i.e., (i) we start from a guess (for Z and ϕ) in the right-hand side, (ii) compute the left part (new, Z and ϕ), (iii) then plug this result to the right again, and repeat the procedure until Z and ϕ are stable with iterations. Both, Z and ϕ are coupled and influence each other via the denominator Θ . Superconductivity occurs whenever a solution is found at non-zero *gap function* ϕ . Critical temperature (T_c) search works as follows: the equations are solved self-consistently for iteratively increasing temperature T (the temperature enters the equations explicitly into the right-hand side and also defines Matsubara meshes). The temperature at which ϕ becomes zero is by definition the critical temperature T_c .

In the next subsections we first (sec. 2.4.1) discuss technicalities in performing the integrals in the Eliashberg equations (eq. 2.2.15-2.2.17). Next (sec.2.4.2), we explain how one can evaluate infinite Matsubara summations in the Coulomb-mediated gap equations. We also discuss the traditional μ^* -approach in Eliashberg theory. And finally, we summarize all approximations in sec. 2.4.3.

2.4.1 Meshes and numerical integrations

Solving the Eliashberg equations involves performing summations of the Matsubara points and energy integrations on the right hand side of eqs. 2.2.15-2.2.16. These integrals and summations are infinite. Therefore, to be performed numerically, they have to be cut (unless particular analytic limits are imposed):

$$\sum_{\omega_{n'}} \int d\xi' \dots \rightarrow \sum_{\omega_{n'} = -\omega_{cut} - E_{cut}}^{\omega_{cut}} \int_{-E_{cut}}^{E_{cut}} d\xi' \dots \quad (2.4.1)$$

The cutoff (ω_{cut} and E_{cut}) will be chosen by convergence checks. We will come back to the convergence issue in sec. 2.5. Convergence is ensured by the structure of the equations and the kernels.

An important role is played by the denominator function Θ (eq. 2.2.17) that makes low energy contributions dominant. From the other side, it will be shown, that convergence occurs at high frequency/energy cut offs. This slow convergence imposes to use special integration meshes. The energy meshes are therefore chosen to be logarithmic from the Fermi energy. High energy Matsubara points are pruned, and the weight is redistributed to a restricted subset of points. In this way one can reach high value of the cutoff limiting the computational cost. The price to pay is that the convergence test must also extend to the pruning (or, skipping) and the logarithmic distribution.

Due to the similar energy scales of phonons and magnons, the corresponding interaction kernels can be put together in the common phonon-paramagnon kernel, in short:

$$\begin{aligned} K_{nn'}^{(ph+m)} &= K_{nn'}^{ph} + K_{nn'}^m, \\ K_{nn'}^{(ph-m)} &= K_{nn'}^{ph} - K_{nn'}^m, \end{aligned} \quad (2.4.2)$$

where, according to eqs. 2.2.15,2.2.16 the first line enters equation for Z , while the second one - the equation for ϕ .

The next simplification comes from the symmetry of fermionic Matsubara points, i.e., $\omega_n = -\omega_{-(n+1)}$ and the fact that Z and ϕ are even functions of frequency, e.g., $Z(i\omega) = Z(-i\omega)$. This allows to perform only a half of the Matsubara sum:

$$[1 - Z_n(\xi)] i\omega_n = T \sum_{\omega_{n'} = \omega_0 - E_{cut}}^{\omega_{cut}} \int_{-E_{cut}}^{E_{cut}} d\xi' N(\xi') \left\{ K_{nn'}^{(ph+m)-} + K_{nn'}^{c-}(\xi\xi') \right\} \frac{Z_{n'}(\xi') i\omega_{n'}}{\Theta_{n'}(\xi')}, \quad (2.4.3)$$

$$\phi_n(\xi) = -T \sum_{\omega_{n'} = \omega_0 - E_{cut}}^{\omega_{cut}} \int_{-E_{cut}}^{E_{cut}} d\xi' N(\xi') \left\{ K_{nn'}^{(ph-m)+} + K_{nn'}^{c+}(\xi\xi') \right\} \frac{\phi_{n'}(\xi')}{\Theta_{n'}(\xi')}, \quad (2.4.4)$$

$$K_{nn'}^{\pm} = K_{nn'} \pm K_{n, -(n'+1)}. \quad (2.4.5)$$

The Coulomb kernel is given by the screened interaction discussed in sec. 1.4.3 and enters the equations above as:

$$K_{nn'}^{c+}(\xi\xi') = 2K_{stat}^c(\xi\xi') + \alpha_{nn'}^{c+}(\xi\xi'), \quad (2.4.6)$$

$$K_{nn'}^{c-}(\xi\xi') = \alpha_{nn'}^{c-}(\xi\xi'). \quad (2.4.7)$$

The final set of equations that has been implemented is the following:

Equations for the Z function:

$$Z_n(\xi) = 1 + Z_n^{ph,m} + Z_n^{c,dyn}(\xi), \quad (2.4.8)$$

$$Z_n^{ph,m} = -\frac{T}{\omega_n} \sum_{\omega_{n'}=\omega_0}^{\omega_{cut}^{ph,m}} \int_{-E_{cut}^{ph}}^{E_{cut}^{ph}} d\xi' N(\xi') K_{nn'}^{(ph+m)-} \frac{Z_{n'}(\xi') \omega_{n'}}{\Theta_{n'}(\xi')}, \quad (2.4.9)$$

$$Z_n^{c,dyn}(\xi) = -\frac{T}{\omega_n} \sum_{\omega_{n'}=\omega_0}^{\omega_{cut}^c} \int_{-E_{cut}^c}^{E_{cut}^c} d\xi' N(\xi') \alpha_{nn'}^{c-}(\xi\xi') \frac{Z_{n'}(\xi') \omega_{n'}}{\Theta_{n'}(\xi')}, \quad (2.4.10)$$

Note, that due to the eq. 2.4.7 the Coulomb part of Z originates only from the dynamical part of the Coulomb interaction (α). The $Z^{ph,m}$ is ξ -independent because of our assumption of the phonon paramagnon kernel to be a $\xi\xi'$ -independent function.

Equations for the ϕ function read:

$$\phi_n(\xi) = \phi_n^{ph,m} + \phi_{stat}^c(\xi) + \phi_n^{c,dyn}(\xi), \quad (2.4.11)$$

$$\phi_n^{ph,m} = -T \sum_{\omega_{n'}=\omega_0}^{\omega_{cut}^{ph,m}} \int_{-E_{cut}^{ph}}^{E_{cut}^{ph}} d\xi' N(\xi') K_{nn'}^{(ph+m)+} \frac{\phi_{n'}(\xi')}{\Theta_{n'}(\xi')}, \quad (2.4.12)$$

$$\phi_{stat}^c(\xi) = -2T \sum_{\omega_{n'}=\omega_0}^{\omega_{cut}^c} \int_{-E_{cut}^c}^{E_{cut}^c} d\xi' N(\xi') K_{stat}^c(\xi\xi') \frac{\phi_{n'}(\xi')}{\Theta_{n'}(\xi')}, \quad (2.4.13)$$

$$\phi_n^{c,dyn}(\xi) = -T \int_{-E_{cut}^c}^{E_{cut}^c} d\xi' N(\xi') \sum_{\omega_{n'}=\omega_0}^{\omega_{cut}^c} \alpha_{nn'}^{c+}(\xi\xi') \frac{\phi_{n'}(\xi')}{\Theta_{n'}(\xi')}. \quad (2.4.14)$$

where the static (frequency-independent) Coulomb kernel $K_{stat}^c(\xi\xi')$ makes the Coulomb gap ϕ_{stat}^c to be also frequency independent. Approximations in the Coulomb part can lead to additional simplifications discussed in sec 2.4.2.1-2.4.2.3.

2.4.2 Special integrations and approximations in the Coulomb part

In the following subsections we discuss the analytical tricks, which allow to extend the cutoff for Matsubara summations in equations for $\phi^{c,dyn}$ and ϕ_{stat}^c up to infinity. In sec. 2.4.2.1 this is done for the $\phi^{c,dyn}$ equation using the plasmon pole approximation, while in sec. 2.4.2.2 it is naturally provided in equation for ϕ_{stat}^c by the limiting behavior of the Z and ϕ functions at high Matsubara frequencies ω_n . In certain approximations to the static interaction the equation for the ϕ_{stat}^c is reduced to the traditional μ^* method, which will be discussed in sec. 2.4.2.3.

2.4.2.1 Plasmon pole approximation

In sec. 2.5.4 we will see that convergence of Matsubara sum with respect to ω_{cut}^c in the equation for the $\phi^{c,dyn}$ (eq. 2.4.14) is extremely slow¹⁰. We can still extend the cutoff to infinity by the following two steps. First, we split the sum into two parts:

$$\sum_{\omega_{n'}=\omega_0}^{\omega_{cut}^c} \alpha_{nn'}^{c+}(\xi\xi') \frac{\phi_{n'}(\xi')}{\Theta_{n'}(\xi')} \rightarrow \left[\sum_{\omega_{n'}=\omega_0}^{\omega_{n'} \leq \omega_{cut}^{c,pp}} + \sum_{\omega_{n'} > \omega_{cut}^{c,pp}}^{\omega_{\infty}} \right] \alpha_{nn'}^{c+}(\xi\xi') \frac{\phi_{n'}(\xi')}{\Theta_{n'}(\xi')}, \quad (2.4.15)$$

¹⁰The situation is better for $Z^{c,dyn}$ (eq. 2.4.10) because of the different kernel construct (α^{c-} versus α^{c+} for the gap).

where $\omega_{cut}^{c,pp}$ is chosen in such a way that the gap has reached a point in which it does not show any relevant variation anymore, i.e., $\phi_{n'}(\xi') \rightarrow \phi_{const}(\xi')$. Second, we introduce a model form of α to be used above $\omega_{cut}^{c,pp}$. We use a plasmon pole approximation with parameters imposed by the continuity of the kernel at $\omega_{cut}^{c,pp}$ (see eq. 1.4.47 and discussions below).

In this condition the infinite part of the sum can be performed analytically¹¹ by splitting it into two parts:

$$\sum_{\omega_{n'} > \omega_{cut}^{c,pp}}^{\omega_{\infty}} \rightarrow \phi_{const}(\xi') \left[\sum_{\omega_{n'} = \omega_0}^{\omega_{\infty}} - \sum_{\omega_{n'} = \omega_0}^{\omega_{cut}^{c,pp}} \right] \frac{\alpha_{nn'}^{c,pl+}(\xi\xi')}{\omega_{n'}^2 + [E(\xi')]^2}, \quad (2.4.16)$$

where $E(\xi') = \sqrt{\xi'^2 + [\phi_{const}(\xi')]^2}$. The first term is evaluated using the analytic form $\phi_n^{PPA}(\xi\xi'E\omega_p)$, and the second term gives the $\phi_n^{PP}(\xi\xi'E\omega_p\omega_{cut}^{c1})$, which is a partial (up to $\omega_{cut}^{c,pp}$) sum. This allows us to rewrite the eq. 2.4.16 as:

$$\sum_{\omega_{n'} > \omega_{cut}^{c1}}^{\infty} \rightarrow [\phi_n^{PPA}(\xi\xi'E\omega_p) - \phi_n^{PP}(\xi\xi'E\omega_p\omega_{cut}^{c,pp})] \phi_{const}(\xi'). \quad (2.4.17)$$

Consequently, we write the final result for the dynamical Coulomb gap function (arguments of $\phi_n^{PP(A)}$ are omitted):

$$\phi_n^{c,dyn}(\xi) = -T \int_{-E_{cut}^c}^{E_{cut}^c} d\xi' N(\xi') \left[\sum_{\omega_{n'} = \omega_0}^{\omega_{cut}^{c,pp}} \frac{\alpha_{nn'}^{c+}(\xi\xi')\phi_{n'}(\xi')}{\Theta_{n'}(\xi')} + \{\phi_n^{PPA} - \phi_n^{PP}\} \phi_{const}(\xi') \right]. \quad (2.4.18)$$

2.4.2.2 Static contribution

Most former studies in the field of superconductivity were restricted to static Coulomb interaction. The reason is that the Coulomb interaction acts much faster (on the scale of the plasma frequency) than the phonon-mediated one. It seems plausible to be considered as instantaneous, neglecting its frequency dependence $V_{kk'}^c(\omega) = V_{kk'}^c(0)$ all together. Then it is a real-valued quantity that does not contribute to α^c (eq. 1.4.39). The static part of the Coulomb interaction contributes to the static part of the gap ϕ_{stat}^c (eq. 2.4.13):

$$\phi_{stat}^c(\xi) = -2T \int_{-E_{cut}^c}^{E_{cut}^c} d\xi' N(\xi') K_{stat}^c(\xi\xi') \sum_{\omega_{n'} = \omega_0}^{\omega_{cut}^c} \frac{\phi_{n'}(\xi')}{\Theta_{n'}(\xi')}, \quad (2.4.19)$$

where $\phi_{n'}(\xi') = \phi_{n'}^{ph} + \phi_{stat}^c(\xi')$. The above Matsubara summations can be further simplified by imposing the high frequency limits of the phononic parts of the self energy: $Z_n^{ph} \rightarrow 0$ (i.e. the total $Z \rightarrow 1$) and $\phi_n^{ph} \rightarrow 0$ for $\omega_n \rightarrow \omega_{cut}^{ph}$. By choosing $\omega_{cut}^{c,stat} \geq \omega_{cut}^{ph}$ we can rewrite the eq. 2.4.19 as:

$$\phi_{stat}^c(\xi) = -2T \int_{-E_{cut}^c}^{E_{cut}^c} d\xi' N(\xi') K_{stat}^c(\xi\xi') \left[\sum_{\omega_{n'} = \omega_0}^{\omega_{cut}^{c,stat}} \frac{\phi_{n'}(\xi')}{\Theta_{n'}(\xi')} + \sum_{\omega_{n'} = \omega_{cut}^{c0}}^{\omega_{\infty}} \frac{\phi_{stat}^c(\xi')}{\omega_{n'}^2 + \xi'^2 + [\phi_{stat}^c(\xi')]^2} \right],$$

where, as one can see, the upper limit of the Matsubara sum is extended to infinity. Using again

¹¹The condition $Z_n \rightarrow 1$ also should be fulfilled for $\omega_n \geq \omega_{cut}^{c,pp}$.

that the infinite sum (eq. 2.3.3) in the expression for ϕ_{stat}^c can be summed exactly, we find:

$$\phi_{stat}^c(\xi) = -2T \int_{-E_{cut}^c}^{E_{cut}^c} d\xi' N(\xi') K_{stat}^c(\xi\xi') \left[\sum_{\omega_{n'}=\omega_0}^{\omega_{cut}^{c,stat}} \frac{\phi_{n'}(\xi')}{\Theta_{n'}(\xi')} + \{A(\xi') - B(\xi')\} \phi_{stat}^c(\xi') \right], \quad (2.4.20)$$

$$A(\xi') = \frac{1 - 2f(E(\xi'))}{4TE(\xi')}, \quad B(\xi') = \sum_{\omega_{n'}=\omega_0}^{\omega_{cut}^{c,stat}} \frac{1}{\omega_{n'}^2 + [E(\xi')]^2}, \quad (2.4.21)$$

with $E(\xi') = \sqrt{\xi'^2 + [\phi_{stat}^c(\xi')]^2}$.

All the discussion above has assumed that we do not have any dynamical Coulomb contribution to the interaction. If the dynamical term is present, the $\phi_{n'}$ contains the $\phi_{n'}^{c,dyn}$ as well and the cutoff frequency $\omega_{cut}^{c,stat}$ has to be taken above the plasmonic energy (i.e., $\sim \omega_{cut}^{c,pp}$ from the previous section).

2.4.2.3 μ^* approach

An even further simplification in the calculation of $\phi_{stat}^c(\xi)$ can be achieved by taking a flat DOS and a flat K_{stat}^c in the eq. 2.4.20. This approximation (introduced in ref. [12, 13]) is extremely popular in computational superconductivity although it does not have a good justification. Within this approximation we assume $N(\xi) = N_F$ and $K_{stat}^c(\xi\xi') = V^c$ and obtain for the (now, energy-independent) Coulomb gap ($\phi_{stat}^c(\xi) \rightarrow \phi_{\mu^*}^c$):

$$\phi_{\mu^*}^c \left(1 + 2T\mu \int_{-E_{cut}^c}^{E_{cut}^c} d\xi' [A(\xi') - B(\xi')] \right) = -2T\mu \int_{-E_{cut}^c}^{E_{cut}^c} d\xi' \sum_{\omega_{n'}=\omega_0}^{\omega_{cut}^{c,\mu}} \frac{\phi_{n'}}{\Theta_{n'}(\xi')}, \quad (2.4.22)$$

where $\mu = N_F V^c$ is units-independent measure of the interaction. After rearranging the terms, we get:

$$\phi_{\mu^*}^c = -2T\mu_1^* \int_{-E_{cut}^c}^{E_{cut}^c} d\xi' \sum_{\omega_{n'}=\omega_0}^{\omega_{cut}^{c,\mu}} \frac{\phi_{n'}}{\Theta_{n'}(\xi')}, \quad (2.4.23)$$

$$\mu_1^* = \frac{\mu}{1 + 2T\mu \int_{-E_{cut}^c}^{E_{cut}^c} d\xi' [A(\xi') - B(\xi')]}. \quad (2.4.24)$$

where μ^* is the so called Coulomb pseudopotential. Such pseudopotential approach was first introduced by Scalapino [13] *et. al.* in the real axis Eliashberg formalism and expression for μ^* was written as:

$$\mu_0^* = \frac{\mu}{1 + \mu \ln E_{cut}^c / \omega_{cut}^{c,\mu}}. \quad (2.4.25)$$

Simple tests show that formulas 2.4.24 and 2.4.25 give almost the same value of μ^* (differences will be discussed in sec. 2.5.6).

The final form in which eq. 2.4.23 was tested and implemented in the present work is:

$$\phi_{\mu^*}^c = -2T \frac{\mu^*}{N_F} \int_{-E_{cut}^c}^{E_{cut}^c} d\xi' N(\xi') \sum_{\omega_{n'}=\omega_0}^{\omega_{cut}^{c,\mu}} \frac{\phi_{n'}}{\Theta_{n'}(\xi')}. \quad (2.4.26)$$

where we have reintroduced the factor $N(\xi)/N_F$ in order to have a minimal way to account for the material's density of states. Obviously this μ^* approach is an oversimplification of the Coulomb problem in superconductors, nevertheless due to its popularity we will consider it and present results in sec. 3.1.

2.4.3 Summary of approximation schemes and nomenclature

The final and complete set of Eliashberg equations solved in this work is summarized here as:

$$\begin{cases} Z_n(\xi) &= 1 + Z_n^{ph,m} + Z_n^{c,dyn}(\xi) \\ \phi_n(\xi) &= \phi_n^{ph,m} + \phi_{stat}^c(\xi) + \phi_n^{c,dyn}(\xi) \end{cases} \quad (2.4.27)$$

We will refer to this as full dynamical Eliashberg equations. The static approximation is done by removing all the dynamical terms (labeled as 'dyn'). Finally, the μ^* approximation is obtained by substituting ϕ_{stat}^c by $\phi_{\mu^*}^c$. The equations for $Z^{ph,m}$, $Z^{c,dyn}$, $\phi^{ph,m}$, ϕ_{stat}^c and $\phi^{c,dyn}$ are also collected in appendix D.1.

The effect of the electron-paramagnon interaction is treated together with electron-phonon interaction (sec. 2.4), and can be eliminated setting $K^m = 0$ in eq. 2.4.2.

Multiband Generalization.

All the derivation so far was done in a fully isotropic form. In certain cases one needs to account for the band anisotropy of the system. For example, in the case of MgB₂ the experiments observe two distinct quasiparticle gaps: the first one ($\Delta_\sigma \sim 7.0 - 7.1$ meV) is attributed to σ bands, while the second one ($\Delta_\pi \sim 2.3 - 2.8$ meV) to π bands¹². To have a minimal (but still accurate) description of this behavior we construct the so called multiband approximation in which the averaging procedures described in sec. D.2 are performed on an arbitrary number of blocks of bands. If the number of blocks is not large the method is still much more efficient and computationally cheaper than a fully anisotropic calculation.

The formal routine of doing that is the following. Suppose we divide the band structure into few subsets (blocks) $b_1, b_2 \dots b_B$ of bands. In each of these blocks we formally take an isotropic limit:

$$\phi_b(\xi) = \sum_{k \in b} \phi_k \delta(\xi_k - \xi), \quad (2.4.28)$$

were the state index (k) sum is running over the chosen subset (b). Clearly, each subset will have its own contribution $N_b(\xi)$ to the total DOS function ($N(\xi) = \sum_b N_b(\xi)$). In this fashion one can derive block-band (multiband) resolved Eliashberg equations, given in appendix D.2. The final multiband equations in the case of the *ab-initio* static Coulomb interaction are:

$$\begin{cases} Z_b &= 1 - \frac{T}{\omega_n} \sum_{b' \omega_{n'}} \int d\xi' N_{b'} \frac{K_{bb'}^{ph-} Z_{b' \omega_{n'}}}{\Theta_{b'}}, \\ \phi_b^{ph} &= -T \sum_{b' \omega_{n'}} \int d\xi' N_{b'} \frac{K_{bb'}^{ph+} \phi_{b'}}{\Theta_{b'}}, \\ \phi_{b,stat}^c &= -2T \sum_{b'} \int d\xi' N_{b'} K_{bb'}^c \left[\sum_{\omega_{n'}} \frac{\phi_{b'}}{\Theta_{b'}} + A_{b'} - B_{b'} \right], \\ \Theta_b &= [Z_b \omega_n]^2 + \xi^2 + \phi_b^2, \end{cases} \quad (2.4.29)$$

where all energy/frequency arguments of ϕ , Z and Θ are omitted for simplicity.

2.5 Convergence and tests

Before applying the Eliashberg equations in this new form to real materials, we will first investigate their properties by studying some model systems (described in detail in sec. 2.5.1). The goal of this investigation is *first* to obtain an understanding of the global properties of this form of the

¹²(these ranges of experimental values is reported in ref. [86])

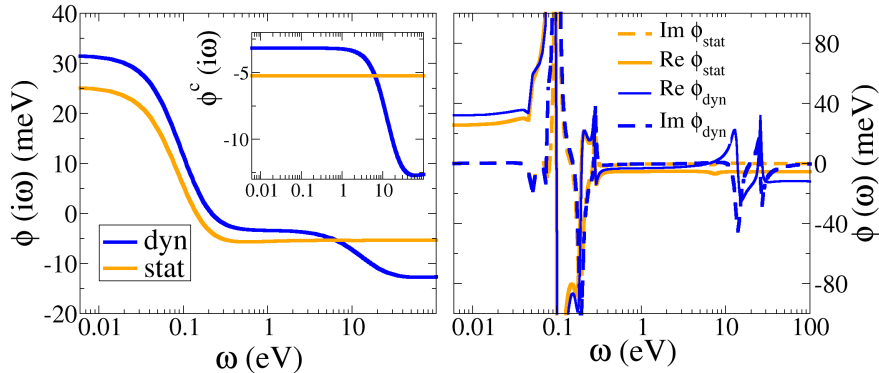


Figure 2.1: The frequency behavior of the total gap function $\phi = \phi^{ph} + \phi^c$ in imaginary (left) and real (right) frequency domain. Results with the static Coulomb interaction (i.e., $\alpha \rightarrow 0$ in eq. 2.5.1) are also given. The inset on the left panel shows the Coulomb contribution ϕ^c to the total gap.

Eliashberg equations, before introducing the additional complexity found in real systems; *second* to study basic convergence issues as the relevant energy scales for frequency and energy integrations in the presence of high energy players like plasmons.

The magnetic correlations will be neglected (this implies the $K^m = 0$ in eq. 2.4.2), hence, a simpler notations will be used, i.e. Z^{ph} and ϕ^{ph} instead of $Z^{ph,m}$ and $\phi^{ph,m}$ respectively. Finally, we consider the static *ab-initio* (sec. 2.5.5) and μ^* -based (sec. 2.5.6) approaches for the gap function.

Models are taken to mimic a realistic system, hence, one can expect the convergence to be similar for real materials that we will study in Chapter 3. Actually, we can already anticipate that this is exactly the case. The cut off studies investigated in this section are prototypical of the convergence behavior that we have observed in real materials.

2.5.1 Models

We adopt two models:

Model A: This first one is a minimalistic model that allows for using a simplified version of the Equations and therefore to have a cross check of the implementation. In this model we assume that all interactions are energy (ξ in our formulation) independent. In frequency, the phononic pairing (eq. 2.2.20) is given by a single Einstein mode (δ -function), and the Coulomb part by a plasmon pole approximation (sec. 1.4.4) and a $\xi\xi'$ -independent static part. Multiplied by a ξ -independent DOS the Coulomb part reads:

$$\begin{aligned} N_F K_{nn'}^c &= N_F (K_{stat}^c + \alpha_{nn'}^c) \\ &= \mu \left(1 + \alpha \frac{\nu_{nn'}^2}{\omega_p^2 + \nu_{nn'}^2} \right). \end{aligned} \quad (2.5.1)$$

In this formulation the strength of the static part is modulated by μ and of the dynamical part by $\mu\alpha$. The resulting simplified form of the Eliashberg equations is presented for completeness in Appendix D.3. The parameters of the model are: phonon energy $\omega_{ph} = 50$ meV, $\lambda^{ph} = 1$, plasmon of $\omega_p = 1$ Ry and Coulomb parings are given by $\mu = 0.5$ and $\alpha = 0.5^{13}$. For this model we will also ignore the mass renormalization effect, i.e. we assume $Z = 1$.

¹³Cut off parameters E_{cut} , ω_{cut}^{ph} and ω_{cut}^c are fixed to 5, 1 and 22 Ry. Infinite tails in Matsubara sums like in the eq. 2.4.18 and 2.4.20 are excluded for simplicity and assumed to be irrelevant for qualitative analysis.

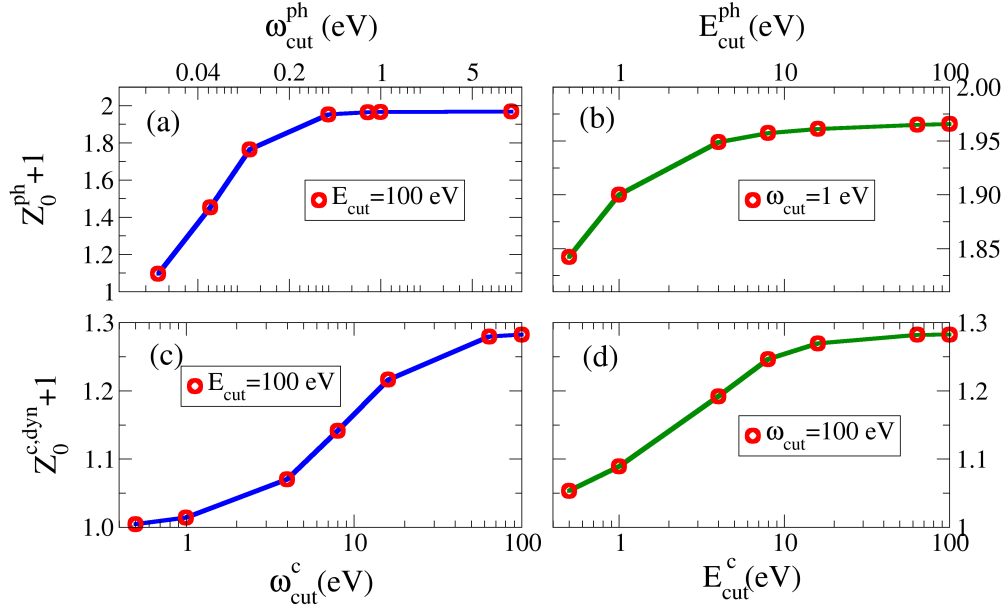


Figure 2.2: Convergence behavior of summations/integrations involved in Eliashberg equations for Z with respect to cut offs. Convergence of the Z^{ph} part of the SE with respect to: (a) ω_{cut}^{ph} (E_{cut}^{ph} is fixed to 100 eV), (b) E_{cut}^{ph} (ω_{cut}^{ph} is fixed to 1 eV). Convergence of the $Z_0^{c,dyn}$ ($\xi = \xi_F$) with respect to: (c) ω_{cut}^c ($E_{cut}^c = 100$ eV), (d) E_{cut}^c ($\omega_{cut}^c = 100$ eV).

Model B: This second model is constructed from an electron gas of $E_F = 11.6$ eV, where we consider an Einstein phonon pairing of $\omega_{ph} = 50$ meV (like for model **A**) but including a line width of ~ 8 meV to make it more physical. Dynamical Coulomb pairing is assumed in the RPA approximation for the electron gas, therefore, constructed from the Lindhard theory discussed in sec. 1.4.5, while the static Coulomb interaction is given by the Thomas-Fermi theory. As result, the electronic part of the interaction is:

$$K_{nn'}^c(\xi\xi') = K_{TF}^c(\xi\xi') + \alpha_{nn'}^c(\xi\xi'), \quad (2.5.2)$$

$$\alpha_{nn'}^c(\xi\xi') = \int_0^\infty \frac{2\omega}{\pi} K_{lind}^c(\xi\xi'\omega) \left\{ \frac{1}{\omega^2 + \nu^2} - \frac{1}{\omega^2} \right\} d\omega, \quad (2.5.3)$$

where the kernels K_{TF}^c and K_{lind}^c are given by eq. 1.4.43 and 1.4.52 respectively. The electronic density of states (per spin) for the electron gas is:

$$N(\xi) = \frac{\sqrt{\xi + E_F}}{4\pi^2} \quad (2.5.4)$$

2.5.2 Model A

Solving the Eliashberg equations (for model **A** a simplified version of those is presented in sec. D.3) at $T = 10$ K, we get the self-consistent total gap $\phi = \phi^{ph} + \phi^c$ plotted in fig. 2.1 as a function of frequency¹⁴ (we display separately the Coulomb gap ϕ^c in the inset of the figure to highlight the plasmonic contribution). The imaginary frequency domain shows the dip of the total gap in high frequency and increase in the low frequency limit in comparison with static case in Coulomb (fig.

¹⁴As soon all our model kernels are $\xi\xi'$ -independent, the resulting gap function is also a ξ -independent function.

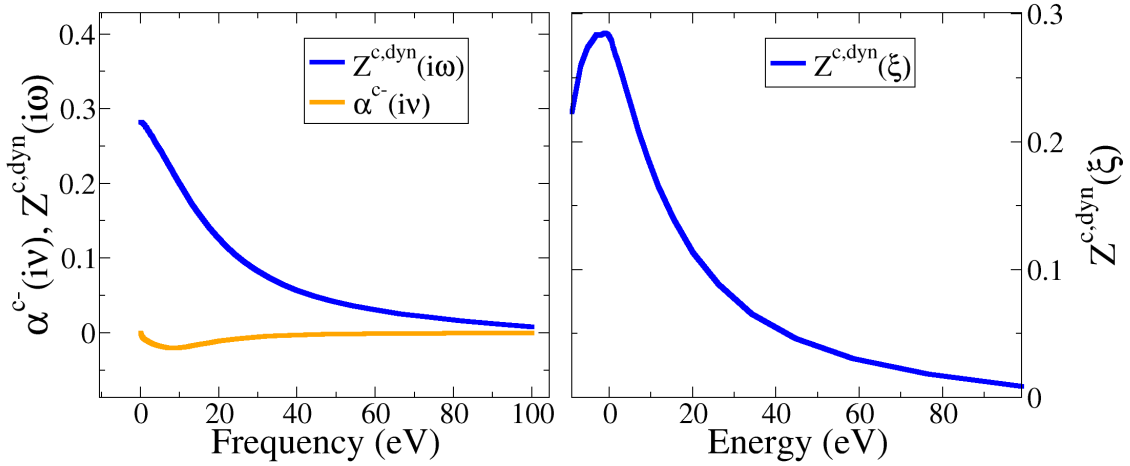


Figure 2.3: (left) Frequency-dependence of the coupling (α^{c-}) and mass renormalization ($Z^{c,dyn}$), both given at the Fermi level ($\xi\xi' = \xi_F$). (right) Plot of $Z^{c,dyn}(\xi)$ for $i\omega_n = i\omega_0$. All units are eV.

2.1, left). This increase of low-frequency gap is a support of the superconducting state, showing that introduced frequency structure of the Coulomb interaction is a source of the superconducting pairing. Note how the gap at zero has increased by about 24%.

More information can be extracted by looking at the same functions on the real axis as obtained by analytic continuation (shortly discussed in sec. 2.2.2). On this physical axis one clearly sees the contribution of phonons at their 50 meV structure, and at higher energy the structure due to plasmons. While the structure of the gap is completely different on the Matsubara and the real frequency axis (left and right of fig. 2.1), it is important to notice that the fingerprint energy scale of the interactions can be clearly observed in both.

2.5.3 Model B: Convergence of the mass renormalization (Z)

In this section we solve equations first for Z^{ph} (eq. 2.4.9) than for $Z^{c,dyn}$ (eq. 2.4.10) ignoring completely contribution of the superconducting gap (normal state). The trends towards the main convergence parameters (see also sec. 2.4.1) are shown in fig. 2.2.

Phonon contribution

In the Matsubara summation for Z^{ph} (eq. 2.4.9) due to the low energy scale of phonons, we observe a fast convergence. And the required cut-off ω_{cut}^{ph} results to be just one order of magnitude larger than the phononic energy scale. In this case, the $1/\Theta_{n'}(\xi') \sim 1/(\omega_{n'}^2 + \xi'^2)$ with small $\omega_{n'}$ insures a fast convergence of the integral over ξ' (with respect to the cut off E_{cut}^{ph}). The corresponding convergence results are presented in fig. 2.2. One can see, that changing the E_{cut}^{ph} from 1 to 10 eV leads to a variation of Z_0^{ph} of 2%, which means that the main contribution to the integral is within the 1 eV interval.

Coulomb contribution

To converge the Matsubara sum in the Coulomb part (eq. 2.4.10) is more challenging, because of the larger energy range of the Coulomb interactions. We cut this sum by ω_{cut}^c and try to reach convergence with respect to this parameter. In this case, the presence of $1/\Theta_{n'}(\xi')$ factors for large $\omega_{n'}$ makes the convergence of the energy integral slower. The convergence investigation presented in fig. 2.2 assumes $Z^{ph} = 0$. Clearly, that for the full convergence we need a cut off of about 100 eV both for ω_{cut}^c and E_{cut}^c . The reason is that, unlike phonons, plasmons have a huge energy scale, as compared to the superconductivity problem. In fact, as shown in fig. 2.3, they induce structures

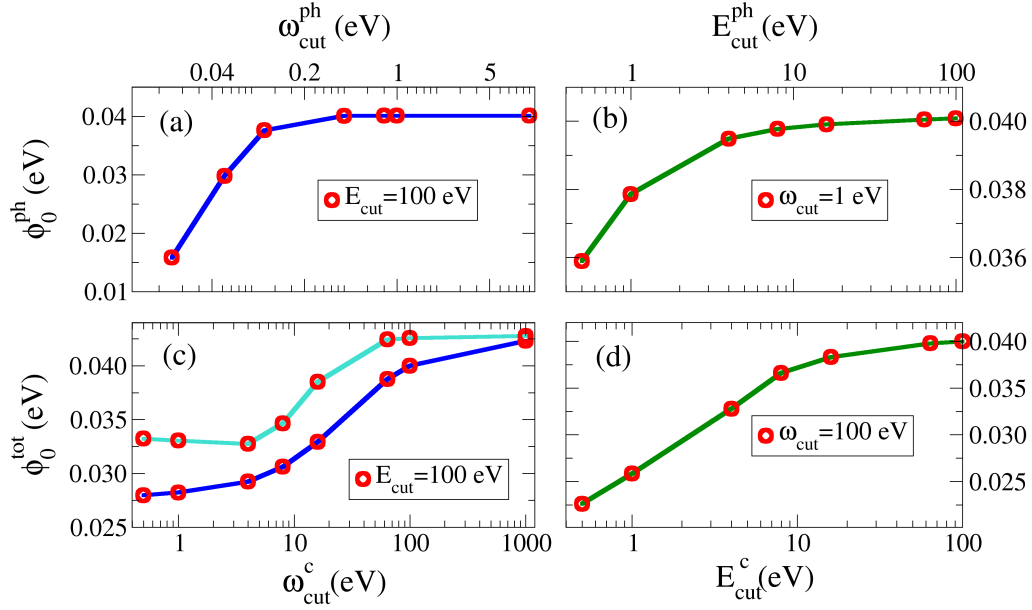


Figure 2.4: Convergence behavior of summations/integrations involved in Eliashberg equations for ϕ with respect to cut offs. Convergence of the ϕ^{ph} part of the SE with respect to: (a) ω_{cut}^{ph} (E_{cut}^{ph} is fixed to 100 eV), (b) E_{cut}^{ph} (ω_{cut}^{ph} is fixed to 1 eV). Convergence of $\phi_0^{tot}(\xi = \xi_F) = \phi^{ph} + \phi_{stat}^c + \phi^{c,dyn}$ with respect to: (c) ω_{cut}^c ($E_{cut}^c = 100$ eV), (d) E_{cut}^c ($\omega_{cut}^c = 100$ eV). At (c) light blue /blue correspond to using/neglecting the plasmon pole tail contribution (see text).

and variations up to high energy and frequency both in the Z function and in the coupling:

$$\alpha^{c-}(i\nu_{nn'}) = \alpha_{nn'}^{c-}(\xi_F \xi_F) = K_{nn'}^c(\xi_F \xi_F) - K_{n,-(n'+1)}^c(\xi_F \xi_F).$$

2.5.4 Model B: Convergence of the gap (ϕ)

To study the convergence of the ϕ part of the gap equation we fix the mass renormalization function to $Z = 1$. The convergence curves for ϕ^{ph} and total ϕ (eq. 2.4.11) are shown in fig. 2.4. It is clearly seen that similarly to what was observed in the previous section for Z , the Coulomb part shows a much slower convergence than the phononic part. The static Coulomb gap ϕ_{stat}^c will be discussed in the next section, for the time being we focus on the dynamical part.

The most important result is shown in fig. 2.4 (c), from which it is clear that convergence with respect to ω_{cut}^c is numerically extremely difficult. As it is achieved only above 1000 eV. For a real material this would clearly have an enormous computational cost. However as discussed in sec. 2.4.2.1, we have introduced an approximation for which we split the frequency sum into two parts. Above the cut off $\omega_{cut}^{c,pp}$ the sum is carried out analytically to infinity but on a plasmon pole model. Therefore, the convergence should be checked with respect to the parameter $\omega_{cut}^{c,pp}$. This is shown in the light blue curve in 2.4 (c). Clearly the convergence is much faster; sufficiently faster to perform calculations on real systems. It is concluded, that we can stick to a cut off $\omega_{cut}^{c,pp} \sim 100$ eV using the plasmon pole tail contribution. E_{cut}^c possess no further problems and can be safely taken on the order of magnitude of 100 eV.

The converged gap functions and kernel:

$$\alpha^{c+}(i\nu_{nn'}) = \alpha_{nn'}^{c+}(\xi_F \xi_F) = K_{nn'}^c(\xi_F \xi_F) + K_{n,-(n'+1)}^c(\xi_F \xi_F),$$

are plotted in fig. 2.5.

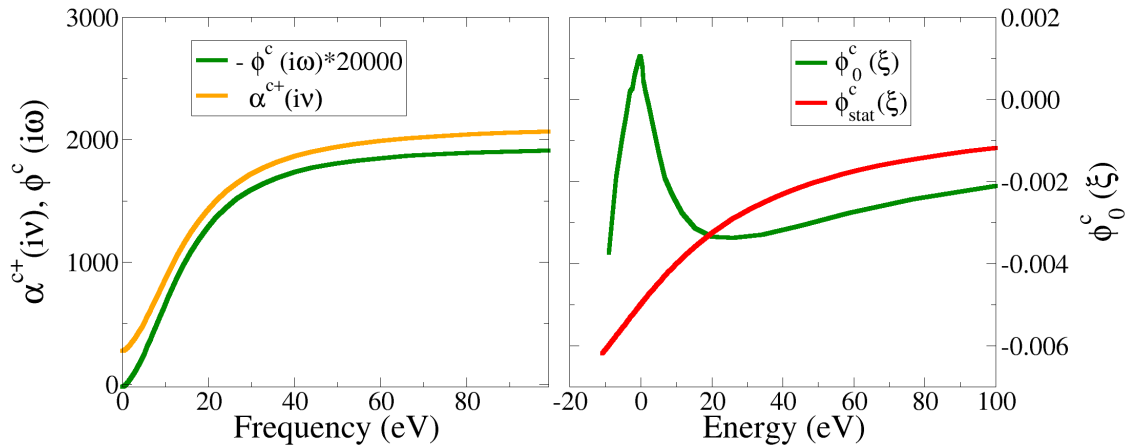


Figure 2.5: (left) Frequency-dependence of the coupling (α^{c+}) and the Coulomb part of the gap ($\phi^c = \phi_{stat}^c + \phi^{c,dyn}$), both given at the Fermi level ($\xi\xi' = \xi_F$). Note that the α^c in principle diverges at $\xi = \xi'$, which results in an extremely high value in the figure. (right) Plot of $\phi_0^c(\xi)$ (full dynamical calculation) and $\phi_{stat}^c(\xi)$ (purely static approach). All units are eV.

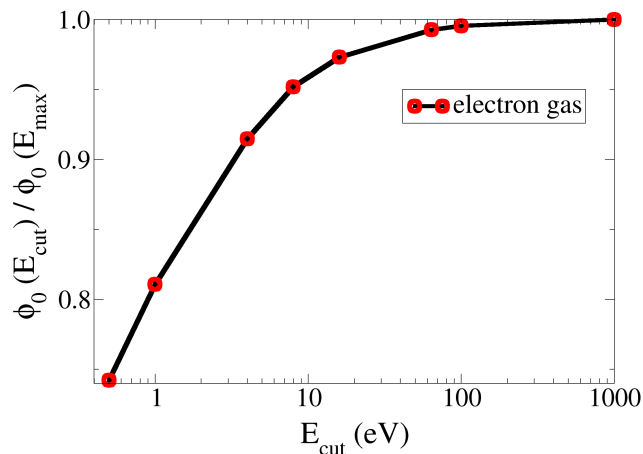


Figure 2.6: Convergence of the total gap function ($\phi_0 = \phi_0^{ph} + \phi^c(\xi = \xi_F)$) with integration cut off E_{cut}^c for the electron gas with $E_F = 11.6$ eV.

On the energy axis one can observe that the low frequency ($n = 0$) Coulomb part of the gap is positive in the presence of dynamical interactions. In our case this means that it has the same sign as the phononic one. It is therefore supporting superconductivity. However, this important issue on the possibility of plasmonic superconductivity will be dropped for the moment. We will come back to this issue in chap. 3 (sec. 3.3).

2.5.5 Static Coulomb kernel

Neglecting any dynamical contribution on the Coulomb interaction (of model **B**) makes the Matsubara sum within $\phi_{stat}^c(\xi)$ (eq. 2.4.20) convergent already at the phononic cutoff, i.e. $\omega_{cut}^{c,stat} = \omega_{cut}^{ph}$, although one should keep in mind that above this cut off, we also include the infinite Matsubara tail contribution as given in eq. 2.4.20. The convergence with respect to E_{cut}^c is shown in fig. 2.6.

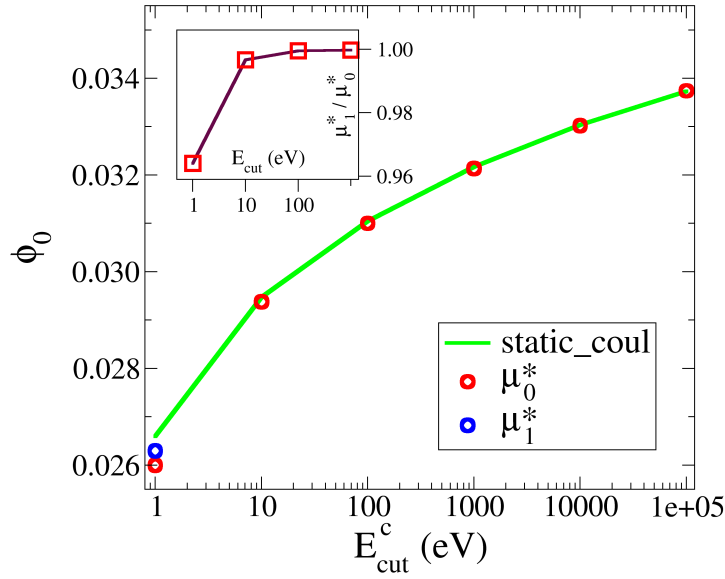


Figure 2.7: Variation of low-frequency total gap ($\phi_0 = \phi_{\mu^*}^c(\phi_{stat}^c) + \phi_0^{ph}$) for the presented model with E_{cut}^c in its full treatment (solid line) and within the reduced μ^* approach ($\mu^* = \mu_0^*$ red dots). The blue dot on the graph is the result of μ^* calculation for a given model, with value of μ^* evaluated via eq. 2.4.24 ($\mu^* = \mu_1^*$). The insets shows a relative variation of μ_1^*/μ_0^* with E_{cut}^c , entering formulas of eq. 2.4.24 and eq. 2.4.25.

2.5.6 Comparison with the μ^* approach

The analytic map of the whole effect of the Coulomb interaction to a single parameter μ^* is provided by two assumptions: a flat DOS and a flat K_{stat}^c (sec. 2.4.2.3). First of all, we would like to show, that this analytical map is exact, i.e., there is no difference between evaluating the gap function of eq. 2.4.20 (with above mentioned assumptions), or first calculate the μ^* , and then to estimate the gap as in eq. 2.4.26.

We stick to some parameters for the model: $N(\xi) = 0.13$ (states/eV/spin) and $K_{stat}^c(\xi\xi') = 1$ (eV) for any $\xi\xi'$. The corresponding value of μ^* is given by eq. 2.4.25. We evaluate the total gap $\phi_n = \phi_{\mu^*}^c(\phi_{stat}^c) + \phi_n^{ph}$ with eq. 2.4.26 (2.4.20) choosing the same cut offs as in the equation for the phonon gap (eq. 2.4.12), i.e., $\omega_{cut}^{ph} = \omega_{cut}^{c,\mu(stat)}$ and $E_{cut}^{ph} = E_{cut}^c$.

In the test we vary the energy cut off ($E_{cut}^c = E_{cut}^{ph}$), fixing all frequency cut offs at $\omega_{cut}^{c,\mu(stat)} = \omega_{cut}^{ph} = 1$ eV. The result is given in fig. 2.7. At the low-energy region, particularly for $E_{cut} = 1$ eV, the result with ϕ_{stat}^c is different from $\phi_{\mu^*}^c$ calculation. The first source of deviation is that we used a real-axis formulation for the μ^* in this test (eq. 2.4.25) instead of eq. 2.4.24. Calculating μ^* via eq. 2.4.24 we get $\mu_1^* = 0.12532$ (against $\mu_0^* = 0.13$, from the eq. 2.4.25), and the corresponding result is marked by a blue dot in the figure. However, using energy cut off E_{cut}^c higher than 10 eV makes both approaches (with ϕ_{stat}^c and $\phi_{\mu^*}^c$) equivalent, independent of the formulation for μ^* .

As the eq. 2.4.25 for μ^* shows, extending the E_{cut}^c to infinity would bring the μ^* to zero and kill completely the effect of the Coulomb interaction. Moreover the behavior would be logarithmic and not convergent at any cutoff. The limit of $E_{cut}^c \rightarrow \infty$ is obtained by neglecting completely the Coulomb part. The resulting phonon only induced gap is $\phi_0 \sim 0.04$ eV.

Chapter 3

Applications

In the previous chapters we have developed a set of Eliashberg equations that lives on the complete electron energy scale, in order to have a tool to account fully from first principles for the Coulomb mediated superconducting pairing. In this chapter we will attempt to apply this method to a set of ten real materials with well known superconducting properties. This set includes some of the most important phononic superconductors, including weak coupling (Al), strong coupling (Pb,Nb) and multiband (MgB_2) cases.

In section 3.1 we will focus on only two of them, and perform an extensive (and very detailed) characterization. We have chosen for this full analysis: MgB_2 and Nb as these are likely the most complex of the set. Then in sec. 3.2 we will present results for the full set. It will be rather evident that within the static Coulomb approximation all materials seem to be quite well described by our theory that predicts critical temperatures in rather good agreement with experimental observations. The inclusion of dynamical Coulomb interactions, will be discussed in sec. 3.3. This worsens the predictivity of the method, leading to significantly overestimated critical temperatures. Eventually we will also discuss the novel approach that involves the introduction of the SCDF correction to the Coulomb self energy (presented in sec. 2.3).

3.1 Superconductivity of Nb and MgB_2 within the static Coulomb interaction

We consider Nb and MgB_2 as examples to present in detail the results of our Eliashberg method. These are two very important materials. Pure bulk Nb as a prototype of a wide class of transition metal superconductors (T_c of Nb is 9.2 K) is broadly studied until today [87, 88, 89, 90]. MgB_2 instead is the phononic superconductor with the highest transition temperature ($T_c = 39$ K) at ambient pressure [79, 91, 92, 81]. The only known superconductor with higher transition temperature is SH_3 very recently discovered but at a pressure of 190 GPa [93, 94]. MgB_2 is also used in industry and has found applications very shortly after its discovery [95].

3.1.1 Normal state properties and pairing interactions

We first present the density of states, the Eliashberg spectral function ($\alpha^2F(\omega)$, eq. 2.2.20), the screened Coulomb interaction given by *ab-initio* static kernel $K_{stat}^c(\xi\xi')$ (discussed in sec. 1.4.3), and in the case of niobium, the spectral function of spin fluctuations ($P(\omega)$, eq. 2.2.24). In addition, the anisotropy of MgB_2 demands, for achieving a correct description, to consider at least

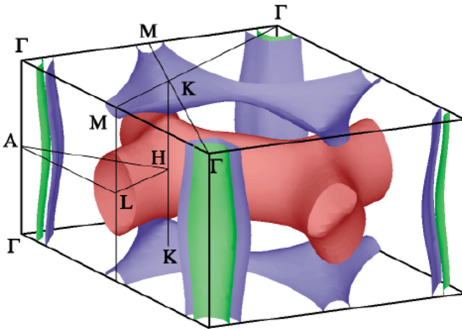


Figure 3.1: Fermi surface of MgB₂ [96]. It is presented by two σ -sheets forming the cylinders along ΓA line, and by two π -sheets in the middle.

a minimal two band anisotropy [97, 79, 81, 15, 92]. This requires a separation of σ and π bands¹ and the introduction of an additional band-block indexing of the Eliashberg equations and listed input quantities, as was discussed in sec. 2.4.3 and D.2.

3.1.1.1 DOS

The Density of states for Nb and MgB₂ is shown in fig. 3.2. The DOS of Nb at the Fermi level has a sharply peaked structure, which originates from the highly localized d bands - typical for most of the transitional metals. This anomalous behavior of the DOS may cause problems, both in the estimation of the electron-phonon coupling and in the superconducting calculations themselves. Localized (flat) bands imply a low Fermi velocity v_F , hence the criteria of applicability of the Migdal's theorem $v_s/v_F \ll 1$ (v_s is the speed of sound) may not be satisfied. This implies that vertex corrections to the SE (discussed in sec. 2.1.3.1 and ref. [98]) may actually be relevant. However, this issue is beyond the scope of the thesis. The niobium DOS at the Fermi level is $N_F = 0.046$ (States/eV/spin/Å³).

The DOS of MgB₂ is given for each band block ($b = \sigma$ or π) component $N_b(\xi)$, where the chosen energy interval for the σ block separation¹ specifies the ξ -interval with non-zero $N_\sigma(\xi)$. The isotropic DOS is also given in this figure and is 0.012 (States/eV/spin/Å) at the Fermi level and $N_\sigma/N_\pi = 0.75$.

3.1.1.2 Electron-phonon interaction

The electron-phonon spectral function is plotted in the same figure (3.2). The corresponding integrated coupling strength (eq. 2.2.21) for niobium is estimated as $\lambda^{ph} = 1.33$. The isotropic coupling strength for MgB₂ is $\lambda_{iso}^{ph} = 0.66$, while its anisotropic contributions² $\lambda_{\sigma\sigma}^{ph}$, $\lambda_{\pi\pi}^{ph}$, $\lambda_{\sigma\pi}^{ph}$

¹Those are separated by an energy interval $[\xi_1, \xi_2]$ and a Brillouin zone division. The Brillouin zone is divided in two parts by a cylinder with radius R located in such a way, that the axis of the cylinder coincides with ΓA symmetry line (see at fig. 3.1 a corresponding Fermi surface (FS) plot). For a given state k , if $\xi_1 \leq \xi_k \leq \xi_2$ and $0 \leq \sqrt{k_x^2 + k_y^2} \leq R$ ($\mathbf{k} = (k_x, k_y, k_z)$), this state belongs to the first band block, otherwise to the second one. Such criteria gives an efficient separation of the FS σ bands (tubes along ΓA) out of the FS π bands (other FS sheets) plus the rest of the band structure, accounting for the needed anisotropy (from now on, we define those blocks of bands with σ and π indices respectively). Values of ξ_1, ξ_2 and R are $-0.12, 0.03$ and 0.311 respectively, given in atomic units.

²The block-band separation for $\alpha^2 F_{bb'}(\omega)$ is equivalent to the one for the Coulomb kernel $K_{bb'}^c(\xi\xi')$, but done at the Fermi level only (because $\alpha^2 F_{bb'}(\omega)$ is defined as a Fermi surface quantity). The band-resolved definition of

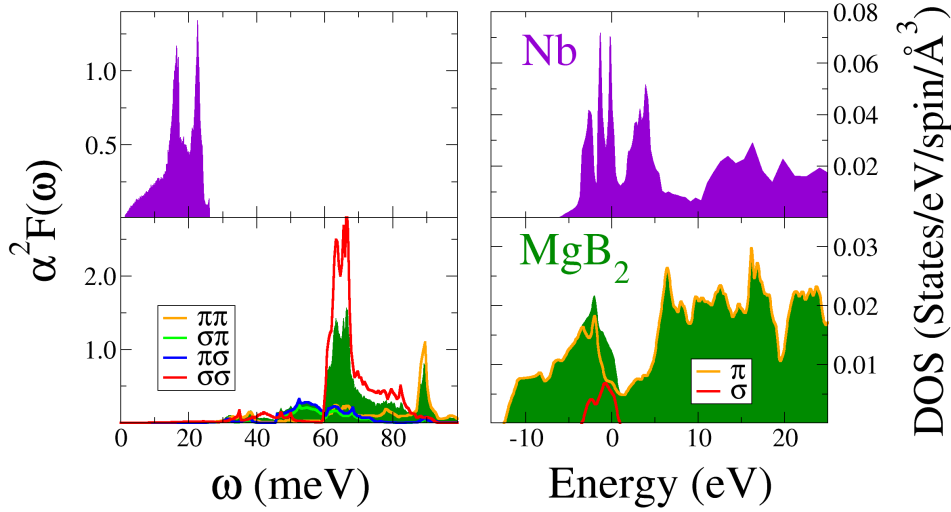


Figure 3.2: Eliashberg spectral functions (left) and DOS (right) for Nb and MgB₂. In the case of MgB₂, a fully isotropic limit is given with green filling, while anisotropic contributions are given by lines (see the text).

and $\lambda_{\pi\sigma}^{ph}$ for MgB₂ are 0.8, 0.26, 0.2 and 0.15 respectively. We know already that the electron-phonon coupling for MgB₂ is hard to converge with respect to the number of \mathbf{q} -points in the conventional electron-phonon calculations, as was demonstrated in ref. [86]. The authors also presented a converged value $\lambda_{iso}^{ph} = 0.748$, and they used a Wannier interpolation to achieve this result. Consequently, our underestimated λ_{iso}^{ph} should lead to the underestimation of T_c .

3.1.1.3 Static Coulomb kernel

As discussed in sec. 2.1.3, the Coulomb interaction in our approach leads to two distinct effects. The first one is exchange and correlation in a GW-like sense (sec. 2.1.3.2), and the second one is due to spin-fluctuations (sec. 2.1.3.4). The screened Coulomb interaction is computed in RPA (sec. 1.4.1.3), while corrections to the RPA are provided by TDDFT-based ALDA approximation (sec. 1.4.1.4).

The RPA-screened static Coulomb kernel K_{stat}^c (eq. 1.4.41) for Nb and MgB₂ is given in fig. 3.3 as color maps. As with the DOS, we normalize it to the unit volume³. All anisotropic contributions for MgB₂ are given together with the fully isotropic limit. The comparison between RPA and ALDA

$\alpha^2 F$ is then follows from the general derivation (given in sec. D.2):

$$\alpha^2 F_{bb'}(\omega) = \frac{1}{N_b} \sum_{k \in b; k' \in b'} \sum_j |g_{kk'}^j|^2 \delta(\xi_k) \delta(\xi_{k'}) \delta(\omega_{\mathbf{k}' - \mathbf{k}}^j - \omega),$$

where the sum over states $k(k')$ is restricted to ones, belonging to a particular block of bands $b(b')$. The corresponding contributions to the effective coupling λ^{ph} are quantitatively estimated via the simple relation:

$$\lambda_{bb'}^{ph} = 2 \int \frac{\alpha^2 F_{bb'}(\omega)}{\omega} d\omega,$$

while the total λ_{iso}^{ph} satisfies:

$$\lambda_{iso}^{ph} = \frac{1}{N_F} \sum_{bb'} N_b \lambda_{bb'}^{ph}.$$

³Which implies a multiplication by the unit cell volume Ω_{WS} (follows from the eq. 1.4.33).

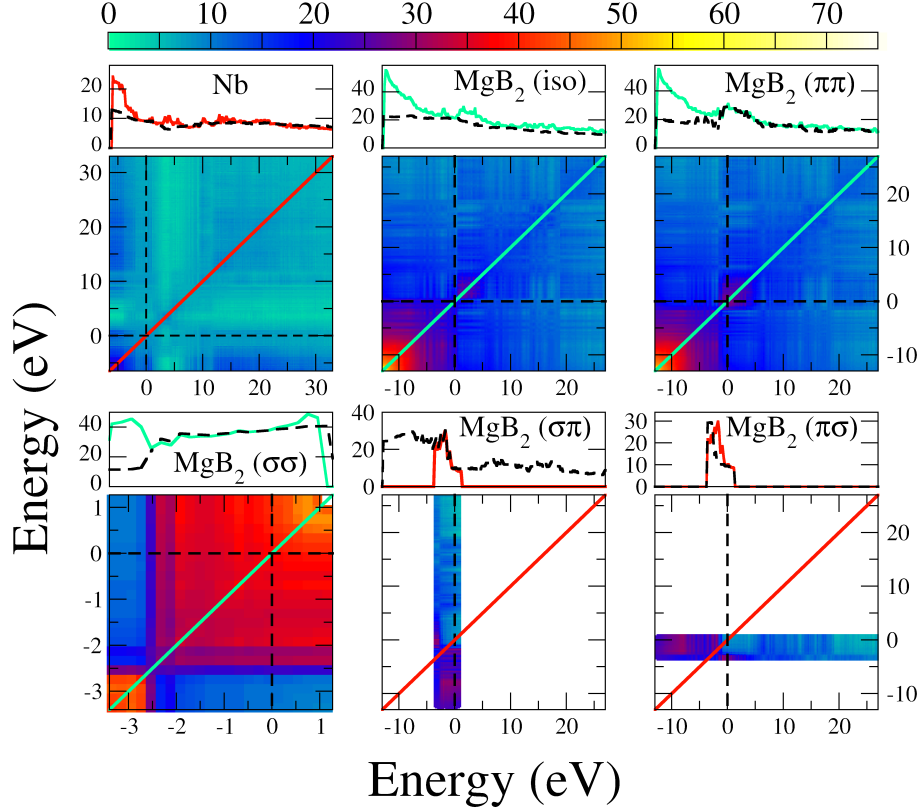


Figure 3.3: Color maps of the static Coulomb interaction kernel for MgB₂ and Nb. All band-resolved components of MgB₂ are also shown on the graph. Diagonal cuts ($K^c(\xi, \xi' = \xi)$, i.e., along solid lines on color maps) and Fermi level cuts ($K^c(0, \xi) = K^c(\xi, 0)$, i.e., along dashed black lines) are given above each color map. All axes (e.g. $\xi\xi'$ of $K^c(\xi\xi')$) are in eV, while the color scale is in eV/Å³

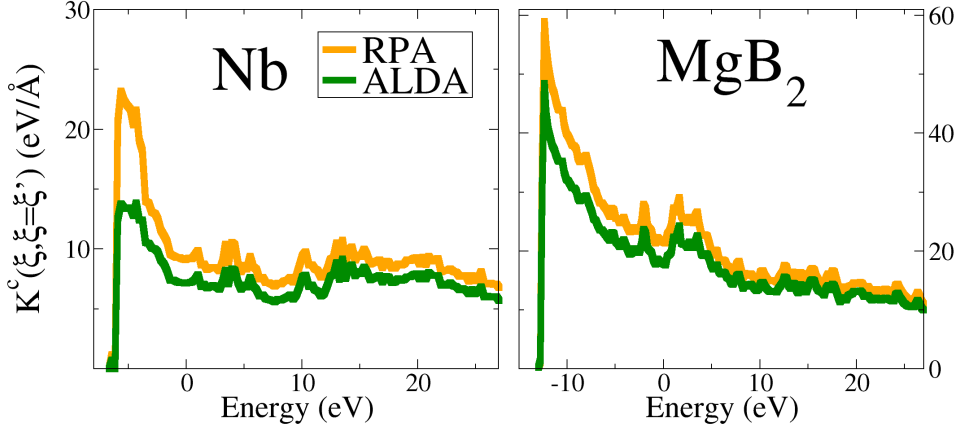


Figure 3.4: Diagonal cuts of the static Coulomb kernel for Nb and MgB₂ respectively; different curves correspond to different models of screening: RPA discussed in sec. 1.4.1.3. ALDA is a TDDFT-based kernel presented in sec. 1.4.1.4.

-screened static kernels ($K_{stat}^c(\xi\xi')$) is presented in terms of diagonal cuts ($K_{stat}^c(\xi, \xi' = \xi)$) in fig. 3.4.

The value of the Coulomb interaction for Nb is about two times lower than for MgB₂, which means that Nb has a significantly better screening. This is due to the fact that the DOS at the Fermi level is almost four times higher than in MgB₂ hence, more electrons participate in the screening. However, in the Eliashberg calculation an integral of the DOS and Coulomb interaction enters (in all equations, collected in sec. D.1), which makes the $\mu = N_F K_{stat}^c(\xi_F \xi_F)$ probably a better number to compare the screening properties. We calculate the RPA μ as 0.47 and 0.256 for Nb and MgB₂ respectively, which is similar to 0.488 and 0.263 known from the literature (refs. [99] and [100]). The anisotropic contributions $\mu_{bb'} = N_{b'}(\xi_F) K_{bb'}^c(\xi_F \xi_F)$ for MgB₂ are also computed as 0.199/0.068/0.052/0.197 for the $\mu_{\sigma\sigma}/\mu_{\sigma\pi}/\mu_{\pi\sigma}/\mu_{\pi\pi}$ components.

The renormalized quantity μ^* enters the traditional Eliashberg approach (sec. 2.4.2.3). In the isotropic case one uses the definition given by eq. 2.4.25, where E_{cut}^c and ω_{cut}^c has to be plugged in. The value for E_{cut}^c is normally an essential electronic energy scale, like the Fermi energy (or chemical potential) or the band width, while the ω_{cut}^c should be the same as a cut off in the Matsubara sum of eq. 2.4.26. We take the $\omega_{cut}^c = 6\omega_{max}^{\alpha^2 F} = 156$ for niobium⁴, where the $\omega_{max}^{\alpha^2 F}$ is the maximum frequency with non-zero $\alpha^2 F(\omega)$ function, while $\omega_{cut}^c = 0.5$ eV for MgB₂. The E_{cut}^c values of 5.23 and 12.43 eV found in the refs. [36] and [100] for Nb and MgB₂ respectively. Using these numbers we get $\mu_{Nb}^* = 0.21$ and $\mu_{MgB_2}^* = 0.142$. Moreover, we can construct a block-band resolved $\mu_{bb'}^*$ out of the mentioned $\mu_{bb'}$ in the same way as in isotropic case (eq. 2.4.25), keeping the ratio E_{cut}^c/ω_{cut}^c unchanged. That gives $\mu_{bb'}^* = 0.121, 0.056, 0.044$ and 0.120 for $\sigma\sigma, \sigma\pi, \pi\sigma$ and $\pi\pi$ blocks.

In addition to the 'charge channel' in Nb, spin-fluctuations (sec. 2.1.3.4) result in strong electron-paramagnon coupling described by the spectral function (sec. 2.2.3.2) presented in fig. B.1 of appendix B.5. The resulting coupling strength (eq. 2.2.26) is $\lambda^{sf} = 0.19$.

3.1.2 Solution of the Eliashberg equations for Nb and MgB₂

Two computational schemes are used in this static limit. The *first* one is a traditional μ^* approach, and the *second* one is our new fully *ab-initio* scheme within this static limit of the Coulomb

⁴The choice of Carbotte (ref. [14]).

| | Nb | MgB ₂ |
|---|---|--|
| N_F (States/eV/spin/Å) | $N_F = 0.046$ | $N_F = 0.012, N_\sigma/N_\pi = 0.75$ |
| λ | $\lambda^{ph} = 1.33$ $\lambda^{sf} = 0.19$ | $\lambda_{iso}^{ph} = 0.66$ $\lambda_{\sigma\sigma}^{ph} = 0.8, \lambda_{\pi\pi}^{ph} = 0.26,$ $\lambda_{\sigma\pi}^{ph} = 0.2, \lambda_{\pi\sigma}^{ph} = 0.15$ |
| μ^* calculated from <i>ab-initio</i> $\mu = K_{stat}^c(\xi_F\xi_F)N_F$ with $K_{stat}^c(\xi_F\xi_F)$ given by the RPA | $\mu^* = 0.21$ ($\omega_{cut}^c = 156$ meV, $E_{cut}^c = 5.23$ eV) | $\mu_{iso}^* = 0.142$ $\mu_{\sigma\sigma}^* = 0.121, \mu_{\sigma\pi}^* = 0.056$ $\mu_{\pi\sigma}^* = 0.044, \mu_{\pi\pi}^* = 0.120$ ($\omega_{cut}^c = 500$ meV, $E_{cut}^c = 12.43$ eV) |
| $T_c^{\mu^*}$ (K) | $T_c^{\mu^*+sf} = 9.5 T_c^{\mu^*} = 14.3$ | $T_c^{\mu_{iso}^*} = 39.9 T_c^{\mu_{bb'}^*} = 31.5$ |
| $\Delta_0^{\mu^*}$ (meV) | $\Delta_0^{\mu^*+sf} = 1.6 \Delta_0^{\mu^*} = 2.5$ | $\Delta_{\sigma}^{\mu_{iso}^*} = 6.8 \Delta_{\pi}^{\mu_{iso}^*} = 1.7$ $\Delta_{\sigma}^{\mu_{iso}^*}/\Delta_{\pi}^{\mu_{iso}^*} = 4.1$ $\Delta_{\sigma}^{\mu_{bb'}^*} = 5.4 \Delta_{\pi}^{\mu_{bb'}^*} = 1.6$ $\Delta_{\sigma}^{\mu_{bb'}^*}/\Delta_{\pi}^{\mu_{bb'}^*} = 3.4$ |
| $\Delta_0^{RPA ALDA}$ (meV) | $\Delta_0 = 1.52 1.61$ | $\Delta_{\sigma} = 5.56 6.14,$ $\Delta_{\pi} = 1.99 2.22$ $\Delta_{\sigma}/\Delta_{\pi} = 2.79 2.76$ |
| $T_c^{RPA ALDA}$ (K) | 13.39 14.31 $T_c^{RPA+sf} = 9.18$ | 31.40 34.38 |
| Δ_0^{exp} (meV) | $\Delta_0^{exp} = 1.5$ | $\Delta_{\sigma}^{exp} = 7.05, \Delta_{\pi}^{exp} = 2.55$ $\Delta_{\sigma}^{exp}/\Delta_{\pi}^{exp} = 2.76$ |
| T_c^{exp} (K) | 9.2 | 39 |

Table 3.1: Numerical estimates of essential properties for Nb and MgB₂

interaction (both summarized in sec. 2.4.3).

Calculations with the μ^* are usually semi-empirical and this value is fitted to get the critical temperature. But for the particular case of Nb and MgB₂ we found all needed ingredients to determine this quantity, hence staying strictly parameter free. The resulting critical temperature for Nb is $T_{c,Nb}^{\mu^*+sf} = 9.5$ K (with the spin fluctuation term included), which is very close to the experimental value of 9.2 K. The low-temperature fundamental gap $\Delta_0 = \Delta(\xi_F, i\omega = 0)$ is 1.6 meV (without spin-fluctuations we get $T_{c,Nb}^{\mu^*} = 14.3$ and $\Delta_{0,Nb}^{\mu^*} = 2.5$ meV). For MgB₂ we do two distinct μ^* calculations. In the first one, we use the isotropic $\mu^* = 0.142$. As result, the effective Coulomb interaction $V^c = \mu^*/N_F$ is isotropic and in multiband calculations we multiply it by block-band⁵ DOS $N_{b'}(\xi')$. The anisotropy is produced in this case by the DOS only. With this scheme we get a $T_c \sim 39.9$ K, which is rather overestimated, in view of underestimated electron-phonon coupling discussed earlier. The fundamental σ and π gaps are $\Delta_{0\sigma}^{\mu^*} = 6.8$ and $\Delta_{0\pi}^{\mu^*} = 1.7$ meV with ratio $\Delta_{0\sigma}^{\mu^*}/\Delta_{0\pi}^{\mu^*} = 4.1$, which is inconsistent with experiment ($\Delta_{\sigma}^{exp}/\Delta_{\pi}^{exp} \sim 2.76$). On

⁵In this case the multiband gap equation reads:

$$\phi_b^c = -2T \frac{\mu^*}{N_F} \sum_{b'} \int d\xi' N_{b'}(\xi') \sum_{\omega_{n'}=\omega_0}^{\omega_{cut}^c} \frac{\phi_{b'n'}}{\Theta_{b'n'}(\xi')},$$

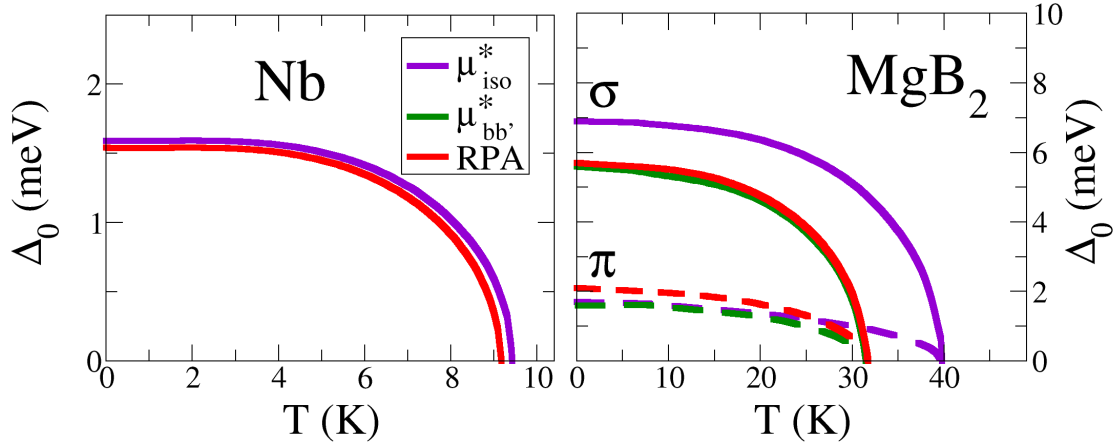


Figure 3.5: Temperature-dependent quasiparticle gap function for Nb and MgB₂ both for μ^* calculations and ones with *ab-initio* static Coulomb kernel.

the other hand, we can improve this result by plugging the anisotropic⁶ $\mu_{bb'}^*$. Doing so, we have obtained fundamental gaps $\Delta_{0\sigma}^{\mu^*} = 5.4$ and $\Delta_{0\pi}^{\mu^*} = 1.6$ (meV) with ratio $\Delta_{0\sigma}^{\mu^*}/\Delta_{0\pi}^{\mu^*} = 3.4$, which is still overestimated. The critical temperature is now lower $T_{c,MgB_2}^{\mu_{bb'}^*} = 31.5$. All essential input and output quantities of the discussed μ^* approach are collected in the tab. 3.1.

The conclusion here should be that, in principle, it is possible to construct μ^* in an *ab-initio* way, but only if one has an estimation of E_{cut}^c in eq. 2.4.25. This cut off may also have a band dependence, which was neglected. It can be viewed as an anisotropic way of renormalizing the Coulomb interaction (i.e., transformation from $\mu_{bb'}$ to $\mu_{bb'}^*$), which may solve the gap ratio problem of the given μ^* calculations. Essentially computing μ^* in this way, seems to us more a way to hide the problem. As we construct an unknown parameter from an ill defined one. From this perspective it is not even surprising that the approach gives still a reasonable result, because the full scheme is constructed not *ab-initio* but by observing that in this way it actually works for conventional superconductors.

In this respect, there is clearly a need for an *ab-initio* approach which takes into account the Coulomb interaction in the full energy range and which solves the gap ratio problem⁷ in MgB₂. This is also important in view of applying the theory to new and different materials (organic, iron based, cuprates) where the *ad hoc* computational schemes invented for known superconductors fail. In many new classes of superconductors (all unconventional in one way or another) the role of Coulomb interactions is still completely open and under discussion.

We now present the results obtained with the *ab-initio* static scheme, where the static Coulomb interaction enters in terms of the kernel K_{stat}^c discussed in sec. 3.1.1.3 (and plotted in fig. 3.3). The resulting low-temperature fundamental gap for Nb is $\Delta_{0,Nb}^{RPA/ALDA} = 1.52/1.61$ (meV) and the critical temperature $T_{c,Nb}^{RPA/ALDA} = 9.18/9.53$ (K) for the RPA/ALDA approaches for the screening. Without the spin fluctuation term those numbers increase in the same way as it was with the μ^*

⁶In the described multiband setup we have to modify corresponding gap equation (eq. 2.4.26) as following:

$$\phi_b^c = -2T \sum_{b'} \frac{\mu_{bb'}^*}{N_{b'}(\xi_F)} \int d\xi' N_{b'}(\xi') \sum_{\omega_{n'}=\omega_0}^{\omega_{cut}} \frac{\phi_{b'n'}}{\Theta_{b'n'}(\xi')},$$

⁷The gap ratio problem in MgB₂ was addressed and solved *ab-initio* within the SCDFt [80, 81], while in investigations within the Eliashberg theory were always a μ^* -dependent calculations.

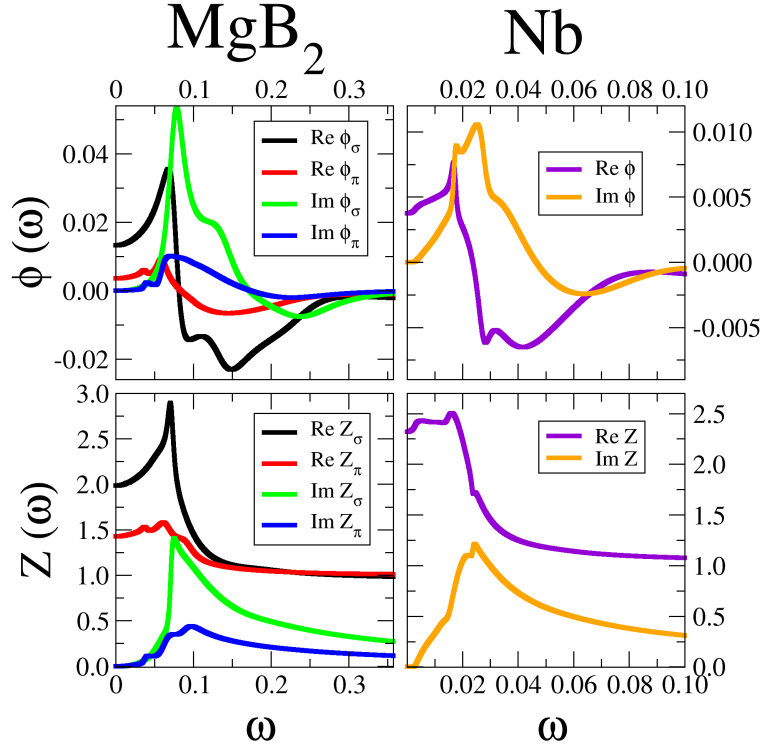


Figure 3.6: Real-frequency $\phi(\xi_F, \omega)$ and $Z(\xi_F, \omega)$ for *ab-initio* static approach. The frequency dependence comes purely from phonons, hence we get similar results with the μ^* calculations, which are not shown here for simplicity.

calculation.

For MgB_2 the T_c we get is lower than the experimental one ($T_{c, \text{MgB}_2}^{\text{RPA/ALDA}} = 31.40/34.38$ K). We attribute this fact to the lower electron phonon coupling (discussed in sec. 3.1.1.2). As was pointed out in ref. [86], the reported experimental values of the low-temperature $\Delta_\sigma^{\text{exp}}$ and Δ_π^{exp} are different. The π gap ranges from 2.3 to 2.8 meV, while the range for the σ gap is 7.0 – 7.1 meV. Hence for the ratio $\Delta_\sigma^{\text{exp}}/\Delta_\pi^{\text{exp}}$ we take the average over reported numbers, which is $\Delta_\sigma^{\text{exp}}/\Delta_\pi^{\text{exp}} \approx 2.76$. Our *ab-initio* calculated low- T gaps within the RPA are $\Delta_\sigma^{\text{RPA}} \sim 5.56$ and $\Delta_\pi^{\text{RPA}} \sim 1.99$ meV hence, the calculated gap ratio $\Delta_\sigma^{\text{RPA}}/\Delta_\pi^{\text{RPA}} = 2.79$ is in excellent agreement with experiments. Gap values for ALDA screening are given in table 3.1. Finally, purely isotropic calculations for MgB_2 resulted in a $T_c = 17.6$ K in our case.

3.1.3 Excitation spectrum and tunneling

As a natural output of the Eliashberg equations, we get the temperature dependence of the fundamental gap shown in fig. 3.5 in comparison with the μ^* results. As discussed in sec. 2.2.2, to compute the tunneling spectrum we have to continue the total Z and ϕ from the imaginary to the real-frequency domain. This is done via the Padé approximant technique [77, 78], and graphs for Z and ϕ within the RPA are shown in fig. 3.6 in the real frequency domain. The ω -structure of Z and ϕ is due to the frequency dependence of interactions, which in the low frequency range is given by the $\alpha^2 F(\omega)$ function. This structure contributes to the measured tunneling DOS $N_{\text{tun}}(\omega)$ (eq. 2.2.13). Thus, from the measured $N_{\text{tun}}(\omega)$ one can deduce the shape of $\alpha^2 F(\omega)$, which is the basis of the tunneling inversion procedure [56].

Two scales of ω are important for us: the gap region, i.e., when $\omega \sim \Delta$, where one can directly observe the quasiparticle gap (as a dip in a $N_{\text{tun}}(\omega)$ for $\omega < \Delta$), and when ω is in the the phononic

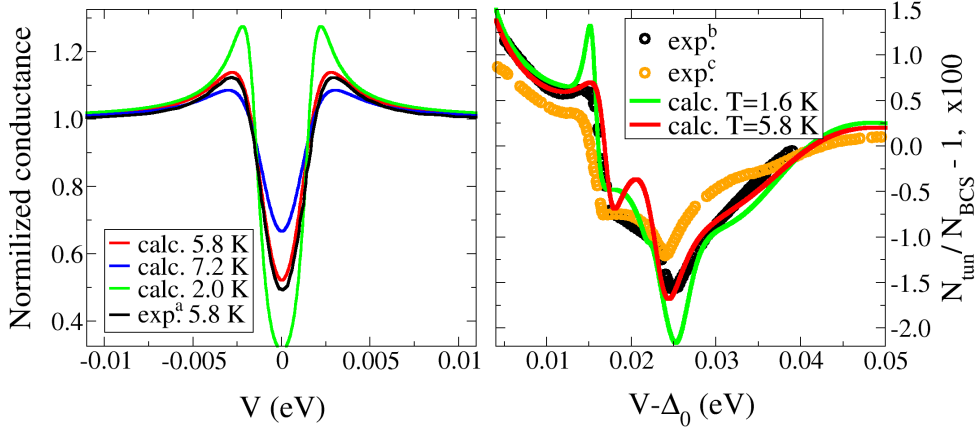


Figure 3.7: Tunneling calculated and experimental data: (left) in the gap energy range and (right) in the phononic energy range, where N_{BCS} is given by $Re[\omega/\sqrt{\omega^2 - \Delta_0^2}]$, i.e. ignoring the frequency dependence of the Δ . The experimental data is from (a) [101], (b) [102] and (c) [57].

energy range, where the structure of $N_{tun}(\omega)$, and, as just discussed, of the $\alpha^2 F(\omega)$ is directly observable. The $N_{tun}(\omega)$ is shown for both energy scales in fig. 3.7 for niobium. For MgB_2 the situation is more complicated, because of its anisotropy. Depending on the orientation of the sample with respect to the tunneling axis, different results are obtained⁸. Because we know that our electron-phonon coupling is lower than it should be, we scale it up about⁹ 8% fitting the calculated T_c to the experimental one for the sake of qualitative comparison. The resulting plots for the calculated and experimental $N_{tun}(\omega)$ are shown in fig. 3.8 (left). The agreement is good.

Surprisingly, the tunneling data at the phononic energy scale (i.e. $\omega \sim \omega^{ph}$) is poorly described in the literature for MgB_2 . We found one reference [104], but the question of anisotropy was not properly studied there, and also the shape of the inverted isotropic $\alpha^2 F(\omega)$ is far too different from what we get fully *ab-initio* and from what was posted recently [86]. In spite of this, we plot only our result for $N_{tun}(\omega)$ for different $\alpha\beta$ (see footnote 8) pairs in fig. 3.8 (right).

3.2 Ab-initio static calculations on a larger set of materials

So far we have investigated only two materials, in order to have enough space to present a complete characterization. However, to validate a new computational/theoretical method one needs to test it on a significant set. This section is devoted to this goal. Eventually, we want to get an idea of how much the predicted critical temperatures deviate from experiments.

⁸ To simulate the variable anisotropy, we can take for the total $N_S(\omega)$ (enters the eq. 2.2.13):

$$N_S^{tot}(\omega) = \alpha N_S^\sigma(\omega) + \beta N_S^\pi(\omega), \quad \alpha + \beta = 1 \quad (3.1.1)$$

$$N_S^{\sigma(\pi)}(\omega) = Re \left[\frac{\omega}{\sqrt{\omega^2 - \Delta_{\sigma(\pi)}^2(\omega)}} \right] \quad (3.1.2)$$

The coefficients α and β are responsible for different directions of the tunneling current. We took $\alpha = 0.13$ and $\beta = 0.87$ as was done in the experimental analysis of ref. [103], and those are empirical parameters which we need.

⁹The experiment we refer to (ref. [103]) is done on the grained samples and consequently, the T_c was lower (37 K) than in the bulk. Hence, the scale of 8% in our $\alpha^2 F(\omega)$ gives a $T_c = 37$ K.

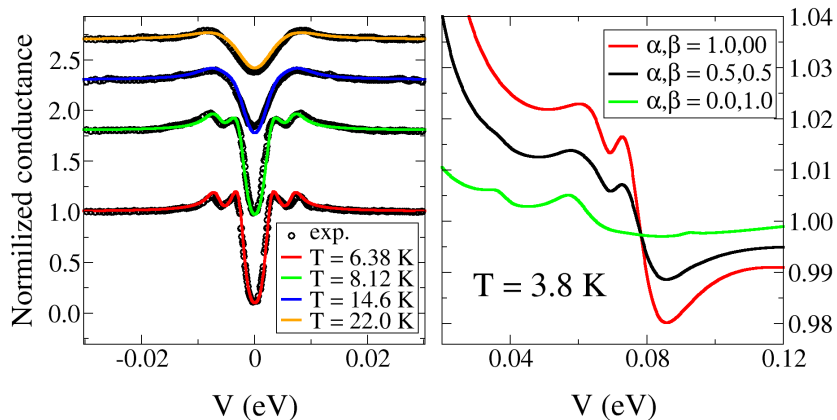


Figure 3.8: Normalized conductance ($\sim N_{tun}(V)$): (left) in the gap energy range and (right) in the phononic energy range. (right) A three cases for $\alpha\beta$ was taken (see eq. 3.1.1 in a footnote 8): first (red) corresponding to taking only σ character ($\alpha = 1, \beta = 0$) into the $N_S(\omega)$ (eq. 3.1.1), second (black) is a mixed case $\alpha = 0.5, \beta = 0.5$, and finally the case of the π character only ($\alpha = 0, \beta = 1$) is shown in green.

3.2.1 Test set of materials

A list of ten phononic superconductors V, Nb, Ta, Al, Pb, Sn, ZrN, CaC₆, V₃Si and MgB₂ is chosen to test our approach. Electronic properties of the chosen systems are different. For example, the densities of states of Al, Pb, Sn are rather smooth in comparison with those of transitional metals and their compounds (see fig. 3.9 and 3.2). Among them, the Pb and Al are traditional examples of the strong and weak coupling superconductors respectively. Coupling strengths for the materials in the set are presented in tab. 3.2 together with other characterizing parameters.

High peaks of the DOS in V, Nb, Ta and V₃Si come from flat d bands, a typical feature of many transition metals, leading to the same issues for the electron-phonon coupling, which we have discussed in sec. 3.1.1.1 for Nb. Moreover, we point out that as soon as the DOS function $N(\xi)$ around the Fermi level is very steep, tiny shifts of the chemical potential (or errors in estimating this quantity) affect the Fermi DOS (N_F) and thus, the $\alpha^2F(\omega)$ (eq. 2.2.20). Consequently, the $\alpha^2F(\omega)$ should probably keep an original energy resolution, i.e., $\alpha^2F(\xi\xi'\omega)$ (eq. 2.2.18), this was neglected for computational convenience. Not less important is the overall shape of $\alpha^2F(\omega)$ (figs. 3.2 and 3.9), that appears to be strongly dependent on the geometry used in calculations. Any phonon calculation has to be performed in an equilibrium geometry. In our calculations we perform internal as well as the lattice relaxations. The lattice relaxation is actually one of the points where the choice of exchange-correlation potential v_{xc} (sec. 1.2.1) is important. We used the PBE functional [105] for all phonon calculations.

3.2.2 Critical temperatures and comparison with experiments

Within this section we use the full *ab-initio* approach in the static limit (sec. 2.4.3). We observe that this scheme is extremely effective and leads to predictions of critical temperatures in a good agreement with experimental observations at reasonably low computational cost.

The Coulomb part is treated with fully *ab-initio* static kernel $K_{stat}^c(\xi\xi')$. The screening has been computed with different approaches: RPA (sec. 1.4.1.3) and with TDDFT-based 'ALDA' (sec. 1.4.1.4). Overall all these approaches show similar qualitative properties and structures, therefore, we give a visualization only for the kernels in the RPA. These are collected in fig. 3.10.

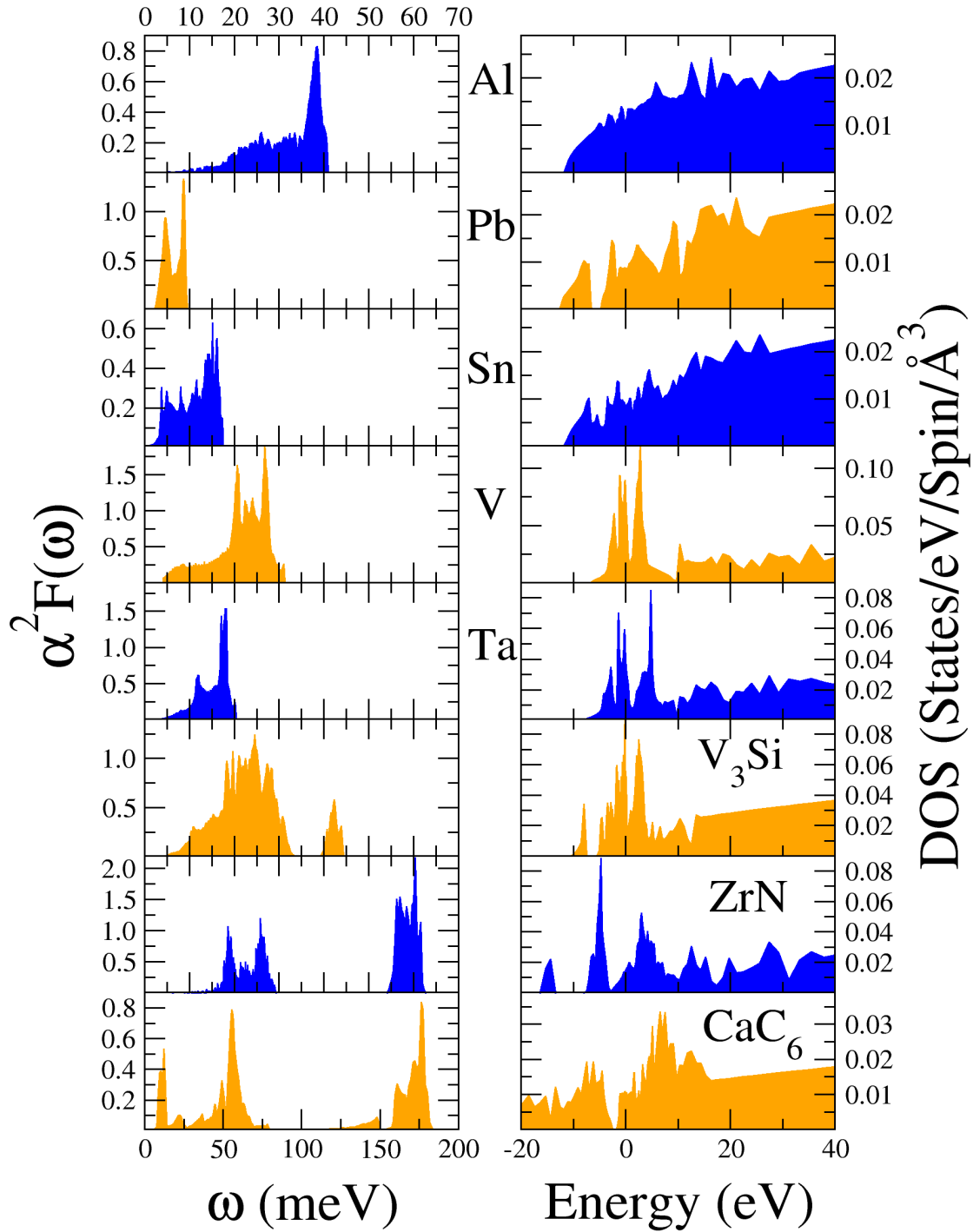


Figure 3.9: Eliashberg spectral functions (left) and the DOS (right) for set of materials.

| mat. | $\lambda^{ph(sf)}$ | $\omega_{log}^{ph(sf)}$ | N_F | $\mu^{RPA ALDA}$ | $T_c^{RPA ALDA ph}$ | | | T_c^{exp} |
|-------------------|--------------------|-------------------------|--------|-------------------|---------------------|------|------|-------------|
| Nb | 1.33 | 12.0 | 0.046 | 0.47 0.37 | 13.3 | 14.1 | 24.1 | |
| (<i>sf</i>) | 0.19 | 1090 | | | 9.1 | 9.6 | 13.1 | 9.2 |
| V | 1.51 | 16.7 | 0.075 | 0.42 0.28 | 21.0 | 23.2 | 35.7 | |
| (<i>sf</i>) | 0.43 | 843 | | | 9.6 | 10.2 | 12.3 | 5.03 |
| Ta | 0.81 | 13.2 | 0.042 | 0.42 0.33 | 6.1 | 6.7 | 14.0 | |
| (<i>sf</i>) | 0.14 | 1129 | | | 3.7 | 4.1 | 6.9 | 4.48 |
| Pb | 1.33 | 5.4 | 0.0086 | 0.21 0.18 | 7.5 | 7.6 | 9.8 | 7.2 |
| Sn | 0.83 | 7.9 | 0.0086 | 0.21 0.18 | 5.2 | 5.4 | 8.6 | 3.72 |
| ZrN | 0.73 | 30.6 | 0.014 | 0.19 0.16 | 13.8 | 14.9 | 27.4 | 10 |
| Al | 0.43 | 26.0 | 0.010 | 0.21 0.17 | 2.3 | 2.7 | 8.3 | 1.2 |
| CaC ₆ | 0.87 | 28.4 | 0.010 | 0.32 0.26 | 11.0 | 12.0 | 33.7 | 11.5 |
| V ₃ Si | 1.43 | 19.6 | 0.055 | 0.39 0.26 | 22.6 | 25.1 | 37.5 | 17 |
| MgB ₂ | 0.66 | 59.1 | 0.012 | 0.26 0.21 | 31.4 | 34.4 | 60.9 | 39 |

Table 3.2: Numerical results for the full set of compounds. Units of ω_{log} , T_c and N_F are meV, K and states/eV/spin/Å respectively. The RPA for Coulomb interaction is considered as the main method of this work and correspondent results are marked with a bold font. Label '*ph*' marks a critical temperatures obtained neglecting the Coulomb interaction.

The overall trend of the interaction is very different for various materials. From the simplicity of Al that, as discussed in sec. 1.4.6, has screening properties very similar to an electron gas, to the complexity of CaC₆, where one observes a rich structure due to the presence in the plotted energy interval of states of very different nature: sp^2 bonds and antibonding states, interlayer π as well as d states.

The resulting critical temperatures are reported in tab. 3.2 and for a visual comparison with the experimental values in fig. 3.11. The predicted critical temperatures are in reasonable agreement with experiment (except for vanadium). The result for Nb and V is improved if one includes the effect of spin fluctuations as in eq. 2.4.2. The error obtained in V₃Si, ZrN and MgB₂ is somehow large, but one has to consider that the error bar for phononic calculations is also significant. And as discussed before, we have arguments to assume that our MgB₂ coupling is underestimated (see sec. 3.1 and ref. [86]).

Overall, the agreement with experiment is good, which shows that the method presented is reliable and can be used for predictions in this static approximation. It will turn out, that the comparison with experiment actually gets worse by including dynamical effects. This issue, solutions and strategies will be discussed in the next section.

3.3 Dynamical screening

In this part we report on the result of superconducting calculations using the full frequency dependent screened Coulomb interaction. Having observed that different approximations in the screening actually lead to minor differences in the final estimation of T_c , we present in this section only results within the RPA. We investigate the effect of dynamical Coulomb interactions in superconductivity on: an electron gas model (sec 3.3.1) for which we can also compare with some existing literature [28]; and for a set of real materials (sec 3.3.2).

The full set of Eliashberg equations, which is summarized by eq. 2.4.27 of sec. 2.4.3, will be used. This involves the calculation of the mass renormalization $Z = 1 + Z^{ph} + Z^{c,dyn}$ and the gap $\phi = \phi^{ph} + \phi_{stat}^c + \phi^{c,dyn}$. Just as reminder, the $Z^{c,dyn}$ and $\phi^{c,dyn}$ are generated by the dynamical

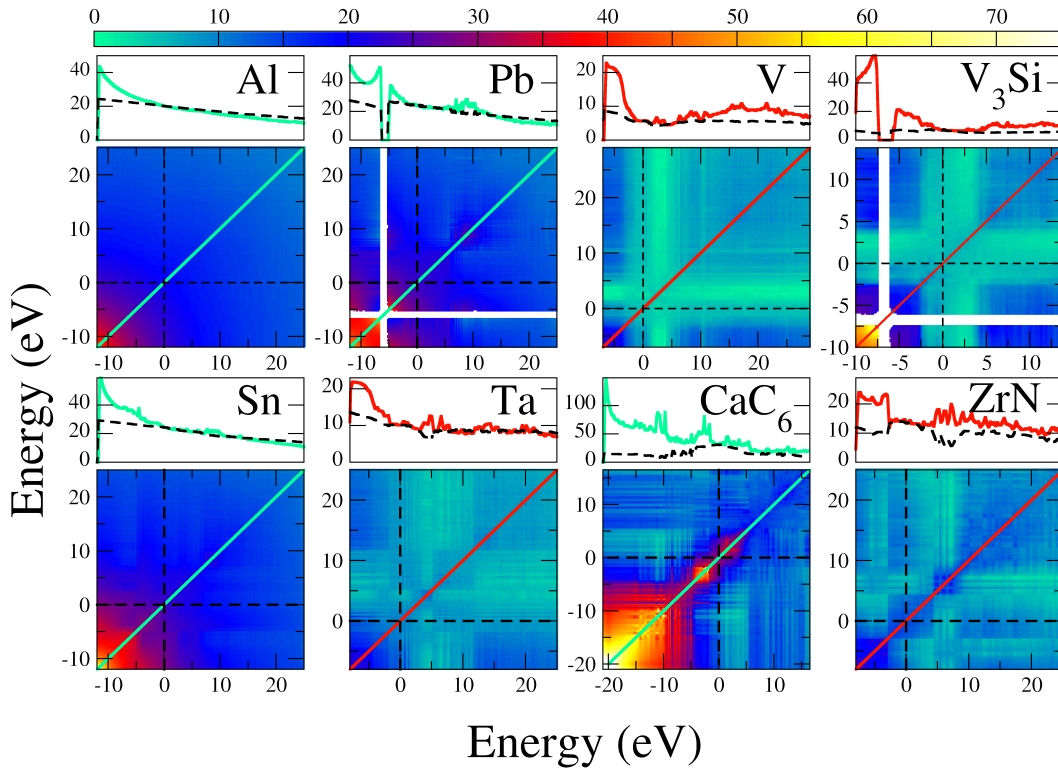


Figure 3.10: Color maps of static Coulomb interaction kernel $K_{stat}^c(\xi\xi')$ for Al, Pb, Sn, Ta, V, V_3Si , CaC_6 and ZrN. Diagonal cuts ($K_{stat}^c(\xi, \xi' = \xi)$, i.e., along solid lines on color maps) and Fermi level cuts ($K_{stat}^c(\xi_F \xi) = K_{stat}^c(\xi \xi_F)$, i.e., along dashed black lines) are given above each color map. All 'argumental' axes (e.g. $\xi\xi'$ of $K_{stat}^c(\xi\xi')$) are in eV, while the color scale is in $eV/\text{\AA}^3$.

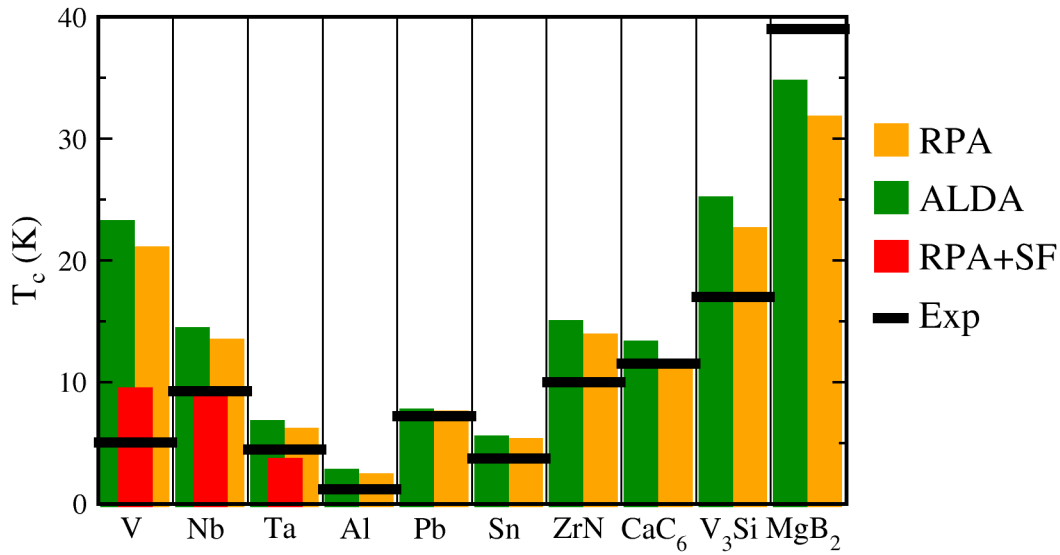


Figure 3.11: Calculated critical temperatures (with RPA and ALDA approximations in Coulomb) together with experimental values for a set of compounds, i.e. the visualization of results from the table 3.2.

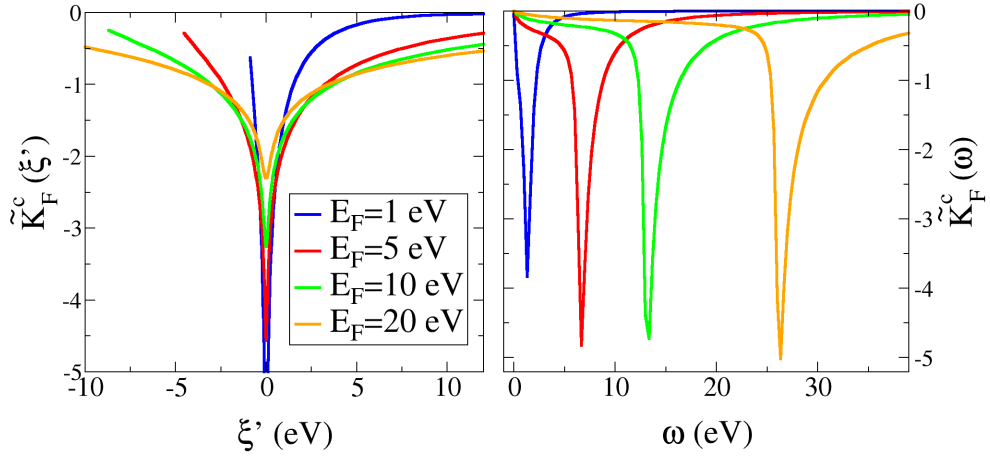


Figure 3.12: Frequency (left) and energy (right) integrated kernels $\tilde{K}_F^c(\xi')$ and $\tilde{K}_F^c(\omega)$ (dimensionless) given by eq. 1.4.54 and 1.4.55 respectively (sec. 1.4.6) within the RPA for electron gas.

part of the Coulomb interaction, which is represented by the kernel $K_{dyn}^c(\xi\xi\omega)$ constructed with eq. 1.4.42 for real materials and with eq. 1.4.52 for the electron gas.

3.3.1 Electron gas

The Coulomb interaction for the electron gas is given by the Thomas-Fermi (in its static limit) and the Lindhard (dynamical part) kernels K_{TF}^c and $K_{lind}^c(\xi\xi'\omega)$ respectively, resulting in the total kernel given by eq 2.5.2. In this section we show how the Coulomb interaction (K_{TF}^c and K_{lind}^c) and superconducting properties depend on the Fermi energy parameter¹⁰ E_F . The electron-phonon interaction, when included, was fixed by the $\alpha^2 F(\omega)$ of model **B** from sec. 2.5.1.

The integrated values $\tilde{K}_F^c(\xi')$ and $\tilde{K}_F^c(\omega)$ (defined in sec. 1.4.6) coming from the dynamical Coulomb kernel¹¹ K_{lind}^c are given in fig. 3.12 for some values of E_F . Both quantities show a single peak, at $\xi' = \xi_F$ for $K_F^c(\xi')$ and at $\omega = \omega_p$ (plasma frequency) for $\tilde{K}_F^c(\omega)$. The corresponding plasma frequencies are collected in tab. 3.3. The dynamical coupling strengths I_F^c (eq. 1.4.56) are also given in the same table and show a clear decrease with increasing E_F parameter.

3.3.1.1 Result with the Eliashberg scheme

Results of the superconducting calculations in the full Eliashberg scheme are collected in fig. 3.13. Where we report the behavior of the self-consistent gap function Δ both in energy (ξ) and frequency (ω) space. As already pointed out in sec 2.5.2 and 2.5.4, the dynamical part of the Coulomb interaction systematically increases the phononic critical temperature (plots e, f, g, h). And it induces superconductivity in the absence of phonon pairing (a,b,c,d) at least in a window for E_F ranging from 0.5 to 3 eV (fig. 3.13a).

The main physical mechanism in which a repulsive interaction like the Coulomb force can help superconductivity is by the Coulomb renormalization process discussed extensively in Chapter 2.

¹⁰It parametrizes the K_{TF}^c and K_{lind}^c , but also the DOS for the electron gas, see sec. 1.4.3, 1.4.5 and 2.5.1

¹¹Plots for both K_{TF}^c and $K_{lind}^c(\xi\xi'\omega)$ for the chosen electron gases are presented in fig. C.4 of appendix C. The essential feature of $K_{lind}^c(\xi\xi'\omega)$, as extensively discussed in sec. 1.4.5, is in its divergence at $\xi = \xi'$ at finite frequency. It comes from the low-q divergence of $Im[\epsilon_{lind}^{-1}(q, \omega)]v_q$, which is used to compute the $K_{lind}^c(\xi\xi'\omega)$ as an isoenergy surface quantity (eq. 1.4.52). The potential $Im[\epsilon_{lind}^{-1}(q, \omega)]v_q$ itself as a function of $q\omega$ is shown in fig. C.5.

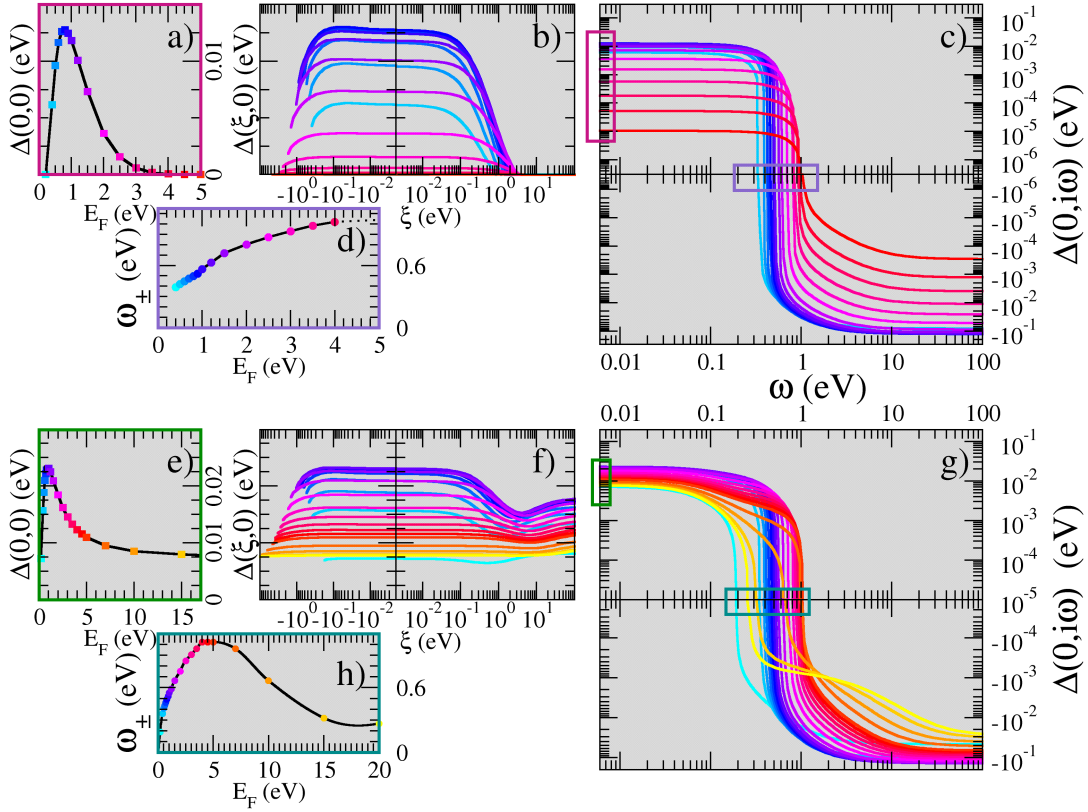


Figure 3.13: Energy (ξ) and frequency (ω) structure of the quasiparticle gap function $\Delta(\xi, i\omega)$ obtained with the full Eliashberg scheme with phonons (e,f,g,h) and without (a,b,c,d). (a and e) The dependence of the fundamental gap on E_F . (b and f) Energy (ξ) structure of the low-frequency gap function. (c and g) Frequency (ω) structure of the gap at the Fermi energy; vertical rectangles are the low-frequency limits specifying the fundamental gaps of panels (a) and (e), while horizontal rectangles specify the upturn frequency ω_{\pm} . (d and h) The gap upturn frequency ω_{\pm} versus E_F . Colors indicate the values of E_F marked by squares and circles in panels (a,e) and (d,h) respectively.

| E_F | I_F^c | ω_p | ω_{log}^c | Δ_0^{stat} | Δ_0^{dyn} | $\Delta_0^{dyn, \cancel{Z}}$ | $\Delta_0^{E+SCDFT}$ | $\Delta_0^{E+SCDFT, \cancel{Z}}$ |
|-------|---------|------------|------------------|-------------------|------------------|------------------------------|----------------------|----------------------------------|
| 1 | 5.22 | 1.3 | 1.4 | 5.2 | 23.1 | 79.9 | 2.94 | 7.82 |
| 5 | 2.20 | 6.6 | 7.5 | 6.4 | 10.9 | 23.3 | 4.92 | 8.75 |
| 10 | 1.53 | 13.1 | 14.9 | 6.9 | 8.5 | 13.6 | 5.70 | 8.65 |
| 20 | 1.08 | 26.3 | 28.7 | 7.4 | 7.8 | 10.5 | 6.41 | 8.63 |

Table 3.3: Results for electron gas calculation with electron-phonon coupling and different approximations in the dynamical Coulomb part. The 'dyn' labels the full original set of Eliashberg equations (sec. 2.4.3). 'dyn, \cancel{Z} ' ignores the mass renormalization $Z^{c,dyn}$ (due to the dynamical Coulomb interaction) in this scheme. 'E + SCDFT' is a calculation with the Kohn-Sham gap in the Coulomb part (introduced in sec. 2.3) of the Eliashberg equation and 'E + SCDFT, \cancel{Z} ' is the same, but ignoring the Coulomb mass renormalization $Z^{c,dyn}$. 'stat' labels the static RPA result. Units for the gaps are meV, while eV stands for the rest (except I_F^c , which is a dimensionless constant).

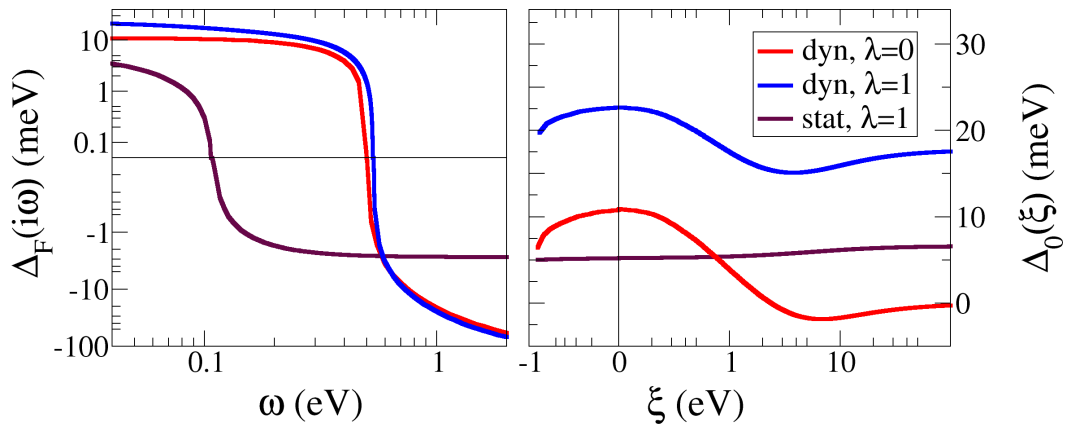


Figure 3.14: The same as in fig. 3.13 but for electron gas of $E_F = 1$ eV. Blue is the result of the full calculation (i.e., with dynamical Coulomb and phonon interactions), red is the result for Coulomb-only ($\lambda^{ph} = 0$) driven superconducting calculation, while the maroon stands for the static approximation in Coulomb (but with $\lambda^{ph} = 1$).

This is triggered by a sign change in the gap function. That is therefore a key element since it indicates the characteristic energy scale of the pairing interaction. In the absence of phonons the upturn frequency (indicated as ω_{\pm} in the figure) grows from zero up to about 1 eV at $E_F \sim 4$ eV, when the superconducting gap becomes exponentially small.

The interplay with a (fix strength) phononic pairing (e,f,g,h) complicates the behavior. At low E_F the plasmonic pairing is zero, therefore superconductivity is purely phononic. Increasing E_F the plasmonic pairing becomes more relevant, $\Delta(0,0)$ ¹² increases (panel e) and at the same time the upturn frequency (panel h) increases from the phononic scale to the plasmonic one), to decrease again, at large E_F when plasmonic pairing becomes less relevant.

All plasmonic effects are stronger around $E_F = 1$. For this particular case we compare the results with those in the static approach for Coulomb in fig. 3.14. The frequency ($i\omega$) shape of the gap in the static Coulomb case was given only by the phonon contribution, while the energy shape (ξ) is due to the energy structure of $K_{TF}^c(\xi\xi')$. The dynamical Coulomb interaction on the other hand contributes strongly to both energy and frequency shape of the gap, rising the fundamental gap Δ_0 up to 22.7 meV, to be compared to the static case of just 5.2 meV. This enormous gap gain due to the dynamical Coulomb interaction shows that this dynamical interaction is able to generate superconductivity without phonons. The calculations with zero electron-phonon coupling ($\lambda^{ph} \rightarrow 0$) are thus performed and the corresponding (to $E_F = 1$ eV) energy/frequency dependent gap function is given also in fig. 3.14. The difference with phonon-included case is that the low-frequency gap $\Delta(\xi, i\omega = 0)$ now changes the sign with energy, and of course it has a lower value of the fundamental gap Δ_0 .

A similar structure of the gap (at $\lambda^{ph} = 0$) is observed in the work of Rietschel and Sham [28], where the Coulomb-only driven superconductivity is studied also within the Eliashberg theory. We obtain quantitatively similar results to this work although there are some conceptual differences between the two approaches. *First*, the gap equation was effectively mapped to the μ^* -based equation, where all high energy/frequency structure of the interaction is folded in the definition of μ^* . This procedure is exact and in principle, should not lead to any difference with our full scale calculations. *Second*, for simplicity we took the Thomas-Fermi kernel K_{TF}^c as the static limit of the

¹² T_c (not shown) follows the same trend.

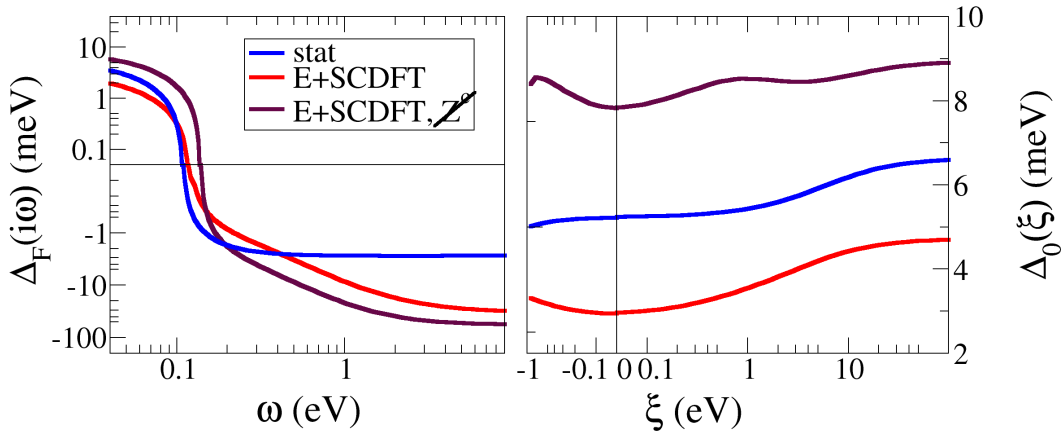


Figure 3.15: The same as in fig. 3.13. Red now is the result of the Eliashberg+SCDFT calculation, and maroon is the same but ignoring the Coulomb mass renormalization $Z^{c,dyn}$. The result of the static Coulomb approach is in blue in this graph. The electron-phonon interaction is included.

interaction, while in the reference it was given by Lindhard everywhere¹³, but we expect that the difference between those is negligible. The *third* difference lies in the fact that in the Eliashberg approach of ref. [28] the chemical potential contribution χ was included. But our goal is to perform the calculations for real materials, for which the normal state quantities, as the starting point of superconducting calculations, are properly described by the DFT. In particular, we assume that the KS band structure includes already the essential part of exchange and correlations, and this allowed us to neglect by the entire $\chi - v_{xc}$ contribution (see sec. 2.2.1 for details).

Fundamental gaps are given in table 3.3 (Δ_0^{dyn} , column). If we exclude the evaluation of $Z^{c,dyn}$, the fundamental gaps greatly increase (values of Δ_0^{dyn,Z^c} in table 3.3), which is consistent with ref. [28].

3.3.1.2 Approach with SCDFT self energy

In sec. 2.3 we have introduced a combined approach that mixes SCDFT and Eliashberg type perturbation theory. This leads to similar equations, with the only difference that on the right hand side of the Coulomb part of the gap (ϕ_{stat}^c and $\phi^{c,dyn}$) the SCDFT KS gap function Δ^s is used instead of the Eliashberg gap (see eq. 2.3.4 and 2.3.6). In this approximation the effect of dynamical Coulomb interaction is very different, and much weaker. The resulting¹⁴ $\Delta_0^{E+SCDFT}$ is lower than the static gap Δ_0^{stat} (table 3.3) and moreover increases with E_F , which is the opposite of what occurs to Δ_0^{dyn} . If we exclude the $Z^{c,dyn}$ from this calculation, we get the resulting $\Delta_0^{E+SCDFT,Z^c}$ higher than in the static case, but lower than Δ_0^{dyn} at the low- E_F region. The frequency/energy shape of $\Delta^{E+SCDFT}$ and $\Delta^{E+SCDFT,Z^c}$ is presented in comparison with static calculations in fig. 3.15. The energy/frequency deviation of $\Delta^{E+SCDFT}$ and $\Delta^{E+SCDFT,Z^c}$ from the static case is much lower than with the original Eliashberg approach.

The gap $\Delta_0 = \Delta(\xi_F, i\omega = 0)$ as a function of E_F , is given in fig. 3.16 for an overall comparison among the various methods presented: full Eliashberg, static approximation and Eliashberg+SCDFT approach¹⁵. Without phononic support only the original Eliashberg scheme has

¹³So far, Lindhard kernel K_{lind}^c was associated with the dynamical part of interaction, i.e., $\sim Im[\epsilon_{lind}^{-1}(q, \omega)]v(q)$ (sec. 1.4.2). Having the Lindhard interaction in the static limit we would use the $\epsilon_{lind}^{-1}(q, \omega = 0)v(q)$ to construct the static kernel instead of K_{TF}^c .

¹⁴This quantity is evaluated from the left-hand side of Eliashberg equation, hence, it is a proper many-body fundamental gap, not the KS gap.

¹⁵Except the $'dyn, Z^c'$ case, which gave an extreme enhancement of the gap (tab. 3.3) and hence, has no practical

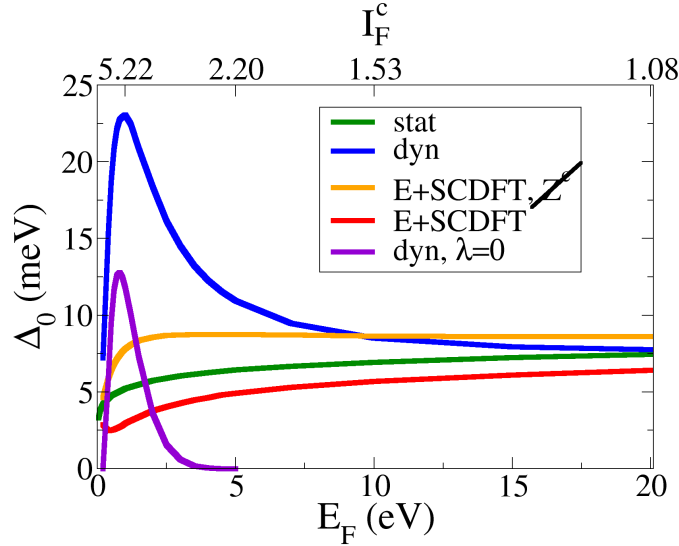


Figure 3.16: Dependence of the self-consistent fundamental gap $\Delta(\xi_F, i\omega \rightarrow 0)$ on the E_F for different computational schemes; The static approximation (green) as well as the E+SCDFT approaches (yellow and red) give a weak dependence. While the full dynamical Eliashberg equations lead to a dome like structure, both with (blue) and without (violet) phononic pairing. Corresponding to $E_F = 1, 5, 10$ and 20 eV coupling strengths I_F^c are given on the upper horizontal axis.

superconducting solutions, while Eliashberg+SCDFT approach gave no superconducting solutions within our numerical precision. From the figure we also conclude that SCDFT corrected methods behave differently at $E_F \rightarrow \infty$: the original $\Delta_0^{dyn}(E_F)$ gets closer to $\Delta_0^{stat}(E_F)$, while the $\Delta^{E+SCDFT}$ and $\Delta^{E+SCDFT, Z}$ lies below and above respectively.

3.3.2 Applications to real materials

Within the static approximation for the Coulomb interaction (sec. 3.2) our Eliashberg scheme has provided a good and quantitatively accurate description of superconducting properties in real materials. Tests on the electron gas have shown that the dynamical part of the Coulomb interaction is not negligible and can drastically increase the superconducting T_c . However, the Eliashberg+SCDFT scheme seems to lead to minor corrections to the static case, at least for the electron gas. In this section we apply the same computational schemes as for the electron gas, but computing the *ab-initio* static and dynamical kernels $K_{stat}^c(\xi\xi')$ and $K_{dyn}^c(\xi\xi'\omega)$ within the RPA¹⁶. The spin-fluctuations are also included in the case of Nb, V and Ta.

The $\tilde{K}_F^c(\xi)$ and $\tilde{K}_F^c(\omega)$ (eqs. 1.4.54 and 1.4.55 respectively) are plotted in fig. 3.17 for the chosen set of compounds¹⁷. The $\tilde{K}_F^c(\xi)$, as for the electron gas (fig. 3.12, left), has a strong peak at the Fermi level, but also, by definition in eq. 1.4.54, contains significant structures mostly induced by the DOS of the material. The frequency structure of $\tilde{K}_F^c(\omega)$ is also quite different throughout the set. The simple electron gas like single-peak structure (fig. 3.12, right) of $\tilde{K}_F^c(\omega)$ is observed only for aluminum, while in other cases the spectral weight is redistributed from the main peak: slightly for Sn and Pb and strongly for the the rest of compounds, forming even a multiple peak structures. The quantitative estimation of the dynamical coupling I_F^c (eq. 1.4.56), where both ξ and ω structure of $K_{dyn}^c(\xi\xi'\omega)$ enters, is given in table 3.4.

use for the real material calculations.

¹⁶Discussed in detail in the chap. 1

¹⁷This set excludes the multiband MgB₂ for simplicity.

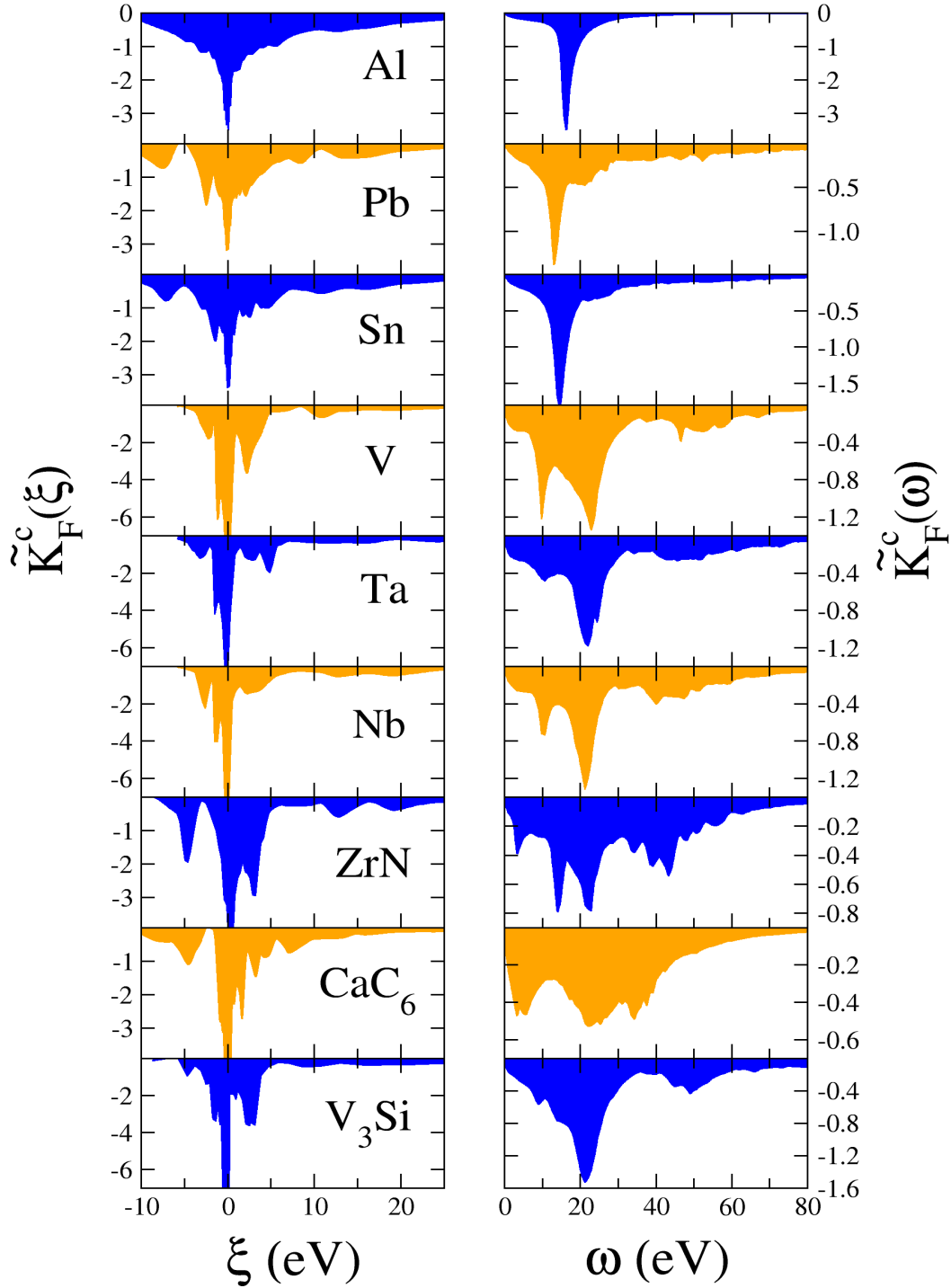


Figure 3.17: Frequency (left) and energy (right) integrated kernels $\tilde{K}_F^c(\xi)$ and $\tilde{K}_F^c(\omega)$ (dimensionless) given by eq. 1.4.54 and 1.4.55 respectively within the *ab-initio* RPA (sec. 1.4.6).

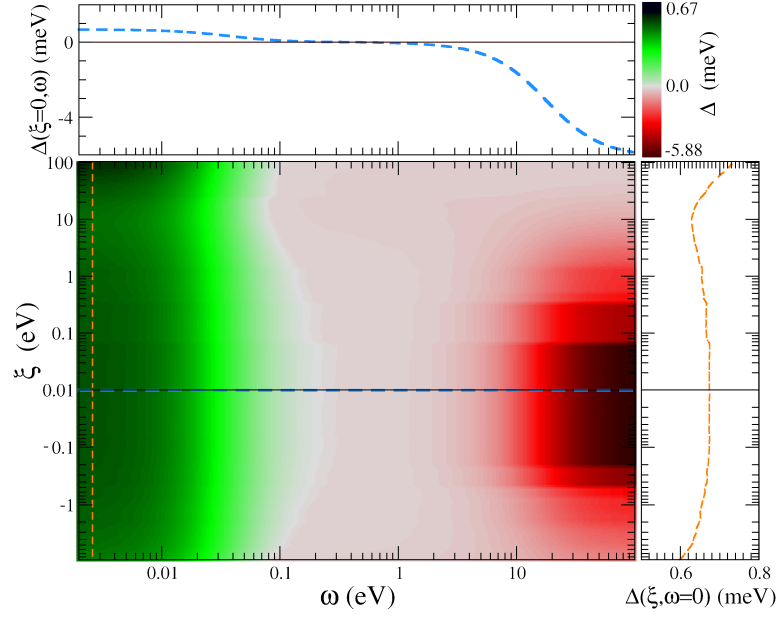


Figure 3.18: Color maps of total gap $\Delta(\xi, i\omega)$ for aluminum in imaginary frequency domain. It is obtained by the full Eliashberg scheme (eq. 2.4.27) with *ab-initio* screened Coulomb interaction given by the RPA. Dashed lines in insets are ω (blue) and ξ (orange) cuts along the corresponding dashed lines on the color map.

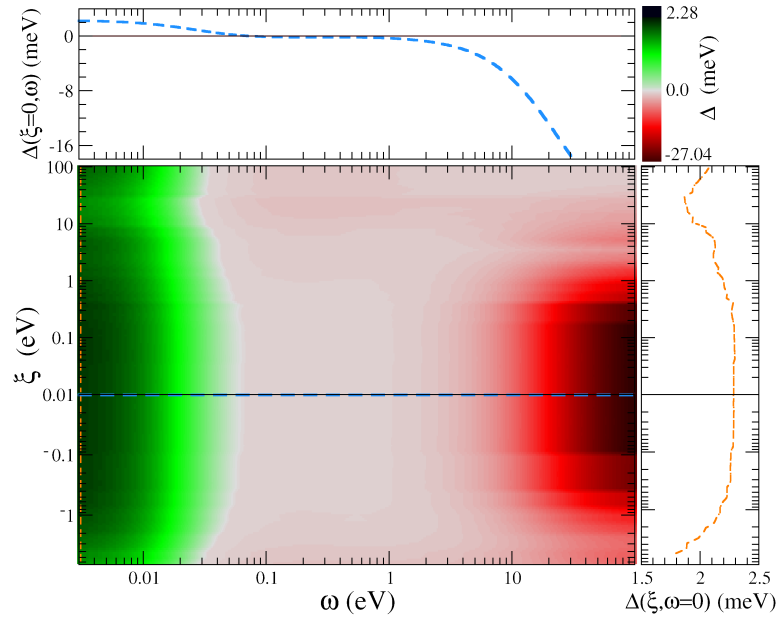


Figure 3.19: The same as in fig. 3.18, but for niobium.

| mat. | I_F^c | $Z_0^{c,dyn}$ | ω_{log}^c | Δ_0^{stat} | Δ_0^{dyn} | $\Delta_0^{E+SCDFT}$ | $\Delta_0^{E+SCDFT,\cancel{Z}^c}$ |
|-------------------|---------|---------------|------------------|-------------------|------------------|----------------------|-----------------------------------|
| Pb | 1.29 | 0.257 | 21.3 | 1.37 | 1.40 | 1.19 | 1.54 |
| Sn | 1.38 | 0.275 | 19.5 | 0.85 | 0.94 | 0.68 | 1.06 |
| ZrN | 1.49 | 0.300 | 24.5 | 2.18 | 3.55 | 1.83 | 2.87 |
| Al | 1.50 | 0.300 | 17.4 | 0.35 | 0.67 | 0.26 | 0.67 |
| Ta | 1.68 | 0.332 | 23.1 | 0.57 | 0.96 | 0.42 | 0.82 |
| Nb | 1.69 | 0.335 | 23.3 | 1.54 | 2.28 | 1.26 | 1.93 |
| CaC ₆ | 1.82 | 0.342 | 20.4 | 1.80 | 3.52 | 1.56 | 2.70 |
| V ₃ Si | 2.09 | 0.408 | 23.2 | 4.03 | 13.10 | 3.40 | 5.11 |
| V | 2.12 | 0.410 | 21.1 | 1.56 | 3.27 | 1.27 | 1.98 |

Table 3.4: Numerical results of dynamical calculations for real materials sorted according to a coupling strength I_F^c . The table contained the calculated low-frequency Coulomb mass renormalization $Z_0^{c,dyn}(\xi_F)$, characteristic frequency ω_{log}^c and fundamental gaps obtained with different schemes. The 'dyn' labels the full original set of Eliashberg equations (sec. 2.4.3), the 'E+SCDFT' is a calculation with Eliashberg+SCDFT scheme (introduced in sec. 2.3) and 'E+SCDFT, \cancel{Z}^c ' is the same, but ignoring the Coulomb mass renormalization $Z^{c,dyn}$. Units of ω_{log}^c is eV, while units of gaps is meV.

3.3.2.1 Eliashberg scheme

In this section we do not use the approach (sec. 2.4.3) without the effective mass renormalization $Z^{c,dyn}$ (i.e. what was the 'dyn, \cancel{Z}^c ' scheme in sec. 3.3.1.1), since we know in advance that this would give enormously high gaps and critical temperatures (tab. 3.3). The full structure of the self-consistent gap on both ξ and $i\omega$ -axes is presented for aluminum and niobium in fig. 3.18 and 3.19 respectively. Qualitatively, it has similar features as observed in the electron gas, therefore we will only focus on quantitative comparisons in terms of gaps and critical temperatures. Fundamental gaps are collected in the table 3.4 for different methods together with the low frequency limit of the mass renormalization $Z^{c,dyn}$ (eq. 2.4.10). The last depends strongly linearly on the coupling I_F^c . The increase of the Δ_0^{dyn} (in comparison with static case) is correlated with I_F^c but it is far from linear, and this correlation for $\Delta_0^{E+SCDFT}$, $\Delta_0^{E+SCDFT,\cancel{Z}^c}$ with I_F^c is not observable. But this is consistent with what we see for the electron gas: the dependence of Δ_0^{dyn} on I_F^c (blue line in fig. 3.16, right) is much stronger than the one for $\Delta_0^{E+SCDFT}$ and $\Delta_0^{E+SCDFT,\cancel{Z}^c}$. Moreover one has to take into account the self-consistent nature of the Eliashberg equations, where all interactions interplay in the resulting gap function. In the extreme case of V₃Si we get the Δ_0^{dyn} three times as large as the Δ_0^{stat} (tab. 3.4), while the deviation of $\Delta_0^{E+SCDFT}$ and $\Delta_0^{E+SCDFT,\cancel{Z}^c}$ from the static gap is within the $\sim 25\%$. Finally, the list of critical temperatures is given in tab. 3.5 for all tested materials.

Clearly, Δ_0^{dyn} is far off from the experiment, especially for higher values of I_F^c . This disagreement could be ascribed to several reasons. First of all, in the self energy (sec. 2.1.3.2) we neglected vertex corrections (apart from spin fluctuation contributions). The effect of this approximation is not known and difficult to estimate (although there have been some studies for the electron gas where it is shown that these vertex corrections could be relevant [106]). This resulting SE has a GW-like form (sec. 2.1.3.3), where the screened Coulomb interaction enters. A second reason for the disagreement may come from the RPA to the screening. Although this is unlikely, since TDDFT corrections (sec 1.4.1.5) seem to have a minor effect. Finally, we have neglected parts of the Eliashberg equations related to the shift in the Fermi energy.

On the other hand, the Eliashberg+SCDFT approach seems to give more physical results. It is difficult to judge why it is like that. In principle, an infinite diagrammatic expansion should

| mat. | T_c^{stat} | T_c^{dyn} | $T_c^{E+SCDFT}$ | $T_c^{E+SCDFT, \cancel{Z}}$ | T_c^{exp} |
|------------------------|--------------|-------------|-----------------|-----------------------------|-------------|
| Pb | 7.49 | 7.77 | 6.71 | 8.30 | 7.2 |
| Sn | 5.20 | 5.77 | 4.28 | 6.37 | 3.72 |
| ZrN | 13.77 | 22.02 | 11.76 | 17.89 | 10 |
| Al | 2.31 | 4.43 | 1.71 | 4.42 | 1.2 |
| Ta | 3.69 | 6.13 | 2.75 | 5.27 | 4.48 |
| Nb | 9.13 | 13.32 | 7.70 | 11.29 | 9.2 |
| CaC ₆ | 11.28 | 21.34 | 9.89 | 16.33 | 11.5 |
| V ₃ Si | 22.56 | 67.19 | 19.82 | 27.65 | 17 |
| V | 9.57 | 18.80 | 7.95 | 11.85 | 5.03 |
| standard deviation (K) | 2.8 | 18.2 | 1.8 | 5.5 | ref. |

Table 3.5: List of critical temperatures obtained with different treatment of the dynamical Coulomb interaction in comparison with static RPA results. The standard deviation from the experimental T_c^{exp} is given by $\sqrt{\frac{1}{N} \sum_i (T_{c,i} - T_{c,i}^{exp})^2}$.

lead to the same result among the two methods. While it seems that within the first order diagrams Eliashberg+SCDFT gives physical results¹⁸. Actually, in better agreement than with the static case, although we believe that deviations are within the error bar in the calculation of the interactions.

¹⁸In sec. 2.2.1 we conclude that the mass renormalization due to the dynamical Coulomb interaction has to be included. Neglect of $Z^{c,dyn}$ leads to a $T_c^{E+SCDFT, \cancel{Z}}$ higher than in the static calculation. In ref. [24], where the same problem was investigated within SCDFT this mass renormalization was not included, and hence, the T_c was overestimated, for example, almost by a factor of 2 for aluminum.

Chapter 4

Summary, Conclusions and Outlook

Eliashberg theory of superconductivity is a leading approach for *ab-initio* superconductivity, surely it is the most used worldwide (in its McMillan parametrized form). The theory is essentially a reformulation of the Dyson equation for the Green's function in Nambu space, and under the assumption of a GW form for the self energy. Originally the theory was developed as perturbative correction from the Hartree approximation. It's modern form instead takes its start from DFT, both as reference unperturbed system, and for the construction of the perturbation Hamiltonian (as reviewed in Chapter 1 of this work). However, the theory has never been investigated in full (at least for realistic systems). To reduce its computational complexity, since the early years, the Coulomb part of the interaction Hamiltonian has always been oversimplified, essentially transforming this powerful framework to a semi-empirical and modellistic theory.

In this work we have reconsidered critically the Eliashberg approach by starting from its general form (Chapter 2). Even with modern computing power this full approach would still be numerically too demanding, certainly if one aims to study real systems. We have therefore constructed a (multiband) isotropic approximation similar to the one previously developed in SCDFE. While this allows for a fully *ab-initio* inclusion of the Coulomb part of the self energy, still it can be made arbitrarily accurate by increasing the number of energy/momentum space divisions. By using special integration schemes both for energy and Matsubara points, we have implemented the method in an efficient and fast Fortran code (not published yet).

The key input of our approach (apart from the standard spectral functions for phonons/ spin fluctuations) requires knowledge of the screened Coulomb interaction. A well known object in normal many body physics and TDDFT. Within the present work it has been implemented and obtained in the ELK full-potential DFT based code [29].

Several issues and subtleties are involved in this Coulomb part of the interaction. The most complex to handle being the integration of the low- q divergence at finite frequency, and the high energy behavior that has to be described analytically in order to be able to reach convergence.

A natural division occurs between static and dynamical parts of the Coulomb interaction, since the two enter the Eliashberg equations in a different way. Also the effect of static Coulomb interaction is already reasonably well known in the literature, from SCDFE studies. While the dynamical one was investigated, so far, only for simple models.

We have applied the theory to an electron gas model and to a validation set of bulk materials: Al, Nb, Pb, V, Ta, Sn, MgB₂, V₃Si, CaC₆, ZrN, covering the main classes of phononic superconductors. The results (Chapter 3) show clearly that a (very) good agreement with experiment is achieved if the dynamical part of the interaction is ignored.

Dynamical effects lead to systematic overestimation of the critical temperature, essentially introducing a very large electron-plasmon interaction that strengthens the Cooper binding in a way that is unphysical. The reason for this has been ascribed to the intrinsic GW approximation

of the Self energy.

Instead of trying to include vertex corrections diagrammatically, that would make the method computationally useless, adding an unaffordable computational cost, we have adopted an alternative strategy. Instead of using interacting Green's functions we have constructed the Coulomb part of the self energy using the SCDF-T-KS Green's functions. This changes the meaning of the GW approximation. Within this approach we observe an excellent agreement with experiments.

Overall the developed approach is an efficient *ab-initio* and predictive approach to superconductivity that can be applied to any system. Still there are some paths that require future investigation.

First, one should try to understand in a deeper way the role of the neglected vertex corrections, and (although this could be very hard) the different behavior of the KS-SCDF-T type of expansion as compared to the many body original form.

Second, the theory should be applied to more and diverse materials. In particular, it would be interesting to apply it to high-temperature superconductors, organic superconductors, and in general to systems where the plasmonic mechanism could play an active role.

Appendix A

Translational symmetry

A.1 Lattice

A.1.1 Direct lattice

In solid state physics one mostly deals with crystals, which are infinite arrays of atoms, molecules or ions arranged in a periodic structure. Those periodic structures are described by so-called Bravais lattices, generated by a set of discrete translations, i.e., rigid shifts by vectors \mathbf{R}_n :

$$\mathbf{R}_n = n_1 \mathbf{a}_1 + n_2 \mathbf{a}_2 + n_3 \mathbf{a}_3, \quad \mathbf{n} = (n_1, n_2, n_3), \quad (\text{A.1.1})$$

where n_i are integers and \mathbf{a}_i are primitive vectors lying in different directions. The parallelepipeds spanned by \mathbf{a}_i form a first unit cell of the lattice and any other cell is its translation by some vector \mathbf{R}_n . The choice of the unit cell is not unique, the most frequently used is the so-called Wigner-Seitz (WS) cell (see the next section for description). The unit cell consists of N_α atoms, which are called a basis. As a result, the position of an arbitrary atom in the crystal (\mathbf{R}_i) is specified by the position of the cell (\mathbf{R}_n) and a position of an atom within this cell \mathbf{R}_α :

$$\mathbf{R}_i = \mathbf{R}_n + \mathbf{R}_\alpha. \quad (\text{A.1.2})$$

In reality, atoms vibrate around their equilibrium positions (\mathbf{R}_i) and an instantaneous displacement around equilibrium is described by vectors $\mathbf{u}_{n\alpha}$, giving a new atomic vectors:

$$\mathbf{R}'_i = \mathbf{R}_n + \mathbf{R}_\alpha + \mathbf{u}_{n\alpha}, \quad \mathbf{u}_{n\alpha} = (u_{n\alpha}^x, u_{n\alpha}^y, u_{n\alpha}^z). \quad (\text{A.1.3})$$

A.1.2 Reciprocal lattice

The reciprocal lattice can be defined as a set of \mathbf{G}_m , such as:

$$e^{i\mathbf{G}_m \mathbf{R}_n} = 1, \quad \forall \mathbf{n}, \quad (\text{A.1.4})$$

There is also a set of primitive vectors \mathbf{b}_i , which gives a \mathbf{G}_m as (m_i are integers):

$$\mathbf{G}_m = m_1 \mathbf{b}_1 + m_2 \mathbf{b}_2 + m_3 \mathbf{b}_3, \quad \mathbf{m} = (m_1, m_2, m_3). \quad (\text{A.1.5})$$

The choice of \mathbf{b}_i is fixed by primitive vectors of the direct lattice:

$$\mathbf{b}_1 = 2\pi \frac{[\mathbf{a}_2 \times \mathbf{a}_3]}{\mathbf{a}_1 \cdot [\mathbf{a}_2 \times \mathbf{a}_3]}, \quad (\text{A.1.6})$$

\mathbf{b}_2 and \mathbf{b}_3 are obtained by cyclic change of all indices: $123 \rightarrow 231 \rightarrow 312$. Orthogonality relations $\mathbf{a}_i \mathbf{b}_j = 2\pi \delta_{ij}$ are straightforward.

The WS cell of the reciprocal lattice with \mathbf{G}_0 at the middle is called the first Brillouin zone (BZ). To construct the BZ, we choose \mathbf{G}_0 and draw all connecting lines to neighboring \mathbf{G}_m . The planes appearing at the middle of those lines surround exactly the BZ. It is useful to note, that for any $\mathbf{k}_1, \mathbf{k}_2 \in BZ$:

$$|\mathbf{k}_1 \pm \mathbf{k}_2| < |\mathbf{G}_m|, \quad \mathbf{m} \neq \mathbf{0}. \quad (\text{A.1.7})$$

A.1.3 Periodic boundary conditions

A single particle wave function of an electron in the crystal is a Bloch state:

$$\phi_{b\mathbf{k}}(\mathbf{r}) = e^{i\mathbf{k}\mathbf{r}} u_{b\mathbf{k}}(\mathbf{r}), \quad (\text{A.1.8})$$

where b is a band index and $u(\mathbf{r}) = u(\mathbf{r} + \mathbf{R}_n)$, i.e. has the periodicity of the lattice. Now, we choose a macroscopic piece of the solid with volume Ω . Each direction of \mathbf{a}_i contains N_i unit cell lengths. The point of the space translated outside the volume Ω by the vector $\mathbf{T} = \sum_i N_i \mathbf{a}_i$ is considered identical to the original one, in particular for the Bloch function:

$$\phi_{b\mathbf{k}}(\mathbf{r} + \mathbf{T}) = e^{i\mathbf{k}\mathbf{T}} e^{i\mathbf{k}\mathbf{r}} u_{b\mathbf{k}}(\mathbf{r}) = \phi_{b\mathbf{k}}(\mathbf{r}), \quad (\text{A.1.9})$$

which restricts possible values of \mathbf{k} to $e^{i\mathbf{k}\mathbf{T}} = 1$. If we expand $\mathbf{k} = \sum_i k_i \mathbf{b}_i$:

$$k_i = \frac{z_i}{N_i}, \quad z_i = 0, 1, \dots, N_i - 1. \quad (\text{A.1.10})$$

If N is the number of WS cells in the volume Ω ($N = N_1 N_2 N_3$), then we use also:

$$\Omega = N \Omega_{WS} \quad (\text{A.1.11})$$

for the following sections. Ω_{WS} is the WS cell volume.

A.2 Fourier transforms

A.2.1 Nuclear coordinates

Nuclear dependent properties are defined with set of $\mathbf{R}_i = \mathbf{R}_n + \mathbf{R}_\alpha + \mathbf{u}_{n\alpha}$. First of all we define the Fourier transform (FT) of the lattice displacement $\mathbf{u}_{n\alpha}$:

$$\mathbf{u}_{\mathbf{q}\alpha} = \frac{1}{\sqrt{N}} \sum_{\mathbf{R}_n \in \Omega} \mathbf{u}_{n\alpha} e^{-i\mathbf{q}\mathbf{R}_n}, \quad (\text{A.2.1})$$

where the sum goes over all N cells in a macroscopic piece of solid with volume Ω . Because of condition A.1.4, $\mathbf{u}_{\mathbf{q}\alpha} = \mathbf{u}_{(\mathbf{q}+\mathbf{G}_m)\alpha}$, i.e., saying that a full set of Fourier components (FC) is defined within the BZ. Hence, the inverse transformation is:

$$\mathbf{u}_{n\alpha} = \frac{1}{\sqrt{N}} \sum_{\mathbf{q} \in \text{BZ}} \mathbf{u}_{\mathbf{q}\alpha} e^{i\mathbf{q}\mathbf{R}_n}. \quad (\text{A.2.2})$$

The orthogonality conditions are also given (note, that \mathbf{q} is a discrete set, because periodic boundary conditions are always implied):

$$\sum_{\mathbf{n}} e^{i\mathbf{q}\mathbf{R}_n} = N \delta_{\mathbf{q},\mathbf{0}}, \quad \sum_{\mathbf{q} \in \text{BZ}} e^{i\mathbf{q}\mathbf{R}_n} = N \delta_{\mathbf{n},\mathbf{0}}. \quad (\text{A.2.3})$$

A.2.2 Electronic coordinates

We often need to calculate a FT of nonlocal functions defined on the lattice (as for dielectric function in sec. 1.4.1.3). In this case, we do a similar thing as in eq. A.1.2, describing an arbitrary position in the solid with $\mathbf{r} = \bar{\mathbf{r}} + \mathbf{T}_n$ ($\bar{\mathbf{r}}$ gives a position within the \mathbf{n} 'th unit cell and \mathbf{T}_n has exactly the same meaning as \mathbf{R}_n previously):

$$f(\mathbf{r}_1, \mathbf{r}_2) = f(\bar{\mathbf{r}}_1 + \mathbf{T}_1, \bar{\mathbf{r}}_2 + \mathbf{T}_2). \quad (\text{A.2.4})$$

Here, \mathbf{T}_i is an appropriate translation vector. We can translate everything on \mathbf{T}_1 , obtaining a $f(\bar{\mathbf{r}}_1, \bar{\mathbf{r}}_2 + \mathbf{T}_2 - \mathbf{T}_1) = f(\bar{\mathbf{r}}_1, \bar{\mathbf{r}}_2, \mathbf{T}_{21})$. The integration over $\Omega = N \Omega_{WS}$ is performed as:

$$\int_{\Omega} d\mathbf{r}.. = \sum_{\mathbf{T}=\mathbf{T}_0}^{\mathbf{T}_N} \int_{\Omega_{WS}} d\bar{\mathbf{r}}.., \quad (\text{A.2.5})$$

and consequently, the FT of the two point function f will be defined as:

$$\begin{aligned}
f(\mathbf{k}_1 + \mathbf{G}_1, \mathbf{k}_2 + \mathbf{G}_2) &= \frac{1}{N\Omega_{WS}} \sum_{\mathbf{T}_1 \mathbf{T}_2} \int \int d\bar{\mathbf{r}}_1 d\bar{\mathbf{r}}_2 e^{-i(\mathbf{k}_1 + \mathbf{G}_1)(\bar{\mathbf{r}}_1 + \mathbf{T}_1)} f(\bar{\mathbf{r}}_1, \bar{\mathbf{r}}_2, \mathbf{T}_{21}) e^{i(\mathbf{k}_2 + \mathbf{G}_2)(\bar{\mathbf{r}}_2 + \mathbf{T}_2)} \\
&= \frac{1}{N\Omega_{WS}} \sum_{\mathbf{T}_1 \mathbf{T}_2} \int \int d\bar{\mathbf{r}}_1 d\bar{\mathbf{r}}_2 e^{-i(\mathbf{k}_1 + \mathbf{G}_1)\bar{\mathbf{r}}_1} f(\bar{\mathbf{r}}_1, \bar{\mathbf{r}}_2, \mathbf{T}_{21}) e^{i(\mathbf{k}_2 + \mathbf{G}_2)\bar{\mathbf{r}}_2} e^{-i(\mathbf{k}_1 + \mathbf{G}_1)\mathbf{T}_1} e^{i(\mathbf{k}_2 + \mathbf{G}_2)\mathbf{T}_2} \\
&= \frac{1}{N\Omega_{WS}} \sum_{\mathbf{T}_1 \mathbf{T}_2} \int \int d\bar{\mathbf{r}}_1 d\bar{\mathbf{r}}_2 e^{-i(\mathbf{k}_1 + \mathbf{G}_1)\bar{\mathbf{r}}_1} f(\bar{\mathbf{r}}_1, \bar{\mathbf{r}}_2, \mathbf{T}_{21}) e^{i(\mathbf{k}_2 + \mathbf{G}_2)\bar{\mathbf{r}}_2} e^{i\mathbf{k}_1(\mathbf{T}_2 - \mathbf{T}_1)} e^{i(\mathbf{k}_2 - \mathbf{k}_1)\mathbf{T}_2} \\
&= \frac{\delta_{\mathbf{k}_1 \mathbf{k}_2}}{\Omega_{WS}} \sum_{\mathbf{T}_{21}} \int \int d\bar{\mathbf{r}}_1 d\bar{\mathbf{r}}_2 e^{-i(\mathbf{k}_1 + \mathbf{G}_1)\bar{\mathbf{r}}_1} f(\bar{\mathbf{r}}_1, \bar{\mathbf{r}}_2, \mathbf{T}_{21}) e^{i(\mathbf{k}_2 + \mathbf{G}_2)\bar{\mathbf{r}}_2} e^{i\mathbf{k}_1 \mathbf{T}_{21}} = \delta_{\mathbf{k}_1 \mathbf{k}_2} f(\mathbf{k}_1 \mathbf{G}_1 \mathbf{G}_2). \tag{A.2.6}
\end{aligned}$$

The reverse one is:

$$f(\mathbf{r}_1, \mathbf{r}_2) = \frac{1}{N\Omega_{WS}} \sum_{\mathbf{q} \mathbf{G}_1 \mathbf{G}_2} e^{i(\mathbf{q} + \mathbf{G}_1)\mathbf{r}_1} f(\mathbf{q} \mathbf{G}_1 \mathbf{G}_2) e^{-i(\mathbf{q} + \mathbf{G}_2)\mathbf{r}_2}. \tag{A.2.7}$$

It is easy to show that, due to the prefactor $1/\Omega$, the $f(\mathbf{q} \mathbf{G}_1 \mathbf{G}_2)$ does not scale with the volume of the integration space. For simplicity, assume a homogeneous approximation ($f(\mathbf{r}_1, \mathbf{r}_2) = f(\mathbf{r}_1 - \mathbf{r}_2)$). Then eq. A.2.6 should be written:

$$f(\mathbf{q}) = \frac{1}{N\Omega_{WS}} \int \int d\mathbf{r}_1 d\mathbf{r}_2 e^{-i\mathbf{q}\mathbf{r}_1} f(\mathbf{r}_1 - \mathbf{r}_2) e^{i\mathbf{q}\mathbf{r}_2} \tag{A.2.8}$$

$$\begin{aligned}
&= \frac{1}{N\Omega_{WS}} \int d\mathbf{r}_2 \int d(\mathbf{r}_1 - \mathbf{r}_2) e^{-i\mathbf{q}(\mathbf{r}_1 - \mathbf{r}_2)} f(\mathbf{r}_1 - \mathbf{r}_2) \\
&= \int d\mathbf{R} e^{-i\mathbf{q}\mathbf{R}} f(\mathbf{R}), \tag{A.2.9}
\end{aligned}$$

where the last line represents the ordinary FT of one-coordinate function, e.g., a bare Coulomb potential:

$$v(\mathbf{q}) = \int d\mathbf{r} v(\mathbf{r}) e^{-i\mathbf{q}\mathbf{r}} = \frac{4\pi}{q^2}. \tag{A.2.10}$$

Convolution. The transform of the next expression is also needed (for example, in sec. 1.4.1.3)¹:

$$h(\mathbf{r}_1, \mathbf{r}_2) = \int d\mathbf{r}_3 f(\mathbf{r}_1, \mathbf{r}_3) v(\mathbf{r}_3 - \mathbf{r}_2), \tag{A.2.11}$$

where in place of v the bare Coulomb potential usually appears and f is a nonlocal function on the lattice. For the moment, we forget about the \mathbf{r}_1 (simply omitted) dependence and try to simplify a transform on the \mathbf{r}_2 subspace (in accordance to eq. A.2.6):

$$\begin{aligned}
&\sum_{\mathbf{T}_2} \int d\bar{\mathbf{r}}_2 \sum_{\mathbf{T}_3} \int d\bar{\mathbf{r}}_3 f(\bar{\mathbf{r}}_3 + \mathbf{T}_3) v(\bar{\mathbf{r}}_3 + \mathbf{T}_3 - \bar{\mathbf{r}}_2 - \mathbf{T}_2) e^{i(\mathbf{k}_2 + \mathbf{G}_2)(\bar{\mathbf{r}}_2 + \mathbf{T}_2)} \\
&= \sum_{\mathbf{T}_3} \int d\bar{\mathbf{r}}_3 f(\bar{\mathbf{r}}_3 + \mathbf{T}_3) e^{i(\mathbf{k}_2 + \mathbf{G}_2)(\bar{\mathbf{r}}_3 + \mathbf{T}_3)} \sum_{\mathbf{T}} \int d\bar{\mathbf{r}} v(\bar{\mathbf{r}} + \mathbf{T}) e^{-i(\mathbf{k}_2 + \mathbf{G}_2)(\bar{\mathbf{r}} + \mathbf{T})} \\
&= \sum_{\mathbf{T}_3} \int d\bar{\mathbf{r}}_3 f(\bar{\mathbf{r}}_3 + \mathbf{T}_3) e^{i(\mathbf{k}_2 + \mathbf{G}_2)(\bar{\mathbf{r}}_3 + \mathbf{T}_3)} v(\mathbf{k}_2 + \mathbf{G}_2), \tag{A.2.12}
\end{aligned}$$

where notation $\bar{\mathbf{r}} + \mathbf{T} = \bar{\mathbf{r}}_3 + \mathbf{T}_3 - \bar{\mathbf{r}}_2 - \mathbf{T}_2$ is used in FT of the bare Coulomb potential. And now we add forgotten \mathbf{r}_1 dependence and a prefactor:

¹clear, that there is a convolution in \mathbf{r}_3 variable, but the following is presented as needed exercise

$$h(\mathbf{k}_1 + \mathbf{G}_1, \mathbf{k}_2 + \mathbf{G}_2) = \frac{1}{N\Omega_{WS}} \sum_{\mathbf{T}_1} \int d\bar{\mathbf{r}}_1 \sum_{\mathbf{T}_3} \int d\bar{\mathbf{r}}_3 \quad (\text{A.2.13})$$

$$e^{-i(\mathbf{k}_1 + \mathbf{G}_1)(\bar{\mathbf{r}}_1 + \mathbf{T}_1)} f(\bar{\mathbf{r}}_1, \bar{\mathbf{r}}_3, \mathbf{T}_{31}) e^{i(\mathbf{k}_2 + \mathbf{G}_2)(\bar{\mathbf{r}}_3 + \mathbf{T}_3)} v(\mathbf{k}_2 + \mathbf{G}_2).$$

It is clear that the FT of f appears on the right hand side, so we get:

$$h(\mathbf{k}_1 + \mathbf{G}_1, \mathbf{k}_2 + \mathbf{G}_2) = f(\mathbf{k}_1 + \mathbf{G}_1, \mathbf{k}_2 + \mathbf{G}_2) v(\mathbf{k}_2 + \mathbf{G}_2). \quad (\text{A.2.14})$$

A.2.3 Applications: Coulomb matrix elements

We calculate the matrix of the screened Coulomb interaction (eq. 1.4.31) out of the FC of the bare Coulomb interaction and a dielectric function. We start with:

$$V_{kk'}^c(\omega) = \int \int d\mathbf{r}_1 d\mathbf{r}_2 \phi_k^*(\mathbf{r}_1) \phi_{k'}^*(\mathbf{r}_2) \left[\int d\mathbf{r}_3 \epsilon^{-1}(\mathbf{r}_1 \mathbf{r}_3 \omega) v(\mathbf{r}_3 \mathbf{r}_2) \right] \phi_{k'}(\mathbf{r}_1) \phi_k(\mathbf{r}_2). \quad (\text{A.2.15})$$

This form gives an infinite contribution. To avoid infinities, we normalize it to the unit cell, i.e., formally we integrate over macroscopic volume Ω (in both \mathbf{r}_1 and \mathbf{r}_2 variables) and then divide by number of contained unit cells N . The expression in the square brackets is rewritten via its FC (see eq. A.2.14):

$$\int d\mathbf{r}_3 \epsilon^{-1}(\mathbf{r}_1 \mathbf{r}_3 \omega) v(\mathbf{r}_3 \mathbf{r}_2) = \frac{1}{N\Omega_{WS}} \sum_{\mathbf{qG}_1 \mathbf{G}_2} e^{i(\mathbf{q} + \mathbf{G}_1)\mathbf{r}_1} \epsilon^{-1}(\mathbf{qG}_1 \mathbf{G}_2 \omega) v(\mathbf{q} + \mathbf{G}_2) e^{-i(\mathbf{q} + \mathbf{G}_2)\mathbf{r}_2}.$$

Plugging it back to our starting point, we have to deal with:

$$V_{kk'}^c(\omega) = \frac{1}{N} \frac{1}{N\Omega_{WS}} \sum_{\mathbf{qG}_1 \mathbf{G}_2} \left\langle \int d\mathbf{r}_1 \phi_k^*(\mathbf{r}_1) e^{i(\mathbf{q} + \mathbf{G}_1)\mathbf{r}_1} \phi_{k'}(\mathbf{r}_1) \right\rangle \quad (\text{A.2.16})$$

$$\times \left\langle \int d\mathbf{r}_2 \phi_{k'}^*(\mathbf{r}_2) e^{-i(\mathbf{q} + \mathbf{G}_2)\mathbf{r}_2} \phi_k(\mathbf{r}_2) \right\rangle \epsilon^{-1}(\mathbf{qG}_1 \mathbf{G}_2 \omega) v(\mathbf{q} + \mathbf{G}_2).$$

We analyze the $\frac{1}{N} \langle \dots \rangle$ overlap:

$$\frac{1}{N} \left\langle \int d\bar{\mathbf{r}} \sum_{\mathbf{T}} \phi_k^*(\bar{\mathbf{r}} + \mathbf{T}) e^{i(\mathbf{q} + \mathbf{G})(\bar{\mathbf{r}} + \mathbf{T})} \phi_{k'}(\bar{\mathbf{r}} + \mathbf{T}) \right\rangle = \frac{1}{N} \sum_{\mathbf{T}} e^{i(\mathbf{k}' - \mathbf{k} + \mathbf{q} + \mathbf{G})\mathbf{T}}$$

$$\times \left\langle \int d\bar{\mathbf{r}} \phi_k^*(\bar{\mathbf{r}}) e^{i(\mathbf{q} + \mathbf{G})\bar{\mathbf{r}}} \phi_{k'}(\bar{\mathbf{r}}) \right\rangle = \delta_{\mathbf{k} - \mathbf{k}', \mathbf{q} + \mathbf{G}} \left\langle \int d\bar{\mathbf{r}} \phi_k^*(\bar{\mathbf{r}}) e^{i(\mathbf{q} + \mathbf{G})\bar{\mathbf{r}}} \phi_{k'}(\bar{\mathbf{r}}) \right\rangle_{WS}.$$

Essentially, the symmetry of Bloch functions allows for any \mathbf{G} in the delta-symbol above ($e^{i\mathbf{G}\mathbf{T}} = 1$), so it can be viewed in a more general way, e.g., $\delta_{\mathbf{k} - \mathbf{k}', \mathbf{q} + \sum_i \mathbf{G}_i}$. The initial overlap we call a polarization matrix (as in ref. [35]):

$$\rho_{kk'}(\mathbf{qG}) = \frac{1}{N} \langle k | e^{i(\mathbf{q} + \mathbf{G})\mathbf{r}} | k' \rangle. \quad (\text{A.2.17})$$

Consequently, we have:

$$V_{kk'}^c(\omega) = \frac{1}{\Omega_{WS}} \sum_{\mathbf{qG}_1 \mathbf{G}_2} \epsilon^{-1}(\mathbf{qG}_1 \mathbf{G}_2 \omega) v(\mathbf{q} + \mathbf{G}_2) \rho_{kk'}(\mathbf{qG}_1) \rho_{kk'}^*(\mathbf{qG}_2). \quad (\text{A.2.18})$$

From here, the scaling properties are also seen quite easily: suppose we double the unit cell, then the matrix element will be twice smaller (overlaps $\rho_{kk'}$ stay the same due to the fact that KS orbitals are normalized to the unit cell). From the other side, the DOS will be twice as big and hence, the dimensionless measure of the interaction $\mu = NV$ will stay unchanged and results of Eliashberg approach will be also fixed because the combination VN persist in Eliashberg equations.

A.2.4 Applications: KS response

We need the FC of the following expression in sec. 1.4.1.3 (χ_0 is the retarded version of P in eq. B.2.7):

$$\chi_0(\mathbf{r}_1\mathbf{r}_2\omega) = 2 \sum_{kk'} \frac{(f_{k'} - f_k)\phi_k(\mathbf{r}_1)\phi_k^*(\mathbf{r}_2)\phi_{k'}(\mathbf{r}_2)\phi_{k'}^*(\mathbf{r}_1)}{\omega - (\xi_k - \xi_{k'}) + i0^+}. \quad (\text{A.2.19})$$

We take the FT as for the two-point function and normalize it to the unit cell (plugging $\frac{1}{N}$ factor as in eq. A.2.16):

$$\begin{aligned} \chi_0(\mathbf{q}\mathbf{G}_1\mathbf{G}_2\omega) &= \frac{1}{N} \frac{2}{N\Omega_{WS}} \sum_{kk'} (f_{k'} - f_k) \\ &\times \frac{\langle \int d\mathbf{r}_1 \phi_{k'}^*(\mathbf{r}_1) e^{-i(\mathbf{q}+\mathbf{G}_1)\mathbf{r}_1} \phi_k(\mathbf{r}_1) \rangle \langle \int d\mathbf{r}_2 \phi_k^*(\mathbf{r}_2) e^{i(\mathbf{q}+\mathbf{G}_2)\mathbf{r}_2} \phi_{k'}(\mathbf{r}_2) \rangle}{\omega - (\xi_k - \xi_{k'}) + i0^+}. \end{aligned}$$

The situation is similar to the one for the screened Coulomb interaction, so we can directly write the result:

$$\chi_0(\mathbf{q}\mathbf{G}_1\mathbf{G}_2\omega) = \frac{2}{\Omega_{WS}} \sum_{kk'} (f_{k'} - f_k) \frac{\rho_{kk'}^*(\mathbf{q}\mathbf{G}_1)\rho_{kk'}(\mathbf{q}\mathbf{G}_2)}{\omega - (\xi_k - \xi_{k'}) + i0^+}. \quad (\text{A.2.20})$$

A.2.5 Analytical properties of χ_0

In this section we would like to note several properties of the KS response (eq. A.2.20). The $(f_{k'} - f_k)$ factor ensures that one of k or k' is above the Fermi level, the other one - below. If k being a conductance state and k' being a valence state, we get $\xi_k - \xi_{k'} \rightarrow \xi_c - \xi_v > 0$ and $f_{k'} - f_k \rightarrow f_v - f_c = 1$. For the reverse situation v and c should be swapped and $\xi_v - \xi_c < 0$ and $f_c - f_v = -1$. As result, we write the KS response as a sum of resonant (r) and anti-resonant (a) parts:

$$\chi_0(\mathbf{q}\mathbf{G}_1\mathbf{G}_2\omega) = \frac{2}{\Omega_{WS}} \sum_{cv} \frac{\rho_{cv}^*(\mathbf{q}\mathbf{G}_1)\rho_{cv}(\mathbf{q}\mathbf{G}_2)}{\omega - (\xi_c - \xi_v) + i0^+} - \frac{2}{\Omega_{WS}} \sum_{cv} \frac{\rho_{vc}^*(\mathbf{q}\mathbf{G}_1)\rho_{vc}(\mathbf{q}\mathbf{G}_2)}{\omega - (\xi_v - \xi_c) + i0^+}. \quad (\text{A.2.21})$$

Denominators contribute as² (P means principle value):

$$\frac{1}{x \pm i0^+} = \frac{P}{x} \mp i\pi\delta(x), \quad (\text{A.2.22})$$

which leads to:

$$\chi_{0ij}(\mathbf{q}\omega) = R_{ij}(\mathbf{q}\omega) - i\pi I_{ij}(\mathbf{q}\omega), \quad (\text{A.2.23})$$

where ($\epsilon_{cv} = \epsilon_c - \epsilon_v$)

$$R_{ij}(\mathbf{q}\omega) = \frac{2}{\Omega_{WS}} \sum_{cv} P \frac{\rho_{cv}^*(\mathbf{q}\mathbf{G}_i)\rho_{cv}(\mathbf{q}\mathbf{G}_j)}{\omega - \epsilon_{cv}} + a.p. = R_{ji}^*(\mathbf{q}\omega) \quad (\text{A.2.24})$$

$$I_{ij}(\mathbf{q}\omega) = \frac{2}{\Omega_{WS}} \sum_{cv} \rho_{cv}^*(\mathbf{q}\mathbf{G}_i)\rho_{cv}(\mathbf{q}\mathbf{G}_j)\delta(\omega - \epsilon_{cv}) + a.p. = I_{ji}^*(\mathbf{q}\omega) \quad (\text{A.2.25})$$

where, $a.p.$ is an anti-resonant part and both R and I are hermitian matrices.

It is necessary to note the ω -behavior at the diagonal ($\mathbf{G}_i = \mathbf{G}_j$), especially the sign change of the I_{ii} :

$$I_{ii}(\mathbf{q}\omega) = I_{ii}^r(\mathbf{q}\omega) + I_{ii}^a(\mathbf{q}\omega) = \frac{2}{\Omega_{WS}} \sum_{vc} |\rho_{cv}(\mathbf{q}\mathbf{G}_i)|^2 \{\delta(\omega - \epsilon_{cv}) - \delta(\omega + \epsilon_{cv})\}, \quad (\text{A.2.26})$$

²Sokhotski–Plemelj theorem

so we write for the imaginary part:

$$\text{Im}[\chi_0(\mathbf{q}\mathbf{G}_i\mathbf{G}_i\omega)] = -\pi I_{ii}(\mathbf{q}\omega) = -\pi |I_{ii}(\mathbf{q}\omega)| \text{sign}[\omega]. \quad (\text{A.2.27})$$

In this way we get the correct sign of the imaginary part for the retarded dielectric function in the $\omega > 0$ case ($\mathbf{G}_i = \mathbf{G}_j$):

$$\text{Im}[\epsilon_{RPA}(\mathbf{q}\omega)] = \text{Im}[1 - v(\mathbf{q})\chi_0(\mathbf{q}\omega)] > 0. \quad (\text{A.2.28})$$

For $\omega = 0$ we see that³

$$R_{ij}(\mathbf{q}0) = -\frac{2}{\Omega_{WS}} \sum_{cv} P \frac{2}{\epsilon_{cv}} \text{Re}[\rho_{cv}^*(\mathbf{q}\mathbf{G}_i)\rho_{cv}(\mathbf{q}\mathbf{G}_j)] = \text{purely real} \quad (\text{A.2.29})$$

$$I_{ij}(\mathbf{q}0) = \frac{2i}{\Omega_{WS}} \sum_{cv} \delta(\epsilon_{cv}) 2\text{Im}[\rho_{cv}^{i*}(\mathbf{q}\mathbf{G}_i)\rho_{cv}^j(\mathbf{q}\mathbf{G}_j)] \sim i(1 - \delta_{ij}) \text{ purely complex or } 0, \quad (\text{A.2.30})$$

which makes the dielectric function at $i = j$ to be purely real.

We also have to deal with hermitian and anti-hermitian parts of matrices (as we do, transforming the dielectric function to the imaginary frequency domain in sec. 1.4.2) and give definitions here with χ_0 as an example. The hermitian part is $\mathbf{Re}\chi_0 = \frac{1}{2}(\chi_0 + \chi_0^\dagger)$, $[\mathbf{Re}\chi_0]_{ij} = \frac{1}{2}(\chi_{0ij} + \chi_{0ji}^*)$:

$$[\mathbf{Re}\chi_0]_{ij} = \frac{1}{2}(R_{ij} - i\pi I_{ij} + R_{ji}^* + i\pi I_{ji}^*) = R_{ij}. \quad (\text{A.2.31})$$

Anti-hermitian part is $\mathbf{Im}\chi_0 = \frac{1}{2i}(\chi_0 - \chi_0^\dagger)$, $[\mathbf{Im}\chi_0]_{ij} = \frac{1}{2i}(\chi_{0ij} - \chi_{0ji}^*)$:

$$[\mathbf{Im}\chi_0]_{ij} = \frac{1}{2i}(R_{ij} - i\pi I_{ij} - R_{ji}^* - i\pi I_{ji}^*) = -\pi I_{ij}. \quad (\text{A.2.32})$$

Note that both R_{ij} and I_{ij} are hermitian matrices.

³To prove this relation, we used $\rho_{vc}^i = \frac{1}{N} \langle v | e^{i(\mathbf{q}+\mathbf{G}_i)r} | c \rangle = \frac{1}{N} \langle v | e^{-i(\mathbf{q}+\mathbf{G}_i)r} | c \rangle = \rho_{cv}^{i*}$ relation (hermitian).

Appendix B

MBPT

B.1 Green's function in KS basis

We start from the definition of the time-ordered GF of an N -particle fermionic system in real space:

$$G_{\alpha\beta}(\mathbf{r}\mathbf{r}'t) = -i \left\langle \Psi_N^0 | T_t \hat{\psi}_\alpha(\mathbf{r}t) \hat{\psi}_\beta^\dagger(\mathbf{r}'0) | \Psi_N^0 \right\rangle, \quad (\text{B.1.1})$$

where the field operators are in Heisenberg representation, i.e., $\hat{\psi}_\alpha(\mathbf{r}t) = e^{iHt} \hat{\psi}_\alpha(\mathbf{r}) e^{-iHt}$ (α is a spin index). Writing explicitly the action of time ordering operator T_t and plugging the

$$1 = \sum_j |\Psi_{N\pm 1}^j\rangle \langle \Psi_{N\pm 1}^j|,$$

where $\Psi_{N\pm 1}^j$ is the j th excited state of the $N \pm 1$ -particle system, we come to:

$$\begin{aligned} G_{\alpha\beta}(\mathbf{r}\mathbf{r}'t) &= -i \sum_j \left\{ \Theta(t) \left\langle \Psi_N^0 | e^{iE_N^0 t} \hat{\psi}_\alpha(\mathbf{r}) e^{-iE_{N+1}^j t} | \Psi_{N+1}^j \right\rangle \langle \Psi_{N+1}^j | \hat{\psi}_\beta^\dagger(\mathbf{r}') | \Psi_N^0 \right\rangle \right. \\ &\quad \left. - \Theta(-t) \left\langle \Psi_N^0 | \hat{\psi}_\beta^\dagger(\mathbf{r}') | \Psi_{N-1}^j \right\rangle \langle \Psi_{N-1}^j | e^{iE_{N+1}^j t} \hat{\psi}_\alpha(\mathbf{r}) e^{iE_N^0 t} | \Psi_N^0 \right\rangle \right\}. \end{aligned} \quad (\text{B.1.2})$$

E_N^0 is the ground state energy of the N -particle system. Decomposing the field operators in the KS basis:

$$\hat{\psi}_\alpha(\mathbf{r}) = \sum_k \hat{c}_{k\alpha} \phi_{k\alpha}(\mathbf{r}), \quad \hat{\psi}_\alpha^\dagger(\mathbf{r}) = \sum_k \hat{c}_{k\alpha}^\dagger \phi_{k\alpha}^*(\mathbf{r}) \quad (\text{B.1.3})$$

we get:

$$\begin{aligned} G_{\alpha\beta}(\mathbf{r}\mathbf{r}'t) &= -i \sum_{jkk'} \phi_{k\alpha}(\mathbf{r}) \phi_{k'\beta}^*(\mathbf{r}') \left\{ \Theta(t) \left\langle \Psi_N^0 | \hat{c}_{k\alpha} | \Psi_{N+1}^j \right\rangle \langle \Psi_{N+1}^j | \hat{c}_{k'\beta}^\dagger | \Psi_N^0 \right\rangle e^{-i(E_{N+1}^j - E_N^0)t} \right. \\ &\quad \left. - \Theta(-t) \left\langle \Psi_N^0 | \hat{c}_{k'\beta}^\dagger | \Psi_{N-1}^j \right\rangle \langle \Psi_{N-1}^j | \hat{c}_{k\alpha} | \Psi_N^0 \right\rangle e^{i(E_{N-1}^j - E_N^0)t} \right\}. \end{aligned} \quad (\text{B.1.4})$$

To simplify the notation we use:

$$d_{jk\alpha}^+ = \langle \Psi_N^0 | \hat{c}_{k\alpha} | \Psi_{N+1}^j \rangle, \quad d_{jk\alpha}^- = \langle \Psi_{N-1}^j | \hat{c}_{k\alpha} | \Psi_N^0 \rangle, \quad (\text{B.1.5})$$

$$E_{N+1}^j - E_N^0 = E_{N+1}^j - E_{N+1}^0 + E_{N+1}^0 - E_N^0 = \omega_j + \mu^+, \quad (\text{B.1.6})$$

$$E_{N-1}^j - E_N^0 = E_{N-1}^j - E_{N-1}^0 + E_{N-1}^0 - E_N^0 = \omega_j - \mu^-, \quad (\text{B.1.7})$$

where the chemical potential (μ) and the excitation energy (ω_j) have been introduced. In systems of our interest (solids), the $\mu^+ = \mu^- = \mu$ is a good approximation. Writing all together:

$$\begin{aligned} G_{\alpha\beta}(\mathbf{r}\mathbf{r}'t) &= -i \sum_{jkk'} \phi_{k\alpha}(\mathbf{r}) \phi_{k'\beta}^*(\mathbf{r}') \left\{ d_{jk\alpha}^+ d_{jk'\beta}^{+*} \Theta(t) e^{-i(\omega_j + \mu)t} - d_{jk\alpha}^- d_{jk'\beta}^{-*} \Theta(-t) e^{i(\omega_j - \mu)t} \right\}, \\ &= \sum_{jkk'} \phi_{k\alpha}(\mathbf{r}) \phi_{k'\beta}^*(\mathbf{r}') \int_{-\infty}^{\infty} \frac{d\omega'}{2\pi} \frac{1}{\omega' + i0^+} \left\{ d_{jk\alpha}^+ d_{jk'\beta}^{+*} e^{-i\omega't} e^{-i(\omega_j + \mu)t} - d_{jk\alpha}^- d_{jk'\beta}^{-*} e^{i\omega't} e^{i(\omega_j - \mu)t} \right\}, \end{aligned} \quad (\text{B.1.8})$$

where

$$\Theta(t) = - \int_{-\infty}^{\infty} \frac{d\omega}{2\pi i} \frac{e^{-i\omega t}}{\omega + i0^+} \quad (\text{B.1.9})$$

is the integral representation of the step function.

We can perform a FT to the frequency domain ($G(\omega) = \int_{-\infty}^{\infty} dt e^{i\omega t} G(t)$), using $\int e^{\pm i(\omega - \omega')t} dt = 2\pi \delta(\omega - \omega')$, leading to:

$$\begin{aligned} G_{\alpha\beta}(\mathbf{r}\mathbf{r}'\omega) &= \sum_{jkk'} \phi_{k\alpha}(\mathbf{r}) \phi_{k'\beta}^*(\mathbf{r}') \int_{-\infty}^{\infty} \frac{d\omega'}{2\pi} \frac{\int_{-\infty}^{\infty} dt e^{i\omega t} \left\{ d_{jk\alpha}^+ d_{jk'\beta}^{+*} e^{-i(\omega' + \omega_j + \mu)t} - d_{jk\alpha}^- d_{jk'\beta}^{-*} e^{i(\omega' + \omega_j - \mu)t} \right\}}{\omega' + i0^+} \\ &= \sum_{jkk'} \phi_{k\alpha}(\mathbf{r}) \phi_{k'\beta}^*(\mathbf{r}') \int_{-\infty}^{\infty} d\omega' \frac{\left\{ d_{jk\alpha}^+ d_{jk'\beta}^{+*} \delta(\omega - \omega' - \omega_j - \mu) - d_{jk\alpha}^- d_{jk'\beta}^{-*} \delta(\omega + \omega' + \omega_j - \mu) \right\}}{\omega' + i0^+} \\ &= \sum_{jkk'} \phi_{k\alpha}(\mathbf{r}) \phi_{k'\beta}^*(\mathbf{r}') \left\{ \frac{d_{jk\alpha}^+ d_{jk'\beta}^{+*}}{\omega - \omega_j - \mu + i0^+} + \frac{d_{jk\alpha}^- d_{jk'\beta}^{-*}}{\omega + \omega_j - \mu - i0^+} \right\} \\ &= \sum_{kk'} \phi_{k\alpha}(\mathbf{r}) \phi_{k'\beta}^*(\mathbf{r}') \left\{ G_{\alpha\beta}^+(kk'\omega) + G_{\alpha\beta}^-(kk'\omega) \right\}. \end{aligned} \quad (\text{B.1.10})$$

In this way we write a general decomposition of the interacting GF in the KS basis with $G_{\alpha\beta}^+(kk'\omega) + G_{\alpha\beta}^-(kk'\omega)$ as coefficients. In the paramagnetic situation, the $G_{\alpha\beta} = \delta_{\alpha\beta} G$, and working with the spin-independent part (G), we omit spin indices for simplicity. Moreover, the GF in direct space should be invariant under translation on \mathbf{T} (see chapter A for definitions). From the other side, the KS orbitals (ϕ_k) are Bloch states and each of those in eq. B.1.10 is multiplied by the $e^{i\mathbf{k}\mathbf{T}}$ factor with such operation. As result, the equation above says: $G(\mathbf{r} + \mathbf{T}\mathbf{r}' + \mathbf{T}\omega) \sim \sum_{kk'} e^{i(\mathbf{k} - \mathbf{k}')\mathbf{T}} \phi_k \phi_{k'}^* \{G^+ + G^-\}$, and thus, the $\delta_{\mathbf{k}\mathbf{k}'}$ factor is automatically (eq. A.2.3) imposed in the decomposition. Although we take the $G^{\pm}(kk'\omega)$ diagonal in \mathbf{k} -vector index, in general it is not diagonal in the band index. With the so-called *band decoupling approximation* we neglected this off-diagonal part in sec. 2.1.2.1. For the non-interacting GF we take a KS one, i.e., presenting Ψ_N^i as single Slater determinant out of KS orbitals. Analyzing the $d_{jk}^+ = \langle \Psi_N^0 | \hat{c}_k | \Psi_{N+1}^j \rangle$ factor in this case, we see that it is non-zero (namely, 1) only if Ψ_{N+1}^j is a Slater determinant, in which an additional electron occupies the j 'th excited state above the Fermi level and necessarily $j = k$ (also implies the k is above the Fermi level). The same analysis works for d_{jk}^- as well, but Ψ_{N-1}^j now contains a hole with $j = k$ state below the Fermi level. Collecting all statements together, we write for the KS GF the following expression:

$$G_0(\mathbf{r}\mathbf{r}'\omega) = \sum_k \phi_k(\mathbf{r}) \phi_k^*(\mathbf{r}') \left\{ \frac{(1 - f_k)}{\omega - \omega_k + i0^+} + \frac{f_k}{\omega + \omega_k - i0^+} \right\}, \quad (\text{B.1.11})$$

where we made a shift in ω variable on the magnitude of μ . We also can write an excitation energy as $\omega_k = \xi_k$, i.e., band energy relative to the Fermi level, then the expression in the brackets is also

simplified¹:

$$G_0(\mathbf{r}\mathbf{r}') = \sum_k \phi_k(\mathbf{r})\phi_k^*(\mathbf{r}') \frac{1}{\omega - \xi_k + i\eta(\xi_k)} \quad (\text{B.1.12})$$

B.2 Polarization propagator

Now we calculate the bare polarization propagator from the normal state Kohn-Sham Green's functions (eq. B.1.12). It is given by a so called bubble diagram (ref. [47]), which results in the following expression:

$$\begin{aligned} P_{00}(\mathbf{r}_1\mathbf{r}_2\omega) &= -2i \int \frac{d\omega'}{2\pi} G_0(\mathbf{r}_1\mathbf{r}_2\omega' + \omega) G_0(\mathbf{r}_2\mathbf{r}_1\omega') \\ &= -2i \sum_{kk'} \phi_k(\mathbf{r}_1)\phi_k^*(\mathbf{r}_2)\phi_{k'}(\mathbf{r}_2)\phi_{k'}^*(\mathbf{r}_1) \int \frac{d\omega'}{2\pi} \frac{1}{\omega + \omega' - \xi_k + i\eta(\xi_k)} \frac{1}{\omega' - \xi_{k'} + i\eta(\xi_{k'})}. \end{aligned} \quad (\text{B.2.1})$$

An essential point is the calculation of

$$I = \int d\omega' \frac{1}{\omega + \omega' - \xi_k + i\eta(\xi_k)} \frac{1}{\omega' - \xi_{k'} + i\eta(\xi_{k'})}. \quad (\text{B.2.2})$$

The expression above is equal to a contour integral around a closed contour in the complex plane. The path is chosen in such a way, that one part of it contains the real axis, $z = \omega'$, while the other part forms a half-circle going to infinity, closing the contour. We also add an $\sim e^{i\delta\omega'}|_{\delta \rightarrow 0}$ factor to insure the convergence.

First we show, that if ξ_k and $\xi_{k'}$ are of the same sign (so, $\eta(\xi_k)$ and $\eta(\xi_{k'})$ as well), then the integral vanishes. Suppose, we are above E_F in both cases (ξ_k and $\xi_{k'}$ are positive). There are two poles in the lower-half plane ($z_1 = -\omega + \xi_k - i0_1^+$ and $z_2 = \xi_{k'} - i0_2^+$) and if the contour is closed in the lower-half plane, the integral is proportional to sum of both residues:

$$\begin{aligned} RES &= Res(z_1) + Res(z_2) \\ &= \frac{1}{-\omega + \xi_k - \xi_{k'} + i0_2^+ - i0_1^+} + \frac{1}{\omega + \xi_{k'} - \xi_k + i0_1^+ - i0_2^+} = 0, \end{aligned} \quad (\text{B.2.3})$$

i.e., is exactly zero. The same result would be obtained if we close the contour in the upper-half plane (there are no poles in this region).

Now we try to take (i) $\xi_k > 0$ and $\xi_{k'} < 0$ and calculate:

$$I = \int d\omega' \frac{1}{\omega + \omega' - \xi_k + i0_1^+} \frac{1}{\omega' - \xi_{k'} - i0_2^+}.$$

There is only one pole in each of the half-planes of complex variable $z \leftarrow \omega'$. Closing contour in the upper-half plane, we get a pole $z_2 = \xi_{k'} + i0_2^+$ there. Again, the contour integral is given by residue in the closed contour:

$$I = (2\pi i) \times Res(z_2) = (2\pi i) \times \frac{1}{\omega + \xi_{k'} - \xi_k + i0_1^+ + i0_2^+}. \quad (\text{B.2.4})$$

Similarly, in the situation with (ii) $\xi_k < 0$ and $\xi_{k'} > 0$, we get:

$$I = (2\pi i) \times \frac{-1}{\omega - \xi_k + \xi_{k'} - i0_1^+ - i0_2^+}. \quad (\text{B.2.5})$$

¹ $\eta(x) = \begin{cases} 0^+ & \text{if } x \geq 0 \\ -0^+ & \text{if } x < 0 \end{cases}$

We can combine (i) and (ii) cases using the Fermi distribution (f_k) at $T = 0$.

$$I = (2\pi i) \times \left\{ \frac{(1 - f_k)f_{k'}}{\omega - (\xi_k - \xi_{k'}) + i\eta(\xi_k - \xi_{k'})} - \frac{f_k(1 - f_{k'})}{\omega - (\xi_k - \xi_{k'}) + i\eta(\xi_k - \xi_{k'})} \right\}, \quad (\text{B.2.6})$$

where the function η reads:

$$\eta(x) = \begin{cases} 0^+, & x > 0 \\ -0^+, & x < 0 \end{cases}.$$

The last expression for the integral can be simplified:

$$I = (2\pi i) \times \frac{f_{k'} - f_k}{\omega - (\xi_k - \xi_{k'}) + i\eta(\xi_k - \xi_{k'})}.$$

Finally, for the eq. B.2.7 we write:

$$\begin{aligned} P_{00}(\mathbf{r}_1 \mathbf{r}_2 \omega) &= -2i \sum_{kk'} \phi_k(\mathbf{r}_1) \phi_k^*(\mathbf{r}_2) \phi_{k'}(\mathbf{r}_2) \phi_{k'}^*(\mathbf{r}_1) \\ &\times \frac{1}{2\pi} (2\pi i) \frac{f_{k'} - f_k}{\omega - (\xi_k - \xi_{k'}) + i\eta(\xi_k - \xi_{k'})} \\ &= 2 \sum_{kk'} \frac{(f_{k'} - f_k) \phi_k(\mathbf{r}_1) \phi_k^*(\mathbf{r}_2) \phi_{k'}(\mathbf{r}_2) \phi_{k'}^*(\mathbf{r}_1)}{\omega - (\xi_k - \xi_{k'}) + i\eta(\xi_k - \xi_{k'})}. \end{aligned} \quad (\text{B.2.7})$$

B.3 EOM for \bar{G}_0 and D

First, we would like to derive the equation of motion (EOM) for the non-interacting Nambu Green's function \bar{G}_0 described in section 2.1.2. We start with τ -derivative and use the definitions given in that section:

$$\begin{aligned} \frac{\partial}{\partial \tau} \bar{G}_0(kk'\tau) &= -\frac{\partial}{\partial \tau} \left\langle T_\tau \hat{\psi}_k(\tau) \otimes \hat{\psi}_{k'}^\dagger(0) \right\rangle_0 \\ &= -\frac{\partial}{\partial \tau} \left\{ \Theta(\tau) \left\langle \hat{\psi}_k(\tau) \otimes \hat{\psi}_{k'}^\dagger(0) \right\rangle_0 - \Theta(-\tau) \left\langle \hat{\psi}_{k'}^\dagger(0) \otimes \hat{\psi}_k(\tau) \right\rangle_0 \right\} \\ &= -\delta_\tau \delta_{kk'} \tau_0 - \left\langle T_\tau \left\{ \frac{\partial}{\partial \tau} \hat{\psi}_k(\tau) \right\} \otimes \hat{\psi}_{k'}^\dagger(0) \right\rangle_0 \end{aligned}$$

The EOM (or, the τ -derivative) for the $\hat{\psi}_k(\tau)$ is given by the commutator:

$$\frac{\partial}{\partial \tau} \hat{\psi}_k(\tau) = [H_0, \hat{\psi}_k(\tau)]_-$$

The normal-state Hamiltonian \hat{H}_0 is given by $\hat{H}^{KS} + \hat{H}^{ph}$ from the eq. 2.1.5. The $\hat{\psi}_k(\tau)$ commutes with phononic field operators in \hat{H}^{ph} , hence, the last can be ignored for a moment. The commutator is calculated as the following:

$$\begin{aligned} [\hat{H}^{KS}, \hat{\psi}_l(\tau)]_- &= \hat{H}^{KS} \hat{\psi}_l(\tau) - \hat{\psi}_l(\tau) \hat{H}^{KS} = \sum_k \xi_k \hat{\psi}_k^\dagger \tau_3 \hat{\psi}_k \hat{\psi}_l(\tau) - \sum_k \xi_k \hat{\psi}_l(\tau) \hat{\psi}_k^\dagger \tau_3 \hat{\psi}_k \\ &= \sum_k \xi_k \left(\hat{\psi}_k^\dagger \tau_3 \hat{\psi}_k \hat{\psi}_l(\tau) - \hat{\psi}_l(\tau) \hat{\psi}_k^\dagger \tau_3 \hat{\psi}_k \right) = \sum_k \xi_k \left(\hat{\psi}_k^\dagger \tau_3 \hat{\psi}_k \hat{\psi}_l(\tau) - \{ \delta_{kl} \tau_0 - \hat{\psi}_k^\dagger \hat{\psi}_l(\tau) \} \tau_3 \hat{\psi}_k \right) \\ &= \sum_k \xi_k \left(\hat{\psi}_k^\dagger \tau_3 \hat{\psi}_k \hat{\psi}_l(\tau) - \delta_{kl} \tau_0 \tau_3 \hat{\psi}_k + \hat{\psi}_k^\dagger \tau_3 \hat{\psi}_l(\tau) \hat{\psi}_k \right) \\ &= \sum_k \xi_k \left(\hat{\psi}_k^\dagger \tau_3 \hat{\psi}_k \hat{\psi}_l(\tau) - \delta_{kl} \tau_3 \hat{\psi}_k - \hat{\psi}_k^\dagger \tau_3 \hat{\psi}_k \hat{\psi}_l(\tau) \right) = -\xi_l \tau_3 \hat{\psi}_l \end{aligned}$$

where the anti-commutation relation of eq. 2.1.3 was used in the second line. Finally, the first equation of this section transforms into:

$$\frac{\partial}{\partial \tau} \bar{G}_0(kk'\tau) + \xi_k \tau_3 \bar{G}_0(kk'\tau) = -\delta_\tau \delta_{kk'} \tau_0,$$

which in Matsubara components (eq. 2.1.12) gives the expression for \bar{G}_0 :

$$\bar{G}_0(kk', i\omega_n) = \delta_{kk'} [\omega_n \tau_0 - \xi_k \tau_3]^{-1} = \delta_{kk'} \bar{G}_0(k, i\omega_n).$$

In similar fashion, we derive the EOM for the non-interacting phonon propagator $D_{qq'}(\tau)$ (where q is a combined branch/wavevector index $q = \{j, \mathbf{q}\}$). But first we substitute the expression of $\hat{\varphi}(\hat{\varphi}^\dagger)$ via the phonon creation/annihilation field operators \hat{b} and \hat{b}^\dagger (eq. 1.3.35):

$$\begin{aligned} D_{qq'}(\tau) &= -\left\langle T_\tau \hat{\varphi}_q(\tau) \hat{\varphi}_{q'}^\dagger(0) \right\rangle_0 \\ &= -\left\langle T_\tau \hat{b}_q(\tau) \hat{b}_{q'}^\dagger \right\rangle_0 - \left\langle T_\tau \hat{b}_{-q}^\dagger(\tau) \hat{b}_{-q'} \right\rangle_0 \\ &= D_{qq'}^I(\tau) + D_{qq'}^{II}(\tau), \end{aligned}$$

where $\sim \hat{b}\hat{b}$ and $\sim \hat{b}^\dagger\hat{b}^\dagger$ terms vanished at the average, and $D_{qq'}^I$ and $D_{qq'}^{II}$ describe the propagation of phonon and phonon 'hole' correspondingly. The EOM for $D_{qq'}^I$ reads:

$$\begin{aligned} \frac{\partial}{\partial \tau} D_{qq'}^I(\tau) &= -\frac{\partial}{\partial \tau} \left\{ \Theta(\tau) \left\langle \hat{b}_q(\tau) \hat{b}_{q'}^\dagger \right\rangle_0 + \Theta(-\tau) \left\langle \hat{b}_q(\tau) \hat{b}_{q'}^\dagger \right\rangle_0 \right\} \\ &= -\delta_\tau \delta_{qq'} - \left\langle T_\tau \frac{\partial \hat{b}_q(\tau)}{\partial \tau} \hat{b}_{q'}^\dagger \right\rangle_0 = -\delta_\tau \delta_{qq'} + \omega_q \left\langle T_\tau \hat{b}_q(\tau) \hat{b}_{q'}^\dagger \right\rangle_0, \end{aligned}$$

where the $\frac{\partial}{\partial \tau} \hat{b}_k(\tau) = -\omega_k \hat{b}_k(\tau)$ equation of motion was used (the derivation is simple and similar to the one for the Fermionic $\hat{\psi}$ operator. The same equation for \hat{b}^\dagger reads $\frac{\partial}{\partial \tau} \hat{b}_k^\dagger(\tau) = \omega_k \hat{b}_k^\dagger(\tau)$ and is used in the derivation for $D_{qq'}^{II}$). After simplification we get:

$$\left\{ \frac{\partial}{\partial \tau} + \omega_q \right\} D_{qq'}^I(\tau) = -\delta_\tau \delta_{qq'}$$

The equation is solved in Matsubara components (eq. 2.1.13):

$$\begin{aligned} \{-i\nu_n + \omega_q\} D_{qq'}^I(i\nu_n) &= -\delta_{qq'} \\ D_{qq'}^I(i\nu_n) &= \frac{-\delta_{qq'}}{-i\nu_n + \omega_q} \end{aligned}$$

Performing the same steps, we find the expression for D^{II} :

$$D_{qq'}^{II}(i\nu_n) = \frac{\delta_{qq'}}{-i\nu_n - \omega_q},$$

which gives the form of the total D by a sum with $D_{qq'}^I$:

$$D_{qq'}(i\nu_n) = \delta_{qq'} \frac{-2\omega_q}{\nu_n^2 + \omega_q^2} = \delta_{qq'} D_q(i\nu_n)$$

B.4 MBPT for magnetic perturbations

In this section we are going to write a perturbation expansion of normal and anomalous GF, using Wick's theorem. We start with the normal GF, which is defined by the following ensemble average [7]:

$$G(k\tau) = - \left\langle T_\tau \hat{c}_{k\uparrow}(\tau) \hat{c}_{k\uparrow}^\dagger(0) \hat{\sigma}(1/T) \right\rangle_0. \quad (\text{B.4.1})$$

All time-dependent operators of this section are in interaction representation, i.e.,

$$\hat{a} = e^{(\hat{H}^0 - \mu \hat{N})\tau} \hat{a} e^{-(\hat{H}^0 - \mu \hat{N})\tau}. \quad (\text{B.4.2})$$

The (non-interacting) ground state ensemble average is calculated as follows:

$$\langle \dots \rangle_0 = \text{tr} \left\{ e^{\frac{\Omega_0 + \mu \hat{N} - \hat{H}^0}{T}} \dots \right\}, \quad e^{\Omega_0} = \text{tr} \left\{ e^{\frac{\mu \hat{N} - \hat{H}^0}{T}} \right\}. \quad (\text{B.4.3})$$

The evolution operator $\hat{\sigma}(1/T)$ is defined by the chosen perturbation ($\hat{H}_{int} = \hat{H}_\pm^m$ from sec. 2.1.3.4, written also in the interaction picture):

$$\begin{aligned} \sigma(1/T) &= T_\tau e^{-\int_0^{1/T} \hat{H}_{int}(\tau) d\tau} \\ &= \sum_{n=0}^{\infty} \frac{(-1)^n}{n!} \int_0^{1/T} \dots \int_0^{1/T} d\tau_1 \dots d\tau_n T_\tau \{ \hat{H}_{int}(\tau_1) \dots \hat{H}_{int}(\tau_n) \} \end{aligned} \quad (\text{B.4.4})$$

The interaction part of the Hamiltonian \hat{H}_{int} is given by one ion spin operator $\hat{S}^{+(-)}$ and two fermionic field operators $\hat{c}^\dagger \hat{c}$ (see eq. 2.1.30). Thus, the first-order term ($n = 1$) in eq. B.4.4 would give an average in eq. B.4.1 out of the one $\hat{S}^{+(-)}$ and four $\hat{c}^{(\dagger)}$ operators. This corresponds to taking into account the magnetization of ionic sites, which should be neglected since we are restricted to paramagnetism when we study superconductivity. Hence, the first contribution to the eq. B.4.1 comes from the second order ($n = 2$) term of eq. B.4.4, in this case average if two spin operators appears. Neglecting terms with $[\hat{S}_{\mathbf{q}}^-]^2$ and $[\hat{S}_{\mathbf{q}}^+]^2$, we write the corresponding contribution to G :

$$\begin{aligned} \delta G^2(k\tau) &= -\frac{1}{2} \int_0^{1/T} d\tau_1 d\tau_2 \sum_{k_1 k'_1} I_{k_1 k'_1} \sum_{k_2 k'_2} I_{k_2 k'_2} \\ &\times \left\{ \left\langle T_\tau \hat{S}_{\mathbf{q}_1}^-(\tau_1) \hat{S}_{\mathbf{q}_2}^+(\tau_2) \right\rangle \left\langle T_\tau \hat{c}_{k\uparrow}(\tau) \hat{c}_{k\uparrow}^\dagger(0) \hat{c}_{k_1\uparrow}^\dagger(\tau_1) \hat{c}_{k'_1\downarrow}(\tau_1) \hat{c}_{k_2\downarrow}^\dagger(\tau_2) \hat{c}_{k'_2\uparrow}(\tau_2) \right\rangle_0 \right. \\ &+ \left. \left\langle T_\tau \hat{S}_{\mathbf{q}_1}^+(\tau_1) \hat{S}_{\mathbf{q}_2}^-(\tau_2) \right\rangle \left\langle T_\tau \hat{c}_{k\uparrow}(\tau) \hat{c}_{k\uparrow}^\dagger(0) \hat{c}_{k_1\downarrow}^\dagger(\tau_1) \hat{c}_{k'_1\uparrow}(\tau_1) \hat{c}_{k_2\uparrow}^\dagger(\tau_2) \hat{c}_{k'_2\downarrow}(\tau_2) \right\rangle_0 \right\} \\ &= \int_0^{1/T} d\tau_1 d\tau_2 \sum_{k_1 k'_1 k_2 k'_2} I_{k_1 k'_1} I_{k_2 k'_2} D_{\mathbf{q}_1 \mathbf{q}_2}^\pm(\tau_1 \tau_2) \\ &\times \left\langle T_\tau \hat{c}_{k\uparrow}(\tau) \hat{c}_{k\uparrow}^\dagger(0) \hat{c}_{k_1\uparrow}^\dagger(\tau_1) \hat{c}_{k'_1\downarrow}(\tau_1) \hat{c}_{k_2\downarrow}^\dagger(\tau_2) \hat{c}_{k'_2\uparrow}(\tau_2) \right\rangle_0. \end{aligned} \quad (\text{B.4.5})$$

The two terms in curly brackets will be equal after swapping variables of integration and summation: $\tau_1 \leftrightarrow \tau_2$ and $k_1 k'_1 \leftrightarrow k_2 k'_2$. Also we define a magnon propagator:

$$D_{\mathbf{q}_1 \mathbf{q}_2}^\pm(\tau_1 \tau_2) = - \left\langle T_\tau \hat{S}_{\mathbf{q}_1}^-(\tau_1) \hat{S}_{\mathbf{q}_2}^+(\tau_2) \right\rangle_0 \quad (\text{B.4.6})$$

According to Wick's theorem, one writes an average of arbitrary number of operators as a sum of all possible contractions of pairs. For the average of six Fermionic operators above we write:

$$\begin{aligned} & \left\langle T_\tau \hat{c}_{k\uparrow}(\tau) \hat{c}_{k\uparrow}^\dagger(0) \hat{c}_{k_1\uparrow}^\dagger(\tau_1) \hat{c}_{k_1\downarrow}(\tau_1) \hat{c}_{k_2\downarrow}^\dagger(\tau_2) \hat{c}_{k_2\uparrow}(\tau_2) \right\rangle_0 = \\ & -G_0(kk_1\tau\tau_1)G_0(k'_1k_2\tau_1\tau_2)G_0(k'_2k\tau_20) - G_0(kk_1\tau\tau_1)F_0(k'_2k'_1\tau_2\tau_1)F_0^\dagger(k_2k\tau_20) \\ & -F_0(kk'_1\tau\tau_1)F_0^\dagger(k_2k_1\tau_2\tau_1)G_0(k'_2k\tau_20) - F_0(kk'_1\tau\tau_1)G_0^\dagger(k_1k'_2\tau_1\tau_2)F_0^\dagger(k_2k\tau_20). \end{aligned}$$

In the formula above we write only those terms, which correspond to exchange-like contributions, i.e., not allowing any of G_0, F_0, G_0^\dagger or F_0^\dagger to have equal time variables. And the definitions of G_0, F_0, G_0^\dagger or F_0^\dagger are:

$$\begin{aligned} G_0(kk_1\tau\tau_1) &= -\left\langle T_\tau \hat{c}_{k\uparrow}(\tau) \hat{c}_{k_1\uparrow}^\dagger(\tau_1) \right\rangle_0, \quad F_0(kk'_1\tau\tau_1) = -\left\langle T_\tau \hat{c}_{k\uparrow}(\tau) \hat{c}_{k'_1\downarrow}(\tau_1) \right\rangle_0 \\ G_0^\dagger(k_1k'_2\tau_1\tau_2) &= -\left\langle T_\tau \hat{c}_{k_1\uparrow}^\dagger(\tau_1) \hat{c}_{k'_2\uparrow}(\tau_2) \right\rangle_0, \quad F_0^\dagger(k_2k_1\tau_2\tau_1) = -\left\langle T_\tau \hat{c}_{k_2\downarrow}^\dagger(\tau_2) \hat{c}_{k_1\uparrow}(\tau_1) \right\rangle_0 \end{aligned}$$

We work within the decoupling approximation, which means that the normal GF is $G^{(\dagger)}(kk') \sim G^{(\dagger)}(k)\delta_{kk'}$ and the anomalous one is $F^{(\dagger)}(kk') \sim F^{(\dagger)}(k)\delta_{k,-k'}$. Thus we rewrite the average using such properties explicitly (omitting arguments of the GF's for a moment):

$$\begin{aligned} \langle T_{\tau\dots} \rangle_0 &= -\delta_{kk_1}\delta_{k'_1k_2}\delta_{k'_2k}G_0G_0G_0 - \delta_{kk_1}\delta_{k'_1,-k'_2}\delta_{k_2,-k}G_0F_0F_0^\dagger \\ &\quad - \delta_{k'_1,-k}\delta_{k_2,-k_1}\delta_{k'_2,k}F_0F_0^\dagger G_0 - \delta_{k'_1,-k}\delta_{k_1k'_2}\delta_{k_2,-k}F_0G_0^\dagger F_0^\dagger \end{aligned}$$

Then, instead of a sum over four arguments $(k_1k'_1k_2k'_2)$, we have a sum over one k' :

$$\begin{aligned} \delta G^2(k\tau) &= \int_0^{1/T} d\tau_1 d\tau_2 \sum_{k'} I_{kk'}^2 D_{\mathbf{q}}^\pm(\tau_1\tau_2) \\ &\quad \times \{G_0(k\tau\tau_1)G_0(k'\tau_1\tau_2)G_0(k\tau_20) + G_0(k\tau\tau_1)F_0(k'\tau_2\tau_1)F_0^\dagger(k\tau_20) \\ &\quad + F_0(k\tau\tau_1)F_0^\dagger(k'\tau_2\tau_1)G_0(k\tau_20) + F_0(k\tau\tau_1)G_0^\dagger(k'\tau_1\tau_2)F_0^\dagger(k\tau_20)\} \end{aligned} \quad (\text{B.4.7})$$

One may argue, that a non-proper time ordering in F and F^\dagger would lead to an effective 'minus' sign in front of the second and third terms. But going to the FT, this would lead to a $-i\omega_n$ argument at that place. And we saw, that F and F^\dagger are symmetric on the frequency axis ($\phi(i\omega_n)$ is symmetric in eq. 2.2.4), thus, one is free to just swap time variables $\tau_1 \leftrightarrow \tau_2$ and consider a 'plus' sign.

The same analysis for $F = -\langle T_\tau \hat{c}_{k\uparrow}(\tau) \hat{c}_{-k\downarrow}(\tau) \hat{\sigma}(1/T) \rangle_0$ leads to:

$$\delta F^2(k\tau) = -\int_0^{1/T} d\tau_1 d\tau_2 \sum_{k'} I_{kk'}^2 D_{\mathbf{q}}^\pm(\tau_1\tau_2) \{G_0G_0F_0 + G_0F_0G_0^\dagger + F_0F_0^\dagger F_0 + F_0G_0^\dagger G_0^\dagger\}$$

In similar fashion, one calculates $\delta G^{\dagger 2}$ and $\delta F^{\dagger 2}$, and now we can collect all contributions

together, omitting some arguments for simplicity:

$$\begin{aligned}
\delta G^2 &= - \int d\tau_1 d\tau_2 \sum_{k'} I_{kk'}^2 D_{\mathbf{q}}^{\pm} \{G_0 G_0 G_0 + G_0 F_0 F_0^\dagger + F_0 F_0^\dagger G_0 + F_0 G_0^\dagger F_0^\dagger\} \\
\delta F^2 &= - \int d\tau_1 d\tau_2 \sum_{k'} I_{kk'}^2 D_{\mathbf{q}}^{\pm} \{G_0 G_0 F_0 + G_0 F_0 G_0^\dagger + F_0 F_0^\dagger F_0 + F_0 G_0^\dagger G_0^\dagger\} \\
\delta G^{\dagger 2} &= - \int d\tau_1 d\tau_2 \sum_{k'} I_{kk'}^2 D_{\mathbf{q}}^{\pm} \{F_0^\dagger G_0 F_0 + F_0^\dagger F_0 G_0^\dagger + G_0^\dagger F_0^\dagger F_0 + G_0^\dagger G_0^\dagger G_0^\dagger\} \\
\delta F^{\dagger 2} &= - \int d\tau_1 d\tau_2 \sum_{k'} I_{kk'}^2 D_{\mathbf{q}}^{\pm} \{F_0^\dagger G_0 G_0 + F_0^\dagger F_0 F_0^\dagger + G_0^\dagger F_0^\dagger G_0 + G_0^\dagger G_0^\dagger F_0^\dagger\}.
\end{aligned}$$

If we use a Nambu GF as usual:

$$\bar{G}_0 = \begin{pmatrix} G_0 & F_0 \\ F_0^\dagger & G_0^\dagger \end{pmatrix}, \quad (\text{B.4.8})$$

those four equations are written into the matrix:

$$\delta \bar{G}^2(k\tau) = - \int_0^{1/T} d\tau_1 d\tau_2 \sum_{k'} I_{kk'}^2 D_{\mathbf{q}}^{\pm} \bar{G}_0 \tau_0 \bar{G}_0 \tau_0 \bar{G}_0. \quad (\text{B.4.9})$$

This is the first non-vanishing perturbative contribution to the Nambu GF.

B.5 Spectral function of spin fluctuations

Following ref. [58], the simplified model of electron-paramagnon interaction (sec. 2.1.3.4) was used to derive the expression for the spin fluctuation spectral function $P(\omega)$ (eq 2.2.24). While in this section we discuss a simple way to estimate the $P(\omega)$, choosing the scheme from ref. [84].

The spin fluctuation propagator, $D_{\mathbf{q}}^{\pm}(\omega)$ (enters eq. 2.2.24) defines a propagation of magnetic excitation through the crystal. This is the transverse part of the full tensor $D_{\alpha\beta}$, which defines the magnetic response of the system:

$$\delta m_{\alpha}^1 = D_{\alpha\beta} \delta v_{\beta}^{ext}.$$

As in sec. 1.4.1.4, one is free to define a (non-interacting) KS magnetic response $D_{0\alpha\beta}$ and express the interacting $D_{\alpha\beta}$ via $D_{0\alpha\beta}$:

$$D_{\alpha\beta} = D_{0\alpha\beta} + D_{0\alpha\beta} I D_{\alpha\beta},$$

the result is similar to the one for the interacting density-density response χ (see eq. 1.4.26) with exchange I instead of $(v + f_{xc})$. The same conclusions were obtained by Vosko and Perdew in their theory of paramagnetism [107]. In the paramagnet, the $D_{\alpha\beta}$ tensor is diagonal with $D_{xx} = D_{yy} = D_{zz}$ (for cubic symmetries) and the transverse magnetic response is $D^{\pm} = D_{xx} + D_{yy} = 2D_{xx}$. The longitudinal KS magnetic response (D_{xx}) is exactly the KS charge-charge response χ_0 , therefore for the total $D_{\mathbf{q}}^{\pm}$ the following is true:

$$D_{\mathbf{q}}^{\pm}(\omega) = \frac{2\chi_0(\mathbf{q}\omega)}{1 - I\chi_0(\mathbf{q}\omega)}, \quad (\text{B.5.1})$$

The sign of exchange interaction is crucial here. Dealing with ferromagnetic interactions, the effective sign is negative, i.e., $I = -I_{ex}$. In this way the interacting $D_{\mathbf{q}}^{\pm}(\omega)$ may be significantly

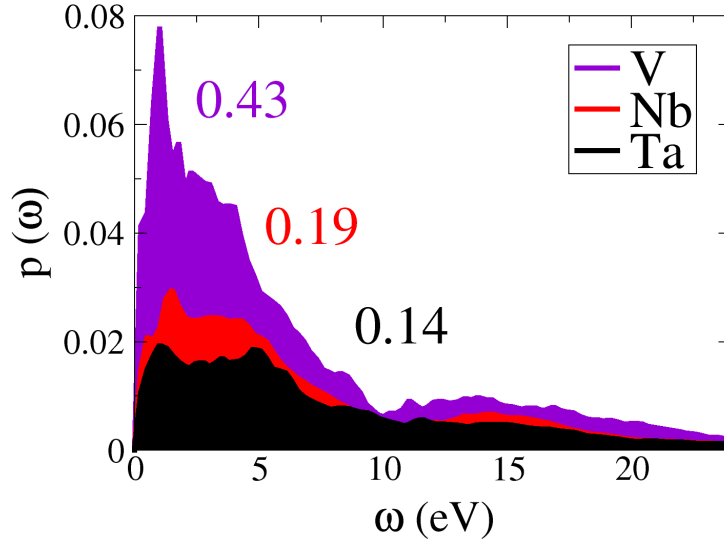


Figure B.1: Spectral function of spin fluctuations for three transitional metals: V, Nb and Ta. Corresponding coupling strength λ^{sf} is given by text.

enhanced (in comparison with χ_0) in the low- \mathbf{q} low- ω region, which will give rise to strong electron-paramagnon coupling. The value of enhancement is estimated with the so-called Stoner parameter:

$$S = [1 + I_{ex}\chi_0(\mathbf{00})]^{-1} = [1 - I_{ex}N_F]^{-1}, \quad (\text{B.5.2})$$

and the corresponding Stoner criterion of ferromagnetic transition is when S becomes negative, or, alternatively $I_{ex}N_F \geq 1$.

Due to translational symmetry, the $D_{\mathbf{q}}^{\pm}$ is, in principle, a matrix in $\mathbf{G}\mathbf{G}'$ (see sec. 1.4.1.3). But if the $D_{\mathbf{q}}^{\pm}(\omega)$ is the most prominent in the low- \mathbf{q} limit (proximity to ferromagnetism), the head of this matrix ($\mathbf{G} = \mathbf{G}' = 0$) dominates and other components can be neglected. Moreover, the dependence I_{ex} on \mathbf{q} also can be safely neglected for the same reason. Equality of longitudinal KS magnetic response ($D_{\mathbf{q}0}^l(\omega)$) and a KS density-density response gives a simple way to define it via basic quantities, like dielectric function (which is calculated in most of the modern solid state codes):

$$D_{\mathbf{q}0}^l(\omega) = \chi_0(\mathbf{q}\omega) = [1 - \varepsilon_{RPA}(\mathbf{q}\omega)]/v(\mathbf{q}),$$

The $P(\omega)$ for V, Nb and Ta is obtained from the above response function and using the eq. 2.2.24. It is given in fig. B.1. The material-dependent exchange parameters I in eq. B.5.1 (also in eq. 2.2.24) were taken from ref. [83] and are 0.0218, 0.0166 and 0.0162 Ry for V, Nb and Ta correspondingly. The essential frequency range is ~ 10 eV, which is far above the phononic one. Although the first peaks appear in $\sim 1 - 2$ eV, our assumption that the spin fluctuation spectral function $P(\omega)$ is a Fermi surface property (like $\alpha^2F(\omega)$) still may fail. Nevertheless we will observe in sec. 3.2.2 that although very simple and rough this approximation still describes qualitatively (and often even quantitatively) the suppression of superconductivity spin fluctuation.

Appendix C

Convergence properties of the Coulomb kernel

C.1 Static case. Superconducting calculations

In this section we present convergence tests of the fully *ab-initio* static Coulomb kernel $K_{stat}^c(\xi\xi')$ (eq. 1.4.41) with respect to the most essential parameters. Within the ELK code [29] those are:

1. k-point grid of the SCF calculation.
2. Number of included reciprocal \mathbf{G} vectors (e.g., in eq. 1.4.33), controlled by the 'gmaxrf' parameter.
3. Number of empty states in the SCF calculation (controlled by 'nempty').

Other parameters, defining the basis for the KS states decomposition, are fixed.

From fig. C.1 it is clear, that the k-point grid for MgB₂ has a greater impact on the T_c as in the case of Nb. This probably is the result of its nested Fermi surface, which is also an issue for the calculation of the electron-phonon coupling (sec. 3.1, [86]). Another crucial parameter is the number of included reciprocal \mathbf{G} vectors. If it is too low, the Coulomb interaction will be overscreened and the resulting T_c thus overestimated. Surprisingly, the effect of empty states was minor. It means that the KS response (eq. B.2.7) is converged with number of empty states quite fast. Of course, this is not true for the dynamical case, i.e., when $\omega \neq 0$ (see also the next section). Note also, that in the last test we fixed the energy cut off E_{cut}^c (see sec. 2.4.2.2) to 10 eV in order to avoid the influence of energy renormalization, i.e., the corresponding changes in the figure are due to the *value* of the Coulomb interaction rather than to its energy range.

C.2 Dynamical case. Lindhard kernel integrations

To investigate the divergence behavior (see sec. 1.4.5) of $K_{lind}^c(\xi\xi'\omega)$ at $\xi \sim \xi'$ limit, we consider the electron gas with $E_F = 0.9 \text{ Ry}$ ¹. We also fix ξ to the Fermi level and construct $K_{lind}^c(\xi\xi'\omega)$ on the ξ' and ω grids, performing an accurate (numerical) angular integration in eq. 1.4.52. The resulting plot of $K_{lind}^c(\xi\xi'\omega)$ is given in fig. C.2. The divergence of $K_{lind}^c(0\xi'\omega)$ at $\xi' \sim 0$ is limited due to numerical accuracy, but from the figure is clear that we still are numerically accurate for $|\xi'| > 0.002 = \delta_0 \text{ Ry}$.

¹Which possesses a plasma frequency $\omega_{plasm} \sim 1.2 \text{ Ry}$.

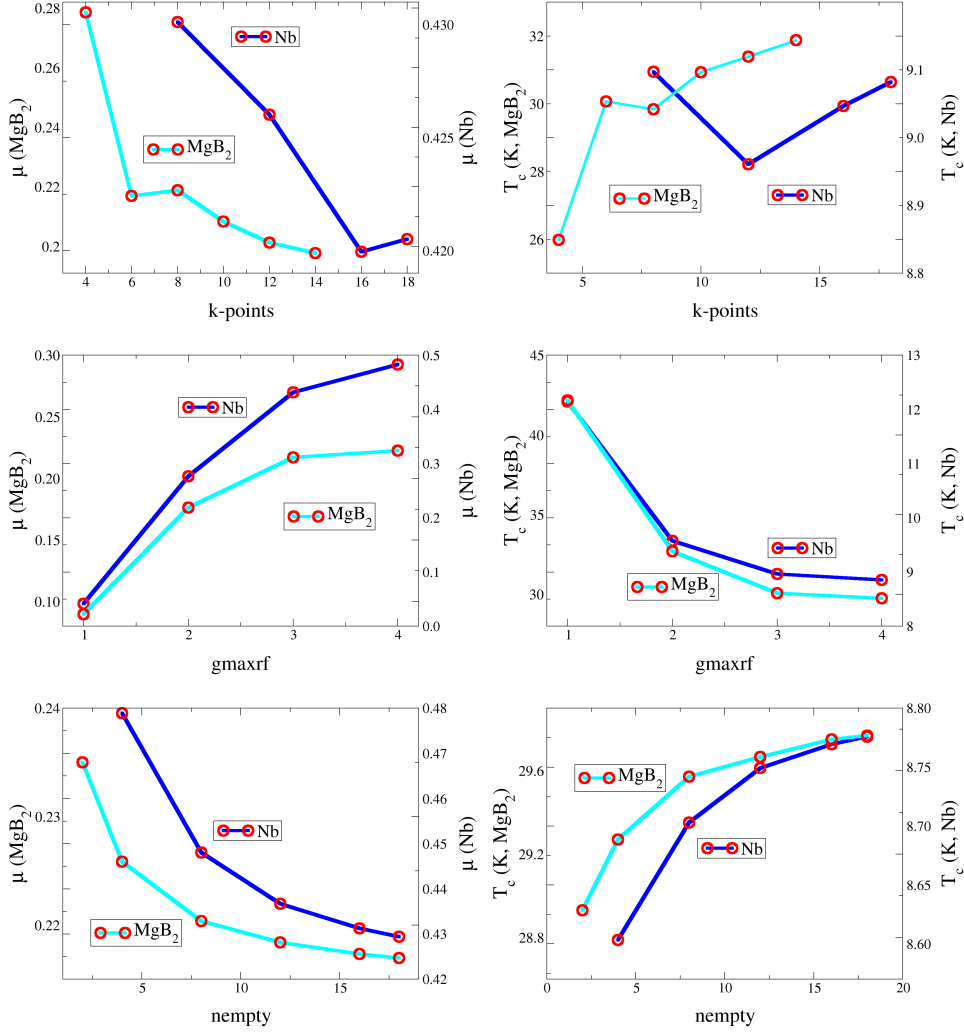


Figure C.1: Convergence of the $\mu = K_{stat}^c(\xi_F \xi_F) N(\xi_F)$ (left column) and Eliashberg T_c (right column) with respect to k-points (first row), 'gmaxrf' (second row) and 'nempty' (bottom row), which are essential parameters in evaluation of $K_{stat}^c(\xi \xi')$.

To investigate whether $K_{lind}^c(0\xi'\omega)$ is integrable in ξ' , we construct the series of $F_{surf}(\omega, \delta_0 < \delta < \Xi)$, such that:

$$F_{surf}(\omega, \delta) = \int_{-\Xi}^{-\delta} d\xi' K_{lind}^c(0\xi'\omega) + \int_{\delta}^{\Xi} d\xi' K_{lind}^c(0\xi'\omega), \quad (\text{C.2.1})$$

where Ξ specifies the peak region (we took $\Xi = 0.3$ Ry). The resulting $F(\omega, \delta)$ is given in fig. C.3 as a function of δ . The $\delta \rightarrow 0$ limit (i.e., $F_{surf}(\omega, \delta = 0)$) is extrapolated linearly² and one can see that $F_{surf}(\omega, \delta = 0)$ is the same as $F_{surf}(\omega, \delta = \delta_0)$ (within the 1% error) which means that such integrals can be converged by direct numerical integrations. Hence, this method of direct integration of the K_{lind}^c will be used when working with the electron gas. In particular, in sec. 3.3.1 we investigate the electron gas of 1,5,10 and 20 eV, for which we plot K_{lind}^c and the corresponding $Im[\epsilon_{lind}^{-1}(q\omega)v_1]$ in fig. C.4 and C.5 respectively.

But in calculations for real materials we cannot perform a precise surface average like eq. 1.4.52 for constructing the kernel, we rather use the eq. 1.4.42 with smeared δ -function. Hence, further we would like to prove that in the last case (i.e. if one constructs the kernel via eq. 1.4.42) the same value of the integral $\int d\xi' K_{lind}^c(0\xi'\omega)$ is obtained. We again appeal to the Lindhard kernel K_{lind}^c in this task. Let us consider the next average:

$$\bar{K}_{lind}^c(\xi\xi'\omega\Delta) = \frac{1}{4\Delta^2} \int_{\xi-\Delta}^{\xi+\Delta} dx \int_{\xi'-\Delta}^{\xi'+\Delta} dy K_{lind}^c(xy\omega), \quad (\text{C.2.2})$$

where K_{lind}^c is given by eq. 1.4.52. In this scope, the \bar{K}_{lind}^c is the volume average, i.e., in the volume between $\xi(\xi') - \Delta$ and $\xi(\xi') + \Delta$ spheres. The integral:

$$F_{vol}(\omega, \Delta) = \int_{-\Xi}^{\Xi} d\xi' \bar{K}_{lind}^c(0\xi'\omega\Delta)$$

is now compared with $F_{surf}(\omega, \delta = 0)$ and found to be the same (less than 1% error, see fig. C.3) for rather large values of Δ . The Δ is measured with respect to $\eta_{lind} = 0.04$ Ry.

It turns out that working with averages like in eqs. 1.4.41 and 1.4.42, using a smeared δ -function, gives the same answer being (analytically) *finite* at $\xi = \xi'$. And the choice is to use a Gaussian normalized to 1:

$$\delta_G(x, \eta_G) = \frac{1}{\sqrt{\pi}\eta_G} e^{-\frac{x^2}{\eta_G^2}} \quad (\text{C.2.3})$$

In this case, the η_G plays the role of Δ in eq. C.2.2, hence one has to choose the η_G large enough to converge the integral out of the K_{dyn}^c (here it should be marked as \bar{K}_{dyn}^c but we omit the head) with k -point grids of *ab-initio* calculations.

C.3 Dynamical case. Superconducting calculations

Here we would like to show the convergence of superconducting calculations with respect to the main parameters of the dynamical Coulomb interaction for the electron gas model. The first

²i.e., we plot the line $y = a + bx$, where $b = \partial F_{surf} / \partial \delta$ at δ_0 and a parameter is a scaling, see fig. C.3 .

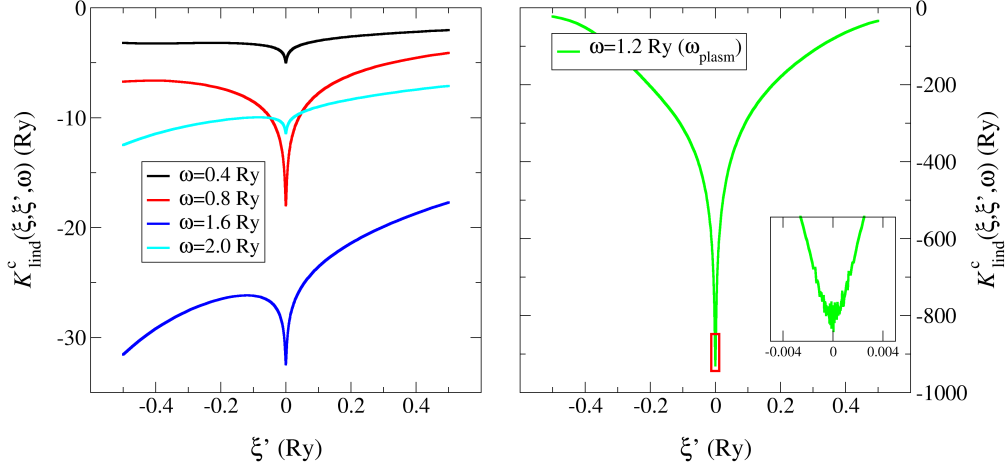


Figure C.2: (left) $K_{lind}^{1c}(0, \xi' \omega)$ for a set of frequencies. (right) The same, but taken at the plasma frequency; the additional inset shows the area in the red rectangle.

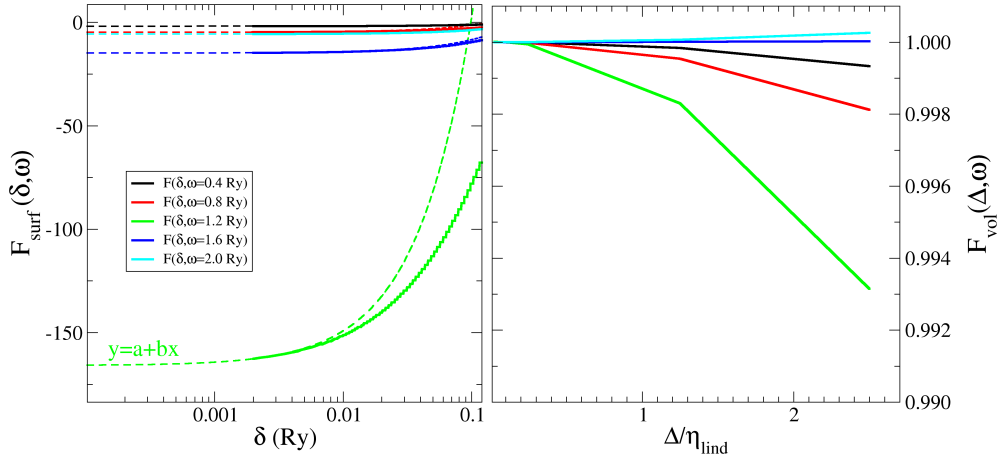


Figure C.3: (left) Integrated Lindhard kernel K_{lind}^{1c} (as a surface average) around the $\xi' = \xi$ divergence according to eq. C.2.1. (right) Integrated \bar{K}_{lind}^{1c} (now, volume average) versus the energy window Δ used to construct \bar{K}_{lind}^{1c} (see eq.C.2.2).

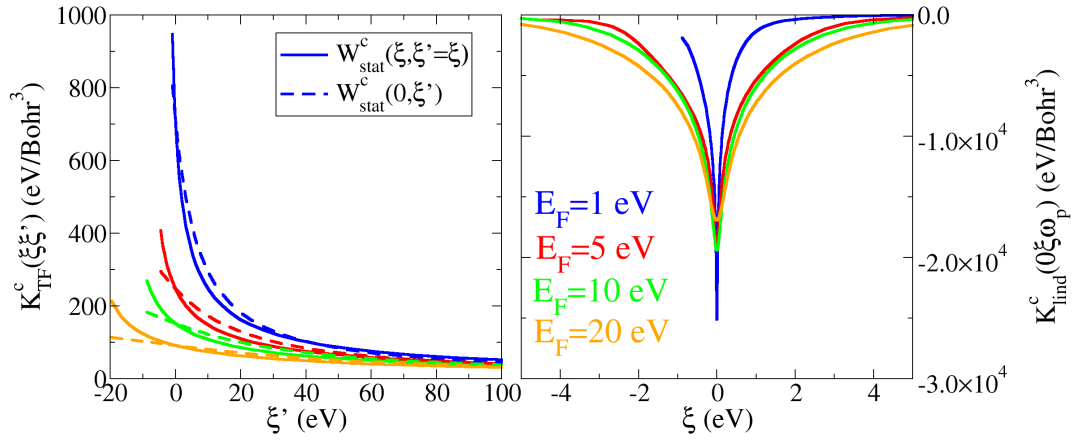


Figure C.4: TF static Coulomb kernel (left), and the dynamical kernel given by Lindhard at the plasma frequency ω_p (right).

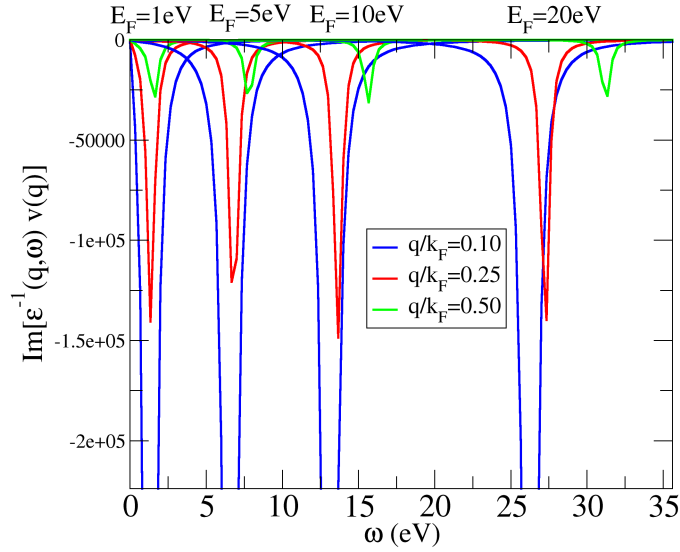


Figure C.5: Frequency-dependent $\text{Im}[\epsilon_{lind}^{-1}(q, \omega)]v_q$ potential used to construct the dynamical kernel for three different q .

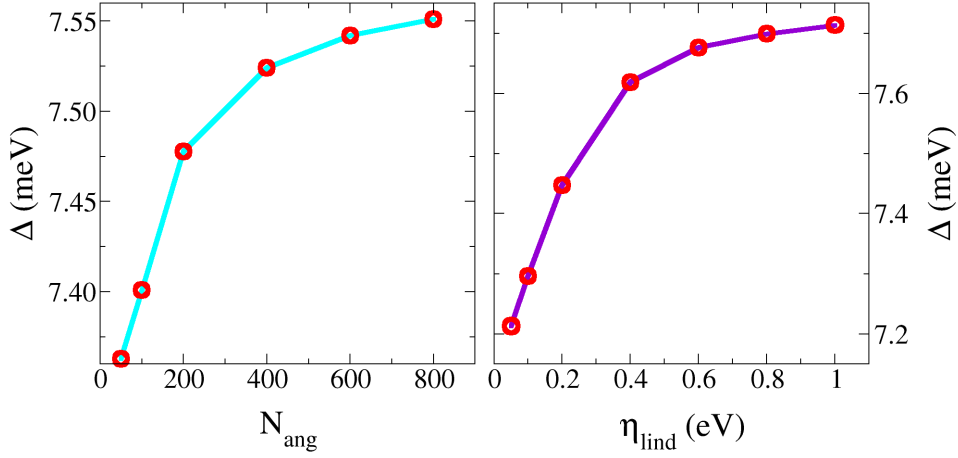


Figure C.6: Dependence of the low-frequency quasiparticle gap function at the Fermi level $\Delta = \Delta(\xi_F, i0)$ on N_{ang} and η_{lind} .

parameter responsible for the accuracy of the energy surface average³ (rewriting the eq. 1.4.52):

$$K_{lind}^c(\xi\xi'\omega) = \frac{1}{S_{k'}} \int_0^\pi d\Theta \int_0^{2\pi} d\phi k'^2 \sin \Theta \tilde{V}_{\mathbf{k}\mathbf{k}'}^{c,lind}(\omega), \quad (\text{C.3.1})$$

is the angular integration grid size N_{ang} (omitting implementation details for simplicity).

In the gap equation (sec. D.1), the following ξ' -integral⁴ has to be converged with N_{ang} :

$$\begin{aligned} \phi_n^{c,dyn}(\xi) &= -T \int_{-E_{cut}^c}^{E_{cut}^c} d\xi' N(\xi') \sum_{\omega_{n'}=\omega_0}^{\omega_{cut}^c} \alpha_{nn'}^{c+}(\xi\xi') \frac{\phi_{n'}(\xi')}{\Theta_{n'}(\xi')}, \\ \alpha^c(\xi\xi' i\nu_{nn'}) &= \int_0^\infty \frac{2\omega}{\pi} K_{lind}^c(\xi\xi'\omega) \left\{ \frac{1}{\omega^2 + \nu^2} - \frac{1}{\omega^2} \right\} d\omega. \end{aligned} \quad (\text{C.3.2})$$

The second parameter affecting the K_{lind}^c , which has not been discussed so far is the smearing width η_{lind} in the dielectric function⁵ ϵ_{lind}^{-1} , which is, in principle, infinitesimal, but in practice numerically always finite.

Instead of investigating the integrals above, we study the dependence of the full dynamical Eliashberg calculations (sec. 2.4.3) on N_{ang} and η_{lind} . The dependence of the obtained quasiparticle gap function on N_{ang} and η_{lind} is shown in fig. C.6. From the figure it is clear, that working with a lower value of N_{ang} (usually we take $N_{ang} \sim 400$), we underestimate the total gap by $\sim 1\%$ (from the one with $N_{ang} \rightarrow \infty$), while working with higher smearing width η_{lind} (usually taken as ~ 0.27 eV) we overestimate the gap by $\sim 5\%$ (from the one with $\eta_{lind} \rightarrow 0$). The total error in our calculation of the gap is about $\sim 4\%$, which is rather low. Hence, this estimation proves that the integration methods are sufficiently accurate and the results are quantitatively reliable.

The calculation of $K_{dyn}^c(\xi\xi'\omega)$ for real systems requires a different surface average, namely:

$$K_{dyn}^c(\xi\xi'\omega) = \frac{1}{N(\xi)N(\xi')} \sum_{\mathbf{k}\mathbf{k}'} \tilde{V}_{\mathbf{k}\mathbf{k}'}^c(\omega) \delta_G(\xi_{\mathbf{k}} - \xi) \delta_G(\xi_{\mathbf{k}'} - \xi'),$$

³To remind, the $\tilde{V}_{\mathbf{k}\mathbf{k}'}^{c,lind}(\omega) = \text{Im}[\epsilon_{lind}^{-1}(\mathbf{q}\omega)]v(\mathbf{q})$ possess a $\sim 1/q^2$ divergence. See sec. 1.4.5.

⁴ α^{c+} is constructed out of α^c , it allows to use a half of Matsubara sum in eq. C.3.2, as discussed in sec. 2.4.

⁵Remember, $\text{Im}[\epsilon_{lind}^{-1}]$ enters the $\tilde{V}_{\mathbf{k}\mathbf{k}'}^{c,lind}(\omega)$ in the eq. C.3.1.

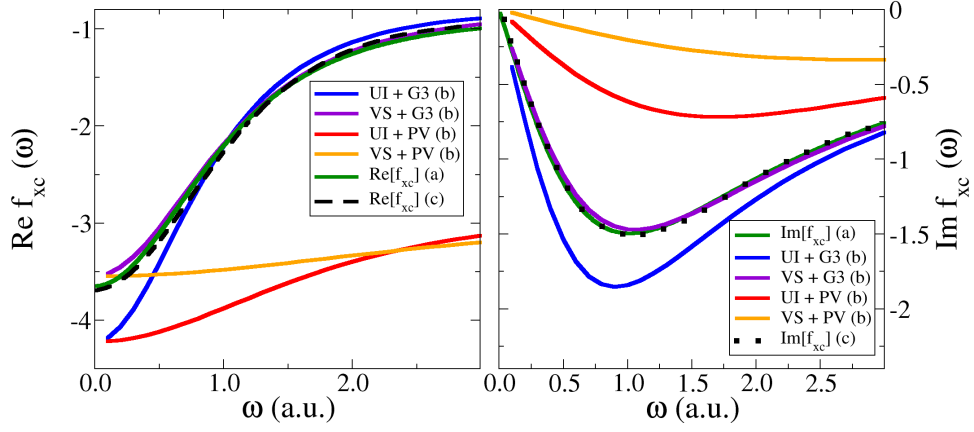


Figure C.7: Comparison between $f_{xc}(q \rightarrow 0, \omega)$ obtained in this work by implementing the modified formulas from ref. [37] (a), the result from ref. [45] (c) and $f_{xc}(q \rightarrow 0, \omega) = -v(q)G(q, \omega)$ (b). All plots are for $r_s = 2$.

where δ_G is actually assumed to be a Gaussian (eq. C.2.3). The role of N_{ang} here is played by the the k -point grid size of the SCF calculation. We observe that the convergence of the full dynamical Eliashberg equations with respect to k -point grid size of the SCF calculations (for K_{dyn}^c) is similar to the one for K_{stat}^c presented in sec. C.1. But, the number of empty states used in the calculation of the susceptibility required to converge K_{dyn}^c is much larger than it was required for K_{stat}^c . The reason is that in order to account for the poles of the response function (eq. B.2.7) at finite ω , one has to have access to the difference $\Delta\xi = \xi_k - \xi_{k'}$ (see denominator of eq. B.2.7) up to energies that are large with respect to ω itself. The frequency range is very large since it should cover all plasmonic peaks of the dielectric function. Consequently, the access⁶ to large $\Delta\xi$ should be provided, and this is controlled by the number of empty states in the SCF calculation (see sec. C.1).

C.4 Gross-Kohn approximation for the ω and q -dependent f_{xc}

In ref. [39], Gross and Kohn developed an approximation for the frequency dependent f_{xc} in the $q \rightarrow 0$ limit. This is given by the Padé-type expression:

$$Im[f_{xc}(q = 0, \omega)] = \frac{a(n)\omega}{[1 + b(n)\omega^2]^{5/4}}, \quad (C.4.1)$$

where a and b are functions of the density n (both expressions are from ref. [37]):

$$\begin{aligned} a(n) &= -c(\gamma/c)^{5/3}[f_\infty(n) - f_0(n)],^{5/3} \\ b(n) &= (\gamma/c)^{4/3}[f_\infty(n) - f_0(n)],^{4/3} \\ \gamma &= [\Gamma(1/4)]^2/(32\pi),^{1/2} \quad c = 23\pi/15 \end{aligned}$$

⁶More precisely, the relevant terms $\Delta\xi = \xi_k - \xi_{k'}$ are with k of a conductance (c) state, while k' of a valence (v) state (or vice versa). It is provided by the Fermi factors in the numerator of eq. B.2.7. The maximum $\Delta\xi_{max}$ is given by $\xi_{c,top} - \xi_{v,bottom}$, where $\xi_{c,top}$ is the top of the conductance states and $\xi_{v,bottom}$ is the bottom of the valence states. Hence, the number of available empty states in the SCF calculation should provide the $\Delta\xi_{max}$ to be greater than the desired frequency range for K_{dyn}^c .

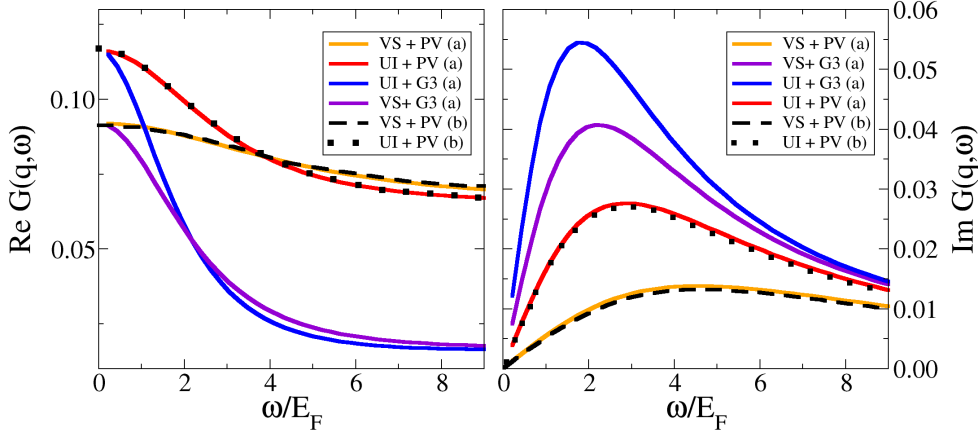


Figure C.8: Comparison between local field corrections $G(q = 0.6, \omega)$ obtained using its different low-frequency (G_0) and high-frequency (G_∞) analytic limits. Black dashed/dotted lines are the result found in ref. [40] with G_0 taken as G_{VS} / G_{UI} , and $G_\infty = G_{PV}$ (see the text for notations), which is reflected in the legends as VS+PV / UI+PV respectively. We could reproduce the same result (red/orange). We also consider the proper high-frequency limit G_3 due to Iwamoto [44] (corresponding cases a labeled as VS+G3 / UI+G3 in the legends). The $r_s = 2$ in this plot.

where as high-frequency limit $f_\infty(n)$ and static limit $f_0(n)$ of $f_{xc}(q \rightarrow 0, \omega)$ one uses the following expressions⁷:

$$f_0(n) = \frac{d^2}{dn^2}[n\epsilon_{xc}(n)], \quad (\text{C.4.2})$$

$$f_\infty(n) = -\frac{4}{5}n^{2/3} \frac{d}{dn}[\epsilon_{xc}(n)/n^{2/3}] + 6n^{1/3} \frac{d}{dn}[\epsilon_{xc}(n)/n^{1/3}], \quad (\text{C.4.3})$$

$$\epsilon_{xc}(n) = \epsilon_x(n) + \epsilon_c(n) \quad (\text{C.4.4})$$

For the correlation energy per particle $\epsilon_c(n)$ we choose the Perdew-Zunger [108] parametrisation and the exchange contribution is given by $\epsilon_x(n) = -3/(4\pi\alpha r_s)$ with $\alpha = (4/9\pi)^{1/3}$. The real part of f_{xc} is given by the Kramers-Kronig relation, which leads to an analytical form (see eq. 210 of ref. [37]):

$$\begin{aligned} \text{Re}[f_{xc}(q=0, \omega)] &= f_\infty(n) + \frac{a(n)}{\pi s^2} \sqrt{\frac{8}{b(n)}} \left\{ 2E\left(\frac{1}{2}\right) - \frac{1+s}{2} \Pi\left(\frac{1-s}{2}, \frac{1}{2}\right) \right. \\ &\quad \left. - \frac{1-s}{2} \text{Re}\left[\Pi\left(\frac{1+s}{2}, \frac{1}{2}\right)\right] \right\}, \quad s(\omega) = \sqrt{1 + b(n)\omega^2}, \end{aligned} \quad (\text{C.4.5})$$

where definitions of complete elliptic integrals of the second (E) and the third (Π) kind are given in ref. [109] and [110] respectively. Also note, that the eq. C.4.5 is different⁸ from the one in ref. [37]. The reason is that in principle, a positive argument $(1+s)/2$ makes the value of Π being a complex number withing the computational tool we used (Mathematica), while the Kramers-Kronig relation for $\text{Re}[f_{xc}]$ implies a principal value integration, which in result should give a real number. To avoid this confusion, we try to use just a real part of the last elliptic integral in eq. C.4.5. To check the modification we reproduce the result of ref. [45] (fig. C.7: black dashed/dotted lines [45])

⁷The last term in eq. C.4.3 is the correction given by Iwamoto [45].

⁸The argument of E is $1/2$ (instead of $1/\sqrt{2}$), which is a consequence of the different from ref. [37] convention (or 'interface') for E function. The same is applied for the second argument of Π .

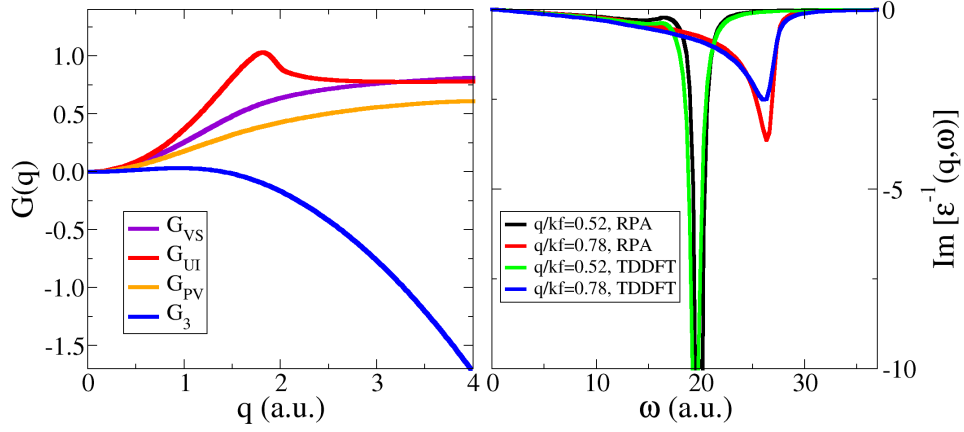


Figure C.9: (left) Static (VS and UI) and high-frequency (PV, G3) limits of the local-field correction $G(q\omega)$. (right) Imaginary part of the inverse dielectric function obtained with RPA and with TDDFT using a frequency and q -dependent f_{xc} .

vs green lines [this work]). A small difference is found because of the different $f_0(n)$ and $f_\infty(n)$ ⁹, which most probably is due to a different parametrization of the correlation energy ϵ_c ¹⁰, while the overall shape of $\text{Re}[f_{xc}]$ is consistent with the literature. Additional check for our modification in eq. C.4.5 coming via comparison between real and imaginary part of the local field correction obtained in this work and the one given by Dabrowski [40], for which the same equations are applied an which does not depend on the choice of ϵ_c .

Following ref. [40], we apply a similar scheme to the frequency and q -dependent local-field correction G , which is related to the $f_{xc}(q, \omega)$ as:

$$f_{xc}(q, \omega) = -v(q)G(q, \omega). \quad (\text{C.4.6})$$

For the G we write similar to eq. C.4.1:

$$\text{Im}[G(q, \omega)] = \frac{a(q, n)\omega}{[1 + b(q, n)\omega^2]^{5/4}},$$

where q -dependent a and b have the following form:

$$\begin{aligned} a(q, n) &= Cq^2 \left[\frac{G_0(q) - G_\infty(q)}{CDq^2} \right]^{5/3}, \\ b(q, n) &= \left[\frac{G_0(q) - G_\infty(q)}{CDq^2} \right]^{4/3}, \\ D &= 0.763 \quad C = 23\alpha r_s/60, \end{aligned} \quad (\text{C.4.7})$$

where $G_0(q)$ represents the static and $G_\infty(q)$ the high-frequency limit of $G(q, \omega)$.

As in the reference, for $G_0(q)$ we use both: the Utsumi and Ichimaru result (UI, ref. [41]) and the Vashishta-Singwi result (VS, ref. [42]). The high-frequency expression $G_\infty(q)$, according to Dabrowski should be given by the Pathak and Vashishta form (PV, ref. [43]). But as in the case with f_∞ , the G from ref. [44] should be used ($G_\infty(q)$ from this approach will be referred as a G_3). We try all listed forms for G_0 and G_∞ in the evaluation of the $q\omega$ -dependent $G(q, \omega)$. The real part $\text{Re}[G(q, \omega)]$ is calculated also via eq. C.4.5, although both a and b are q -dependent now.

⁹ f_0 and f_∞ are -3.64896 and -1.00222 respectively for $r_s = 2$.

¹⁰The Vosko-Wilk-Nussair parametrization [111] was chosen in ref. [45].

All results are given in fig. C.8. We conclude that our result is consistent with the one of Dabrowski, although one should mind the error bar we might have extracting the limiting G 's: the $G_{PV}(q)$, $G_{VS}(q)$ and $G_{UI}(q)$ either taken from the tabulated data (UI and VS) or digitized figure (PV), with subsequent interpolation in q . It should be noted, that using the proper high-frequency limit G_3 in place of G_∞ (eq. C.4.7) strongly modifies the behavior of $G(q, \omega)$. To understand what is the best choice for the $G_\infty(q)$ and $G_0(q)$ we plot the low- q limit of eq. C.4.6 together with the result of ref. [45] in fig. C.7. The best fit to f_{xc} of ref. [45] is provided by taking $G_{VS}(q)$ for $G_0(q)$ and $G_3(q)$ for $G_\infty(q)$. All limiting $G_i(q)$ are shown in fig. C.9.

In the same figure we compare the frequency dependent dielectric function obtained with frequency dependent f_{xc} (eq. 1.4.27) and the one with RPA ($f_{xc} = 0$). The main conclusion, which is important for us, is that $f_{xc}(q, \omega)$ slightly modifies the shape of the plasmon dispersion and its damping, but does not significantly modify the low- q behavior of the dielectric function. Moreover, our tests show that it does not lead to important quantitative differences in the strength of the dynamical part of the Coulomb interaction. Hence, we do not adopt this method in sec. 3.3 considering only RPA to reproduce the dynamical screening.

Appendix D

Eliashberg equations

This appendix assembles the complete information about the details of implementation of our Eliashberg approach. First, (sec. D.1), we collect the complete set of Eliashberg equations in the fully isotropic limit. Second, (sec. D.2), we present the multiband extension to the fully isotropic limit of the Eliashberg equations. And finally (sec. D.3), we write the simplified form of equations, which was used for the model investigation in sec. 2.5.2.

D.1 Review of the different sets of Eliashberg equations

Basically we rewrite the equations appeared in the chap. 2. Those define the mass renormalization $Z_n(\xi) = 1 + Z_n^{ph,m} + Z_n^{c,dyn}(\xi)$ and the Eliashberg gap function $\phi_n(\xi) = \phi_n^{ph,m} + \phi_{stat}^c + \phi_n^{c,dyn}(\xi)$ (sec. 2.4.1). We group them according to integral kernels.

1) Phonon and magnon part:

$$Z_n^{ph,m} = -\frac{T}{\omega_n} \sum_{\omega_{n'}=\omega_0}^{\omega_{cut}^{ph}} \int_{-E_{cut}^{ph}}^{E_{cut}^{ph}} d\xi' N(\xi') K_{nn'}^{(ph+m)-} \frac{Z_{n'}(\xi') \omega_{n'}}{\Theta_{n'}(\xi')}, \quad (D.1.1)$$

$$\phi_n^{ph,m} = -T \sum_{\omega_{n'}=\omega_0}^{\omega_{cut}^{ph}} \int_{-E_{cut}^{ph}}^{E_{cut}^{ph}} d\xi' N(\xi') K_{nn'}^{(ph-m)+} \frac{\phi_{n'}(\xi')}{\Theta_{n'}(\xi')}. \quad (D.1.2)$$

2) static Coulomb part:

$$\phi_{stat}^c(\xi) = -2T \int_{-E_{cut}^c}^{E_{cut}^c} d\xi' N(\xi') K_{stat}^c(\xi\xi') \left[\sum_{\omega_{n'}=\omega_0}^{\omega_{cut}^{c,stat}} \frac{\phi_{n'}(\xi')}{\Theta_{n'}(\xi')} + A(\xi') - B(\xi') \right] \quad (D.1.3)$$

or:

$$\phi_{\mu^*}^c = -2T \frac{\mu^*}{N_F} \int_{-E_{cut}^c}^{E_{cut}^c} d\xi' N(\xi') \sum_{\omega_{n'}=\omega_0}^{\omega_{cut}^c} \frac{\phi_{n'}(\xi')}{\Theta_{n'}(\xi')}. \quad (D.1.4)$$

3) Dynamical Coulomb part

$$Z_n^{c,dyn}(\xi) = -\frac{T}{\omega_n} \sum_{\omega_{n'}=\omega_0}^{\omega_{cut}^c} \int_{-E_{cut}^c}^{E_{cut}^c} d\xi' N(\xi') \alpha_{nn'}^{c-}(\xi\xi') \frac{Z_{n'}(\xi')\omega_{n'}}{\Theta_{n'}(\xi')}, \quad (\text{D.1.5})$$

$$\begin{aligned} \phi_n^{c,dyn}(\xi) &= -T \int_{-E_{cut}^c}^{E_{cut}^c} d\xi' N(\xi') \\ &\times \left[\sum_{\omega_{n'}=\omega_0}^{\omega_{cut}^{c,pp}} \frac{\alpha_{nn'}^{c+}(\xi\xi')\phi_{n'}(\xi')}{\Theta_{n'}(\xi')} + \{\phi_n^{PPA} - \phi_n^{PP}\} \phi_{const}(\xi') \right], \end{aligned} \quad (\text{D.1.6})$$

where the common denominator:

$$\Theta_n(\xi) = [Z_n(\xi)\omega_n]^2 + \xi^2 + \phi_n^2(\xi),$$

and the total Z and ϕ are chosen according to the approximation (see sec. 2.4.3).

D.2 Block-band resolved approach

Basically we proceed here almost in the same way as in sec. 2.2.3. For illustrative reasons, we rewrite the starting point, i.e., the fully anisotropic Eliashberg equations (eq. 2.2.5-2.2.6) restricting to Z and ϕ contributions¹:

$$[1 - Z_n(k)] i\omega_n = T \sum_{k'\omega_{n'}} \left[V_{kk'nn'}^{ph} + V_{kk'nn'}^c \right] \frac{Z_{n'}(k')i\omega_{n'}}{\Theta_{n'}(k')}, \quad (\text{D.2.1})$$

$$\phi_n(k) = -T \sum_{k'\omega_{n'}} \left[V_{kk'nn'}^{ph} + V_{kk'nn'}^c \right] \frac{\phi_{n'}(k')}{\Theta_{n'}(k')}. \quad (\text{D.2.2})$$

The multiband isotropization scheme now is constructed slightly differently than it was in sec. 2.2.3. First, we divide the band structure in subsets of bands indexed with b_1, b_2, \dots, b_B . Consequently, the sums over k' can be equivalently rewritten as:

$$\sum_{k'} \rightarrow \sum_{k' \in b_1} + \sum_{k' \in b_2} + \dots + \sum_{k' \in b_B} = \sum_{b; k' \in b}$$

Then we construct the interaction, which is b -dependent, but isotropic at each b :

$$\begin{aligned} K_{bb';nn'}^c(\xi\xi') &\equiv V_{bb'nn'}^c(\xi_k\xi_{k'}) \\ &= \frac{1}{N_{b'}(\xi')N_b(\xi)} \sum_{k \in b; k' \in b'} V_{kk'nn'}^c \delta(\xi_k - \xi) \delta(\xi_{k'} - \xi'), \end{aligned} \quad (\text{D.2.3})$$

$$K_{bb';nn'}^{ph}(\xi\xi') = V_{bb'nn'}^{ph}(\xi_k\xi_{k'}) \quad (\text{D.2.4})$$

$$= \frac{1}{N_{b'}(\xi')N_b(\xi)} \sum_{k \in b; k' \in b'} V_{kk'nn'}^{ph} \delta(\xi_k - \xi) \delta(\xi_{k'} - \xi'), \quad (\text{D.2.5})$$

where band-block DOS:

$$N_b(\xi) = \sum_{k \in b} \delta(\xi_k - \xi)$$

¹Here we are neglecting the interaction with paramagnons for simplicity.

was introduced. Using the fact that the sum $\sum_{b;k' \in b}$ is equivalent to ξ -integration with the $\sum_{b'} N_{b'}(\xi)$ factor, we arrive to the final multiband-isotropic form of equations:

$$[1 - Z_{bn}(\xi)] i\omega_n = T \sum_{\omega_{n'}} \int d\xi' \sum_{b'} N_{b'}(\xi') \quad (\text{D.2.6})$$

$$\times \left\{ K_{bb';nn'}^{ph}(\xi\xi') + K_{bb';nn'}^c(\xi\xi') \right\} \frac{Z_{b'n'}(\xi') i\omega_{n'}}{\Theta_{b'n'}(\xi')},$$

$$\phi_{bn}(\xi) = -T \sum_{\omega_{n'}} \int d\xi' \sum_{b'} N_{b'}(\xi') \quad (\text{D.2.7})$$

$$\times \left\{ K_{bb';nn'}^{ph}(\xi\xi') + K_{bb';nn'}^c(\xi\xi') \right\} \frac{\phi_{b'n'}(\xi')}{\Theta_{b'n'}(\xi')},$$

$$\Theta_{bn}(\xi) = [Z_{bn}(\xi)\omega_n]^2 + \xi^2 + \phi_{bn}^2(\xi), \quad (\text{D.2.8})$$

Due to the low phononic energy scale, the phonon kernel can be taken at the Fermi level:

$$K_{bb';nn'}^{ph}(\xi\xi') \rightarrow K_{bb';nn'}^{ph}(\xi\xi') \rightarrow K_{bb';nn'}^{ph},$$

which leads to the multiband Eliashberg spectral function $\alpha^2 F_{bb'}(\omega)$ via the following derivation (using the same steps as in sec. 2.2.3.1):

$$\begin{aligned} K_{bb';nn'}^{ph} &= \frac{1}{N_{b'}(\xi_F) N_b(\xi_F)} \sum_{k \in b; k' \in b'} \sum_j |g_{kk'}^j|^2 D_{\mathbf{q}nn'}^j \delta(\xi_k) \delta(\xi_{k'}) \\ &= \frac{1}{N_{b'}(\xi_F) N_b(\xi_F)} \int d\omega \sum_{k \in b; k' \in b'} \sum_j |g_{kk'}^j|^2 \delta(\xi_k) \delta(\xi_{k'}) \delta(\omega_{\mathbf{q}}^j - \omega) D_{\mathbf{q}nn'}^j \\ &= \frac{1}{N_{b'}(\xi_F)} \int d\omega \alpha^2 F_{bb'}(\omega) D_{nn'}(\omega), \end{aligned} \quad (\text{D.2.9})$$

The difference between eqs. D.2.6, D.2.7 and the fully isotropic limit (eqs. 2.2.15, 2.2.16) is minor: the Z , ϕ and Θ now have an additional band index, interaction kernels are square matrices with respect to band indexes, and finally, one has to perform an additional sum over b' on the right-hand side. One can just use this observation and easily transform any set of Eliashberg equations (in sec. D.1) to the multiband case.

D.3 Model A (details)

In this section we would like to detail the model used in sec. 2.5.2 to discuss the basic properties and structure of the solutions of the Eliashberg equations in our approach.

If the Eliashberg spectral function is taken as a δ -peak $\alpha^2 F(\omega) = N\delta(\omega - \omega_{ph})$ normalized to the $\lambda^{ph} = 1$ (eq. 2.2.21), the normalization constant N is then derived in the following way:

$$\begin{aligned} \lambda^{ph} &= 2 \int d\omega \frac{\alpha^2 F(\omega)}{\omega} = 2 \int d\omega \frac{N\delta(\omega - \omega_{ph})}{\omega} = \frac{2N}{\omega_{ph}} \\ &\rightarrow N = \frac{\lambda\omega_{ph}}{2} \end{aligned}$$

Taking the DOS to be a flat function of energy we write its product with the phonon kernel (eq.

2.2.18) as:

$$\begin{aligned} N_F K_{nn'}^{ph} &= \int d\omega \alpha^2 F(\omega) D_{nn'}(\omega) = \frac{\lambda \omega_{ph}}{2} \int d\omega \delta(\omega - \omega_{ph}) \frac{-2\omega}{(\omega_n - \omega_{n'})^2 + \omega^2} \\ &= \lambda \frac{-\omega_{ph}^2}{\nu_{nn'}^2 + \omega_{ph}^2} \end{aligned}$$

The total Coulomb kernel of sec. 2.5.2 is modeled as a $\xi\xi'$ -independent object but with proper frequency behavior, namely:

$$N_F K_{nn'}^c = \mu(1 + K_{nn'}^{pl}) = \mu(1 + \alpha \frac{\nu_{nn'}^2}{\omega_p^2 + \nu_{nn'}^2}),$$

where the frequency structure of the $K_{nn'}^{pl}$ is precisely the one of the plasmon pole approximation (sec. 1.4.4). Plugging it all together in the Eliashberg gap equations (eq. 2.4.13-2.4.14 and ignoring all mass renormalization effects, i.e., $Z = 1$) we obtain the following form:

$$\begin{aligned} \phi_n^{ph} &= T\lambda \int_{-E_{cut}}^{E_{cut}} d\xi' \sum_{\omega_{n'}=\omega_0}^{\omega_{cut}^{ph}} \check{K}_{nn'}^{ph\pm} \frac{\phi_{n'}(\xi')}{\Theta_{n'}(\xi')}, \\ \check{K}_{nn'}^{ph\pm} &= \frac{\omega_{ph}^2}{\omega_{ph}^2 + \nu_{nn'}^2} + \frac{\omega_{ph}^2}{\omega_{ph}^2 + \nu_{n,-(n'+1)}^2}, \\ \phi_n^c &= -2T\mu \int_{-E_{cut}}^{E_{cut}} d\xi' \left\{ \sum_{\omega_{n'}=\omega_0}^{\omega_{cut}^c} (1 + \frac{\alpha}{2} \check{K}_{nn'}^{p\pm}) \frac{\phi_{n'}(\xi')}{\Theta_{n'}(\xi')} \right\}, \\ \check{K}_{nn'}^{p\pm} &= \frac{\nu_{nn'}^2}{\omega_p^2 + \nu_{nn'}^2} + \frac{\nu_{n,-(n'+1)}^2}{\omega_p^2 + \nu_{n,-(n'+1)}^2}, \quad \phi = \phi^{ph} + \phi^c, \\ \Theta_{n'}(\xi') &= \omega_{n'}^2 + \xi'^2 + \phi_{n'}^2(\xi'), \end{aligned}$$

where the notations $\check{K}_{nn'}^{ph\pm}$ and $\check{K}_{nn'}^{p\pm}$ for the frequency dependence of the kernels are introduced, and ϕ_{stat}^c (eq. 2.4.13) is combined with $\phi^{c,dyn}$ (2.4.14) into the Coulomb gap $\phi_n^c(\xi)$ for simplicity. In this form the overall size of the Coulomb interaction is expressed by μ in the static case and by the product $\mu\alpha$ in the dynamic one.

Bibliography

- [1] J. Bardeen, L. N. Cooper, and J. R. Schrieffer, “Theory of Superconductivity,” *Phys. Rev.*, vol. 108, pp. 1175–1204, Dec. 1957.
- [2] H. K. Onnes, “The resistance of pure mercury at helium temperatures,” *Commun. Phys. Lab. Univ. Leiden*, vol. 12, no. 120, p. 1, 1911.
- [3] G. R. Stewart, “Superconductivity in iron compounds,” *Reviews of Modern Physics*, vol. 83, pp. 1589–1652, Dec. 2011.
- [4] J. Paglione and R. L. Greene, “High-temperature superconductivity in iron-based materials,” *Nature Physics*, vol. 6, pp. 645–658, Aug. 2010.
- [5] P. A. Lee and X.-G. Wen, “Doping a Mott insulator: Physics of high-temperature superconductivity,” *Reviews of Modern Physics*, vol. 78, pp. 17–85, Jan. 2006.
- [6] H. Fröhlich, “Theory of the Superconducting State. I. The Ground State at the Absolute Zero of Temperature,” *Phys. Rev.*, vol. 79, pp. 845–856, Sept. 1950.
- [7] A. L. Fetter and J. D. Walecka, *Quantum Theory of Many-particle Systems*. Courier Corporation, 2003.
- [8] A. A. Abrikosov, L. P. Gorkov, and I. E. Dzyaloshinski, *Methods of Quantum Field Theory in Statistical Physics*. Courier Corporation, 2012.
- [9] G. M. Eliashberg, “1437. translation: Sov. Phys.,” *JETP*, vol. 11, no. 696, p. 12, 1960.
- [10] S. Baroni, S. de Gironcoli, A. D. Corso, and P. Giannozzi, “Phonons and related properties of extended systems from density-functional perturbation theory,” *Reviews of Modern Physics*, vol. 73, p. 52, July 2000.
- [11] S. Y. Savrasov and D. Y. Savrasov, “Electron-phonon interactions and related physical properties of metals from linear-response theory,” *Physical Review B*, vol. 54, pp. 16487–16501, Dec. 1996.
- [12] P. Morel and P. W. Anderson, “Calculation of the Superconducting State Parameters with Retarded Electron-Phonon Interaction,” *Physical Review*, vol. 125, pp. 1263–1271, Feb. 1962.
- [13] D. J. Scalapino, J. R. Schrieffer, and J. W. Wilkins, “Strong-Coupling Superconductivity. I,” *Physical Review*, vol. 148, pp. 263–279, Aug. 1966.
- [14] J. P. Carbotte, “Properties of boson-exchange superconductors,” *Reviews of Modern Physics*, vol. 62, pp. 1027–1157, Oct. 1990.

- [15] I. I. Mazin, O. K. Andersen, O. Jepsen, A. A. Golubov, O. V. Dolgov, and J. Kortus, “Comment on ”First-principles calculation of the superconducting transition in MgB2 within the anisotropic Eliashberg formalism”,” *Physical Review B*, vol. 69, p. 3, Feb. 2002.
- [16] M. M. Rieger, L. Steinbeck, I. White, H. Rojas, and R. Godby, “The GW space-time method for the self-energy of large systems,” *Computer Physics Communications*, vol. 117, pp. 211–228, Mar. 1999.
- [17] F. Aryasetiawan and O. Gunnarsson, “The GW method,” *Physical Review*, vol. 139, no. 3A, p. 75, 1997.
- [18] L. N. Oliveira, E. K. U. Gross, and W. Kohn, “Density-Functional Theory for Superconductors,” *Phys. Rev. Lett.*, vol. 60, pp. 2430–2433, June 1988.
- [19] W. Kohn and L. J. Sham, “Self-Consistent Equations Including Exchange and Correlation Effects,” *Physical Review*, vol. 140, pp. A1133–A1138, Nov. 1965.
- [20] M. Born and R. Oppenheimer, “Zur Quantentheorie der Molekeln,” *Annalen der Physik*, vol. 389, no. 20, pp. 457–484, 1927.
- [21] J. Lindhard, “On the properites of a gas of charged particles,” *Kgl. Danske Videnskab. Selskab, Mat-fys. Medd.*, vol. 28, p. 8, 1954.
- [22] E. Runge and E. K. U. Gross, “Density-Functional Theory for Time-Dependent Systems,” *Phys. Rev. Lett.*, vol. 52, pp. 997–1000, Mar. 1984.
- [23] M. A. L. Marques, N. T. Maitra, F. M. S. Nogueira, E. K. U. Gross, and A. Rubio, *Fundamentals of Time-Dependent Density Functional Theory*, vol. 837 of *Lecture Notes in Physics*. Berlin, Heidelberg: Springer Berlin Heidelberg, 2012.
- [24] R. Akashi and R. Arita, “Density functional theory for plasmon-assisted superconductivity,” *Journal of the Physical Society of Japan*, vol. 83, p. 061016, 2014.
- [25] J. Ashkenazi, C. Kuper, and R. Tyk, “Soft plasmon theory of the new high-temperature superconductors,” *Solid State Communications*, vol. 63, pp. 1145–1148, Sept. 1987.
- [26] S.-M. Cui and C.-H. Tsai, “Plasmon theory of high- T_c superconductivity,” *Physical Review B*, vol. 44, pp. 12500–12510, Dec. 1991.
- [27] Y. Takada, “Plasmon Mechanism of Superconductivity in Two- and Three-Dimensional Electron Systems,” *Journal of the Physical Society of Japan*, vol. 45, pp. 786–794, Sept. 1978.
- [28] H. Rietschel and L. J. Sham, “Role of electron Coulomb interaction in superconductivity,” *Physical Review B*, vol. 28, pp. 5100–5108, Nov. 1983.
- [29] “ELK,” <http://elk.sourceforge.net/>, 2004.
- [30] R. M. Dreizler and E. K. U. Gross, *Density Functional Theory*. Berlin Heidelberg New York London Paris Tokio Hong Kong Barcelona: Springer-Verlag, 1990.
- [31] P. Hohenberg and W. Kohn, “Inhomogeneous electron gas,” *Physical review*, vol. 136, no. 3B, p. B864, 1964.
- [32] R. D. Mattuck, *A Guide to Feynman Diagrams in the Many-Body Problem*. Dover Books on Physics, Dover Publications, 2012.

- [33] E. K. U. Gross, E. Runge, and O. Heinonen, “Many-Particle Theory, Hilger,” 1991.
- [34] M. van Schilfgaarde, T. Kotani, and S. Faleev, “Quasiparticle Self-Consistent GW Theory,” *Phys. Rev. Lett.*, vol. 96, p. 226402, June 2006.
- [35] F. Sottile, *Response functions of semiconductors and insulators*. PhD thesis, Ecole Polytechnique, Palaiseau (France), 2003.
- [36] N. W. Ashcroft and N. D. Mermin, *Solid State Physics*. Holt, Rinehart and Winston, 1976.
- [37] E. K. U. Gross, J. F. Dobson, and M. Petersilka, “Density-functional theory of time-dependent phenomena,” in *Topics in current chemistry*, vol. 181, pp. 81–172, Springer, Berlin, 1996.
- [38] L. Hedin, “New method for calculating the one-particle Green’s function with application to the electron-gas problem,” *Physical Review*, vol. 139, pp. A796–A823, Aug. 1965.
- [39] E. K. U. Gross and W. Kohn, “Local density-functional theory of frequency-dependent linear response,” *Physical Review Letters*, vol. 55, no. 26, pp. 2850–2852, 1985.
- [40] B. Dabrowski, “Dynamical local-field factor in the response function of an electron gas,” *Physical Review B*, vol. 34, no. 8, p. 4989, 1986.
- [41] K. Utsumi and S. Ichimaru, “Dielectric formulation of strongly coupled electron liquids at metallic densities. II. Exchange effects and static properties,” *Physical Review B*, vol. 22, no. 11, p. 5203, 1980.
- [42] P. Vashishta and K. S. Singwi, “Electron correlations at metallic densities. v,” *Physical Review B*, vol. 6, no. 3, p. 875, 1972.
- [43] K. N. Pathak and P. Vashishta, “Electron Correlations and Moment Sum Rules,” *Physical Review B*, vol. 7, no. 8, p. 3649, 1973.
- [44] N. Iwamoto, E. Krotscheck, and D. Pines, “Theory of electron liquids. II. Static and dynamic form factors, correlation energy, and plasmon dispersion,” *Physical Review B*, vol. 29, no. 7, p. 3936, 1984.
- [45] N. Iwamoto and E. K. U. Gross, “Correlation effects on the third-frequency-moment sum rule of electron liquids,” *Physical Review B*, vol. 35, no. 6, p. 3003, 1987.
- [46] A. Sanna, *Applications of Density Functional Theory for superconductors to real materials*. PhD thesis, University of Cagliari, Cagliari, Italy, 2007.
- [47] J. R. Schrieffer, *Theory of Superconductivity*. Advanced Book Program, Perseus Books, 1983.
- [48] A. Sanna, G. Profeta, A. Floris, A. Marini, E. K. U. Gross, and S. Massidda, “Anisotropic gap of superconducting CaC6: A first-principles density functional calculation,” *Physical Review B - Condensed Matter and Materials Physics*, vol. 75, p. 20511, Jan. 2007.
- [49] A. Floris, A. Sanna, S. Massidda, and E. K. U. Gross, “Two-band superconductivity in Pb from ab initio calculations,” *Phys. Rev. B*, vol. 75, p. 54508, Feb. 2007.
- [50] P. B. Allen and B. Mitrović, “Theory of superconducting Tc,” *Solid state physics*, vol. 37, pp. 1–92, 1983.

- [51] M. A. L. Marques, M. Lüders, N. N. Lathiotakis, G. Profeta, A. Floris, L. Fast, A. Continenza, E. K. U. Gross, and S. Massidda, “Ab initio theory of superconductivity. II. Application to elemental metals,” *Physical Review B*, vol. 72, p. 024546, July 2005.
- [52] G. Giuliani and G. Vignale, *Quantum Theory of the Electron Liquid*. Cambridge University Press, 2005.
- [53] W. L. McMillan, “Transition temperature of strong-coupled superconductors,” *Physical Review*, vol. 167, pp. 331–344, Mar. 1968.
- [54] P. B. Allen and R. C. Dynes, “Transition temperature of strong-coupled superconductors reanalyzed,” *New York*, vol. 12, pp. 905–922, Aug. 1975.
- [55] A. Sanna, S. Pittalis, J. K. Dewhurst, M. Monni, S. Sharma, G. Umrigar, S. Massidda, and E. K. U. Gross, “Phononic self-energy effects and superconductivity in CaC₆,” *Physical Review B*, vol. 85, p. 184514, May 2012.
- [56] W. L. McMillan and J. M. Rowell, “Lead phonon spectrum calculated from superconducting density of states,” *Physical Review Letters*, vol. 14, pp. 108–112, Jan. 1965.
- [57] E. L. Wolf, J. Zasadzinski, J. W. Osmun, and G. B. Arnold, “Proximity electron tunneling spectroscopy I. Experiments on Nb,” *Journal of Low Temperature Physics*, vol. 40, pp. 19–50, July 1980.
- [58] S. Vonsovsky, Y. Izyumov, and E. Kurmaev, *Superconductivity of transition metals*. Berlin: Springer, 1982.
- [59] A. B. Migdal, “Interaction between electrons and lattice vibrations in a normal metal,” *Sov. Phys. JETP*, vol. 7, no. 6, pp. 996–1001, 1958.
- [60] F. Essenberger, *Density Functional Theory for Superconductors : Extension to a Pairing Mediated by Spin Excitations*. PhD thesis, Martin Luther University Halle-Wittenberg, 2013.
- [61] J. J. Rehr, “Lars Hedin and the quest for a theory of excited states,” *Physica Scripta*, vol. T115, pp. 19–23, 2006.
- [62] P. G. A. DE GENNES, *Superconductivity of Metals and Alloys*. Advanced Book Classics, Addison-Wesley Publishing Company, 1966.
- [63] M. Lüders, M. A. L. Marques, N. N. Lathiotakis, A. Floris, G. Profeta, L. Fast, A. Continenza, S. Massidda, and E. K. U. Gross, “Ab initio theory of superconductivity. I. Density functional formalism and approximate functionals,” *Physical Review B*, vol. 72, p. 24545, July 2005.
- [64] M. Lüders, *Density Functional Theory for Superconductors: A first principles approach to the superconducting phase*. 1998.
- [65] G. Profeta, C. Franchini, N. N. Lathiotakis, A. Floris, A. Sanna, M. A. L. Marques, M. Lüders, S. Massidda, E. K. U. Gross, and A. Continenza, “Superconductivity in Lithium, Potassium, and Aluminum under Extreme Pressure: A First-Principles Study,” *Physical Review Letters*, vol. 96, p. 047003, Feb. 2006.

- [66] A. Sanna, C. Franchini, A. Floris, G. Profeta, N. N. Lathiotakis, M. Lüders, M. A. L. Marques, E. K. U. Gross, A. Continenza, and S. Massidda, “Ab initio prediction of pressure-induced superconductivity in potassium,” *Physical Review B*, vol. 73, p. 144512, Apr. 2006.
- [67] P. Cudazzo, G. Profeta, A. Sanna, A. Floris, A. Continenza, S. Massidda, and E. K. U. Gross, “AbInitio Description of High-Temperature Superconductivity in Dense Molecular Hydrogen,” *Physical Review Letters*, vol. 100, p. 257001, June 2008.
- [68] P. Cudazzo, G. Profeta, A. Sanna, A. Floris, A. Continenza, S. Massidda, and E. K. U. Gross, “Electron-phonon interaction and superconductivity in metallic molecular hydrogen. I. Electronic and dynamical properties under pressure,” *Physical Review B*, vol. 81, p. 134505, Apr. 2010.
- [69] P. Cudazzo, G. Profeta, A. Sanna, A. Floris, A. Continenza, S. Massidda, and E. K. U. Gross, “Electron-phonon interaction and superconductivity in metallic molecular hydrogen. II. Superconductivity under pressure,” *Phys. Rev. B*, vol. 81, p. 134506, Apr. 2010.
- [70] N. F. Berk and J. R. Schrieffer, “Effect of Ferromagnetic Spin Correlations on Superconductivity,” *Physical Review Letters*, vol. 17, pp. 433–435, Aug. 1966.
- [71] H. Rietschel and H. Winter, “Role of spin fluctuations in the superconductors Nb and v,” *Physical Review Letters*, vol. 43, pp. 1256–1260, Oct. 1979.
- [72] F. Essenberger, P. Buczek, A. Ernst, L. Sandratskii, and E. K. U. Gross, “Paramagnons in FeSe close to a magnetic quantum phase transition: Ab initio study,” *Physical Review B*, vol. 86, p. 060412, Aug. 2012.
- [73] F. Essenberger, A. Sanna, A. Linscheid, F. Tandetzky, G. Profeta, P. Cudazzo, and E. K. U. Gross, “Superconducting pairing mediated by spin fluctuations from first principles,” *Physical Review B*, vol. 90, p. 214504, Dec. 2014.
- [74] F. Essenberger, A. Sanna, P. Buczek, A. Ernst, L. Sandratskii, and E. K. U. Gross, “Ab-initio theory of Iron based superconductors,” Nov. 2014.
- [75] T. Kasuya, “A Theory of Metallic Ferro- and Antiferromagnetism on Zener’s Model,” *Progress of Theoretical Physics*, vol. 16, pp. 45–57, July 1956.
- [76] Linscheid Andreas, *Density Functional Theory of Superconductivity in the Presence of a Magnetic Field*. PhD thesis, Martin Luther University Halle-Wittenberg, 2013.
- [77] v. Osolin and R. Žitko, “Padé approximant approach for obtaining finite-temperature spectral functions of quantum impurity models using the numerical renormalization group technique,” *Physical Review B*, vol. 87, p. 245135, June 2013.
- [78] O. Gunnarsson, M. W. Haverkort, and G. Sangiovanni, “Analytical continuation of imaginary axis data for optical conductivity,” *Phys. Rev. B*, vol. 82, p. 165125, Oct. 2010.
- [79] H. J. Choi, D. Roundy, H. Sun, M. L. Cohen, and S. G. Louie, “The origin of the anomalous superconducting properties of MgB(2).,” *Nature*, vol. 418, pp. 758–60, Aug. 2002.
- [80] A. Floris, G. Profeta, N. N. Lathiotakis, M. Lüders, M. A. L. Marques, C. Franchini, E. K. U. Gross, A. Continenza, and S. Massidda, “Superconducting properties of MgB2 from first principles,” *Physical Review Letters*, vol. 94, p. 037004, Jan. 2005.

- [81] A. Floris, A. Sanna, M. Lüders, G. Profeta, N. N. Lathiotakis, M. A. L. Marques, C. Franchini, E. K. U. Gross, A. Continenza, and S. Massidda, “Superconducting properties of MgB₂ from first principles,” *Physica C: Superconductivity and its Applications*, vol. 456, no. 1-2, pp. 45–53, 2007.
- [82] S. V. Halilov, A. Y. Perlov, P. M. Oppeneer, and H. Eschrig, “Magnon spectrum and related finite-temperature magnetic properties: A first-principle approach,” *Europhysics Letters (EPL)*, vol. 39, no. 1, pp. 91–96, 2007.
- [83] M. M. Sigalas and D. A. Papaconstantopoulos, “Calculations of the total energy, electron-phonon interaction, and Stoner parameter for metals,” *Physical Review B*, vol. 50, pp. 7255–7261, Sept. 1994.
- [84] M. Wierzbowska, “Effect of spin fluctuations on T_c from density-functional theory for superconductors,” *The European Physical Journal B*, vol. 48, p. 11, June 2005.
- [85] M. Marques, “Density Functional Theory for Superconductors : Exchange and Correlation Potentials for Inhomogeneous Systems,” 2000.
- [86] E. R. Margine and F. Giustino, “Anisotropic Migdal-Eliashberg theory using Wannier functions,” *Physical Review B*, vol. 87, p. 024505, Jan. 2013.
- [87] A. Chainani, T. Yokoya, T. Kiss, and S. Shin, “Photoemission Spectroscopy of the Strong-Coupling Superconducting Transitions in Lead and Niobium,” *Physical Review Letters*, vol. 85, pp. 1966–1969, Aug. 2000.
- [88] P. Dhakal, G. Ciovati, G. R. Myneni, K. E. Gray, N. Groll, P. Maheshwari, D. M. McRae, R. Pike, T. Proslie, F. Stevie, R. P. Walsh, Q. Yang, and J. Zasadzinski, “Effect of high temperature heat treatments on the quality factor of a large-grain superconducting radio-frequency niobium cavity,” *Physical Review Special Topics - Accelerators and Beams*, vol. 16, p. 042001, Apr. 2013.
- [89] Y. Togawa, K. Harada, T. Akashi, H. Kasai, T. Matsuda, F. Nori, A. Maeda, and A. Tonomura, “Direct Observation of Rectified Motion of Vortices in a Niobium Superconductor,” *Physical Review Letters*, vol. 95, p. 087002, Aug. 2005.
- [90] X. H. Zheng and D. G. Walmsley, “Evidence for effective weakening of electron-phonon interaction in superconducting tantalum, niobium, lead and aluminum,” *Journal of Low Temperature Physics*, vol. 173, pp. 120–142, June 2013.
- [91] J. Nagamatsu, N. Nakagawa, T. Muranaka, Y. Zenitani, and J. Akimitsu, “Superconductivity at 39 K in magnesium diboride,” *Nature*, vol. 410, pp. 63–4, Mar. 2001.
- [92] S. Tsuda, T. Yokoya, Y. Takano, H. Kito, A. Matsushita, F. Yin, J. Itoh, H. Harima, and S. Shin, “Definitive Experimental Evidence for Two-Band Superconductivity in MgB₂,” *Physical Review Letters*, vol. 91, p. 127001, Sept. 2003.
- [93] A. P. Drozdov, M. I. Erements, and I. A. Troyan, “Conventional superconductivity at 190 K at high pressures,” Dec. 2014.
- [94] N. Bernstein, C. S. Hellberg, M. D. Johannes, I. I. Mazin, and M. J. Mehl, “What superconducts in sulfur hydrides under pressure and why,” *Physical Review B*, vol. 91, no. 6, 2015.

- [95] V. Braccini, D. Nardelli, R. Penco, and G. Grasso, “Development of ex situ processed MgB₂ wires and their applications to magnets,” *Physica C: Superconductivity*, vol. 456, pp. 209–217, June 2007.
- [96] J. Kortus, I. I. Mazin, K. D. Belashchenko, V. P. Antropov, and L. L. Boyer, “Superconductivity of metallic Boron in MgB₂,” *Physical Review Letters*, vol. 86, pp. 4656–4659, May 2001.
- [97] E. Cappelluti, S. Ciuchi, C. Grimaldi, L. Pietronero, and S. Strässler, “High T(c) superconductivity in MgB₂ by nonadiabatic pairing,” *Physical review letters*, vol. 88, no. 11, p. 117003, 2002.
- [98] A. Birnboim and H. Gutfreund, “Localized description of superconductivity in narrow-band metals,” *Physical Review B*, vol. 9, pp. 139–146, Jan. 1974.
- [99] K.-H. Lee and K. Chang, “Linear-response calculation of the Coulomb pseudopotential μ^* for Nb,” *Physical Review B*, vol. 54, pp. 1419–1422, July 1996.
- [100] C. Y. Moon, Y. H. Kim, and K. J. Chang, “Dielectric-screening properties and Coulomb pseudopotential μ^* for MgB₂,” *Physical Review B - Condensed Matter and Materials Physics*, vol. 70, p. 104522, Sept. 2004.
- [101] A. Kohen, Y. Noat, T. Proslie, E. Lacaze, M. Aprili, W. Sacks, and D. Roditchev, “Fabrication and characterization of scanning tunneling microscopy superconducting Nb tips having highly enhanced critical fields,” *Physica C: Superconductivity and its Applications*, vol. 419, no. 1-2, pp. 18–24, 2005.
- [102] Z. Khim, D. Burnell, and E. Wolf, “Equivalence of optimized conventional and proximity electron tunneling (PET) for niobium,” *Solid State Communications*, vol. 39, pp. 159–161, July 1981.
- [103] M. Iavarone, G. Karapetrov, a. E. Koshelev, W. K. Kwok, G. W. Crabtree, D. G. Hinks, W. N. Kang, E.-M. Choi, H. J. Kim, H.-J. Kim, and S. I. Lee, “Two-Band Superconductivity in MgB₂,” *Physical Review Letters*, vol. 89, p. 187002, Oct. 2002.
- [104] A. I. D’yachenko, V. Y. Tarenkov, A. V. Abal’oshev, and S. J. Lewandowski, “Evidence of strong electron-phonon interaction in superconducting MgB₂ from electron tunneling,” Jan. 2002.
- [105] J. P. Perdew, K. Burke, and M. Ernzerhof, “Generalized Gradient Approximation Made Simple,” *Phys. Rev. Lett.*, vol. 77, pp. 3865–3868, Oct. 1996.
- [106] T. Büche and H. Rietschel, “Superconductivity in the homogeneous electron gas: Exchange and correlation effects,” *Physical Review B*, vol. 41, pp. 8691–8697, May 1990.
- [107] S. H. Vosko and J. P. Perdew, “Theory of the Spin Susceptibility of an Inhomogeneous Electron Gas via the Density Functional Formalism,” *Canadian Journal of Physics*, vol. 53, pp. 1385–1397, July 1975.
- [108] J. P. Perdew and A. Zunger, “Self-interaction correction to density-functional approximations for many-electron systems,” *Phys. Rev. B*, vol. 23, pp. 5048–5079, 1981.
- [109] “Mathematica,” <http://mathworld.wolfram.com/EllipticIntegraloftheSecondKind.html>.

- [110] “Mathematica,” <http://mathworld.wolfram.com/EllipticIntegraloftheThirdKind.html>.
- [111] S. H. Vosko, L. Wilk, and M. Nusair, “Accurate spin-dependent electron liquid correlation energies for local spin density calculations: a critical analysis,” *Canadian Journal of physics*, vol. 58, no. 8, pp. 1200–1211, 1980.

Acknowledgements

It is not the places that grace the men, but men the places. When I think about my five-years stay at MPI Halle, I completely agree with this expression. I would like to thank all of the MPI family for the support, for the fruitful working atmosphere and for the bright events which we had at MPI.

In particular, I am proud to be the first official PhD-student of Dr. Antonio Sanna, from whom I learned everything I know now. His advises always helped me to solve the difficulties I faced during my PhD. I am grateful for his patience with the way I formulate things. I would like to thank Dr. John Kay Dewhurst and Dr. Sangeeta Sharma who gave me opportunity to contribute into the ELK code, from which I gained all of my current programming skills. And of course nothing would be possible without having such a brilliant head of our department, Prof. Dr. E.K.U. Gross. I really hope to see and to work with these people again in the future.

I would also like to mention my colleges and first officemates C. Bersier and H. Glawe, I will never forget their jokes and funny stories started immediately after I arrived in Halle. At the same time I met N. Sardana and A. Senichev, we were recognized as "Russian mafia" afterwards (in fact, not completely Russian and not completely mafia). I would like to thank M. Santo for a great help at the very beginning of my stay in Halle, for the beautiful apartment which she helped me to find.

I appreciate our mini-office-coffee seminars with my new officemates T. Müller and E. Kraisler. I am grateful for the reliable work of our secretary I. Goffin, who could solve any administrative problem. And finally, I would like to thank my family and my wife for their support, for their patience and for being with me all this time.

The work presented in the thesis was sponsored within the International Max Planck Research School (IMPRS) program.

Curriculum Vitae

Personal Details

Name: Arkadiy Davydov
Born: 1986 in Severouralsk, UdSSR
Citizenship: Russian Federation
Address: Gräfestr. 21, 06110 Halle (Saale)
Email: ark.davydov.1986@gmail.com

Education

1996-2004: High school
09/2004 - 06/2008: Bachelor's diploma - Ural State University in Ekaterinburg, Russia
09/2008 - 06/2010: Master's diploma - Ural State University in Ekaterinburg, Russia
02/2011 - 07/2015: Ph.D. Student - MPI for Microstructure Physics in Halle (Saale)

Current Position

08/2015 - until the present: Postdoc - MPI for Microstructure Physics in Halle (Saale)

Publications

Ab-initio Eliashberg theory of superconductivity with static and dynamic Coulomb interactions
A. Davydov, A. Sanna, S. Sharma, J.K. Dewhurst and E.K.U. Gross
- in preparation

Ab-initio theory of Plasmonic Superconductivity: the hybrid Eliashberg-SCDFT approach
A. Davydov, A. Sanna, S. Sharma, J.K. Dewhurst and E.K.U. Gross
- in preparation

Eidesstattliche Erklärung

Hiermit erkläre ich gemäß 5 Abs. 4 der Promotionsordnung der Naturwissenschaftlichen Fakultät II - Chemie, Physik und Mathematik der Martin-Luther Universität Halle-Wittenberg vom Februar 2011, dass ich die vorliegende Arbeit selbständig und ohne fremde Hilfe verfasst habe. Es wurden keine, außer die angegebenen Quellen und Hilfsmittel benutzt und die den benutzten Werken wörtlich oder inhaltlich entnommenen Stellen wurden als solche kenntlich gemacht. Desweiteren erkläre ich gemäß 5 Abs. 5 der Promotionsordnung, dass ich bisher keine vergeblichen Promotionsversuche an dieser oder einer anderen Fakultät unternommen habe.

Halle, den 15.09.2016

Arkadiy Davydov